Multi-functional Cyclopentadienyl Complexes for Theranostic Applications

---

Dissertation

zur

Erlangung der naturwissenschaftlichen Doktorwürde

(Dr. sc. nat.)

vorgelegt der

Mathematisch-naturwissenschaftlichen Fakultät

der

Universität Zürich

von

Angelo Frei

aus

Diepoldsau-Schmitter SG

Promotionskommission

Prof. Dr. Roger Alberto (Vorsitz)

Prof. Dr. Nathan Luedtke

Prof. Dr. Nils Metzler-Nolte

Zürich, 2018

“As with most of life's problems, this one can be solved by a box of pure radiation.”
— Andy Weir, The Martian

Per meis frar e meis bazegner
Per meis genituors

Table of Contents

Acknowledgement

The amazing rollercoaster of experiences that the last four years have been were made entirely possible by Prof. Dr. Roger Alberto agreeing to take me on as his PhD student. As far as I can tell, this decision was made on a first impression and a very good word put in by my Master-thesis supervisor Prof. Dr. Gilles Gasser (which is highly appreciated). Having heard more than one horror story about bosses in academia over the years I feel quite privileged to say that Roger was a great supervisor. From day one, he gave me the freedom to completely follow my own ideas while also being there for advice and support whenever I needed it. I also want to thank him for his immense support in finding a post-doc position and the successful application for an SNF-fellowship. Apart from the science, I thoroughly enjoyed our discussions about all things science-fiction as well as our shared trips to South Africa.

Next, I need to thank my “second supervisor” Prof. Dr. Andreas Roodt. For the hours and hours of intense kinetic discussions, the shared stories and experiences as well as the unparalleled hospitality you have shown me in South Africa.

I also would like to thank Prof. Dr. Nathan Luedtke, who “accompanied” me throughout my studies in the context of lectures, my master exam and my SNF postdoc application, for agreeing to be part of my PhD committee. I am also thankful to Prof. Nils Metzler-Nolte for being my external committee member. Thanks also to Prof. Dr. Jason Holland, for a fruitful collaboration and helpful career advice.

The whole “university-machine” would break down in chaos if not for the many many people keeping things going. I especially thank Ramona for always being available and helpful and for keeping the ex-ACI (and the whole department really) going and somewhat organized. Thanks to Dr. Thomas Fox, Prof. Bernhard Spingler, Heinz Spring, Dr. Ferdinand Wild, Hanspeter Stalder, Serkan Sariyildiz, Dr. Eliane Fischer, Yvonne Forster and the whole Bigler Group, Simon Jurt, Sascha Giger, Mirko Hofer, Nathalie Melunsky, Dr. Sabine Stockhause, the rest of the HR-department and the Betriebsdienst for all your work and effort in keeping things going and always being available when I needed something.

Special thanks go to Dr. Henrik Braband for continuously helping me with any problem I had in the radiolab and always having an open door for me.

During these four years I had the chance to visit several overseas conferences, which would not have been possible without the financial support through travel awards by the SCNAT/SCS, SBIC and the CMSZH Graduate School. Further thanks to the CMSZH for the monthly apéros, the BBQ's, the excellent soft-skill courses and last but not least for the organization of the yearly and amazing Retreats (Shout-out to the 2016 Orgateam: Elena, Marianthi, Matteo, Marco, Lucas, Sabine and honorary members Nicola, Cristina, Andy and Bea).

At this point I would also like to acknowledge google, reaxys, scifinder, wolframalpha, scihub, wikipedia and twitter, for making knowledge accessible the way they do, it is hard for me to imagine a world without these incredible resources. I would also like to thank my coffee machine for it's flawless service throughout the years.

A big thank you goes to all past and present members of the Alberto group for making my four years very enjoyable. In particular, I want to thank Michel for being a great labmate and my go-to person for everything from weird online videos, my enthusiastic space-outbreaks, my frustrations and my first external opinion on abstracts, grants, graphics and this thesis. Also, thanks for being my non-daltonic pair of eyes when I need them. Many thanks to Carla for keeping up with the entropy in our lab and all the things you do to keep our workplace in order. I also want to thank Giusi for all the helpful discussions in the last years as well as all the good times at DoBars and apéros. Thanks to Robin B. for your dry humor and always keeping me busy by injecting weird things into HPLCs or throwing radioactive stuff where you should not. Thanks Raphael for picking up my project and caring it on, I'm happy that it is in very good hands with you. Thanks Bradley for all the good discussions and your excellent help with the ICP-MS. Thanks to Daniel for following in my footsteps in the South-Africa exchange and being open to all the things to explore "that side". Further thanks also the other current members Nico, Mathias, Peter, Anna, Maruan, Paul, Benji, Prerna, Chris and Franziska and former members Craig, Benz, Michi, Immi, Stephan, Benz, Evelyne, Johannes and Cyril.

Thanks to all the students (except one) I got to supervise during the years, I have learned a lot by teaching and supervising you.

Thanks to all the amazing people I met around the Uni and around the world with whom I had a drink, a chat or some other adventure. Thanks to Ruben, Rebecca, Mr. Mohammed, Alabel, Tinus, Renier, Shaun, Pi, T5, Mutente, Lindy, the Australians, Paul, Robyn, Alex, Sofia, Matteo, Alma, Jelena, Elena, Loïc, Matthias, Mylene, Aaron, Faustine, Phuc, MicBac, Dominik, Tobi, Flo, Sandro, Marco, Robin and Karla.

Thanks to David for your friendship, all the hours we spent at the gym together and your computational support when I needed it.

Shout-out to my former room-mates that are now scattered around the globe but still am happy to count as friends. Thanks to Sam & Dahye in Lausanne, Kostas in London and Ding in New York.

Also thanks to former fellow students Lars and Denise for keeping in touch even though we don't see each other that often anymore.

There are a few people that deserve a special note for the friendship that we developed or maintained during this time of my life. Thank you, Lucas, for being part of this No-Homo-Bromance, for being a great travel companion on ~~three~~ four continents, the uncountable fikas and gin tonics and your great friendship and support throughout the years. Grazie Jefe!

Thank you Cristina for all the coffee breaks, dinners, BBQ's, trips and fun moments we shared. Thank you Marjorie for your great humor, your hilarious laugh, your openness and the will to endure my stubborn discussions. Thanks to Manon (+ French Concorde) and Klara for being part of an amazing group of friends and for all the Foies Gras, Champagne, Mascottes and vegetarian Lasagnes.

From my heart, thank you Sara for being a pillar in my life for the last 10 years. Thanks for being my best friend, the one person I can trust with anything, always having an open ear and being there in both the good and the bad times (TVB).

Thanks to my "Italian division": Dario, Giovanni & Will. Grazie per l'amicizia e per avermi sempre fatto sentire come a casa quando sto con voi.

Moving to a different continent, thank you Orbett for an extraordinary friendship across hemispheres. Thanks for (hesitantly) following me on all sorts of crazy adventures like

bush-walking, hyena-braais, shark-diving, lake-zurich swimming etc. I hope we will have many more together.

I also want to thank the two other Marraus, Pennie and Tom for a great companionship and the numerous drinks, braais and parties on two continents. Ketlaobona ditapoles!

Moving on to yet another continent, I want to thank my ~~Gorman~~ New Zealand princess Hannah for embarking on a crazy-amazing globe-spanning adventure together with me and all the love, support and encouragement you have given me (<3).

Finally, a very big thank you to my parents, for all your support and never questioning my life choices, even when it involves moving to the other side of the globe.

Grazia fich per tuot vos sustegn dürant nö be ils ultims quatter ons ma daspö adüna!

Thank you ! - Grazia ! - Merci ! - Danke ! - Grazie !

Summary

In the last decades ^{99m}Tc has dominated the market as the most frequently used radionuclide for diagnostic purposes in the clinics. The unparalleled success of technetium stems from its near-ideal properties, such as a half-life of 6 hours, optimal energy for SPECT imaging as well as easy, cost-friendly and worldwide availability.

However, in recent years there has been a severe lack of new technetium based nuclear imaging agents, with only two new compounds being approved since 2001. This can partly be attributed to the preference for a so-called pendent approach in the design of radiotracers. The concept of the pendent approach is to attach a targeting unit *via* a linker to a chelator of the radiometal. This approach is synthetically straightforward and hence the most frequently pursued one, even though the use of linkers and usually bulky chelators affects the biodistribution of the radiotracer in unpredictable ways. The more elegant but in turn more challenging integrated approach involves the rational introduction of the radiometal and its chelator into the chemical structure of a biomolecule with known *in vivo* distribution profile. This application would also enable a theranostic approach were the ^{99m}Tc complex is used for diagnostics and the analogous non-radioactive Re-compound for therapy.

Cyclopentadiene (Cp) is well-suited ligand to address the issues of current systems. It is small in size and forms stable neutral complexes with both Re and ^{99m}Tc. Additionally, the vast potential for the chemical functionalization Cp-ligands has been relatively unexplored. The goal of this work was the development of a chemically versatile Cp-ligand synthesis and its application towards pendent as well as integrated approaches with Re and ^{99m}Tc.

In the first and main part of this thesis a novel synthetic route towards multifunctional Cp-ligands was developed. The synthesis was optimized for routine preparation of up to gram-scale batches of Cp's containing at least three functionalities. With these ligands, the corresponding rhenium and technetium-99m complexes could be prepared in a straightforward manner. The respective complexes are homo- or hetero functionalized, depending on the specific requirements. In a second part, these ligands were applied in biological settings by synthesizing Cp-complexes conjugated to one or two prostate cancer targeting moieties. It was shown that the species containing two inhibitor-units exhibits binding affinity in the low nanomolar range and was significantly

more potent than the complex containing only one. In a third project the same ligand platform was used to prepare a rhenium-mimic of the anticancer drug pemetrexed following an integrated approach. The aromatic ring in pemetrexed was replaced by a Cp-ring, leading to a Re-analogue of unprecedented structural similarity to the lead-compound.

Part B explores the applicability of multifunctional Cp's with other metals. Both metallocene and mixed-sandwich type complexes were prepared with ruthenium and iron, introducing the potential for further functionalization of these types of complexes with possible applications in catalysis and medicinal chemistry.

The more fundamental Part C deals with the study of basic rhenium building blocks and their behavior in solution towards ligand exchange. It is shown that rhenium tricarbonyl can undergo rapid carbonyl exchange in solution. ^{13}C NMR spectroscopy was the tool to study the intricate mechanism of CO exchange in these complexes. These findings enable the targeted preparation of ^{13}C-labeled rhenium synthons which are key to study the basic reaction mechanisms of these complexes.

Finally, Part D focuses on the different synthetic strategies towards hitherto unexplored polynuclear complexes of Re incorporating ^{99m}Tc. By comparing pure Re-clusters with ^{99m}Tc-containing ones it is shown that radiolabeled multinuclear complexes can be prepared by both pre-assembly and self-assembly approaches. The easy and well-defined synthesis of these complexes lends itself to nuclear imaging applications where such structures have not found much notice yet.

Overall, this thesis entails the design and implementation of a Cp-ligand platform for the synthesis of cancer-targeting diagnostic and therapeutic metal complexes. Additionally, this toolkit is generally relevant to the field of organometallic chemistry and will find applications in different domains of this field.

Zusammenfassung

Der radiopharmazeutische Markt der letzten Jahrzehnte wurde von dem am häufigsten klinisch eingesetzten Radionuklid Technetium-99m dominiert. Der beispiellose Erfolg von ^{99m}Tc kann seinen nahezu idealen Eigenschaften wie der vorteilhaften Halbwertszeit von sechs Stunden, optimalen Zerfallsenergie für SPECT-Bildgebung sowie der einfachen, kostenfreundlichen und globalen Verfügbarkeit zugeschrieben werden. In den letzten Jahren hat sich jedoch ein deutlicher Mangel an neuen Technetium-basierten Pharmazeutika für nukleare Bildgebungsverfahren abgezeichnet. Seit 2001 wurden nur zwei neue Verbindungen zur klinischen Anwendung zugelassen. Dieser Mangel kann teilweise dem Trend, wonach Radiodiagnostika anhand des sogenannten pendenten Ansatzes konzipiert werden, zugeschrieben werden. Beim pendenten Ansatz wird das Radiometall durch einen Chelator über einen Linker an eine zielorientierte biologische Einheit angehängt. Obwohl der Einsatz von Linkern und normalerweise sperrigen Chelatoren die Bioverteilung des Tracers auf unvorhersehbare Weise beeinflussen ist dies der synthetisch einfachere und daher öfters verwendete Ansatz. Beim eleganteren aber auch schwierigerem integrierten Ansatz wird das Radiometall und der Chelator in die chemische Struktur eines Biomoleküls mit bekanntem *in vivo* Verhalten eingefügt. Dies würde eine theranostische Anwendung ermöglichen, in welcher der ^{99m}Tc-Komplex für die Diagnose und die analoge nicht-radioaktive Rhenium Verbindung für eine anschliessende Therapie benutzt wird.

Cyclopentadien (Cp) ist ein gut geeigneter Ligand, der die Schwachstellen von heutigen Chelator-Systemen umgehen kann. Cp-Liganden sind klein und bilden stabile, neutrale Komplexe mit Re und ^{99m}Tc. Das grosse Potential der chemischen Derivatisierung von Cp-Liganden wurde zudem bisher erst wenig erforscht. Das Ziel dieser Arbeit war die Entwicklung einer chemisch vielfältigen Cp-Ligandsynthese und dessen Anwendung in sowohl pendenten als auch integrierten Ansätzen mit Re und ^{99m}Tc.

Der erste Teil dieser Dissertation beschreibt die Entwicklung eines neuen Syntheseweges für multifunktionelle Cp-Liganden. Diese Synthese wurde optimiert um routinemässig Cp-Liganden mit mindestens drei Funktionalitäten im Gramm-Massstab herzustellen. Die Rhenium und Technetium-99m Komplexe dieser Liganden konnten

auf einfachem Weg hergestellt werden und können je nach Bedürfnissen homo- oder heterofunktionell substituiert sein. Im zweiten Projekt wurden diese Liganden in einem biologischen Kontext eingesetzt. Es wurden Cp-Komplexe synthetisiert, die mit einer oder zwei Einheiten derivatisiert waren, welche vorzugsweise von Prostatakrebszellen aufgenommen werden. Die Verbindung mit zwei Prostatabindungseinheiten wies eine Affinität im tiefen nanomolaren Bereich für diese Krebszellen auf und war der Substanz mit nur einer Bindungseinheit um ein Vielfaches überlegen.

In einem dritten Projekt wurde dasselbe Ligandensystem benutzt um ein Rheniumanalogon des Krebsmedikamentes Pemetrexed nach einem integrierten Ansatz zu synthetisieren. Dazu wurde der aromatische Ring im Medikament durch einen Cp-Ring ersetzt, was zu einem Rheniumkomplex mit neuartiger struktureller Ähnlichkeit zur Ausgangsverbindung führte.

Teil B befasst sich mit der Komplexierung von diesen multifunktionellen Cp-Liganden mit anderen Metallen. Sowohl Metallocene als auch gemischte Sandwichkomplexe konnten mit Ruthenium und Eisen hergestellt werden. Dies ergab Komplexe, welche potentiell weiter funktionalisiert werden und somit mögliche Anwendungen in der Katalyse oder der medizinischen Chemie haben könnten.

Im Teil C wird das Ligandenaustauschverhalten von grundlegenden Rhenium-Synthesebausteinen in Lösung untersucht. Es wird gezeigt, dass bei Rhenium-Tricarbonyl Verbindungen in Lösung schneller CO-Austausch beobachtet werden kann. Mithilfe von ^{13}C NMR-Spektroskopie konnte dieser komplizierte Mechanismus im Detail studiert werden. Diese Ergebnisse ermöglichen eine gezielte Anreicherung von ^{13}C in elementaren Rhenium-Bausteinen, welche essentiell sind, um die grundsätzlichen Reaktions-mechanismen dieser Verbindung zu untersuchen.

Im letzten Teil D liegt der Fokus auf bisher wenig studierten Synthesestrategien um ^{99m}Tc in mehrkernigen Rhenium-Komplexen zu inkorporieren. Durch Vergleich von rein Rhenium-haltigen Komplexen mit ^{99m}Tc enthaltenden Verbindungen konnte gezeigt werden, dass radiomarkierte Komplexe sowohl nach einem "Voranordnungs" als auch nach einem "Selbstanordnungsansatz" synthetisiert werden können. Diese einfache und wohldefinierte Synthese bietet sich zur Anwendung in nuklearen Bildgebungsanwendungen an wo solche Strukturen bisher wenig Beachtung fanden.

Insgesamt beinhaltet diese Doktorarbeit die Entwicklung und Umsetzung eines Cp-Ligandensystems welches die Synthese von Krebspezifischen diagnostischen und therapeutischen Metallkomplexen ermöglicht. Generell ist dieses Ligandensystem auch für das Forschungsgebiet der Organometallchemie relevant, wo es Anwendungen in verschiedenen Gebieten dieses Feldes finden wird.

Riassunt

Dürant ils ultims decennis ha dominà il radioisotop tecnetium-99m (^{99m}Tc) il marchà sco radionuclid chi vegn dovrà il plü suvent illas clinicas. Quist success unic as poja ingrazchar a las qualitats plü o main idealas, sco il temp da mezza-vita da ses uras, optimala energia per la diagnostica SPECT e la disponibilità globala favuraivla. Ma i'ls ultims ons as ha manifestada üna s-charsdà da farmaceuticas chi's basan sül tecnetium. Be duos formulaziuns sun stattas admissas per l'adöver in clinicas daspö il 2001. Quista mancanza as poja declerar per part cul trend da concipir radiodiagnostics tenor la metoda pendenta. Pro la metoda pendenta vegn attachà il metal radioactiv ad ün chelator intuorn il qual es attachà per travers üna colliaziun ad ün'unità biologica cun ün böt specific. Cumbain cha l'adöver da colliaziuns e chelators chi sun normalmaing massitschs ha ün effet sün la distribuziun biologica da l'unità diagnostica chi nu's riva da preverer es quista metoda la plü simpla e perquai la plü populara. Ün'otra metoda plü eleganta, ma eir plü difficila es quella integrada. In quist cas sun il radiometal ed il chelator inchastrats aint illa structura chemica dad ün molekül cun cumportamaint e culla distribuziun biologica cuntschainta. Quai pussibilitess ün'applicaziun theranostica, ingiò cha'l cumplex cun ^{99m}Tc vain dovrà per la diagnosa e la colliaziun analoga na-radioactiva cun rhenium (Re) per la terapia.

Cyclopentadien (Cp) es ün ligant chi'd es fich adattà per surmuntar ils puncts debels da chelators actuals. Ligants da Cp sun pitschens e fuorman cumplex stabils e neutrals cun Re e ^{99m}Tc. Implü nun esa fin uossa amo gnü fat blera retschercha a reguard il grond potenzial aint illa derivatisaziun chemica da Cp's. L'intenziun da quista lavur d'eira da sviluppar üna sintesa multifaria per ligants da Cp e lur applicaziun tant illas metodas pendentas sco eir in quellas integradas cun Re e ^{99m}Tc.

La prüma part da quista dissertaziun descriva il svilup dad üna nouva ruta sintetica per ligants da Cp multifuncziunals. La sintesa es gnüda optimada per la preparaziun da rutina aint illa scala da grams da Cp's cun almain trais funcziunalitats. Ils cumplexs da rhenium e tecnetium cun quists ligants sun gnüts preparats in maniera simpla e pon esser funcziunalisats in maniera omogena o eterogena. Aint il seguond progect sun gnüts applichats quists ligants in ün context biologic. I sun gnüts sintetisats cumplexs cun ligands da Cp chi d'eiran derivatisats cun üna o duos unitats specificas chi vegnan

tuttas sü pustüt da cellas da cancar dal pancreas. Il molekül cun duos unitats ha muossà ün'affinità illa regiun nanomolara per quistas cellas da cancar e seis effet es stat bler plü grond co quel dal molekül cun be üna unità.

Aint il terz project es gnü dovrà l'istess sistem per sintetisar ün analog dal medicamaint da cancar pemetrexed chi cuntegna rhenium, inspirà da la metoda integrada. Il rinch aromatic dal medicamaint es gnü substitui cun ün Cp, quai ha manà ad ün cumplex da rhenium cun üna gronda sumglientscha structurala al medicamaint original.

La part B da quista lavur as occupa culla cumplexaziun da quists ligants da Cp multifuncziunals cun oters metals. Id eis stat pussibel da preparar cumplexs dal tip metallocen ed eir cumplexs masdats da "sandwich", cun ruthenium e fier. Quists cumplexs as pudessa funcziunalisar inavant per applicaziuns aint illa catalisa o illa chemia medicinala.

Illa part C vain examinà il cumportamaint da barat dals ligands aint in blocs da sintesa basics dal rhenium in soluziun. I's po observar chi dà ün barat svelt tanter moleküls da rhenium cun trais ligands da monoxid carbonic. Cun l'agüd da la spectroscopia da resonanza magnetica da charbun-13 esa stat pussibel dad eruir in detagl quist mecanissem cumplichà. Ils resultats da quist proget permettan üna concentraziun da charbun-13 aint in blocs da sintesa basics da rhenium. Quai es essenzial per examinar ils mecanissems da reacziun da quistas substanzas.

L'ultima part D as focussescha sün strategias da sintesa per incorporar ^{99m}Tc aint cumplexs da rhenium poly-nuclears. Cun congualar cumplexs chi cuntegnan be rhenium cun quels chi cuntegnan eir technetium s'haja pudü muossar cha cumplexs radiomarcats pon esser sintetisats tenor il princip da pre-arrandschamaint opür il princip dad auto-arrandschamaint. Quista sintesa simpla as douvra per l'applicaziun illa diagnostica nucleara ingiò cha quistas structuras nu sun fin uossa amo gnüdas resguardadas uschè suvent.

Tuot in tuot cumpiglia quist doctorat il svilup e l'implementaziun d'ün sistem da ligands chi's basan sün Cp. Grazcha a quist sistem es statta pussibla la sintesa da cumplexs cun tecnetium e rhenium, diagnoistics e therapeutics specifics pel cancar. In general sun quists ligands da Cp eir interessants per il chomp da perscrutaziun da la chemia organometallica ingio chi chattaran applicaziuns in diversas domenas da quist chomp.

1. Introduction

1.1 Inorganic Medicinal Chemistry

While the pharmaceutical market is dominated by purely organic compounds, metal-based drugs have firmly established themselves as an essential cornerstone of modern medicine. Inorganic compounds often have access to properties and modes of action which are not achievable with organic compounds alone, such as ligand exchange, reactive oxygen species (ROS) generation, redox activity and a significantly more pronounced 3D geometry.[1, 2]

The prime example of a metal-based drug is the anticancer drug cisplatin (Figure 1), approved for clinical use in 1978, and still used in over 50% of all cancer treatments today.[3, 4] Even though it suffers from significant drawbacks, such as various side-effects (ranging from nausea and vomiting to nephro- and neurotoxicity) and the development of resistance amongst certain cancer cell lines, cisplatin has increased the cure rate for testicular cancer to over 95 %.[5] Inspired by its outstanding success, many thousands of platinum based compounds have been synthesized in the last decades. However, only two Pt(II) compounds (carboplatin and oxaliplatin, cf. Figure 1) have been globally approved by the clinics. More recently, a series of studies have reported the promising preclinical results of platinum(IV) prodrugs, which are reductively activated to the cytotoxic Pt(II) compound in the tumor cells.[6]

In the last two decades, the field of metal-based medicinal chemistry has widened its focus and compounds based on ruthenium, gallium and iron have made it into human clinical trials.[7] The first ruthenium-based compound to make it into a phase I clinical trial is known as NAMI-A ([ImH][*trans*-$RuCl_4$(dmso-S)(Im)] (dmso-S = sulfur-bonded dimethyl sulfoxide, Im = imidazole, Figure 1), developed by the group of Alessio.[8, 9] This compound had shown favorable and selective anti-metastatic activity in mice, but without significant effects on the primary tumor growth. The phase I study followed by a limited phase II clinical trial however deemed it "*insufficiently effective for further use*".[10] It is uncertain if the failure is attributable to a design flaw of the clinical trials as stated by Alessio in a recent personal view. It is however evident, that NAMI-A paved the way for non-platinum metal-based drugs to enter clinical trials.[9] The second and so far only other ruthenium complex to make it into human trials is NKP-1339

(Figure 1). Based on a lead compound (KP418) reported by Keppler and Rupp in 1986,[11] NKP1339 showed encouraging activity against both primary tumors and metastases and minimal side effects were reported in a first small clinical phase I trial.[12, 13]

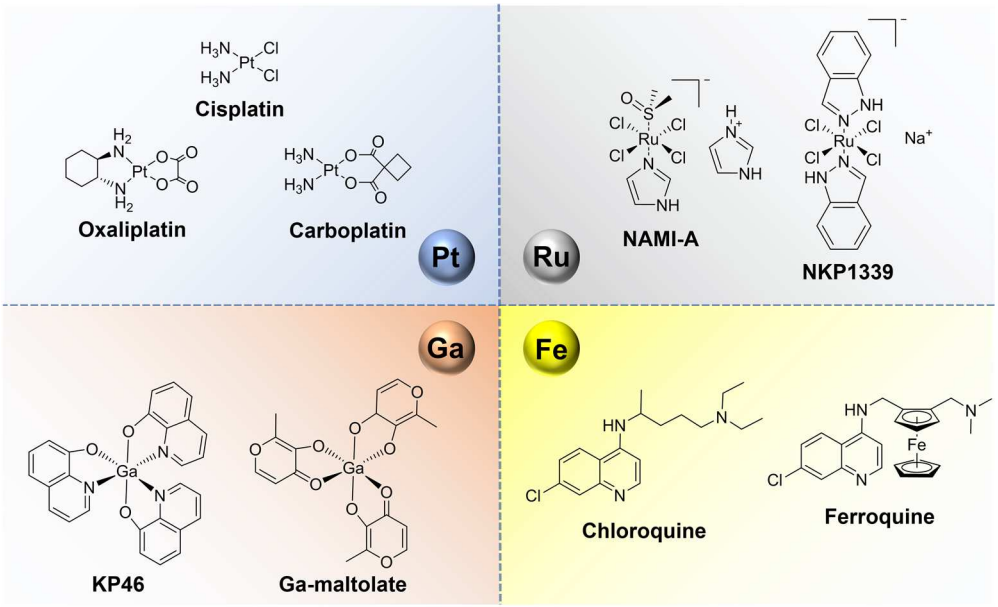

Figure 1. Overview of the structures of metal-based drugs in clinical use or that have been evaluated in human clinical trials

Gallium, an element that shares many physicochemical characteristics with Fe(III) in its +3 oxidation state has also shown promising antitumor activity.[14] Two compounds are currently in early clinical trials, KP46 and gallium maltolate (Figure 1). Both complexes showed no dose-limiting toxicities and more potent tumor cell proliferation inhibition than gallium salts in phase I studies.[15]

Another up-and-coming metal-based drug candidate comes from the field of anti-malaria drugs. Ferroquine is a ferrocene-based derivative of the known drug chloroquine (Figure 1). In contrast to the previous examples, this compound does not represent an entirely new chemical structure but an integration of the redox-active ferrocene-moiety into the active scaffold of chloroquine. This has been shown to circumvent the chloroquine resistance in certain strains of malaria.[16] Ferroquine has very recently completed a phase II clinical trial with promising results.[17] Furthermore, phase II trials in combination with other antimalarial compounds are currently ongoing.[18]

While metals have most definitely proven their potential in a clinical setting, there has not been a metal-based compound approved for human use in decades. Part of the hurdle of getting more compounds tested in humans is both the challenge to understand the metabolic fate of these drugs but also a certain resistance of established pharmaceutical companies to “touch” these, in their eyes, un-orthodox molecules. Since clinical development is a high-risk and very expensive endeavor, the aversion of “Big Pharma” to consider them is partially understandable. It is probably going to be up to smaller and less risk-averse biotech companies to show the world that metals will still play an important role in modern medicine in the future.

1.2 Radiochemistry

1.2.1 A Brief History of Diagnostic Radiochemistry

Modern medicine has contributed significantly to the drastic increase in life expectancy in the last 100 years. New and better drugs keep prolonging our lives by curing previously untreatable diseases, but the early diagnosis and detection of malignancies as well as the monitoring of therapy progress also plays a crucial role in better treatment outcomes. Diagnostics is a very widespread field ranging from optical observations by doctors to intricate detection of specific molecules in the bodies of patients. Since its discovery, radioactivity represented an interesting potential tool to investigate patients bodies as the primary radiation from γ-decays and the secondary radiation from β^+-decays penetrate human tissue easily and without causing significant damage. From the discovery of radioactivity by Henri Becquerel in 1896 it only took four decades until the first use of radioactive material (^{32}P) in animals in 1935.[19] The radionuclide iodine-131 was first produced in 1938 and its use as the first radioactive diagnostic tool in humans was published in 1939.[20, 21] Today, a vast array of radionuclides are used or being investigated for their use in clinical diagnosis.[22-24] For reasons that will be highlighted in the following chapters, ^{99m}Tc has become the most widely applied radio-isotope.

1.2.2 The Rise of ^{99m}Tc

By accounting for over 80 % of all diagnostic nuclear medicine studies, technetium-99m is the most widely used radionuclide today.[25, 26] Originally discovered by Perrier and Segré in 1937 and isolated by deuteron bombardment of molybdenum, technetium-99 (from the greek “technètos” = artificial) was the first artificial element made by man.[27] It’s relatively shortlived isomer ^{99m}Tc was reported by Seaborg and Segré in 1939.[28] The dominance of ^{99m}Tc in the field of diagnostic nuclear medicine can be attributed to its many favorable properties. The radionuclide decays to ^{99}Tc with a half-life of 6 hours, emitting a 141 keV gamma photon with 89% abundance.[29] This is ideal for the gamma cameras used in nuclear medicine. The half-life allows for a long enough signal detection, while also ensuring that the patients are only exposed to the radioactive radiation for the minimum time.

Another decisive factor in the success of ^{99m}Tc is its cost. Most other radioisotopes require a nearby synchrotron for their generation and therefore have a significant price-tag. Technetium-99m on the other hand, can be obtained continuously during multiple weeks from so-called generators where ^{99}Mo ($t_{1/2}$ = 66 h) continually decays into the desired isotope. The development of these generators in the Brookhaven National Laboratory (BNL) in 1950 allowed the ^{99}Mo to be packaged as $[^{99}MoO_4]^{2-}$ and shipped in the form of an alumina column, from which the ^{99m}Tc can easily and safely be eluted as $[^{99m}TcO_4]^-$ in sterile saline with high radionuclide purity.[30] The ^{99}Mo on the other hand is conveniently a side product of nuclear fission and is readily available and transportable. However, the current global movement away from nuclear energy is threatening this constant supply stream and other production methods might have to take over in the near future.[31-33] An additional advantage of ^{99m}Tc over its competitors is its diverse chemistry. Being a group VIIB element, it exists in 9 different oxidations states which opens up a plethora of possibilities in terms of geometries and structures available.[27]

The favorable properties of ^{99m}Tc are validated by its unparalleled success in the clinics. As of now, a total of 67 imaging agents based on ^{99m}Tc have been approved by the FDA, of which 28 are still in use today.[34] The two most successful agents, cardiolite and myoview (Figure 2), are both heart imaging agents and accounted for

over 600 million USD in revenue in 2007. However, since 2001, only two new kits based on molecular entities have been approved.[35]

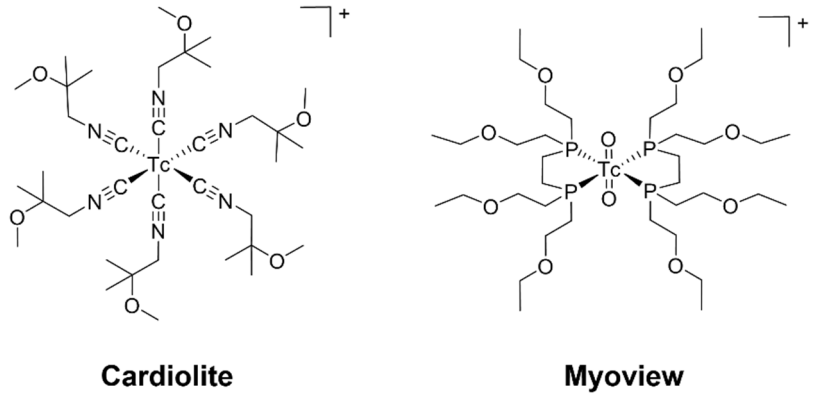

Figure 2. Structure of the two ^{99m}Tc "blockbusters" cardiolite and myoview.

1.2.3 The $[TcCO_3]^+$ Kit

In the early 2000s, Alberto *et al.* reported the convenient synthesis of $[^{99m}Tc(OH_2)_3(CO)_3]^+$ in one step from $[^{99m}TcO_4]^-$.[36, 37] This procedure, and it's subsequently commercially available kit-formulation, promised a re-invigoration of the somewhat stagnant field. This new Tc(I) building block offered both a stable backbone through the three carbonyl ligands, as well as the possibility for chemical diversity through the labile aquo ligands. In subsequent years, a myriad of new technetium tricarbonyl complexes were synthesized and reported.[26, 38] The fact, that the corresponding "cold" rhenium analogue can usually readily be prepared, significantly facilitates the characterization of the new ^{99m}Tc compounds. Generally, the technetium concentration available through ^{99}Mo generators is too low for most analytical techniques such as mass spectrometry (MS), nuclear magnetic resonance (NMR) and/or X-ray crystallography. Hence, a HPLC-coinjection of both the ^{99m}Tc and the beforehand completely characterized Re-complex is commonly accepted as proof-of-identity. Despite the large number tricarbonyl-based ^{99m}Tc(I) complexes that have been prepared and studied, to date only one tricarbonyl based compound has made it to clinical trials in 2010. **^{99m}Tc-MIP1404** consists of a hydrophyilic tridentate chelator that coordinates the $^{99m}TcCO_3$-core attached to a short tripeptide (Figure 4). This tripeptide

is a high affinity binder for the prostate specific membrane antigen (PSMA), a receptor which is highly overexpressed on prostate cancer cells.[39] It completed phase III clinical trial testing in late 2017 with very encouraging results, suggesting that there is indeed a future for $^{99m}TcCO_3$-based radiopharmaceuticals when a "rational design" approach is followed.[40]

In summary, the rich chemistry of technetium with its many oxidations states has been extensively explored since its discovery in 1937. Its favorable properties and low cost have made it the "work-horse" of clinical imaging. While supply problems and a lack of new imaging compounds in the pipeline are looming over its spotlight, the very recent success of the tricarbonyl-based prostate imaging agent **^{99m}Tc-MIP1404** may just be the spark needed to re-ignite the field of ^{99m}Tc chemistry.

1.3 Principles in the Design of Nuclear Imaging Probes

One of the most important goals when designing an imaging probe, is to achieve a high signal-to-noise ratio between the area of interest that is to be imaged and the rest of the patient. Hence, the focus of radio-imaging research has more and more shifted towards the development of more target-specific compounds. In general, two approaches are possible: the pendent approach and the integrated approach.

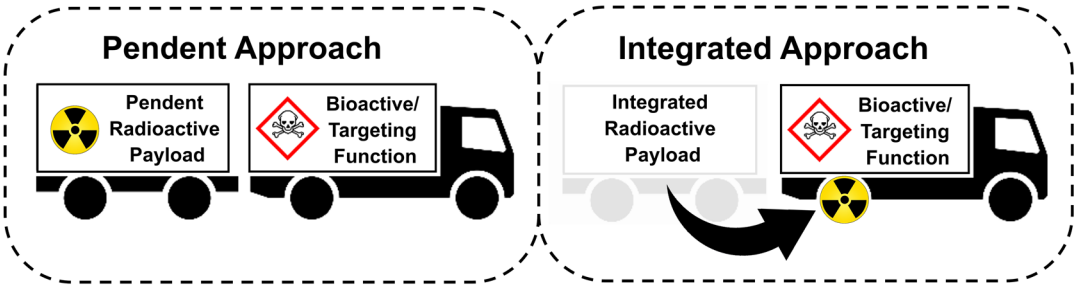

Figure 3. Schematic overview of the pendent and the integrated approach in the development of a nuclear imaging probe.

1.3.1 The Pendent Approach

The modular nature of the pendent approach makes it the synthetically more straightforward and hence also the more pursued one. The well-understood and vast

amount of different small chelators available, as well as a large array of chemical tools for coupling the chelator to the bioactive and/or targeting functions are the main drivers of this approach. Over the years, hundreds if not thousands of ^{99m}Tc-chelates were conjugated to a bioactive and/or targeting function. The results of these studies are summarized in numerous excellent reviews.[41-51] Giving a complete summary of these results would exceed the scope of this thesis. Hence an overview on targeted ^{99m}Tc-complexes that have been approved for clinical use or have recently entered clinical trials is given.

The last approval of a "pendent imaging agent" based on technetium-99m dates back to the year 2000. [^{99m}TcO]depreotide (**NeoTect®**) is a somatostatin receptor binding sequence containing a cyclic hexapeptide connected to a tetrapeptide which forms a coordination complex with a technetium(V) core by coordinating with three amide nitrogens and a cysteine-derived sulfur (Figure 4). The compound behaved as a somatostatin mimic *in vivo* and was successfully used in the differentiation of malignant and benign lung tumors. However, due to poor commercial performance, the compound was withdrawn from the market in 2010.[48, 52]

The only other clinically approved technetium-labeled targeting peptide is [^{99m}TcO]apcitide, which was approved as **AcuTec®** by the FDA in 1998. Analogous to **NeoTect®**, the technetium core is coordinated by a short peptide sequence (namely the C-terminal Gly-Gly-Cys), which is part of the native sequence of the 13 amino acid peptide apcitide (Figure 4). This compound was used for the detection and localization of deep vein thrombosis but has since also been discontinued.[52] The commercial failure of these two compounds might be one of the reasons why the field has been rather unfruitful in the last two decades. Only five ^{99m}Tc compounds have been in active clinical development since the turn of the century (Figure 4).

The elevated metabolic rate of cancer cells has the downstream effect of increased folate-dependent enzyme expression in certain types of cancer.[53] Thus, both therapeutics and diagnostic agents targeting folate receptor (FR) over-expressing cells have been widely explored in the current literature and some drugs are already used in clinics today. **^{99m}Tc-EC20** (^{99m}Tc-etarfoladite) is an effort to use FR-positive cells as an imaging target with ^{99m}Tc (Figure 4). The Tc(V)-based complex was first reported by Leamon *et al.* in 2002 and displayed promising tumor accumulation in a mouse

model.[54] The imaging agent candidate first entered human clinical trials the same year and has since completed multiple phase I & II studies. A phase III trial was suspended in 2015 for unknown reasons. However, at least two further phase II studies are currently ongoing, underscoring the continued interest in folate-mimicking nuclear imaging agents.[55]

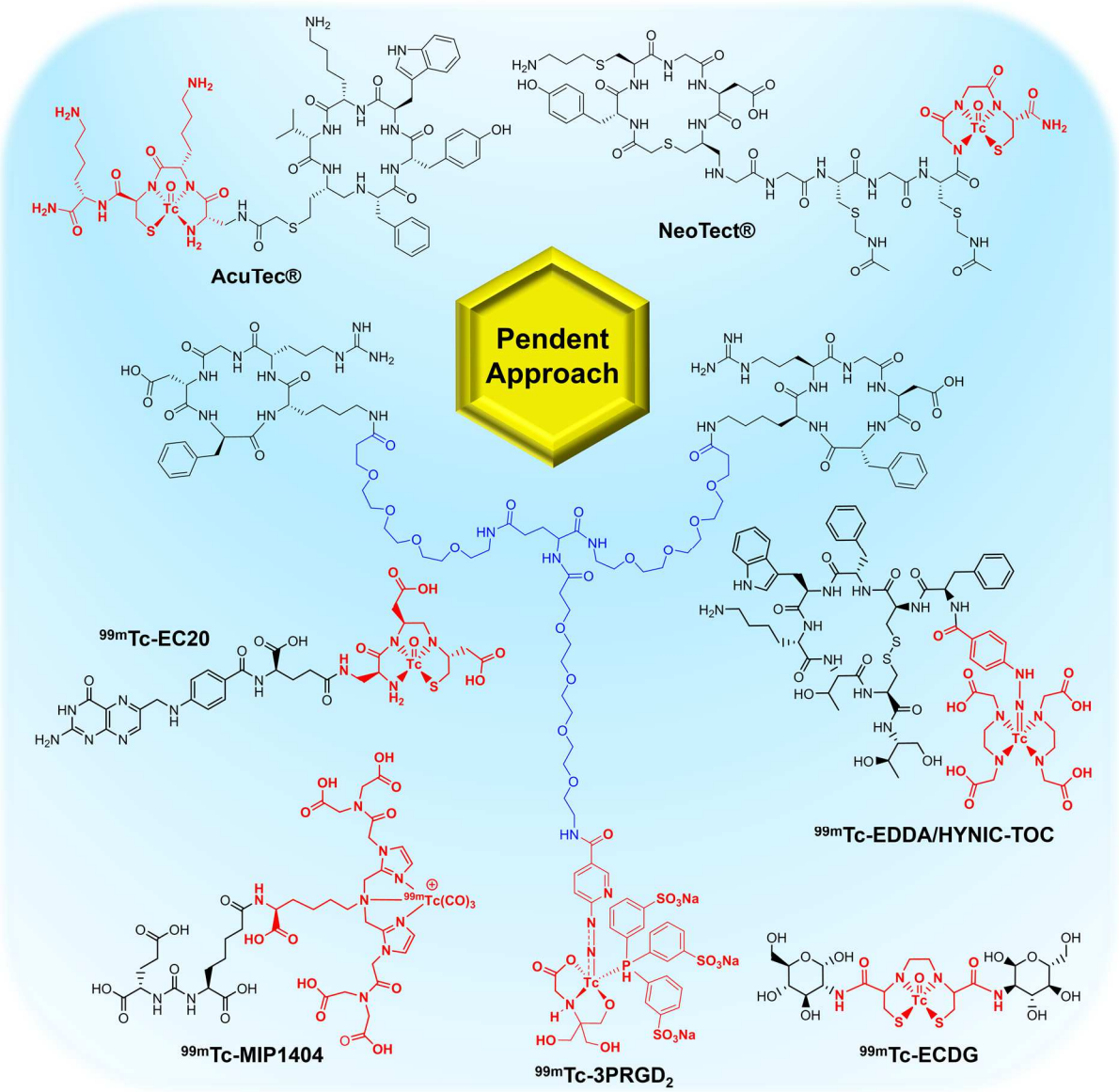

Figure 4. Overview of ^{99m}Tc-based radiotracers previously approved for clinical use or currently in clinical trials.

Another promising target in cancer targeting is integrin $\alpha_v\beta_3$. Briefly, integrins are membrane-attached receptors and are involved in many fundamental cellular

processes ranging from cell-matrix adhesion to stress response. The reason integrins are interesting for cancer imaging is the observation that certain classes of them are overexpressed on tumor cells.[56] The integrin $\alpha_v\beta_3$ is involved in tumor angiogenesis and metastasis, usually the stage where a cancer transitions from a minor malignancy to a life-threatening disease. It is therefore not surprising that significant efforts have been made to develop both the drugs to target these proteins as well as the tools to monitor the effect of the latter. Cyclic, so-called RGD (Arg-Gly-Asp) peptides have early been shown to be potent inhibitors of $\alpha_v\beta_3$ and to induce apoptosis.[57] Since $\alpha_v\beta_3$ is located on the cell surface it was hypothesized that higher binding affinity could be obtained with multimeric cyclic RGD peptides.[58] The verification of this idea led to the development of a range of multimeric RGD-based technetium imaging agents culminating in the clinical candidate **^{99m}Tc-3PRGD$_2$** (Figure 4). The separation of a cyclic RGD-peptide dimer and the metal core by a PEG_4 linker lead to significantly enhanced tumor targeting.[59] The compound has entered early phase I clinical trials for diagnosis of esophagus, breast, and lung cancer as well as for rheumatoid arthritis. In the case of lung cancer, preliminary results indicate that in patients with suspected lung lesions the imaging sensitivity with visual analysis could be drastically improved. Unfortunately, the specificity was somewhat lower.[60] More results from these early studies are expected in the next years and most likely the success or failure of **^{99m}Tc-3PRGD$_2$** will have a significant effect on the future of the field of technetium-based integrin imaging agents.[61]

In **^{99m}Tc-EDDA/HYNIC-TOC** the somatostatin mimic, octreotide, is conjugated *via* a tyrosine to the established hydrazinonicotinyl (HYNIC) linker and ligand to a ^{99m}Tc(V)-core with ethylenediaminediacetic acid (EDDA) as the co-ligand system (Figure 4). Preclinical evaluation showed that the peptide retained somatostatin receptor affinity upon technetium coordination and the compound displayed higher tumor/organ ratios than the clinically approved agent ^{111}In-DTPA.[62] Early reports of small clinical studies further demonstrate the potential of the compound.[63] Since 2016, **^{99m}Tc-EDDA/HYNIC-TOC** is in a phase II clinical trial for the diagnosis of neuroendocrine tumors.[64]

The increased metabolism of cancer cells also leads to a higher demand for energy, which can be obtained, for example, in the form of glucose. Hence, many glucose-

receptor targeting imaging agents such as the ^{18}F agent fluorodeoxyglucose (FGD) have been developed (Figure 5). Though highly successful and widely applied in clinics, the use of ^{18}F comes with several disadvantages such as its short life, long synthesis times, limited availability and high cost of the isotope. Hence the demand for a ^{99m}Tc-based glucose-mimic remains high.

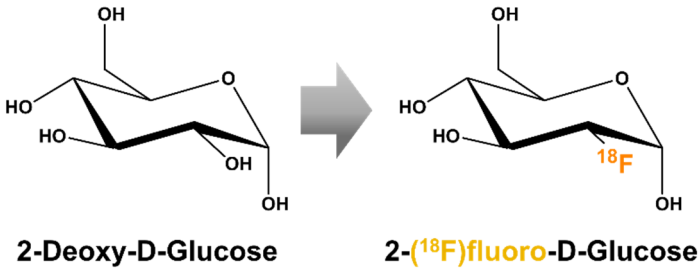

Figure 5. Chemical structures of native glucose and FGD.

^{99m}Tc-ECDG is currently the clinically most advanced of these candidates (Figure 4). The oxo-Tc(V) core is coordinated by a ethylenedicysteine moiety (EC) which in turn is functionalized with two deoxyglucose residues (DG). *In vitro* experiments showed that **^{99m}Tc-ECDG** displayed higher tumor/brain and tumor/muscle uptake ratios than FDG.[65] The compound entered clinical trials for non-small cell lung cancer in 2010 and a phase III trial was started in 2017. Additionally it is also being investigated in a further phase II study for imaging coronary artery disease.[66] A ^{99m}Tc based FGD-replacement appears close to commercial clinical use. This would be a significant contribution to the field of nuclear medicine due to the easy, widespread availability and relatively low cost of the radioisotope.

All the compounds described to this point are built around a $^{99m}Tc(V)$-core. The previously mentioned $[Tc(I)CO_3]^+$-core seems to be out of favor. Clinical candidate **^{99m}Tc-MIP1404** might be able to reverse this trend. As mentioned in the previous chapter, the structure consists of a PSMA-targeting tripeptide connected to a hydrophilic chelator and the technetium tricarbonyl core. The first clinical trial for prostate cancer imaging with this compound was started in 2010. The compound has now passed four phase I trials as well as a follow-up phase II trial.[64] A very recent report on the ongoing phase III study indicates that **^{99m}Tc-MIP1404** has a high probability of detecting PSMA-positive lesions and medical professionals could recommend treatment adjustments for 74% of the screened patients.[67]

Altogether, even though thousands of molecules have been synthesized, only a handful of them made it into human studies. This is of course partially a reflection of what is commonplace in the drug-discovery world. But it also seems that the full potential of ^{99m}Tc-chemistry has not been exploited yet, especially with regards to the $[Tc(I)CO_3]^+$-core.

1.3.2 The Integrated Approach

One can strive to design the imaging unit in such a way, that its physicochemical properties allow a targeted accumulation without further intervention. In practice, even with the vast knowledge of chemistry, drug design, pharmacology and biochemistry available today, such a *de novo* approach is of insurmountable difficulty. The next best thing to designing a completely new molecular entity is to start from something that is known. In what was coined as the "integrated approach", a known molecular entity with established biological distribution and/or activity is taken as a starting point (Figure 6). The radionuclide is then rationally introduced into the lead compound with a minimum amount of chemical alteration. A compound where the integrated approach has probably been applied with unsurpassable simplicity is the previously mentioned ^{18}F derivative of glucose FDG (Figure 5).[68, 69] Of course, the inclusion of a radio*metal* into an active structure poses a considerably more difficult challenge. The example of ferroquine (and to a lesser extent the tamoxifen analogue ferrocifen[70]) has demonstrated that it is possible to very elegantly introduce a metal into a bioactive structure without tampering with its native activity, even going as far as introducing additional mode of actions.[16] In the realm of ^{99m}Tc, only a handful of such attempts have been reported, as the synthetic obstacles towards an integrated approach are often of prohibitive difficulty.

One of the first examples for the implementation of the integrated approach was reported in 1992 by Chen and Janda. In their communication they described the synthesis of a water-stable adenosine-^{99m}Tc(V) complex (Figure 6), which displayed binding affinity to ribonuclease comparable to the bench-mark vanadate complexes.[71] These results together with the more in-depth studies with the respective Re(V)

complex indicate that the introduction of the oxometal-moiety does not have a deleterious effect on the native properties of the adenosine.[72]

Neurotransmitter receptors have long been in the spotlight as there is still a lack of appropriate technetium brain imaging agents. In 1994, Lever *et al.* described the preparation of a $^{99/99m}$Tc-complex based on the very potent muscarinic acetylcholine receptor (mAChR) inhibitor I-QNB (Figure 6). Although the technetium-99m compound did accumulate in the brain, the *in vitro* binding affinity to mAChR was found to be too low to warrant further investigations.[73] Nevertheless, this work demonstrated that technetium-analogues of neuroreceptor ligands could be prepared in an integrated way. In another example, Brandau and co-workers synthesized ^{99m}Tc compounds inspired by the potent nonspecific antagonist spiperone in 1995 (Figure 6). Unfortunately, their complexes showed poor brain uptake in *in vivo* experiments. However, the authors did observe significant uptake in heart, kidney, and lung tissues, which also contain high concentrations of dopamine receptors. This indicates that while binding the appropriate target, their complexes may just not have been able to cross the blood-brain-barrier (BBB).[74]

A synthetically very creative approach was pursued by the group of Katzenellenbogen. Systematically, they prepared a series of estradiol mimics containing an oxorhenium species (representative example shown in Figure 6).[75-77] The initial stability issues could be overcome with more refined compounds, but all of them showed only poor binding affinities for the estrogen receptors and were rather lipophilic in nature. Although it is an elegant execution of the integrated approach, the geometric and electronic differences between the native ligand and the oxorhenium complex were probably too stark in this case.

In recent years even fewer studies on the integrated approach have been reported. It is likely that lack of success as in the previously mentioned examples resulted in a shift of focus towards the synthetically more feasible pendent approach. Though in 2006, Caiyun *et al.* described a further attempt of integrating oxometal(V) species of rhenium and technetium-99m into a σ-receptor ligand framework (Figure 6).[78] *In vivo* biodistribution studies showed moderate tumor uptake suggesting that further modifications to the chelate-structure could generate higher affinity tumor imaging agents.

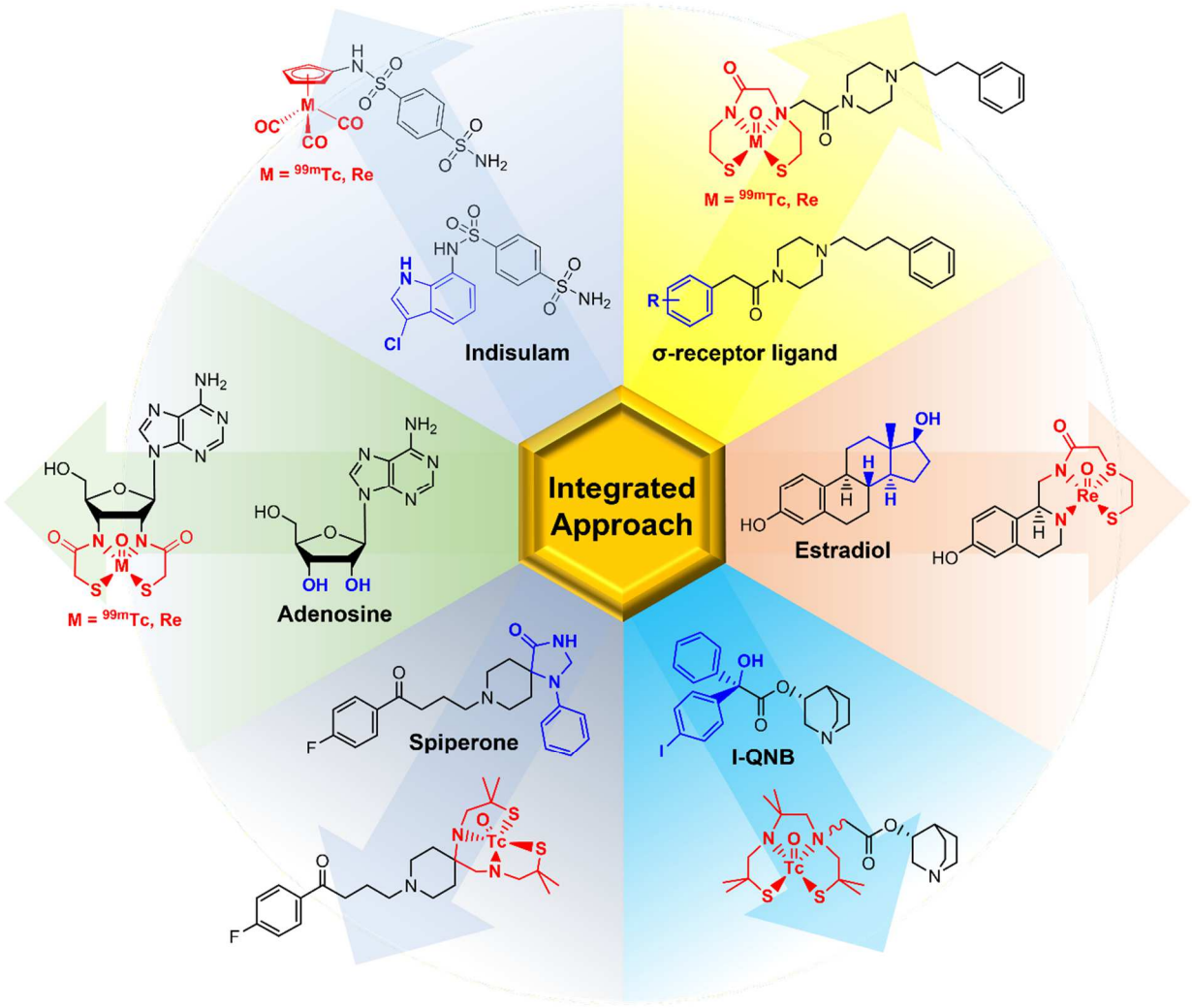

Figure 6. Overview of selected applications using the integrated approach.

Remarkably, as with the pendent approach, most hitherto published examples were based on the oxometal(V) synthon of rhenium and technetium. Recently, our group has turned its attention to Re(I) and ^{99m}Tc(I) complexes of the type [(Cp-R)M(CO)$_3$] and we reported on their synthesis as selective human carbonic anhydrase (CA) inhibitors.[79] The structure of the complexes is very similar to the structure of Indisulam (E7070), one of the most potent sulfonamide CA inhibitors ever reported.[80] Both the rhenium and ^{99m}Tc complexes could be readily obtained and the binding affinity of one rhenium complex was found to be higher than the current standard.[79]

Mimicking the structure of a compound with known bioactivity opens up the possibility for a theranostic system with rhenium and technetium-99m. In this case, the ^{99m}Tc complex is the diagnostic tool. Additionally, the rhenium complex, which can be

obtained in macroscopic quantities, is used as the therapeutic entity with a homologous structure to the radiotracer. Effectively both diagnosis and therapy can then be achieved with the same ligand framework. Since the integrated approach has not been explored very extensively yet it is not surprising that a theranostic system with Re and ^{99m}Tc has also not been investigated yet.

1.3.3 Cyclopentadiene and ^{99m}Tc, a Perfect Match?

It is undeniable that the implementation of the integrated approach is a synthetically daunting task. This is also reflected by the very limited examples that are found in the current literature compared to the myriad of examples on the pendent approach. Nevertheless, the elegance of the approach remains alluring. The small cyclopentadiene ligand as the chelating unit has early-on caught the eye of several researchers, including the Alberto group. Cyclopentadiene (Cp) is most famously known for its use in the synthesis of ferrocene, one of the most iconic compounds of organometallic chemistry.[81, 82] Since then, the field of Cp-chemistry has highly diversified with complexes with nearly every element having been reported. Scifinder lists almost 4000 publications with the key-word “cyclopentadiene” for the last five years, indicating that it is still a highly relevant compound today. Already in 1962, the first ^{99}Tc-Cp complex was prepared through neutron bombardment of the analogous molybdenum compound.[83] But it took another 30 years until the corresponding ^{99m}Tc could be synthesized by Wenzel *et al.* in 1992.[84] In 1998, Katzenellenbogen and coworkers reported the “double ligand transfer” (DLT) reaction for {(η^5-C_5H_5)^{99m}Tc and {(η^5-C_5H_5)Re}. The previously mentioned octreotide and estradiol were successfully conjugated to a ^{99m}Tc moiety via a CP-ligand along the DLT approach.[85, 86] However, the scope of the DLT reaction is limited by the accessibility of the corresponding ferrocene precursor and the high temperatures required to transfer the functionalized Cp and the CO ligands to ^{99m}Tc.

All these approaches have the sensitivity of the Cp-precursors and a limitation in biomolecules in common. Nonetheless, the Cp-ligand remains an interesting ligand due to its small size, low-molecular weight and innocence towards the metal center.

Additionally, the complexes formed with the *fac*-$[M(CO)_3]^+$ core are very stable and neutral in charge. In practice, two major problems remain to be solved:

1.) The low water solubility of simple Cp-ligands prevents its use in the synthesis of radiopharmaceuticals with ^{99m}Tc, as these syntheses must be carried out in aqueous solutions.
2.) The number of synthetic routes available to Cp-ligands to either be conjugated or integrated to/into a bioactive and/or targeting function is very limited.

In the last years, the Alberto group has worked towards addressing these issues of Cp-ligands. The first milestone was the development of a convenient synthesis of mono-functional complexes of the type $[(Cp\text{-}R)^{99m}Tc(CO)_3]$ in one step from functionalized "Thiele's acid" (the Diels-Alder dimer of HCp-COOH) and $[^{99m}Tc(OH_2)_3(CO)_3]^+$ (a direct "one-pot" reaction from $[^{99m}TcO_4]^-$ is also possible).[87, 88] In further work, a bifunctional, water-soluble and stable sodium salt of the form $C_5H_3(COOR)_2$ was prepared.[89]

2. Objectives

The goal of this PhD thesis is the development of a synthetically versatile Cp-ligand synthesis and its application to both pendent and integrated approaches (Figure 7).

The Cp-ligands should be easy to synthesize in useful quantities as well as air-, water- and temperature-stable. They should possess multiple sites for functionalization and ideally their physicochemical properties can be manipulated through the insertion/modification of functional groups. Finally, their respective Re and ^{99m}Tc complexes should be synthetically accessible. In the case of ^{99m}Tc the synthesis of the Cp-complexes has to proceed at tracer-level concentrations of metal (nM), in water and within short reaction times.

In a second step, the developed Cp-ligands and their complexes are to be implemented into a model pendent approach by conjugating a biological targeting unit to the system.

The final goal is to use the versatility of the Cp-platform to prepare a $CpM(CO)_3$ compound that can be integrated into a known bioactive molecule in a way that the rhenium complex could be used for therapy and the technetium for diagnosis.

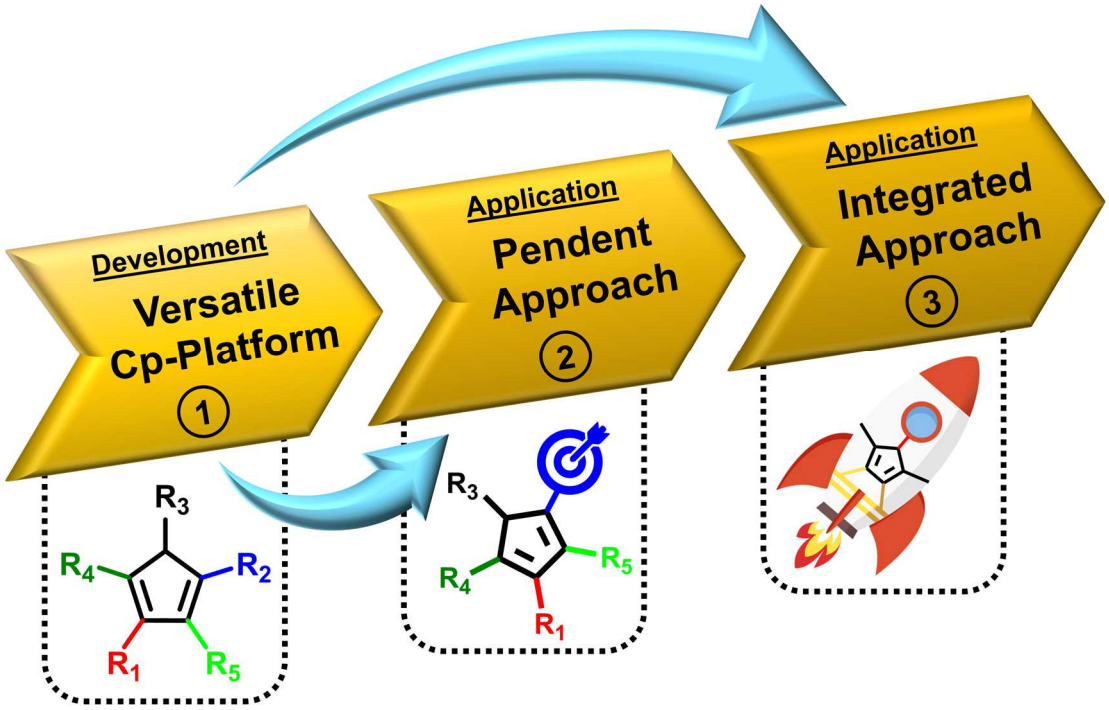

Figure 7. Overview of main objectives of this thesis.

3. Results & Discussion

Part A: Multifunctional Cp-Complexes for the Development of Pendent and Integrated Theranostic Agents.

3.1 Development of a Versatile Cp-Ligand Platform

3.1.1 Preface

In 2008, the Alberto group reported the synthesis of monofunctional Cp-complexes of both rhenium and technetium-99m (Scheme 1).[87]

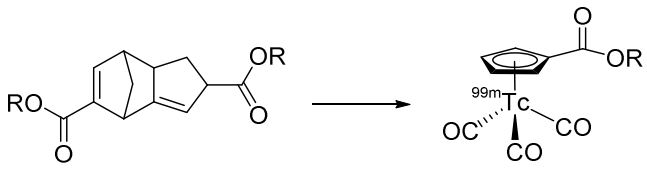

Scheme 1. General reaction scheme towards monofunctional $Cp^{99m}Tc(CO)_3$ complexes via a retro-Diels-Alder reaction.

In a follow-on project we prepared a difunctional Cp with two ester groups in either 1,2- or 1,3-position from sodium cyclopentadienide. The ligands **S1a** and **S1b** could be obtained in gram quantities as an inseparable mixture in a 9:1 ratio. The respective Re and ^{99m}Tc complexes could be synthesized in both water and organic solvents and the ester groups could readily be cleaved off under basic conditions.[89]

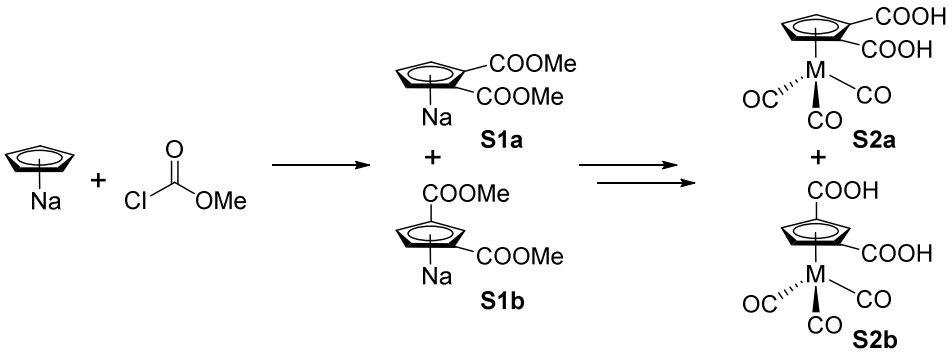

Scheme 2. Synthetic route towards 1,2- and 1,3-bifunctional CpRe and $Cp^{99m}Tc$-complexes (**S2a**, **S2b**)

The subsequent functionalization of either the ligand or the metal complexes turned out more difficult than expected. Hydrolysis of the free ligands **S1a** and **S1b**, was not

possible under basic conditions. Furthermore, attempts at direct amide bond formation did not yield any detectable product.

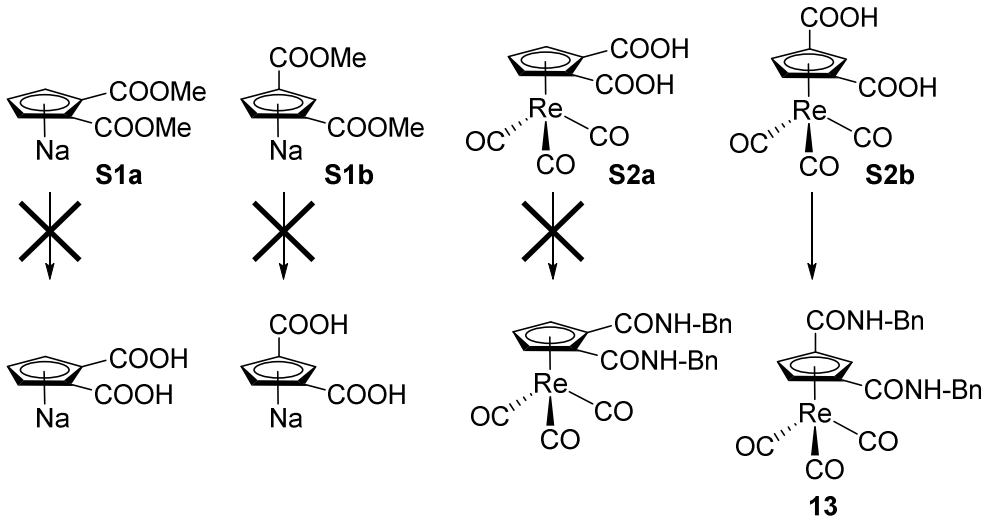

Scheme 3. Summary of synthesis attempts towards functionalization of 1,2- and 1,3-substituted Cp-ligands and complexes.

After complexation with rhenium, the 1,2- and 1,3-isomers of the complex were isolated and hydrolyzed. However, the functionalization of the latter with a model amine (benzylamine) only led to product formation for the 1,3-isomer (Scheme 3, **13**). This complex could be characterized by MS, ^{1}H-NMR and an X-ray crystallography (unrefined, Figure 8).

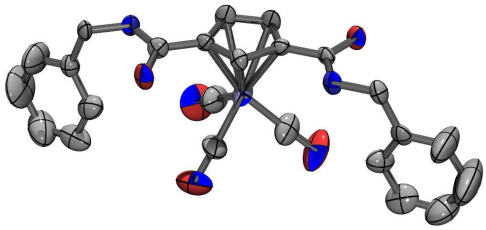

Figure 8. Unrefined X-ray structure of **13**

However, since the functionalization only worked with the rhenium complex and also only with the minor 1,3-isomer (**S2b**), it became clear that a different Cp-ligand system was needed to further pursue the goal of multifunctional compounds.

An unconventional synthetic route to both multifunctional Cp-ligands and complexes was reported by Kuninobu *et al.* in 2008. They found that dirhenium decacarbonyl could catalyze the formation of substituted Cp's from *α,β*-unsaturated ketimines and *α,β*-

unsaturated carbonyl compounds (Scheme 4). Addition of equimolar amounts of the rhenium catalyst resulted in the direct formation of the respective $CpRe(CO)_3$ complex. It was also shown that the reaction was relatively substrate tolerant and different substituents could be introduced into the Cp-system. [90]

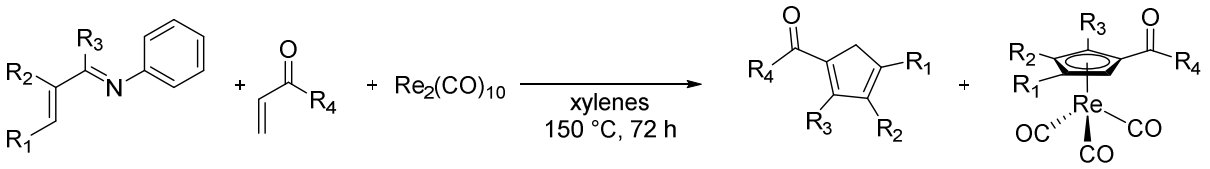

Scheme 4. General synthetic route to substituted Cp-ligands and Re-complexes reported by Kuninobu *et al.*

Based on this information, **16** was designed as a model compound to expand the Kuninobu-route to poly-substituted Cp-ligands that could be functionalized further (Scheme 5, route A).

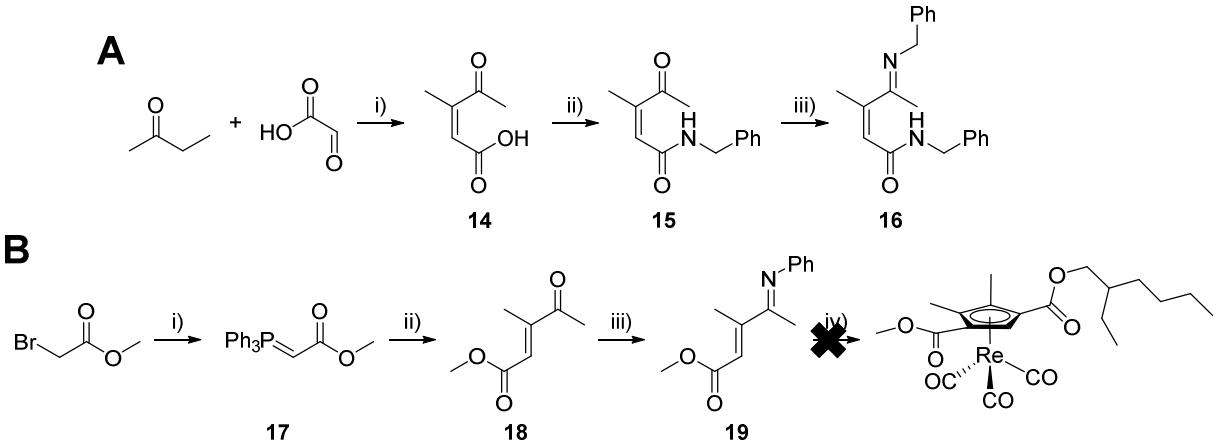

Scheme 5. Reaction conditions: **A** i) conc. H_3PO_4, 85 °C, overnight, 32 %. ii) benzylamine, HBTU, DIPEA, DMF, RT, 4h, 28 %. iii) benzylamine, toluene, 170 °C, 16 h, 41 %. **B** i) PPh_3, dry toluene, RT, 16 h, 91%. ii) DCM, $NaHCO_3$ (10%), RT, 30 min, 77%. iii) 2,3-butanedione, DCM, RT, 24 h, 55%. iv) aniline, toluene, 175 °C, 16 h, 62%.

Starting from commercially available starting materials the first step was an aldol condensation according to a literature procedure (**14**).[91] In the next step the free carboxylic acid (which was found to hinder the imine formation in the following step) was "protected" through an amide bond formation with benzylamine forming **15**. Finally, the imine was formed under Dean-Stark conditions yielding compound **16** as characterized by ^{1}H-NMR.

Unfortunately, ^{1}H-NMR-NOE experiments showed that the compound was present exclusively as the *cis*-isomer and not the required *trans*-isomer (Figure 9).

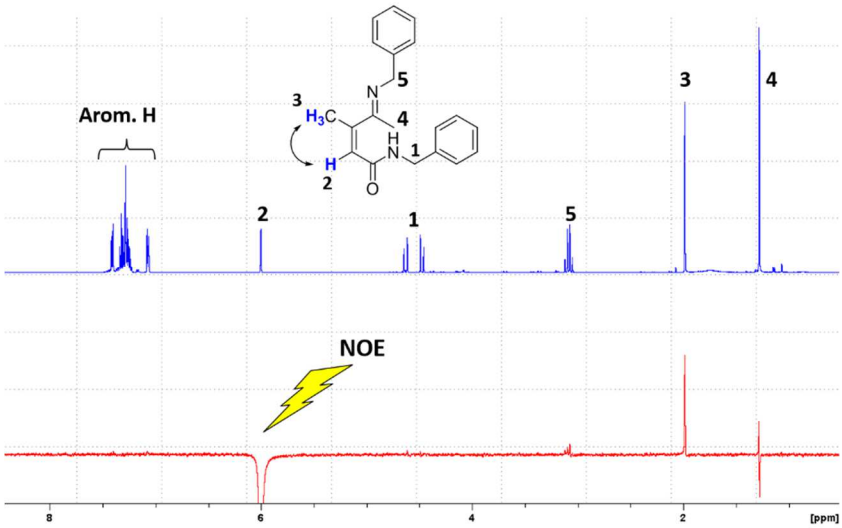

Figure 9. ^{1}H-NMR-NOE spectra showing an NOE between the *cis*-lying proton (**2**) and methyl group (**3**), which would not be observable in the *trans*-isomer.

An alternative synthetic route was hence devised (Scheme 5, route B). Compounds **17** and **18** could be prepared according to literature procedures.[92, 93] The imine **19** could then be obtained using the same Dean-Stark conditions as for **16**. Unfortunately reacting **19** under the reported conditions to form the corresponding rhenium complex was not successful.

Another interesting route to poly-substituted Cp-ligands was published very recently by Ichitsuka *et al.* They reported a nickel-mediated [3+2] cycloaddition of 2-trifluoromethyl-1-alkenes with alkynes yielding multifunctional Cp's containing a fluorine atom.[94] Due to the relative novelty of the publication, a reproduction of a sample reaction was first attempted (Scheme 6). Following the literature procedure, product **20** could indeed be isolated and characterized by ^{1}H-NMR.

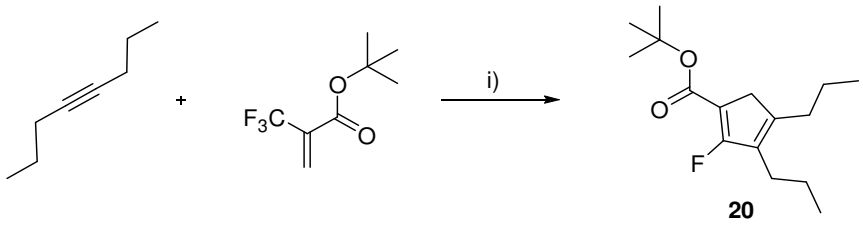

Scheme 6. Reaction conditions: [Ni(cod)$_2$], PCy$_3$, toluene, 23 °C, 48 h.

Multiple attempts to expand the synthesis with dimethyl acetylenedicarboxylate as the alkyne yielded no desired product. It is possible that the proximity of the ester functions to the alkyne altered its electronical properties in a detrimental way. Introducing an alkyl chain between the alkyne and the ester functions could potentially solve this problem. Unfortunately, the synthesis suffers a number of other draw-backs. Firstly, the nickel cyclooctadiene precursor is highly air and temperature sensitive and hence, reactions have to be carried out in a glovebox. Also, the nickel compound is expensive (177 CHF for 2 g from Sigma-Aldrich/Merck) and used in stoichiometric amounts in these reactions, making them hard to scale up.

Finally, both mentioned approaches were abandoned in favor of a third one. Building upon work reported by Hatanaka *et al.*[95] the following manuscript was put together and submitted for publication.

3.1.2 Manuscript

Multi-functional Cyclopentadiene as a Scaffold for Combinatorial Bioorganometallics in $[(\eta^5\text{-}C_5H_2R_1R_2R_3)M(CO)_3]$ (M = Re, ^{99m}Tc) Piano-stool Type Complexes

Angelo Frei,[a] Bernhard Spingler[a] and Roger Alberto[a]*

[a] Department of Chemistry, University of Zürich, Winterthurerstr. 190, CH-8057 Zürich Switzerland

Introduction

The combination of organometallic complexes with biologically active, organic molecules or fragments has become a strongly researched (sub)field in medicinal inorganic chemistry. Bioorganometallic complexes benefit from a series of properties different from typical coordination compounds. They can form integrated structures in pharmaceutically active lead structures such as the tamoxifen/ferrocifen couple[70], exert cytotoxicity through metal-mediated interactions with proteins or nucleic acids as in the case of the $[(\eta^6\text{-arene})Ru]^{2+}$ fragment[96] or form *de novo* parts in existing inhibitors as in bioorganometallic kinases for instance.[97] Ferrocene (Fc) probably represents the main fragment in this field and the cyclopentadiene (Cp) ligand plays an important role in all Fc-based bioorganometallic concepts. The majority of Cp-based bioorganometallic complexes comprises one additional functionality, a pendent targeting moiety, a cytotoxic or otherwise biologically active agent. Cp-ligands are not only found in ferrocene but also in Re/^{99m}Tc piano-stool type complexes. We reported recently two examples in which such Re/^{99m}Tc complexes were conjugated to carbonic anhydrase inhibitors or cytotoxic doxorubicin.[79, 98] Since biological activities of group 7 piano-stool complexes are rather overall structure- than metal-based, a combination of rhenium and ^{99m}Tc complexes is a complementary strategy in theranostics; the rhenium complex for therapy and its ^{99m}Tc homologue for imaging. This combination is interesting since ^{99m}Tc is still core in Single Photon Emission Tomography (SPECT)[42,

[99-101] due to its half-life ($t_{1/2}$ = 6.02 h), decay characteristics and, of growing importance, its price.[29, 35, 102, 103] Since 2001 only a limited number of new ^{99m}Tc imaging agents have been introduced into clinical routine. This mirrors the challenges encountered when aiming at introducing a well-defined transition metal complex into a targeting molecule in quantitative yields and in one step.[104-106] The preparation of *fac*-$[^{99m}Tc(OH_2)_3(CO)_3]^+$ was a step in this direction and a wide variety of complexes based on the fac-$[^{99m}Tc(CO)_3]^+$ core have been explored since.[36, 37, 79, 107, 108] Recently, a PSMA targeting biovector made it into phase III clinical trials.[109-113] The general concept of targeted radiotracers is the conjugation of a receptor binding molecule with a ligand for coordination to the respective metal center or complex fragment, also referred to as the bifunctional ligand approach.

Current pharmaceutical research aims at combining multiple modalities such as targeting and cytotoxicity, in one single molecule. However, this approach has not yet found the consideration it deserves in bioorganometallic chemistry, probably due to the fact that the modalities should typically be conjugated to one single ligand. This concept is further hampered by the fact that a multi-modality ^{99m}Tc complex must be synthesized in one single step from $[^{99m}TcO_4]^-$ and in water.

Cp-ligands represent a scaffold to which multiple functionalities can be bound according to elaborate organic synthetic strategies. In addition, Cp is small, has a low molecular weight and is innocent. After coordination to the *fac*-$[M(CO)_3]^+$ core, the complexes are highly inert and of zero charge. Our group reported a one-pot synthesis of singly functionalized $\{(\eta^5\text{-}C_5H_5)^{99m}Tc\}$ complexes in water under moderate heating.[114, 115] By derivatizing di-cyclopentadiene “Thiele’s acid” through amid bond formation, chemically stable and functionalized Cp-precursors and complexes of the type $[(\eta^5\text{-}C_5H_4R)^{99m}Tc(CO)_3]$ became accessible.[79, 87, 116] The bifunctional ligand approach, with or without Cp, does not immediately comprise the option of combining multiple, different or equal, targeting vectors. Multimeric molecular imaging agents would offer many new opportunities such as targeting of different sites, enhancing binding affinities and/or addition of a cytotoxic payload. Only a few multimeric molecular ^{99m}Tc imaging agents have been reported thus far, mainly by Liu *et al.* on integrin $\alpha_v\beta_3$ targeting multimeric cyclic-RGD peptide oligomers.[117, 118] For Cp, all

approaches described above are synthetically incompatible with multi-functionalization as required for multimeric targeting agents.

We reported recently the synthesis of water soluble Re/^{99m}Tc complexes, comprising a Cp-ligand for coordination to the $\{^{99m}Tc(CO)_3\}^+$ core and two carboxylato groups in 1,2-position for potential conjugation to two biomolecules.[89]

In this study, we extend the flexibility of the multi-functional Cp-approach to a $C_5H_3R_1R_2R_3$-type scaffold, which can be mono- (Figure 10A) or homo (Figure 10B) and hetero (Figure 10B) di-functionalized with respect to targeting molecules or other biovectors. The choice of biovectors or molecular functionalities attached to the central Cp-core is highly flexible which allows for the discovery of new imaging compounds. The ligands as such do not undergo Diels-Alder dimerization and are water and air-stable at room temperature and up to 220 °C. Mono-, homo- and hetero-functionalization of the ligand was demonstrated with model vectors on both the free ligand and the "cold" rhenium complexes. The corresponding ^{99m}Tc complexes could be prepared in a one-pot reaction from $[^{99m}TcO_4]^-$ and in high radiochemical yields. Altogether we present a ligand platform that allows for the synthesis of tetra-functional Re/^{99m}Tc complexes. Combinatorial variation of all pendent groups will lead to a wide variety of structurally different but functionally identical matched-pair complexes.

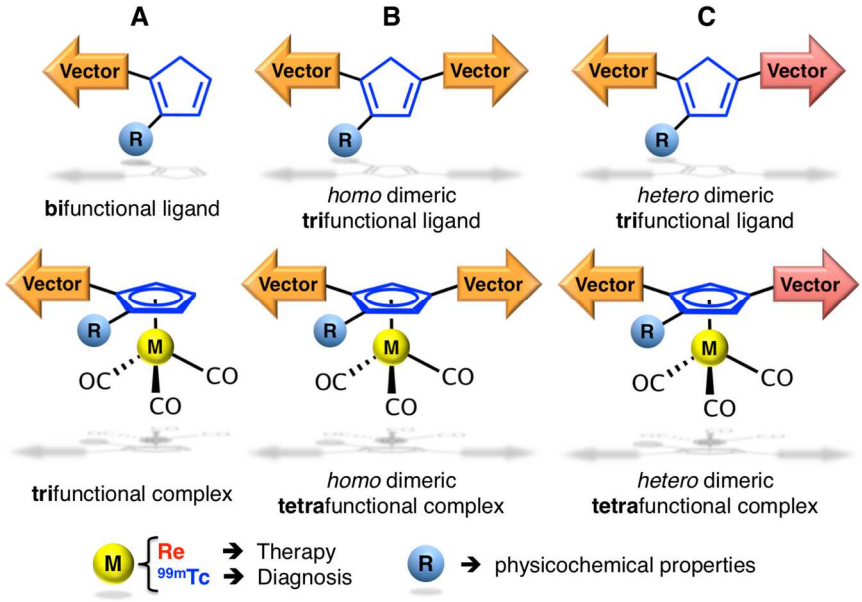

Figure 10. Overview of the different poly-modalities accessible with the new multifunctional Cp's.

Results and Discussion

Design of Cp-Ligands.

The syntheses of the multi-functional Cp-ligands in this study as shown in Figure 10 were based on a procedure by Hatanaka *et al.*[95]. A variety of triphenyl-phosphonium salts with different substituents R_1 react with α-bromo-ketones under mild conditions to form triply substituted Cp's in good yields. The most general concept towards such multi-functionalized Cp's is shown in Scheme 7 (top). The carboxylate group directly attached to the Cp-ring (R_4, green in Scheme 7) and the terminal carboxylate in R_2 (blue) allow for later conjugation of two equal or different biological functions V_1 and V_2. This synthetic approach thus enables a versatile alteration of three functionalities; R_1 for guiding the chemical properties and the two carboxylate groups for conjugation of bioactive functionalities (Scheme 7, A and B). The original literature also highlights the possibility to vary R_2 and to introduce further functionalities at R_3, while modifications of R_4 and R_5 are also conceivable.

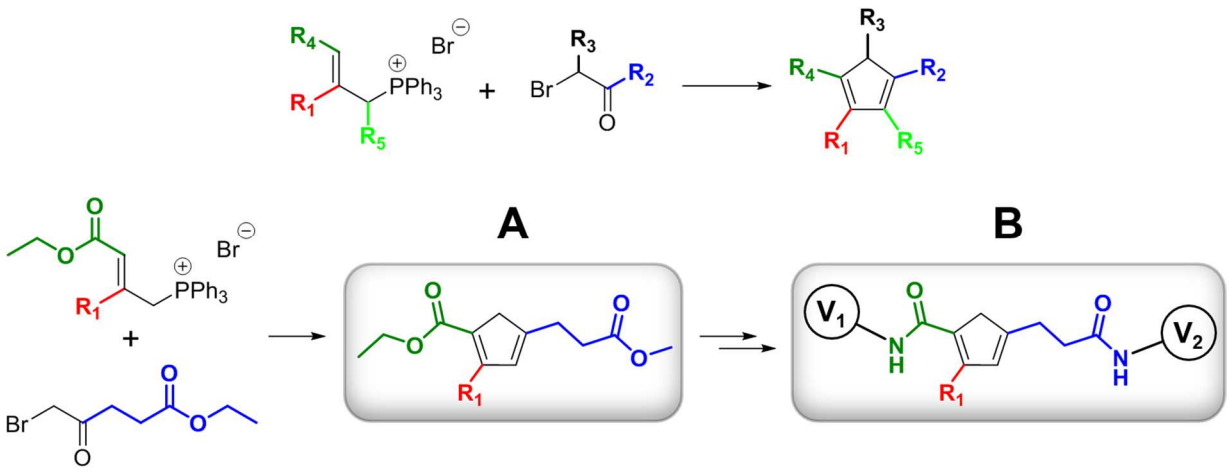

Scheme 7. General synthesis of multifunctional Cp-ligands (top) and the synthetic strategy pursued in this study (bottom): A) variation of R_1 to modify the chemical properties of the Cp. B) variation of the conjugated vectors (V_1, V_2) to modify biological properties of the Cp.

We did not alter all these positions on the central cyclopentadiene scaffold but choose ethyl 5-bromo-4-oxopentanoate (**0.1** Scheme 8) as the standard α-bromo-ketone for the bi-functionalization, keeping R_2 thereby constant with the option of conjugating a biovector V_2 to this position. The $(CH_2)_2$-spacer in R_2 was introduced in this building block design to reduce interference of the terminal ester group with the reactivity of the

α-ketone. Furthermore, this spacer suppresses the undesired rearrangement of the Cp-double bond in the final ligand, as previously observed in our group in mono-functional Cp's with one CH_2 group between Cp and the ester group. The ester group on the phosphonium building block (R_4, green in Scheme 7) was also kept constant but will enable the conjugation of a 2nd bioactive moiety V_1 to the Cp-scaffold after cyclization. In its essence, the approach towards multi-functionalized Cp derivatives focuses on the building block A in Scheme 7, prepared from ethyl 5-bromo-4-oxopentanoate and phosphonium salts with a methyl (**1a**), a phenyl (**4a**) and a methoxy (**6a**) group as R_1, red in Scheme 7 to show that both electron donating and withdrawing groups can equally be bound to the Cp-ring. Introduction of V_1 and V_2 will lead to the trifunctional Cp derivatives as shown with B in Scheme 7. We suggest that Cp derivatives of type B can equally be applied to other metal centers such as iron, to make corresponding ferrocene derivatives.

Synthesis and Characterization.

The ligands **1a**, **4a** and **6a** represent the cores of the later trifunctional Cp-systems. These precursors were synthesized following the reported procedure with minor changes to improve yields and isolations (see Supplementary Information for details).[95] Notably, the radical brominations of **1.1**, **4.1**, and **6.1** (Scheme 8) to yield **1.2**, **4.2** and **6.2** were carried out under microwave conditions in less than 15 min (30s at 85 °C for **6.1**). The harmful solvent CCl_4 could be replaced by methylacetate without loss of performance. Subsequent reactions with triphenyl-phosphine and cyclizations with 5-bromo-4-oxopentanoate lead straight to the Cp-ligands **1a**, **4a** and **6a** in moderate to good yields and in up to gram quantities after purification by silica column chromatography.

The rhenium complexes **1b**, **4b** and **6b** with all three Cp-derivatives were obtained by refluxing the respective ligand **1a**, **4a** and **6a** with Re_2CO_{10} for multiple days in *o*-xylene (Scheme 9). Under microwave conditions, the reaction solutions were heated to 220 °C and the reaction time reduced to 15 min as described in the supplementary information without loss of yields. For **1b** quantitative conversion was observed and no purification was necessary. Complexes **4b** and **6b** were purified by column chromatography on silica. Ester hydrolysis to **2b**, **5b** and **7b** was achieved under basic conditions by either

refluxing overnight under basic conditions or by microwave heating at 120 °C for 15 min.

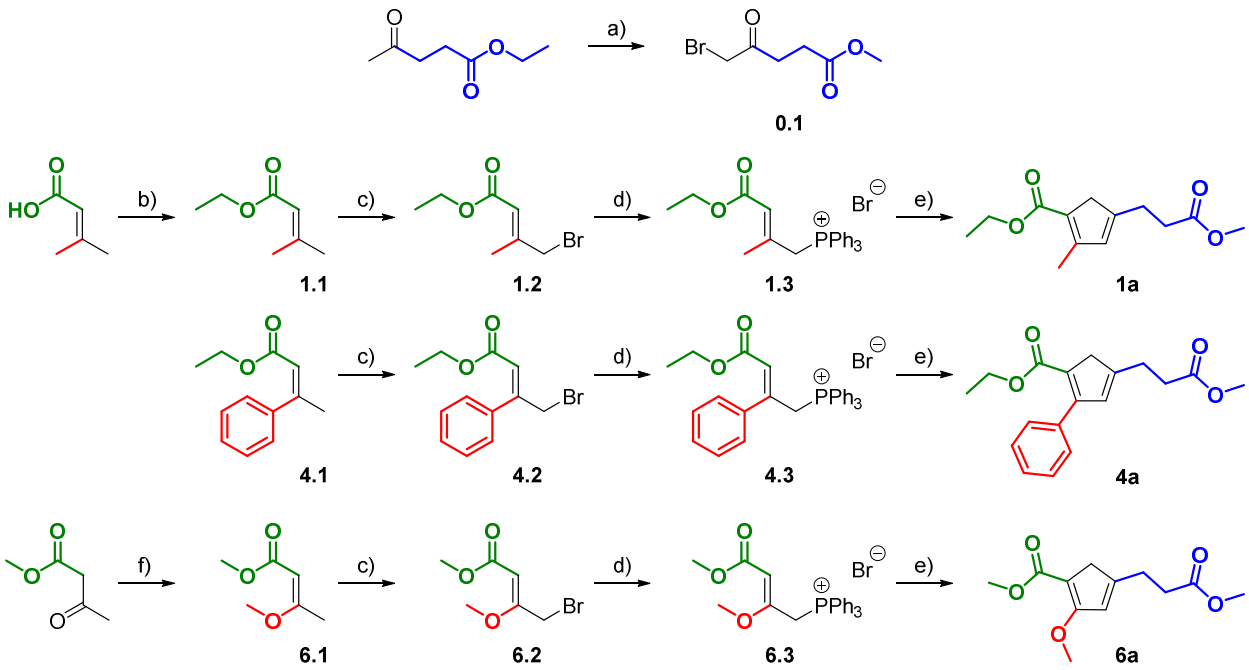

Scheme 8. Synthetic route to the Cp-ligands **1a**, **4a**, **6a**. Reaction conditions: a) Br_2, MeOH, 0 °C, 24 h, 23%. b) cat. H_2SO_4, EtOH, reflux, overnight, 87%. c) NBS, cat. AIBN, MeOAc, MW; 110 °C, 15 min (**1.2**, 83%); 110 °C 12 min (**4.2**, 97%); 85 °C, 30 s (**6.2**, 73%). d) PPh_3, dry toluene, 25 °C, 24 h (**1.3**, 84%; **4.3**, 65%; **6.3**, 54%). e) **0.1**, DCM/sat. $NaHCO_3$, 25 °C, 48 h (**1a**, 66%; **4a**, 27%; **6a**, 23%). f) Trimethoxymethane, H_2SO_4, 25 °C, 25 h, 82%.

Bis-homo functionalization of rhenium complexes: Complexes **2b**, **5b** and **7b** are the precursors for introducing two identical functionalities, either for targeting of for any other interaction with biological modalities. To demonstrate these possibilities and for preparing rhenium model complexes for later comparison with the ^{99m}Tc homologues, two molecules of benzyl-amine were coupled to the two carboxylate groups in **2a**. Standard peptide coupling was achieved with the reagents Hydroxybenzotriazole (HOBt) and 1-Ethyl-3-(3-dimethyl-aminopropyl)carbodiimide (EDC) at room temperature (Scheme 9). The products were then purified by preparative HPLC and fully characterized by NMR, HPLC and high resolution ESI-MS. For complexes **2b** and **3b** single crystals suitable for X-ray diffraction were obtained by slow evaporation of methanolic solutions of the compounds. ORTEP presentations for these two complexes are given in Figure 11.

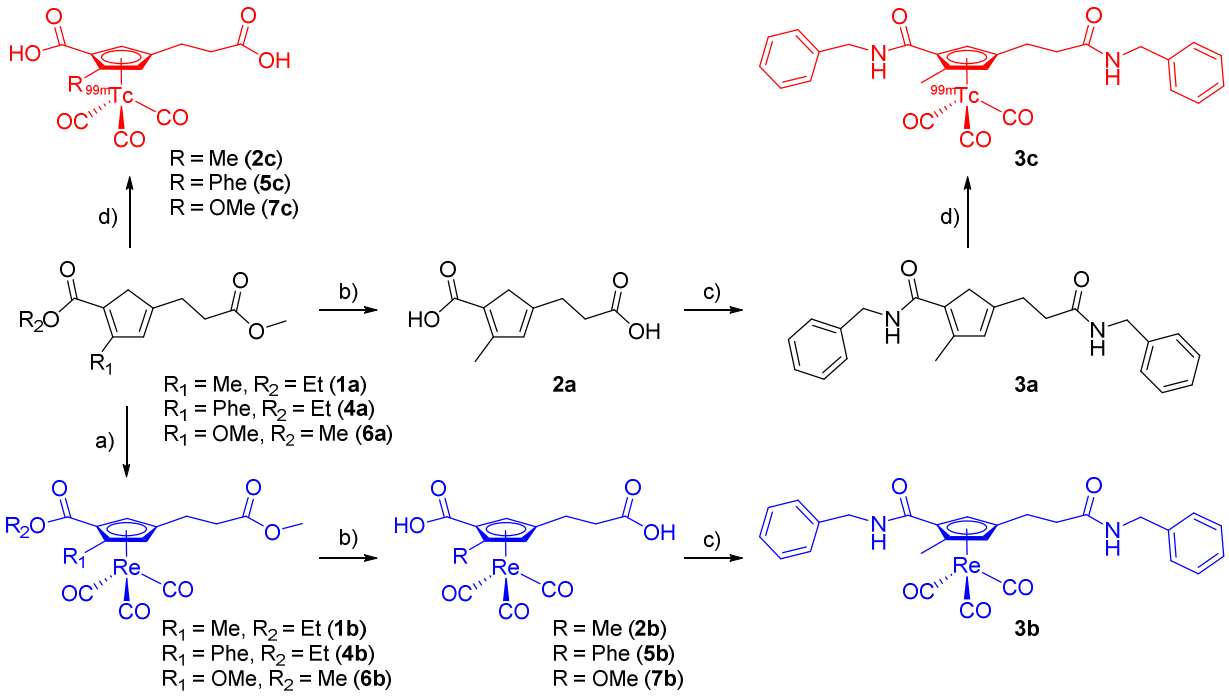

Scheme 9. Synthetic route towards homo-functionalized Re and ^{99m}Tc complexes. Reaction conditions: a) Re_2CO_{10}, *o*-Xylene, MW, 220 °C, 15 min (**1b**, 76%; **4b**, 83%; **6b**, 44%). b) NaOH, MeOH, MW, 120 °C, 15 min (**2b**, 68%; **5b**, 92%; **7b**, 48%). c) benzylamine, HOBt, EDC, DMF, 25 °C, 24 h, (**3a**, 38%; **3b,** 16%) d) $[TcO_4]^-$, sodium boranocarbonate, sodium tartrate, sodium tetraborate, H_2O, MW, 120 °C, 30 min.

Bis-hetero functionalization of the Cp-ligand 1a: To assess the full potential of this approach and to open a scope towards two different functions V_1 and V_2, thus bis-hetero functionalized Cp-ligands and complexes, the individual carboxylato groups must be conjugated stepwise to biovectors. We exemplify this strategy with the Cp ligand **1a**, which comprises the methyl group at the R_1 position. The first mono-functionalization was achieved by hydrolysis of **1a** with slightly less than one equivalent of NaOH, yielding exclusively **8a** (Scheme 10). One could expect a statistical distribution of hydrolysis at both ester functions but the one at the R_2 position is obviously more susceptible, leaving R_4 untouched. Subsequent amide bond formation under the previously mentioned conditions gave **9a** in good yields. By further and careful tuning of the reaction conditions, **9a** could selectively be hydrolyzed to **10a**. Reaction times longer than 5 min and pressures over 5 bar usually resulted in decomposition of the compound. For subsequent bis-hetero-functionalization, we chose O-^{t}butyl-L-phenylalanine to demonstrate that our approach is substrate tolerant

with the option of extension to e.g. peptides. Along a standard peptide bond formation strategy (see experimental section), **10a** was converted into **11a**, containing two different functionalities on the Cp-ring.

Bis-hetero functionalization of the rhenium complex 2b: Unlike the Cp-ligand **1a** itself, selective mono-hydrolysis of **1b** was not possible. Addition of one equivalent of NaOH and subsequent heating gave a statistical mixture of ester-hydrolyzed products. Thus, to accomplish the rhenium complex **8b**, a direct reaction between the mono-acid ligand **8a** and Re_2CO_{10} in DMF under microwave irradiation was performed. The obtained crude mixture was directly reacted under standard peptide coupling conditions to give **9b** after purification by preparative HPLC (Scheme 10). Complex **9b** was then easily further hydrolyzed and functionalized with O-^{t}butyl-L-phenylalanine, yielding **11b** after preparative HPLC in 26% yield. The *tert*-butyl protecting group of **11b** could be cleaved by treatment with TFA in DCM at 80 °C, yielding **12b** as a model for the later ^{99m}Tc complexes. The chiral center in the attached amino acid together with the chiral planarity of the asymmetric Cp-ligand leads to the formation of two diastereomers (see Figure 69). This was confirmed by the observation of two identical sets of NMR signals in both ^{1}H and ^{13}C NMR spectra of **11b** and **12b** (Figure 67-68). All compounds were fully characterized by NMR, HPLC and high resolution ESI-MS.

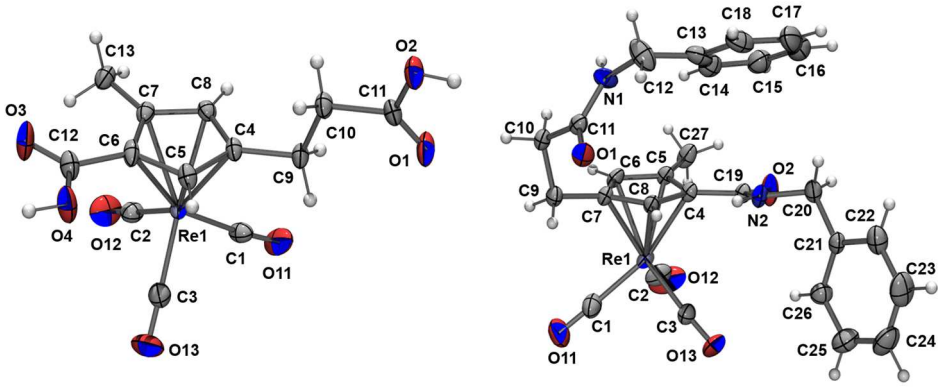

Figure 11. Crystal structures of **2b** and **3b**. Displacement ellipsoid representation. Ellipsoids are drawn at 50% probability. Important bond lengths (Å): **2b** Re-centroid of Cp: 1.950(2), **3b** Re-centroid of Cp: 1.945(3).

These synthetic results clearly imply that more complex biomolecules can be conjugated to both, the free ligand and to the rhenium complexes themselves. For

rhenium, ligand **8a** and complex **8b** are key since they will allow the consecutive introduction of two different functionalities on the ligand (**8a**) for later labeling with ^{99m}Tc (vide infra) or on the rhenium complex (**8b**) for biological evaluation and comparison with the ^{99m}Tc complex.

Radiolabeling with ^{99m}Tc: It is the common notion that cyclopentadiene systems, capable of binding in aqueous solution to the $[^{99m}Tc(CO)_3]^+$ fragment, have to comprise electron withdrawing groups directly on the Cp scaffold. This would sufficiently acidify the ring to have at least small amounts deprotonated and therefore prone to coordination. Accordingly, most of the approaches towards $[(\eta^5\text{-}C_5H_4\text{-}R)^{99m}Tc(CO)_3]$ type complexes comprise a carbonyl function directly on the Cp ring.[79, 87, 107] First, we radiolabeled the basic ligands **1a**, **4a** and **6a** which follow this concept and should therefore readily react with the $[^{99m}Tc(OH_2)_3(CO)_3]^+$ precursor.

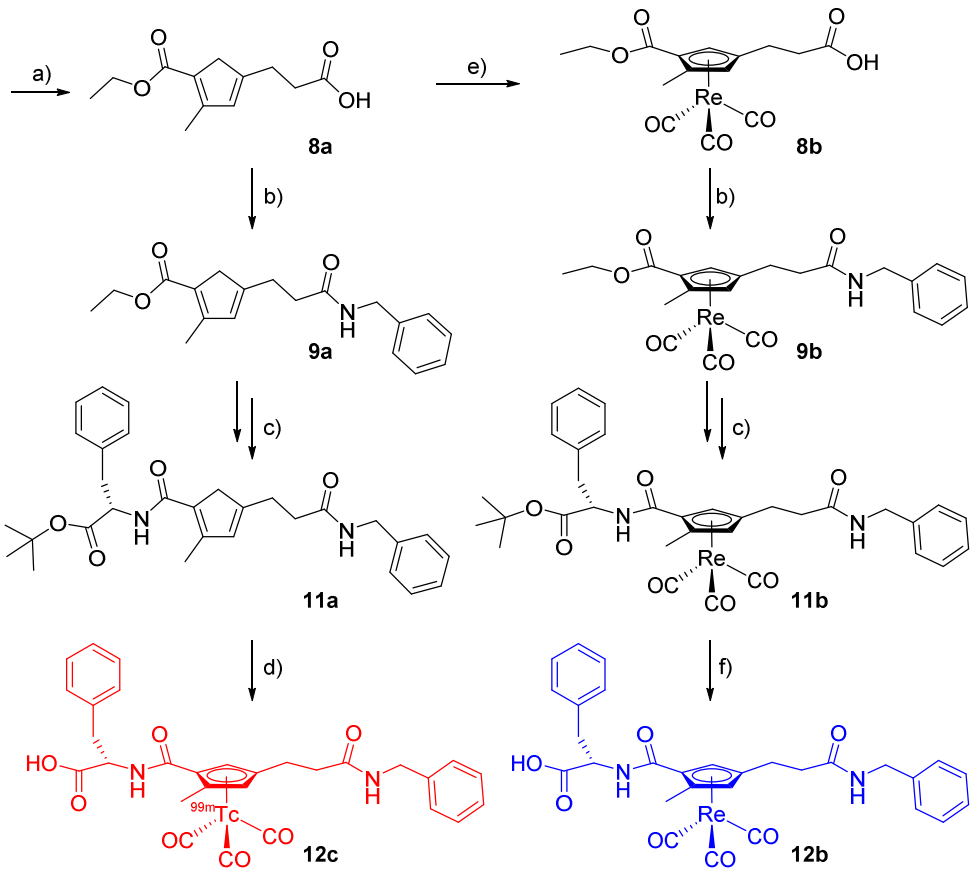

Scheme 10. Synthetic route towards hetero-functionalized Re and ^{99m}Tc complexes. Reaction conditions: a) NaOH, MeOH, MW, 120 °C, 15 min. b) benzylamine, HOBt, EDC, DMF, 25 °C, 48 h, 69%. c) i) NaOH, MeOH, MW, 120 °C, 15 min. ii) O-tertbutyl-L-Phenylalanine, HOBt,

EDC, DMF, 25 °C, 24 h, 26%. d) $[TcO_4]^-$, sodium boranocarbonate, sodium tartrate, sodium tetraborate, H_2O, MW, 140 °C, 30 min. e) Re_2CO_{10}, DMF, MW, 220 °C, 15 min. f) TFA, DCM, MW, 80 °C, 15 min, 80%.

In a two-step approach, *fac*-$[^{99m}Tc(OH_2)_3(CO)_3]^+$ was prepared and then reacted with ligands **1a**, **4a** and **6a** at millimolar concentrations. Along this path, the ^{99m}Tc complexes **2c**, **5c** and **7c** (Scheme 3) could all be obtained in high radiochemical yields under alkaline conditions and microwave heating at 120 °C for 30 min (see experimental part). Having shown that radiolabeling of these ligands with *fac*-$[^{99m}Tc(OH_2)_3(CO)_3]^+$ was straight-

forward, we attempted the direct synthesis of the ^{99m}Tc complexes (**2c**, **5c** and **7c**) directly from $[TcO_4]^-$ in a "one-pot" approach. Mixing all components together in a vial and adding directly the generator eluate containing the $[^{99m}TcO_4]^-$ complexes **2c**, **5c** and **7c** formed quantitatively through an improved procedure under microwave conditions in 30 min at 120 °C (Figure 12). We emphasize that these are conditions compatible with routine applications in clinics. As typical ^{99m}Tc concentrations are too low for standard chemical characterizations of the formed complexes by e.g. NMR, the accepted procedure for their characterizations is HPLC co-injection with the "cold" rhenium homologue and comparison of retention times (γ-trace for ^{99m}Tc, UV-trace for Re). Figure 12 shows the HPLC traces of the respective ^{99m}Tc complexes as obtained after direct preparations in quantitative yields with all three ligands from $[^{99m}TcO_4]^-$. Further purification was not required. Due to the basic conditions, the ester groups hydrolyzed during the labelling process, wherefore co-injections were performed with the di-acid rhenium analogues (**2b**, **5b** and **7b**). The retention times match, corroborating the identity of the two homologous complexes with Re and ^{99m}Tc. The Cp compounds **3a** and **11a** bear two model functionalities V_1 and V_2 at positions R_2 and R_4 in the basic Cp structure, conjugated via an amide to the two carboxylate groups. These ligands represent the basic structure for a combinatorial approach since essentially any two biovectors can be added at this time point. The labeling of such more complex systems in general and **3a** and **11a** in particular is an exemplary step in the preparation of multi-functional molecular imaging agents. Accordingly, by following the preparations as described above, ligands **3a** and **11a** could be labelled along the one-pot procedure directly from $[^{99m}TcO_4]^-$, giving the corresponding ^{99m}Tc complexes

3c and **12c** in good yields (Figure 13). Slightly higher temperatures and reaction times were required. As a convenient "side effect", the *tert*-butyl protective group was concertedly cleaved of during the reaction in case of **11a**.

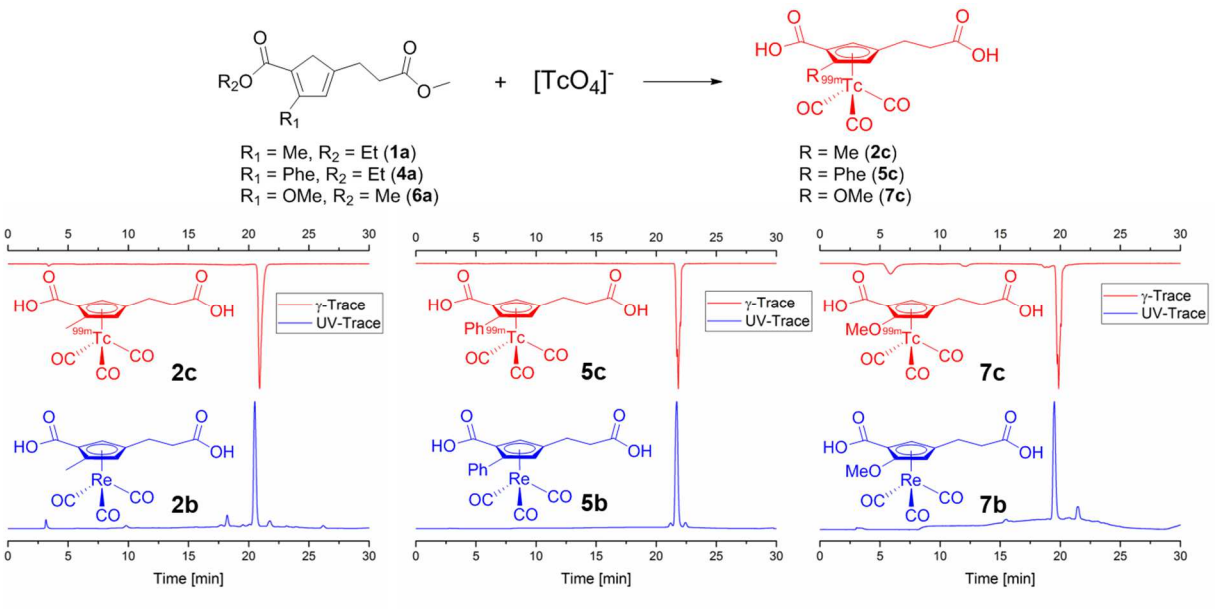

Figure 12. General reaction scheme for the one-pot reaction of ligands **1a**, **4a** and **6a** with $[TcO_4]^-$ (top). Reaction conditions: $[TcO_4]^-$, sodium boranocarbonate, sodium tartrate, sodium tetraborate, H_2O, MW, 120 °C, 30 min. UV- and y-traces of the co-injection of the rhenium compounds **2b**, **5b** and **7b** with the ^{99m}Tc compounds **2c**, **5c** and **6c** respectively (bottom). Differences in retention times are due to detector separation.

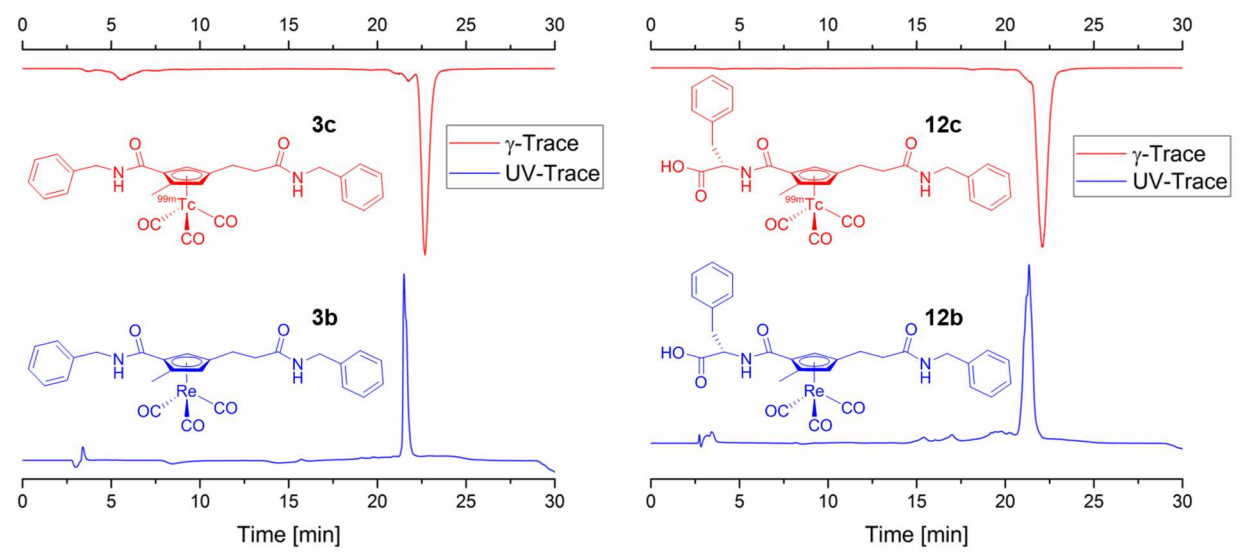

Figure 13. UV/vis- and y-traces of the co-injection of the rhenium compounds **3b** and **12b** with the ^{99m}Tc compounds **3c** and **12c** respectively. Time differences are due to detector separation.

Taken together, these results demonstrate the possibility to synthesize ^{99m}Tc piano-stool type molecular imaging agents with structurally complex and multifunctional Cp ligands in one step and from $[^{99m}TcO_4]^-$ in a straightforward and efficient way. The option of altering V_1 and V_2 (phenyl-alanine and benzyl-amine in our case) opens a path towards further combinations of biologically active moieties.

Conclusion

In this work, we present versatile synthetic routes towards multiply substituted cyclopentadiene, which are base for the subsequent preparation of multifunctional ligands. Both, the physico-chemical (group R_1) as well as the biological properties (V_1 and V_2) can be tuned individually in the same ligand. We have furthermore shown that these cyclopentadiene scaffolds serve as a ligand platform in bioorganometallic ^{99m}Tc chemistry that allows the introduction of multiple modalities in a straightforward way. The ligands as such can be prepared separately with functionalities V_1 and V_2 according to the targets needs. The "innocent" group R_1 on the Cp scaffold influences the physico-chemical properties such as lipo/hydrophilicity while leaving the targeting properties untouched. The three representative ligands (**1a**, **3a**, **5a**) with different R_2 groups have been synthesized, fully characterized and coordinated to the *fac*-$[Re(CO)_3]$ moiety. As a further proof-of-concept, **1a** was both bis-homo - and bis-hetero functionalized with two simple biovector-models. Established amide bond formation chemistry for the vector conjugation, ensures its applicability to a wide variety of modalities. The combination of these ligands with the theranostic pair Re and ^{99m}Tc leads to tetra-functional complexes. Their synthesis is both straightforward, highly tolerant to different functionalities and, most importantly, the ^{99m}Tc homologous are prepared in one step directly from generator eluted $[^{99m}TcO_4]^-$. We envision that this ligand platform will enable a combinatorial approach towards targeted and multimodal bioorganometallic complexes.

3.1.3 Extended Discussion of the Manuscript

Analogous to **3b**, complexes **5b** and **7b** were also homo-functionalized with benzylamine with the standard procedure (Scheme 11). The bis-amide complexes **21** and **22** were purified by preparative HPLC and characterized by ^{1}H- and ^{13}C-NMR, HR-ESI-MS and IR spectroscopy.

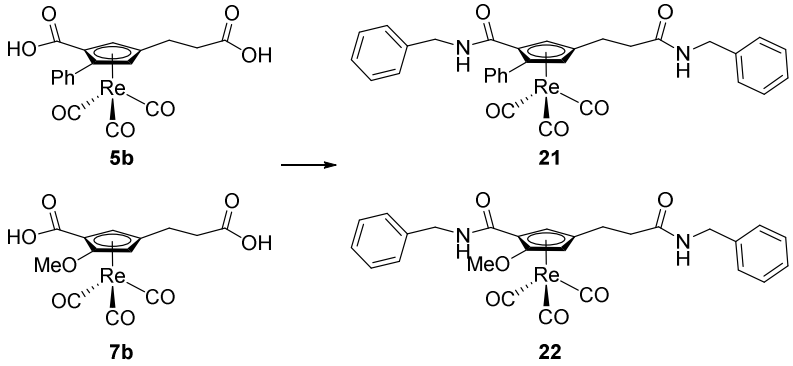

Scheme 11. Reaction conditions: benzylamine, HOBt, EDC, DMF, 25 °C, 48 h, **21**, 49%; **22**, 25 %).

In addition to the Cp-ligands discussed in the above manuscript several other Cp-ligands were pursued as well. An overview of the attempts is shown in Scheme 12.

To obtain a simpler kind of Cp, the synthesis of **Cp-A** was pursued. Starting from commercially available 4-bromo-trans-crotonic acid ethyl ester, a white precipitate was isolated upon stirring at room temperature in dry toluene overnight with triphenylphosphine. The presumed **23** was dried and directly reacted with **0.1** under standard conditions. No product formation was observed by UPLC even after 48 h.

Another strategy was the introduction of a third ethyl ester at the same position to obtain a Cp with three sites that could potentially be functionalized (**Cp-B**). **25** was obtained staring from citraconic acid in two steps following literature procedures.[119, 120] By reacting **25** with triphenylphosphine in dry toluene, the phosphonium salt **26** could be isolated as the precipitate and was characterized by ^{1}H-NMR. However, the reaction of **26** with the bromoketone **0.1** was not successful**.** The route towards a trifluoromethyl-substituted Cp-ligand (**Cp-C**) had a similar fate. The radical bromination of (*E*)-3-trifluoromethyl-2-butenoic acid ethyl ester could be carried as described in the literature.[121] The synthesis of the phosphonium salt **28** was performed under the same conditions as for **26**, yielding a white powderish solid that could be characterized by

^{1}H-NMR. Again, the final Cp-forming step to **Cp-C** was not successful. It seems that introducing a strongly electron-withdrawing group at this position prevents the ring-forming step from occurring. Potentially introducing a linker between the ring and the functional group could lead to better results.

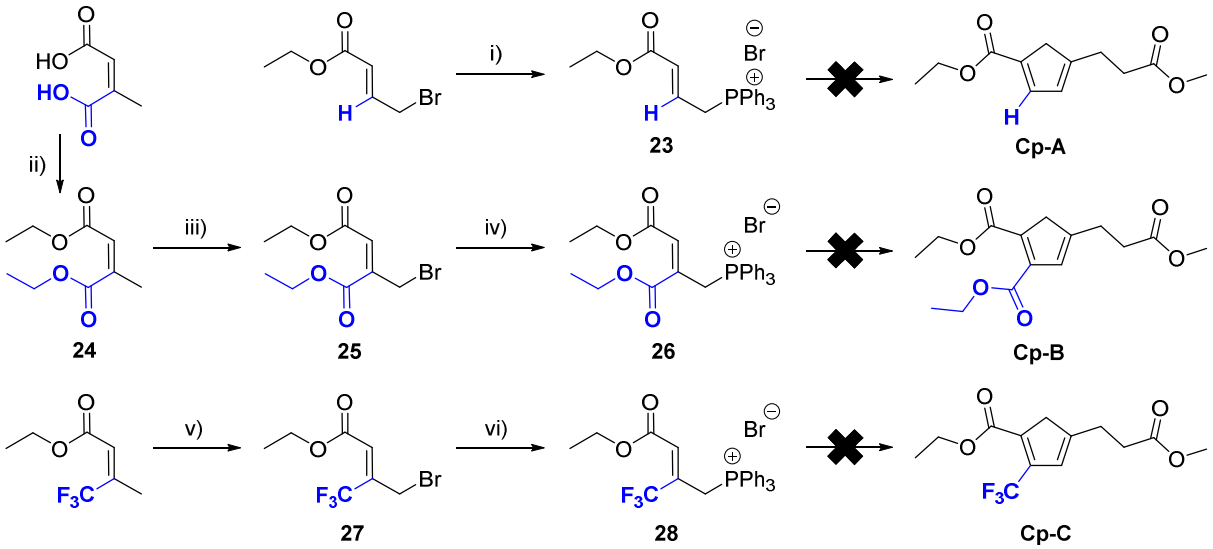

Scheme 12. Reaction conditions: i) PPh_3, dry toluene, 24 h, RT. ii) EtOH, cat. H_2SO_4, reflux, overnight. iii) NBS, cat. AIBN, CCl_4, reflux, 4 h. iv) PPh_3, dry toluene, 24 h, RT. v) NBS, cat. AIBN, CCl_4, reflux, 4 h. vi) PPh_3, dry toluene, 24 h, RT.

Several more approaches to introducing different functional groups at various positions of the Cp-ring were pursued and are summarized briefly in the following section.

The introduction of an amine group directly to the Cp was of high interest, as the resulting ligand and complex would have aminoacid-like character. The first step involved protection of the free amine with the *boc*-protecting group leading to **I**. Unfortunately, all attempts to brominate both the protected as well as the free amine were not successful.

Another strategy involved the modification of the bromoketone instead of the phosphonium salt (Scheme 13). Both the introduction of an alcohol and a protected amine group failed at the Cp-ring forming step. Protecting the bromoketone carboxylic acid orthogonally to the ester on the phosphonium salt e.g. with a *tert*-butyl ester group (**VI**), would have led to another path towards hetero-functionalization of the Cp. However, the conditions of the bromination to **VII** were such, that the *tert*-butyl group

was mostly cleaved off in the process. Also, this strategy was abandoned when the mono-hydrolysis of **1a** was found to be successful.

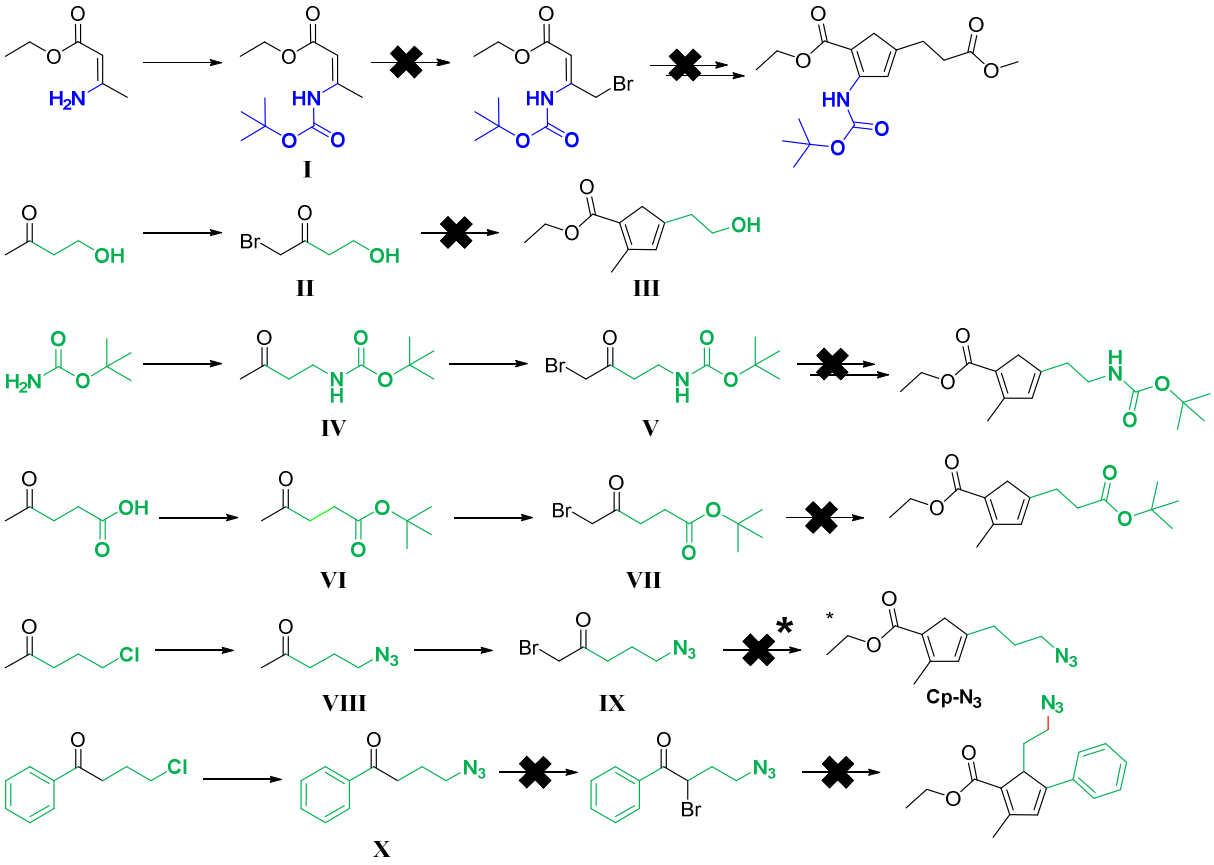

Scheme 13. Overview of explored paths to the introduction of different functionalities into the Cp-ligand. *This reaction was later on optimized and successful in the hands of another group-member.

The azide functional group and the robust "click"-chemistry developed around it prompted the investigation into azide-Cp derivatives. Although first steps were successful (**VIII** and **IX**), the synthesis of a N_3-containing Cp-system could not be achieved (of note, **Cp-N_3** could recently be synthesized and characterized by a fellow group member).

3.1.4 Outlook

The possibilities that are accessible through the synthetic strategy to multifunctional Cp's presented in this work are numerous. The recent success in the introduction of an azide group *via* the bromoketone has opened up the whole field of "click"-chemistry

to this system. Modifications on the two remaining sites of the Cp-ring were not explored within this work but could very well lead to even more versatile ligands.

3.2 The Pendent Approach: Synthesis and Biological Evaluation of Novel PSMA-Cp-M Conjugates

3.2.1 Preface

Having developed a Cp-ligand platform that is both versatile and can readily coordinate both rhenium and technetium-99m, the next obvious step was the application of the latter in a biological setting. We decided to start with a pendent approach and chose a well-established prostate specific membrane antigen (PSMA) inhibitor as the targeting moiety. The synthesis, characterization and *in vitro* evaluation of both mono- and di-substituted Re and ^{99m}Tc complexes led to the following manuscript.

(Note: at the time of submission, the ^{99m}Tc-PSMA binding experiments were not completed yet and could hence not be included).

3.2.2 Manuscript

Two is Better than One. Dimeric High-affinity PSMA Probes Based on a [CpM(CO)$_3$] (M = Re/^{99m}Tc) Scaffold

Angelo Frei,[a] Eliane Fischer,[a] Bradley Childs,[a] Jason Holland[a] and Roger Alberto[a]*

[a] Department of Chemistry, University of Zürich, Winterthurerstr. 190, CH-8057 Zürich Switzerland

In the 21st century, one out of nine men will be diagnosed with prostate cancer during his lifetime. While current treatments have vastly increased the mean survival rate of patients, 30'000 people are still expected to die from prostate cancer in 2018 in the US alone.[122] The most common cause for mortality in prostate cancer patients is the occurrence of metastases. A major factor in reducing the death toll of this disease is the improvement of early detection and monitoring techniques. The prostate specific membrane antigen (PSMA) is an extracellular receptor and a promising target for nuclear imaging as its overexpression is proportional to the stage and grade of tumor progression.[123] PSMA-binding imaging agents based on ^{11}C, ^{18}F, ^{64}Cu, ^{68}Ga, ^{99m}Tc, ^{111}In have been reported, but so far, only ^{11}C, ^{18}F and ^{111}In-based radiotracers are used in the clinics for prostate cancer imaging.[124] These isotopes share the disadvantage of requiring a cyclotron for their generation and the associated limited availability and high cost of production compared to the cheaper and generator-available radio-isotopes ^{68}Ga and ^{99m}Tc. New imaging agents based on both gallium and technetium chelators coupled to a high PSMA-affinity Lys-urea-Glu (LuG) motif are currently in advanced clinical trials.[40, 125] Multimeric radiotracers containing more than one binding unit are thought to possess higher binding affinity to membrane-proteins. This has already been exploited with integrin $\alpha_v\beta_3$ protein-targeted radiotracers linked to cyclic arginine-glycine-aspartic (RGD) peptides.[126, 127] Multiple studies found superior binding for dimeric RGD-chelates compared to their monomeric counterparts. Indeed, ^{99m}Tc-3PRGD$_2$ is a dimeric cyclic RGD-based imaging agent which is currently undergoing multiple phase I clinical trials. In the light of these promising results it is surprising that only little work has been done on multimeric PSMA-targeting compounds. In 2012, Schäfer *et al.* reported a ^{68}Ga-based structure containing two LuG units that displayed

improved PSMA affinity, higher cell uptake and prolonged cell surface retention time compared to the monomeric analogue.[128] To the best of our knowledge, the only ^{99m}Tc-complexes conjugated to multiple binding units were reported by Frangioni and coworkers in 2007. They prepared dimeric and trimeric compounds based on a phosphinyl-containing PSMA-ligand. The bi- and trifunctional complexes showed significantly higher PSMA affinities than their monomeric counterpart.[129] These promising preliminary results clearly indicate that there is unexplored potential in multimeric PSMA-targeted radiotracers.

In this work we describe the synthesis and evaluation of a compact Re/^{99m}Tc system containing either one or two LuG units. By using a multifunctional cyclopentadiene (Cp) as both the metal-coordinating moiety as well as the linker to the two PSMA-ligands the chelator only accounts for a small fraction of the resulting complex.

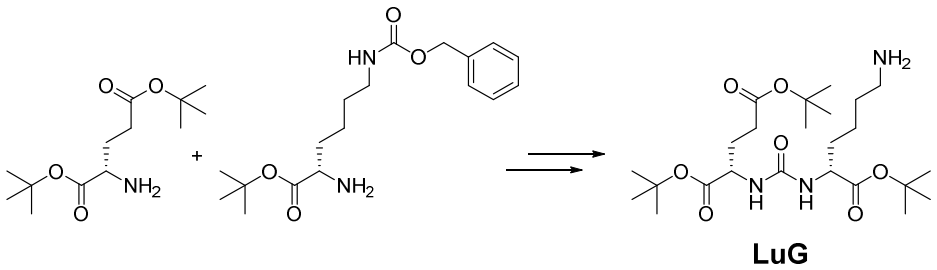

Scheme 14. Synthesis of **LuG**. Reaction conditions: i) triphosgene, NEt_3, dry CH_2Cl_2, 0 – 25 °C, 6 h, 65 %. ii) H_2, Pd/C (10 %), MeOH, 25 °C, 16 h, 96 %.

The “cold” rhenium complexes **30** and **32** were prepared from **1a** based on a synthetic strategy recently reported by our group (Scheme 15).[130] **LuG** was prepared according to a previously reported procedure (Scheme 14) and reacted with **8b** and **2b** using HOBt and EDC.[131] The resulting complexes (**29** and **31**) were purified by preparative HPLC. In the case of **31**, the two diastereoisomers resulting from combining the planar chirality of the rhenium complex with the enantiomerically pure **LuG** could be separated and characterized individually. The *tert*-butyl protecting group cleaved with NaOH in MeOH under microwave conditions and further purification by preparative HPLC yielded pure **30** and **32** (For **32** a 1:1 mixture of **31a** and **31b** was used). The complexes were characterized by NMR spectroscopy and high-resolution mass spectrometry.

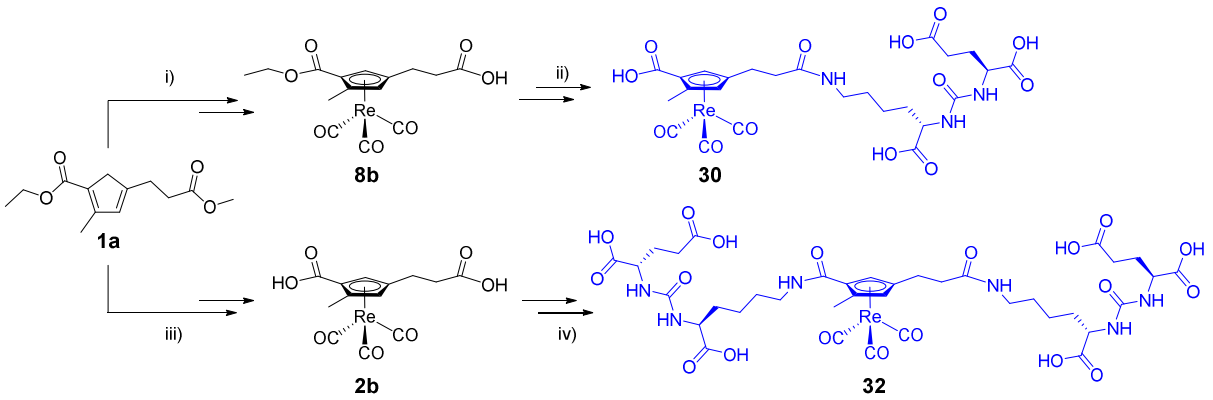

Scheme 15. Synthetic route to **30** and **32**. Reaction conditions: i) a) NaOH, MeOH, MW, 120 °C, 15 min. b) Re_2CO_{10}, DMF, MW, 220 °C, 15 min. ii) a) **LuG**, HOBt, EDC, DIPEA, DMF, 25 °C, 24 h, 30 % (from **1a**). b) NaOH, MeOH, MW, 120 °C, 15 min, 76 %. iii) a) Re_2CO_{10}, *o*-Xylene, MW, 220 °C, 15 min, 76 %. b) NaOH, MeOH, MW, 120 °C, 15 min, 68 %. iv) a) **LuG**, HOBt, EDC, DIPEA, DMF, 25 °C, 24 h, 31 %. b) NaOH, MeOH, MW, 120 °C, 15 min, 56 %.

To determine the PSMA-binding affinity of **30** and **32** LnCap (PSMA-positive) and PC3 (PSMA-negative) cells were incubated for 1 h with different concentrations of the rhenium complexes. The cells were then washed, digested and the total amount of Re bound was determined by ICP-MS. Both compounds displayed binding affinities in the low nanomolar range (Table 1). With a K_D of 1.6 nM, the binding affinity of the dimeric complex **32** is 8 times higher than for the monomeric **30**, and comparable with PSMA-binders currently in clinical trials.[132] Interestingly, the amount of rhenium detected at the highest incubation concentrations for **30** is almost twice as high as for **32**. Since roughly the same number of cells were used for both assays, this indicates that **32** occupies two binding sites per metal atom.

In order to confirm the results obtained with the rhenium complexes, the free ligands **33** and **35** were prepared from **1a** and **LuG** in two steps (Scheme 16). The pure ligands were then used directly and without deprotection for radiolabeling with ^{99m}Tc. Reacting **33** and **35** with $[^{99m}Tc(OH_2)(CO)_3]^+$ at 140 °C in a microwave reactor under basic condition led to formation of **34** and **36** as diastereoisomeric mixtures within 15 min, as evidenced by HPLC co-injection with the respective rhenium complex (Figure 14). The only detectable side-products were $[^{99m}TcO_4]^-$ and $[^{99m}Tc(OH_2)(CO)_3]^+$. Of note, under

the employed reaction conditions, all the *tert*-butyl protecting groups are cleaved off and the fully deprotected compounds are obtained directly.

	K_d [nM]
30	1.6 ± 0.2[a]
32	12.5 ± 5[a]
34	TBD[b]
36	TBD[b]

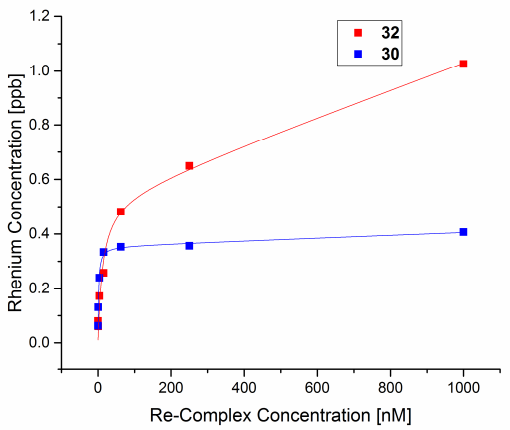

Table 1. PSMA-binding affinity of complexes **30**, **32**, **34** and **36**. [a]Binding affinities obtained by fitting rhenium content of cell-samples incubated with different concentrations of complex. Each data point is the average of three different samples.

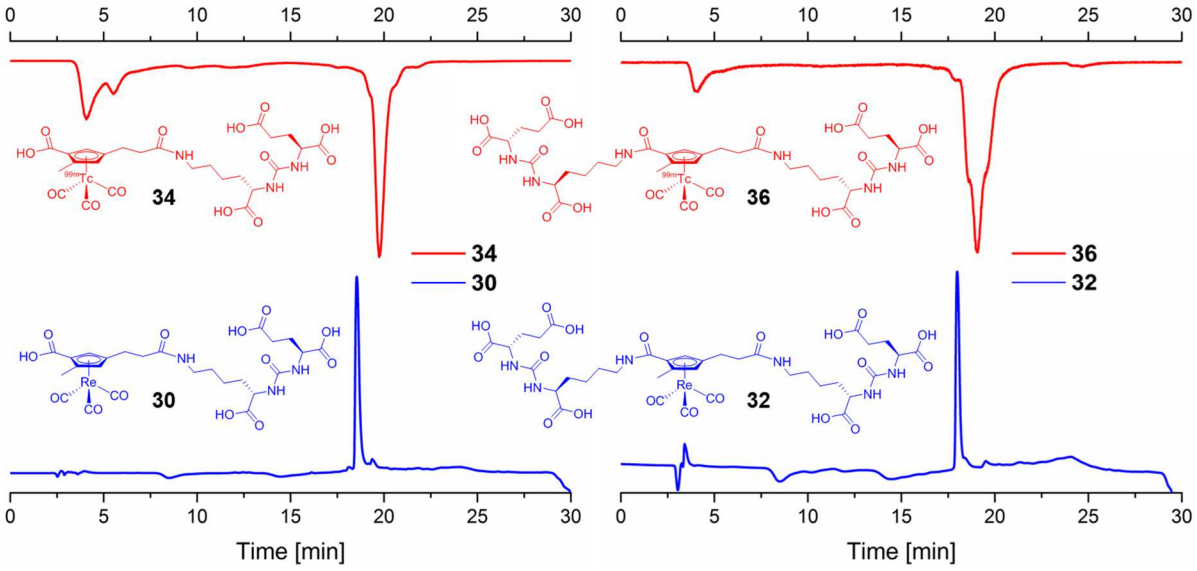

Figure 14. UV/vis- and y-traces of the co-injection of the rhenium compounds **30** and **32** with the ^{99m}Tc compounds **34** and **36** respectively. Time differences are due to detector separation.

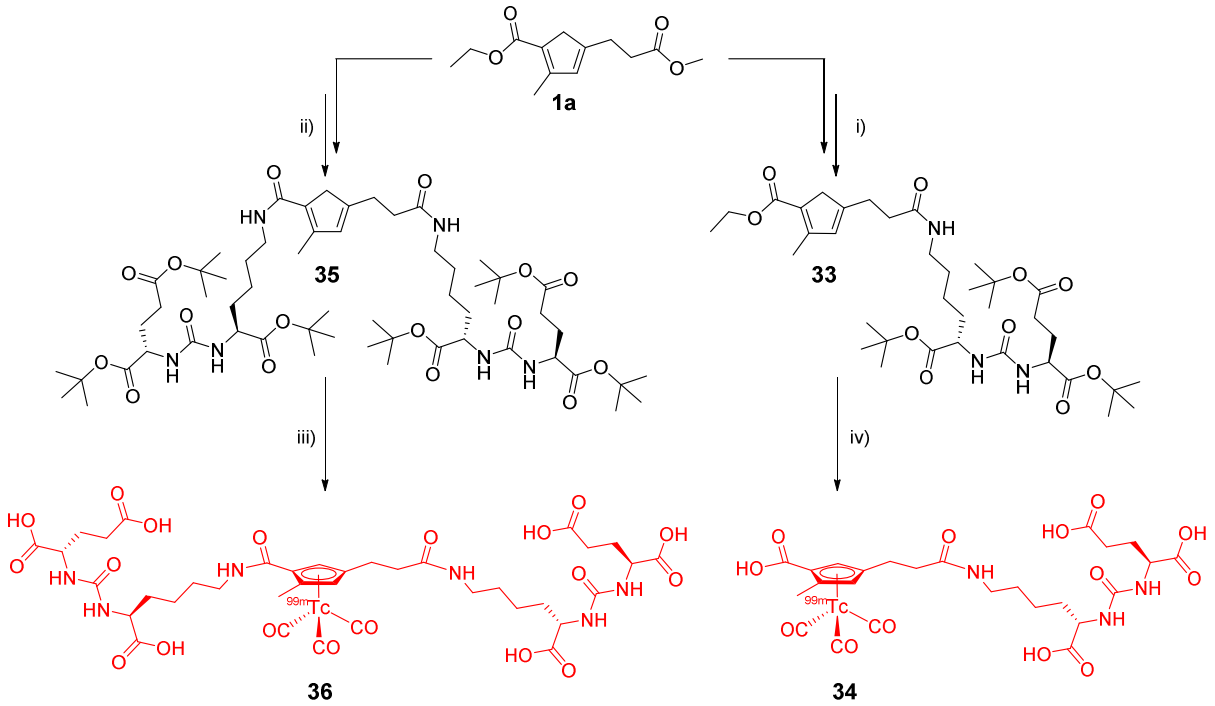

Scheme 16. Synthetic route to **34** and **36**. Reaction conditions: i) a) 0.93 eq. NaOH, MeOH, MW, 120 °C, 15 min. b) **LuG**, HOBt, EDC, DIPEA, DMF; 25 °C, 24 h, 17 % (from **1a**). ii) a) NaOH, MeOH, MW, 120 °C, 15 min. b) **LuG**, HOBt, EDC, DIPEA, DMF; 25 °C, 24 h, 15 % (from **1a**). iii) $[^{99m}Tc(OH_2)_3(CO)_3]^+$, NaOH, MW, 140 °C, 15 min. iv) $[^{99m}Tc(OH_2)_3(CO)_3]^+$, NaOH, MW, 140 °C, 10 min.

3.2.3 Outlook

This work demonstrates that the herein developed Cp-system lends itself to easy and straightforward functionalization with biomolecules. The coupling reactions proceed with good overall yields and the products are readily purified by preparative HPLC. Importantly, the synthesis of the respective ^{99m}Tc complexes is also possible from highly functionalized Cp-ligands. The successful conjugation of a targeting unit to our platform opens up the possibility to additionally attach a cytotoxic moiety to the complex. This would lead to a true theranostic system: The ^{99m}Tc complex is directed to prostate cancer cells but due to the low concentrations of the radionuclide it will not induce apoptosis *in situ*. On the other hand, the analogous rhenium complex would localize in the same way as its Tc-congener but in higher concentrations thereby inducing a therapeutic effect. In conclusion this proof-of-concept evidences the

potential of the multifunctional Cp-ligands and encourages its application with further targeting and bioactive modalities.

3.3 The Integrated Approach: Synthesis of Pemetrexed-Mimics

3.3.1 Discussion of Preliminary Results

We have shown that our ligand platform can be used to conjugated one or multiple targeting functions to rhenium and technetium. The ultimate goal, however, was always to use the versatility of the Cp-ligand synthesis to pursue an integrated approach as inspired by the antimalaria compound ferroquine.[16] The first step was to find an organic molecule with known anticancer activity, containing a phenyl-ring system with a substitution pattern similar to our Cp-system. We turned our attention to the antifolate class of anticancer compounds, particularly the drug pemetrexed (Figure 15).[133] The *para*-substituted central phenyl ring was an ideal candidate to be replaced by a Cp. Additionally, the two phenyl-pendent moieties could be obtained in a straightforward way. L-Glutamic acid (Figure 15, red) is commercially available and the synthesis of the 6,5-fused pyrrolo[2,3-d]pyrimidine nucleus (Figure 15, blue) including an additional amine group was already reported in the literature.[134]

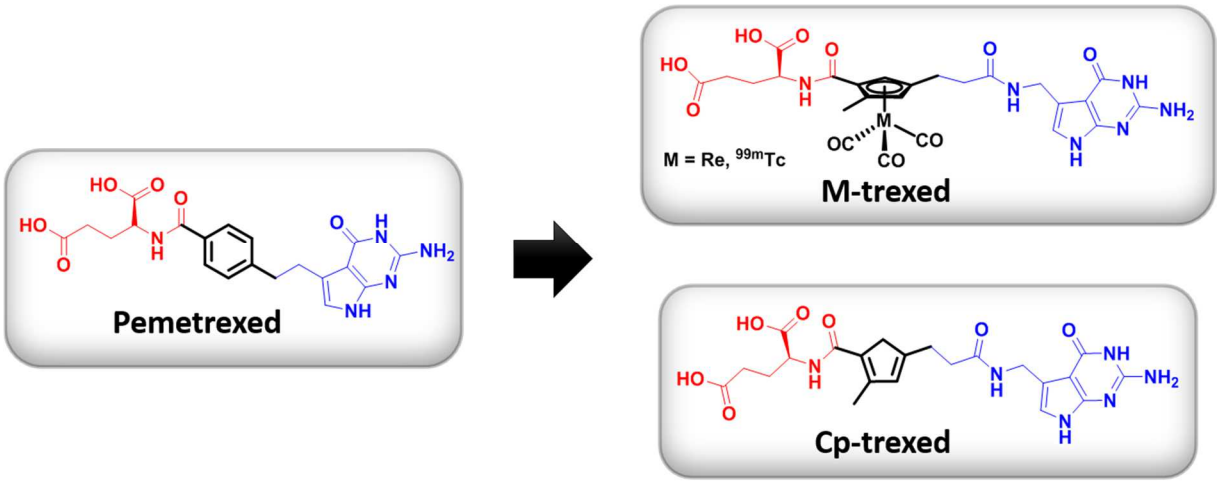

Figure 15. The integrated approach applied to pemetrexed.

Pemetrexed was first reported in 1992 by Taylor *et al.* and subsequently developed for clinical evaluation in a cooperation with Eli Lilly.[135] As an antifolate, pemetrexed inhibits several folate-dependent enzymes that are essential for DNA synthesis and cell proliferation.[136] Today, pemetrexed is approved for use against malignant pleural mesothelioma and non-small cell lung cancer (NSCLC) in the U.S. and the E.U. Due to its proven clinical relevance as well as the afore-mentioned synthetic accessibility

we proposed complexes **Re-trexed/43**, **^{99m}Tc-trexed** and ligand **Cp-trexed** (Figure 15) as metal-based pemetrexed mimics following an integrated approach.

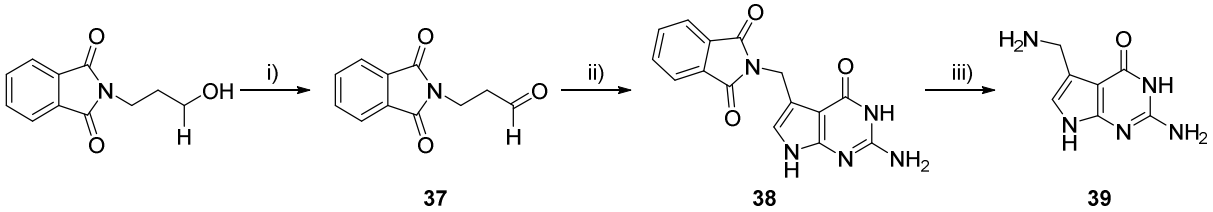

Scheme 17. Reaction conditions: i) Dess-Martin periodinane, DCM, RT, 16 h, 54%. ii) a) Me_3SiBr, ACN/DMSO, RT, 4 h. b) 2,6-diamonopyrimidin-4-one, AcOH, H_2O, RT, 16 h, 30%. iii) $NH_2NH_2{\cdot}H_2O$, EtOH, reflux/RT, 2 h/ 8 h.

The building block **39** was prepared in three steps starting from commercially available 2-(3-hydroxypropyl)isoindoline-1,3-dione according to a literature procedure (Scheme 17).[134] In the reported synthesis, the deprotection of **38** was followed by an *in situ boc*-protection as the free amine could not be isolated in good yields. In our case we skipped the *boc*-protection and used the crude of the **38** phtalimide-deprotection directly for the amide coupling with a crude reaction mixture of **8b**, yielding **40** after preparative HPLC purification (Scheme 18). Hydrolysis of the ethyl ester was followed by a second amide coupling with L-glutamic acid di-*tert*-butyl ester and **42** was obtained as a mixture of two diastereoisomers after purification by preparative HPLC. As before, the two diastereoisomers occur due to the combination of the planar chirality of the Cp-ligand with the chiral center on the glutamic acid. Deprotection with TFA and triethylsilane finally gave the target compound **43**.

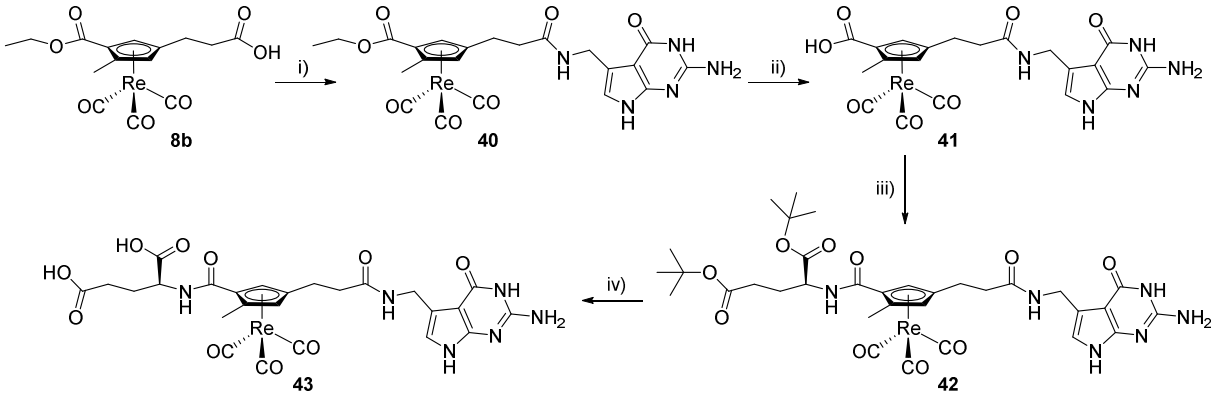

Scheme 18. Synthetic route towards **43**. Reaction conditions: i) **39**, HOBt, EDC, DIPEA, DMF, RT, 24 h, 20 % (from **38**). ii) NaOH, MeOH, MW, 120 °C, 15 min. iii) H-Glu(OtBu)-OtBu.HCl, HOBt, EDC, DIPEA, DMF, RT, 24 h, 62 % (from **40**). iv) TFA, triethylsilane, CH_2Cl_2, 25 °C, 24 h, 38 %.

Overall, the synthesis of **43** is analogous to the model synthesis of a heterodimeric tetrafunctional complex reported above (**12c**), highlighting once more the easy application of this concept to relatively complex target compounds.

A similar route can be followed to obtain the respective free Cp-ligand that can then be labelled with ^{99m}Tc (Scheme 19). Due to a lack of time, this synthesis was not pursued before submission of this thesis.

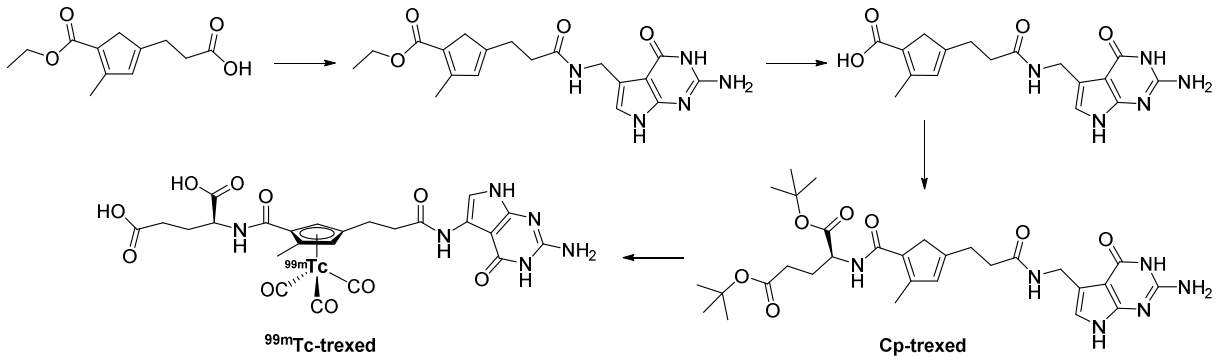

Scheme 19. Proposed synthetic route towards the free Cp-ligand (**Cp-trexed**) and ^{99m}Tc-analogue of **43** (**^{99m}Tc-trexed**).

In conclusion the newly developed Cp-platform allowed the straightforward synthesis of **Re-trexed**/**43**, an analogue of the clinically approved anticancer drug pemetrexed, with unprecedented structural similarity. While *in vitro* and *in vivo* evaluation of these compounds is still pending, it is clear that this approach can very easily be applied to a myriad of other compounds, opening up a new avenue in the research of Re/^{99m}Tc theranostic agents.

Part B: Multifunctional Cp-Complexes with Iron and Ruthenium

3.4 Synthesis of Mixed-sandwich and Metallocene Complexes with Polysubstituted Cp-ligands

The availability of the water-soluble Cp **S1** prompted exploratory investigations into the aqueous synthesis of Cp-containing complexes with other metals. Although iron was the first candidate of choice, reactions of **S1** with $FeCl_2$ only lead to the detection of trace amounts of the corresponding ferrocene product by UPLC-MS under various attempted conditions. We therefore turned our attention to ruthenium. The dimers **44** and **47** were prepared according to literature procedures (Scheme 20).[137] Suspending these complexes in H_2O and addition of silver nitrate, resulted in a color change and formation of a dark precipitate. Subsequent addition of **S1** at room temperature and precipitation with NH_4PF_6 yielded complexes **45** and **48**. Both compounds were characterized by NMR and single crystals suitable for X-ray analysis could be obtained by slow evaporation of a MeOH solution of **45** (Figure 15).

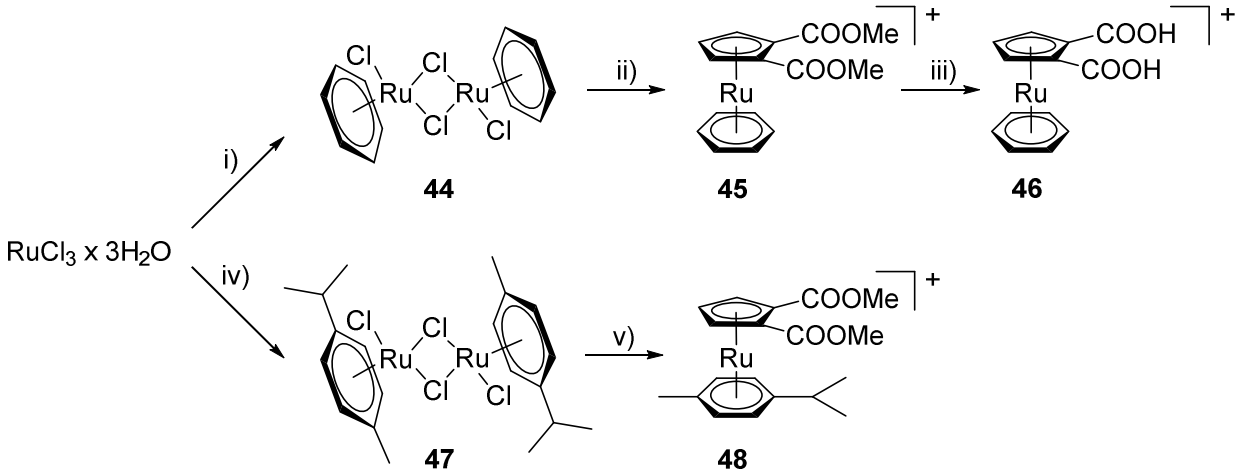

Scheme 20. Reaction conditions: i) 1,3-cyclohexadiene, EtOH, reflux, 4 h, 93% ii) a) 4 eq. $AgNO_3$, H_2O, RT, 1 h; b) 1 eq. **S1**, H_2O, RT, 1 h, 41%. iii), NaOH, MeOH, RT, 6 h. iv) α-terpinene, MeOH, MW, 140°C, 1 min, 59% v) a) 4 eq. $AgNO_3$, H_2O, RT, 1 h; b) 1 eq. **S1**, H_2O, RT, 1 h, 73%.

By using the water-soluble Ru(II) synthon $Ru(DMSO)_4Cl_2$, and heating it with **S1** in H_2O by microwave at 120 °C for 10 min, the ruthenocene **49** could be obtained and purified by a simple extraction (Scheme 21). The complex was characterized by NMR and single crystals were obtained by vapor diffusion of hexane into a solution of **49** in DCM (Figure 16).

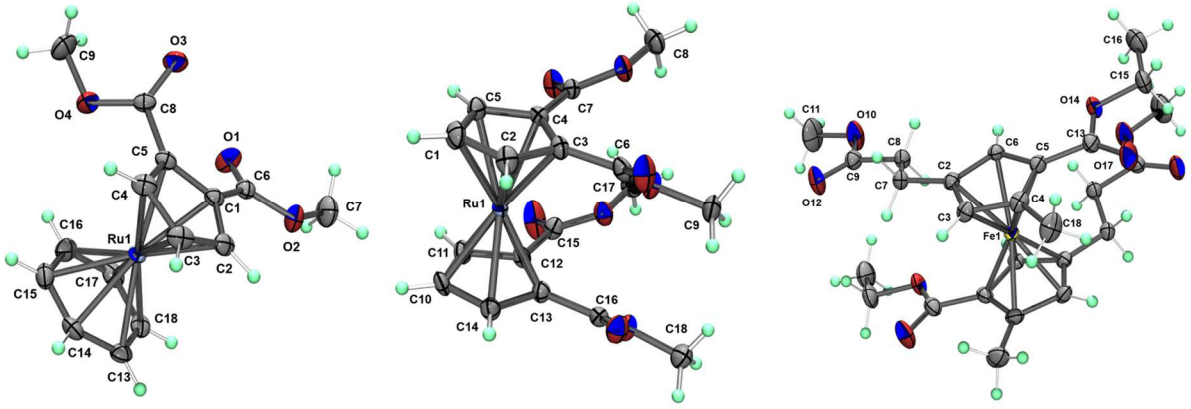

Figure 16. ORTEP diagrams of **45**, **49** and **51**, with ellipsoids at 50% probability level.

In both **45** and **49**, the ester groups could easily be cleaved by stirring a solution of the complex in MeOH with KOH for several hours. The obtained compounds (**46** and **50**) display high water solubility and could potentially exhibit cytotoxic properties as has been shown for other ruthenium arene/Cp complexes.[96]

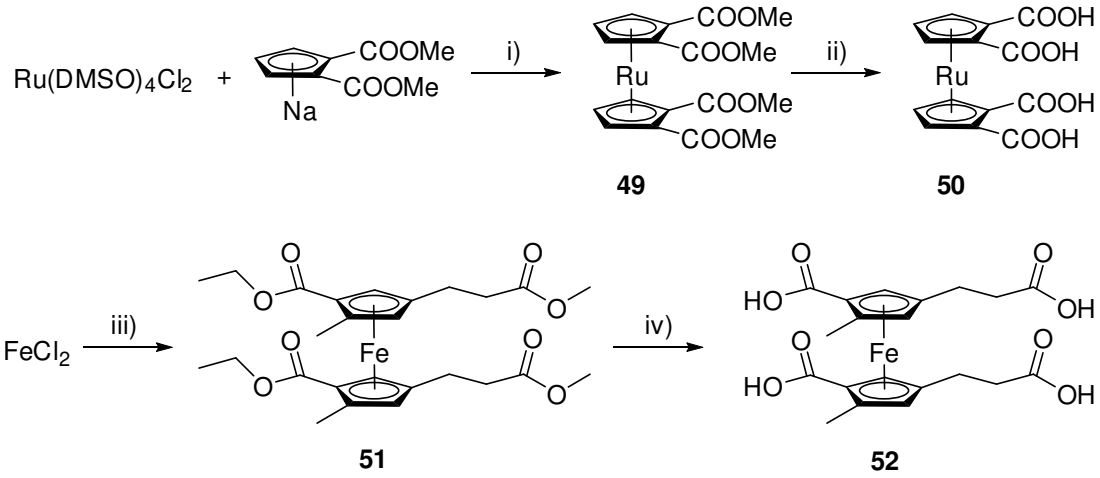

Scheme 21. Reaction conditions: i) H_2O, MW, 120°C, 10 min, 67%. ii) KOH, MeOH, RT, 1 h, 54 % iii) KOH, diglyme, DMSO, RT, 2 h. iv) NaOH, MeOH, MW, 120 °C, 30 min.

While reactions of $FeCl_2$ with **S1** were not very successful, it was possible to obtain multifunctional ferrocene derivatives from **1a** by following a procedure analogous to an early ferrocene synthesis protocol.[138] Due to the planar chirality of **51**, two isomers were detected by UPLC but could not be separated. The compound was characterized by MS and NMR. Single crystals suitable for X-ray analysis could be obtained by the slow evaporation of a methanolic solution of **51** (Figure 15). In a trial reaction of the hydrolysis of the ester groups in **51**, the formation of a couple peaks was observed at significantly lower retention time (i.e. more hydrophilic species), hinting at the formation of **52**. Due to time constraints, this was not investigated further.

These preliminary results clearly indicate that these multifunctional Cp-ligands offer the possibility to prepare interesting compounds with other metals as well.

Part C: Fundamental Investigations into the solution-behavior of basic rhenium and technetium synthons

3.5 ^{13}CO exchange in $Re(CO)_3$ and $^{99}Tc(CO)_3$-based complexes

3.5.1 Preface

Understanding the behavior of fundamental rhenium and technetium synthons is of high importance when designing complexes containing these metals. Since the carbonyl ligands in the *fac*-$[M(CO)_3]^+$-core are thought to be mostly inert, they represent an interesting potential probe into fundamental reaction mechanisms occurring at the metal center. In collaboration with the group of Prof. Andreas Roodt at the University of the Free State in South Africa, we embarked on a project to study these reactions. Our initial strategy envisaged the enrichment of $[NEt_4]_2[ReBr_3(^{12}CO)_3]$ with ^{13}CO in order to investigate the reaction of the metal core with Cp-ligands. Surprisingly, addition on ^{13}CO gas to a solution of the rhenium tricarbonyl in DMF rapidly led to the formation of a new, at first unknown, species. Further studies showed that a rhenium tetracarbonyl species is formed in the process. The results obtained during the thorough examination of this process led to an in-depth understanding of the solution behavior of the tricarbonyl-core and to the publication of the following manuscript.

3.5.2 Manuscript

Kinetics and Mechanism of CO Exchange in $[MBr_2(solvent)(CO)_3]^-$ (M=Re, ^{99}Tc)

Angelo Frei,[a] David Sidler,[a] Pennie Mokolokolo,[b] Henrik Braband,[a] Thomas Fox,[a] Bernhard Spingler,[a] Andreas Roodt[b] and Roger Alberto*[a]*

[a] Department of Chemistry, University of Zürich, Winterthurerstr. 190, CH-8057 Zürich Switzerland

[b] Department of Chemistry, University of the Free State, P.O. Box 339, Bloemfontein 9300, South Africa

Abstract

The self-exchange kinetics of CO ligands in the solvated forms of the commonly used complex $[MBr_3(CO)_3]^{2-}$ (M=Re, ^{99}Tc) were investigated in-depth by ^{13}C NMR spectroscopy in organic solvents such as DMF and MeOH. The two homologues exhibit a surprisingly different chemical behaviour. In the case of rhenium, the stable intermediate $[NEt_4][ReBr_2(CO)_4]$ was isolated and characterized by ^{13}C NMR and IR spectroscopy as well as by single crystal X-ray diffraction. For technetium, no such intermediate could be identified. The activation parameters ($\Delta H^{\neq}$ = 110 ± 7 kJ mol^{-1} and $\Delta S^{\neq}$ = 127 ± 22 J mol^{-1} K^{-1}) and the observed influences of different ligands and solvents suggest a dissociative-interchange-type mechanism with a 2nd order rate constant for the formation of $[NEt_4][ReBr_2(CO)_4]$ k_1 = 0.039 ± 0.001 M^{-1} s^{-1} at 274 K. Based on variable temperature NMR experiments, kinetic simulations and DFT calculations, a complete model for the CO self-exchange including all respective rate constants is reported.

Introduction

Among the current imaging modalities in diagnostic medicine, single photon emission computed tomography (SPECT) is one of the most important methods. In SPECT, well over 80% of all diagnostic nuclear medicine studies are performed with ^{99m}Tc compounds.[42, 99-101] In parallel, rhenium complexes are developed for chemo- and radioimmunotherapy applications.[139-142] The labeling of targeting biomolecules with radionuclides such as ^{99m}Tc requires building blocks, ready to bind to chelators pendent to the targeting molecules. In recent years, *fac*-$[^{99m}Tc(OH_2)_3(CO)_3]^+$ and its rhenium homologue were extensively studied for this purpose since high kinetic stability of the CO ligands and the relative ease of water exchange are predominant and favorable characteristics.[143] At least one compound finished Phase II clinical trials.[38, 144-154,112, 155, 156] The precursor $[^{99m}Tc(OH_2)_3(CO)_3]^+$ is readily accessible from commercially available $[^{99m}TcO_4]^-$.[37] For rhenium, a common starting material for $[Re(OH_2)_3(CO)_3]^+$ and complexes thereof is $[NEt_4]_2[ReBr_3(CO)_3]$. The Br^- ligands are readily exchanged by solvent molecules, either directly after dissolution in e.g. water or after precipitation with silver salts in less strongly coordinating solvents such as DMF (dimethyl-formamide).[157] $[Re(OH_2)_3(CO)_3]^+$ is of highest importance due to its chemistry, paralleling the one of its prominent ^{99m}Tc counterpart.[112, 155, 156] The structural and synthetic chemistry of low valent 4d and 5d elements is similar, wherefore rhenium complexes are often taken as models for technetium complexes. They differ, however, in their kinetic properties whereas thermodynamic properties such as redox potentials are very similar. A common feature among the group 7 triad complexes $[M(OH_2)_3(CO)_3]^+$ is the lability of the water ligands. This lability contrasts the high inertness of the CO ligands.[18] Indeed, a literature survey reveals that the CO ligands rarely exchange by entering ligands in $[Re(OH_2)_3(CO)_3]^+$ or its ^{99m}Tc homologue. Only in organic solvents and under high temperature conditions, replacement of one CO by other ligands was reported.[158-161] In contrast, the water exchange kinetics in $[M(OH_2)_3(CO)_3]^+$ for all group 7 elements has been studied extensively by Merbach et al., our own group and others.[162-167] A detailed review of the respective literature was presented by Helm et al.[143] The method of choice for these investigations was NMR spectroscopy, which allowed for a quantitative determination of exchange rate constants, spanning 15 orders of magnitude.[168] Isotopically enriched

ligands, such as $H_2{}^{17}O$, further enhance the sensitivity and applicability of this technique. While the water ligands found much attention, the exchange of CO ligands was only of scarce interest, if ever. In *fac*-$[^{99}Tc(CO)_3(H_2O)_3]^+$, the three ^{12}CO ligands could be exchanged for ^{13}CO under 44 bar within 35 h, resulting in all complexes $[^{99}Tc(OH_2)_n(^{13}CO)_{6-n}]^+$ (n=3-6). CO exchange was shown to be up to three orders of magnitude slower than the substitution of H_2O.[169] In order to obtain best reaction conditions for radiopharmaceuticals, it is of fundamental interest to elucidate in detail similarities and/or differences in the chemical behaviour between the common rhenium and technetium starting materials.

The behaviour of the CO ligands is of particular interest since the option of replacing them would lead to new classes of building blocks for molecular imaging agents. In that respect, rates and mechanisms of CO self-exchange rates are basic. Herein, we report an in depth investigation into self-exchange kinetics of the CO ligands in $[ReBr_3(CO)_3]^{2-}$ and its solvato complexes. Beside kinetic rates, we found $[ReBr_2(CO)_4]^-$ as a surprisingly stable intermediate, which could be isolated and fully characterized. High-level theoretical calculations and kinetic simulations support the proposed self-exchange mechanism as deduced from the kinetic measurements.

Results and Discussion

Solution behaviour of $[NEt_4]_2[ReBr_3(CO)_3]$. Upon dissolution of $[NEt_4]_2[ReBr_3(CO)_3]$ in coordinating solvents, up to four (Scheme 22, **1a-1d**) species are potentially present, according to the binding strength of the solvent and the anion respectively. For “strong solvents” such as H_2O or acetonitrile, one might expect the exchange of all halides, which is not the case as shown later (vide infra). Although **1a-1d** could be detected and differentiated by ^{13}C NMR, this has not been done before by this method to the best of our knowledge. Structures **1a** and **1d** for example exhibit equivalent carbonyl carbons, which results in a single peak in ^{13}C NMR for each complex. For each complex **1b** and **1c**, a two-peak pattern with a relative integral intensity of 2:1 should be observed (Scheme 22). In case of one single signal in the ^{13}C NMR spectrum, precipitation of Br^- in **1a** and eventual signal shift will then allow to discriminate between **1a** and **1d**. The ^{13}C NMR of a concentrated sample of $[NEt_4]_2[ReBr_3(CO)_3]$ in weakly coordinating, deuterated DMF depicted two peaks at 200.4 and 195.0 ppm (red

spectrum in Figure 17), a pattern indicative for **1b** or **1c**. Refluxing $[Re(CO)_5Br]$ in DMF overnight must yield only compound **1c** (blue spectrum in Figure 17) after cleavage of two CO ligands due to the *cis*-influence of the axial Br^-.[170] The ^{13}C NMR spectrum shows two peaks at 198.0 and 193.1 ppm. By comparing the two spectra and taking the integral of the coordinated solvent peak into account, it is evident that dissolution of $[NEt_4]_2[ReBr_3(CO)_3]$ in DMF leads to the exclusive formation of **1b**.

Scheme 22. Compounds in equilibria upon dissolution of $[NEt_4]_2[ReBr_3(CO)_3]$ in DMF.

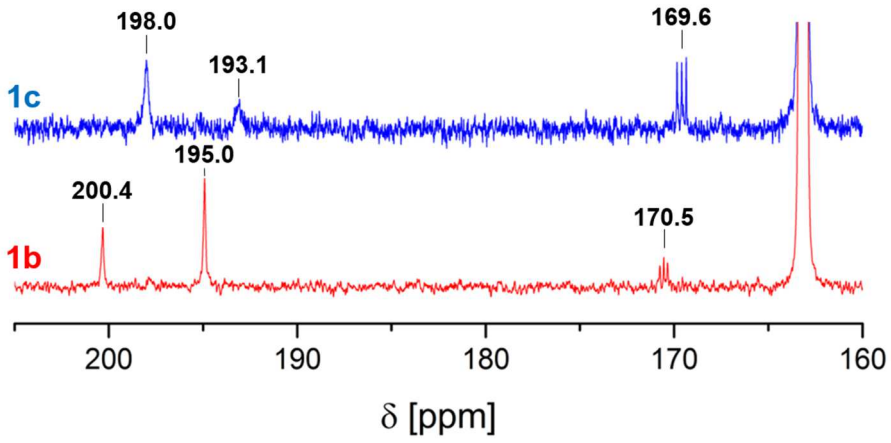

Figure 17. ^{13}C NMR spectrum of **1c** (blue, 120 mM, 300 K) and **1b** (red, 177 mM, 300 K) in d^7-DMF (163.15 ppm).

In stronger coordinating solvents such as methanol (CH_3OH), the equilibrium is shifted towards **1c** upon dissolution of $[NEt_4]_2[ReBr_3(CO)_3]$. Dissolving $[NEt_4]_2[ReBr_3(CO)_3]$ in CD_3OD, the ^{13}C NMR spectrum evidenced the di-solvated $[ReBr(HOCH_3)_2(CO)_3]$ and to a very minor extent the mono-solvated $[ReBr_2(HOCH_3)(CO)_3]^-$ (Figure 107). In acetonitrile (d^3-MeCN), we unambiguously identified only the mono-solvated complex $[ReBr_2(NCMe)(CO)_3]^-$ (Figure 108). This contrasts previous reports which described the formation of $[Re(NCMe)_3(CO)_3]^+$ in this solvent without previous precipitation of the bromides.[171]

Synthesis and Characterization of $[NEt_4][ReBr_2(CO)_4]$. A solution of $[NEt_4]_2[ReBr_3(CO)_3]$ in d^7-DMF, containing $[ReBr_2(DMF)(CO)_3]^-$ (**1b**) as major

constituent, was bubbled with ^{13}CO at room temperature. The ^{13}C NMR spectrum showed the rapid formation of a single new peak at 187.9 ppm within minutes (solvated ^{13}CO in DMF: 185.4 ppm; Figure 110). The signals of **1b** disappeared or were not detectable anymore due to low concentrations. When the solution was left standing for several days at r.t. or was heated to 310 K for 4 hours, three more peaks appeared at 187.1, 195.0 and 200.4 ppm. The latter two peaks are identical to the ones of previously described **1b** by comparison of chemical shifts and relative integrals. Clearly, a new compound formed under the presence of ^{13}CO and at the same time ^{12}CO in the original **1b** did exchange for ^{13}CO in a statistical distribution, making **1b** "visible" in the ^{13}C NMR spectra. If the solution was left to equilibrate, the peak at 187.1 ppm eventually reached the same integral as the one at 187.9 ppm.

A concentrated solution of $[NEt_4]_2[ReBr_3(CO)_3]$ in DMF was kept with stirring for a week in a sealed flask under 1 atm ^{13}CO to determine whether the peaks at 187.9 and 187.1 ppm belong to the same species. This yielded a mixture of compounds with high ^{13}CO abundance (blue spectrum, Figure 18).

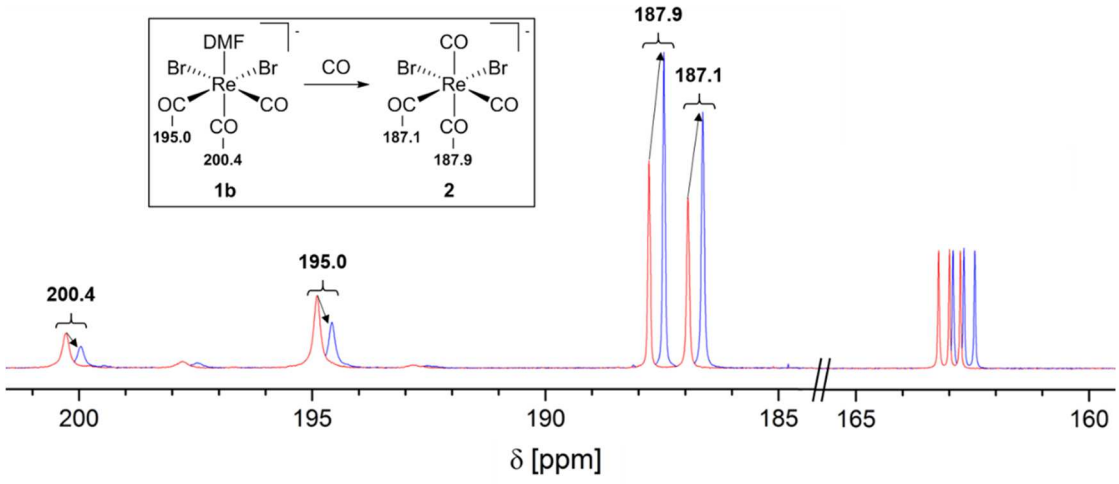

Figure 18. ^{13}C-NMR of ^{13}CO enriched **1b** and **2** before (red) and after (blue) addition of further ^{13}CO (DMF-d^7, 100 mM, 300 K). Peaks at 163 ppm correspond to d^7-DMF.

After removal of $^{13}CO/^{12}CO$ from the head space, a second exposition of this solution to fresh ^{13}CO resulted in a rapid and simultaneous decrease of the two peaks belonging to **1b** by 50 % (200.4 and 195.0 ppm), while the other two peaks of the so far unknown compound at 187.1 and 187.9 ppm increased simultaneously (red spectrum, Figure 18). The equal rate of appearance of these two peaks strongly suggests that

they belong to the same species. The integral ratio of 1:1 points towards the formation of a complex comprising the $[Re(CO)_4]^+$ core with two pairs of equivalent CO's. To corroborate this hypothesis, a solution of $[NEt_4]_2[ReBr_3(CO)_3]$ in DMF was continuously bubbled with ^{12}CO for 6 h. The infrared spectrum of the white solid obtained after removal of the solvent showed four strong vibration bands (2110, 1995, 1968 and 1909 cm^{-1}, Figure 109) in the CO region. The pattern and the relative intensities are in good agreement with those expected for an octahedral complex of C_{2v} symmetry for which examples with rhenium have been reported in literature.[172-175] As a confirmation, single crystals suitable for X-ray diffraction analysis could be obtained by slow evaporation of a DMF solution of $[NEt_4]_2[ReBr_3(CO)_3]$ with a stream of CO gas. An ORTEP of $[NEt_4][ReBr_2(CO)_4]$ (**2**) is depicted in Figure 19 and affirms the conclusions from the NMR experiment (see also Table 11-12).

Although one would expect one of the two trans-coordinating CO ligands to be easily released, complex **2** showed surprisingly high stability. Even after 4 weeks in DMF at room temperature, only trace amounts of **1b** formed as evident from the ^{13}C NMR spectrum (Figure 111). We note that the observation of a very slow CO release from **2** to form **1b** is of particular importance for the deduction of the mechanism and the interpretation of kinetic data (vide infra). The rapid coordination of CO to **1b** to form **2** does not follow a general pattern since the fully solvated complex **1d** did not coordinate additional CO ligands in solution, both at 274 K and at r.t (Figure 112). This suggests a cooperative role of the equatorially bound bromide ligands, crucial for stabilization of **2** as will be described later in the kinetic studies.

^{99}Tc behaves distinctly different from rhenium. We did not observe the formation of homologous complexes with ^{99}Tc, e.g. the formation of $[^{99}TcCl_2(CO)_4]^-$ when starting from $[^{99}TcCl_3(CO)_3]^{2-}$ in DMF under else identical reaction conditions. For assessing if the cooperative behaviour of Br^- would make the difference between ^{99}Tc and Re, the three Cl^- of $[^{99}TcCl_3(CO)_3]^{2-}$ in DMF where precipitated with $Ag[PF_6]$ to form $[Tc(CO)_3(DMF)_3]^+$ and 3 eq. of $[NEt_4]Br$ were then added to have the same conditions as with rhenium (Figures 113 - 115). While the rhenium complex **2** forms very rapidly (vide supra), no such reaction was observed for ^{99}Tc, even under constant CO flow (~ 1 atm) for extensive time periods. ^{99}Tc and Re therefore behave clearly different,

which is rather uncommon for such simple reactions of 4d and 5d complexes in low valencies.

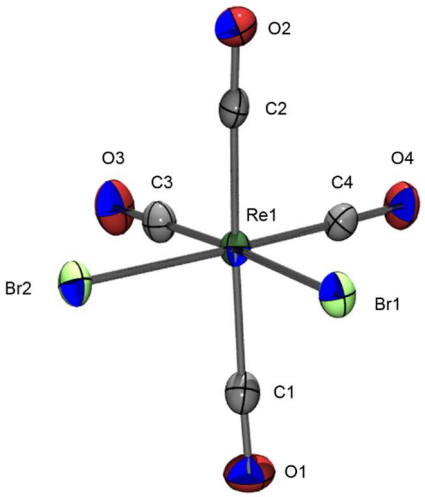

Figure 19. Crystal structure of $[ReBr_2(CO)_4]^-$ **2** ($[NEt_4]^+$ cation omitted for clarity). Ellipsoids are drawn on the 50 % probability level. Important bond lengths (Å) and angles (°) are: Re1-C1 2.011(3), Re1-C2 1.983(3), Re1-C3 1.914(4), Re1-C4 1.900(3), Re1-Br1 2.6200(4), Re1-Br2 2.6395(3), Br1-Re1-Br2 88.906(10), C1-Re1-C2 171.08(13).

Formation kinetics of $[NEt_4][ReBr_2(CO)_4]$. We chose DMF as solvent since the solubilities of $[NEt_4]_2[ReBr_3(CO)_3]$ and ^{13}CO are reasonably good in this solvent (for CO around mM levels). After dissolution, the starting material is exclusively present as **1b** (vide supra), facilitating the interpretation of the ^{13}C NMR data. Complex **2** forms rapidly in DMF when exposed to ^{13}CO. The new peak evolving at 187.9 ppm corresponds to the ^{13}CO ligand coordinated trans to another CO ligand in **2**. Since no other signals appeared on the same time scale, we conclude, that the entering ^{13}CO replaces the originally coordinated DMF ligand in **1b** and not a Br^-. Simultaneously, the formation kinetics of **2** can be quantified by monitoring the disappearance of the signal of dissolved ^{13}CO. An NMR spectrum of ^{13}CO dissolved in DMF is shown in Figure 110. Since all subsequent “isomerization“ reactions are slow in comparison to this initial formation step of **2**, its kinetics can be analyzed separately. We studied the rate of formation under *pseudo* first-order conditions with **2** in excess over ^{13}CO. A precise concentration of **1b** altered over a certain range (based on **1a**) is obtained simply by weighing corresponding mass amounts into solution. The ^{13}C NMR experiments were

performed at 274 K as the reaction was otherwise too fast for obtaining a satisfactory signal-to-noise ratio by ^{13}C NMR. The integrals of the peaks at 185.4 ppm (^{13}CO) and 187.9 ppm (**2**) were plotted against time and fitted to a 1st order exponential. Figure 20 illustrates a "waterfall" plot, showing the disappearance of free ^{13}CO and the rise of the signal of the newly trans-coordinated ^{13}CO. Linear correlation of k_{obs} values vs. concentrations (Figures 116-117 and Table 7) gave a 2nd order rate constant at 274 K k_1 of 0.039 ± 0.001 M^{-1} s^{-1}.

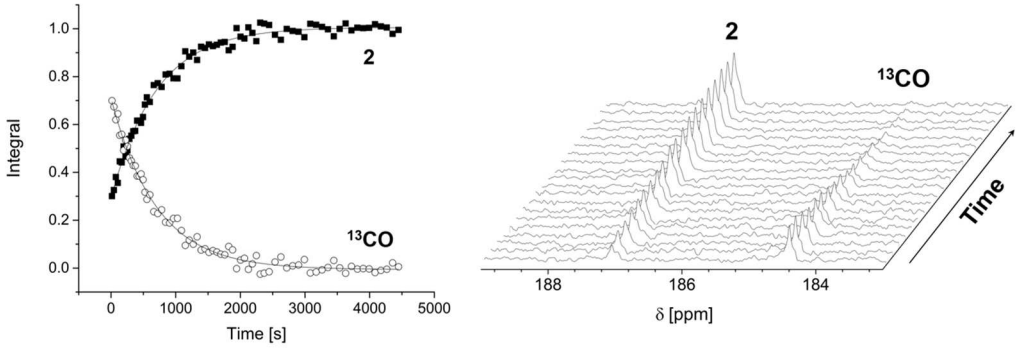

Figure 20. A plot of the time-dependent integrals of **2** (48 mM) and free ^{13}CO (4 mM) and waterfall plot of the ^{13}C NMR spectra, recorded during a typical measurement at 274 K.

The question about the activation mechanism for this relatively rapid substitution of DMF by ^{13}CO is evident. Therefore, an Eyring plot, i.e. the temperature dependence of k_1, was recorded in a range between 274 K and 253 K (Figure 21). The range for these experiments was limited since the rate became too fast on the NMR time scale and solubility of ^{13}CO too low above 274 K. Similarly, the rate became too slow below 253 K. The activation parameters from the Eyring plot are $\Delta H^{\neq}$ = 110 ± 7 kJ mol^{-1} and $\Delta S^{\neq}$ = 127 ± 22 J mol^{-1} K^{-1} (Table 8 and Figure 118). The estimated standard deviations (esd) for the activation parameters are probably underestimated given the fact that the individual kinetic runs show variation with respect to accurate integration. By subjecting this data in total to a global fit, this is indeed confirmed (global fit: $\Delta H^{\neq}$ = 129 ± 23 kJ mol^{-1} and $\Delta S^{\neq}$ = 198 ± 80 J mol^{-1} K^{-1}).[55, 176] The significantly positive $\Delta S^{\neq}$ value is a clear indication for a strong, dissociative activation of the substitution reaction. The activation enthalpy is comparable with work by Bengali *et al.*[55], where the substitution of THF by MeCN in a $LRe(CO)_2$ system was shown to occur via a dissociative-type mechanism.

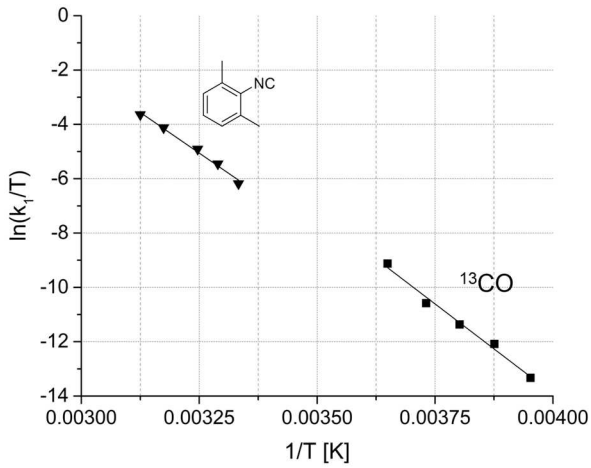

Figure 21. Eyring plot for the reaction of **1b** with CO and Xyl-NC.

The distinctly positive $\Delta S^{\neq}$ value raised the question, if similar entering ligands would behave comparably. Therefore, the kinetics for the reaction of **1b** with 2,6-dimethylphenyl-isocyanide (Xyl-NC), a ligand with comparable electronic properties than CO reaction, was done and the activation parameters for the process were determined. Upon addition of Xyl-NC to a solution of **1b** in DMF, both ^{13}C NMR (Figure 119-120) and subsequent isolation and analysis of the product by single crystals X-ray diffraction evidenced formation of the complex $[NEt_4][ReBr_2(CO)_3(Xyl\text{-}NC)]$ (**4**) (Figure 129, Table 13-14). In these experiments, the formation of **4** could be followed by UV/vis spectroscopy since the spectra of the starting materials **1b** and Xyl-NC differ significantly from the product at 326 nm (Figures 121-122). The same rate law was operative for this substitution process as for the CO exchange (Figure 123 and Table 9). The combined Eyring plots of the two reactions (Figure 21) display a very similar reaction rate and activation parameters ($\Delta H^{\neq} = 99 \pm 6$ kJ mol^{-1} and $\Delta S^{\neq} = 84 \pm 20$ J mol^{-1} K^{-1} for the reaction of **1b** with Xyl-NC, Table 10) within the experimental error margins. By subjecting this data for Xyl-NC as entering ligand to **1b** to a global fit, a marginal variation in values and larger esd's, but still in very good agreement with those listed above, are obtained, ($\Delta H^{\neq} = 93 \pm 8$ kJ mol^{-1} and $\Delta S^{\neq} = 64 \pm 24$ J mol^{-1} K^{-1}). These findings imply that the nature of the entering ligand does not affect the rate significantly but that the dissociation of the solvent is most probably the rate determining elementary step.

A solvent dependence of the rate is expected since the formation of **2** and **4** are accompanied with the dissociation of a solvent ligand. Therefore, the reaction rates for the formation of **2** were also quantified in d^3-MeCN under else identical conditions as in DMF. The 2nd order rate constant k_1 for d^3-MeCN is $0.0056 \pm 0.0007\ M^{-1}\ s^{-1}$ (Figure 124). The reaction rate is slower in MeCN than in DMF. At the same time DMF is a more Lewis basic solvent as expressed, for example, by the donor strength scale (D_S) by Persson *et al.* (MeCN: 12, DMF: 24).[177] This corroborates the influence of the solvent-rhenium bond and supports the previous findings of a dissociatively activated substitution mechanism. However, the observation that the more Lewis basic solvent induces a faster reaction rate suggest an interchange-type of mechanism, where the solvent molecule is still present in the transition state. In D_2O, the solubility of ^{13}CO is very low and a white precipitate formed during the reaction with CO. The IR spectrum of this precipitate was identical to the one of **2** which is essentially insoluble in D_2O. Due to these constraints it was not possible to measure any exchange kinetics in D_2O. Altogether, these experimental data, in particular the strongly positive $\Delta S^{\neq}$ value, are consistent with a dissociative-interchange mechanism.

Mechanism of CO exchange. The observation of rapid ^{13}CO coordination to **1b** does not explain why the ^{13}CO NMR shows, after some time, ^{13}CO also coordinated to the equatorial plane and not only in the *trans*-$[Re(^{13}CO)(CO)]^+$ moiety. The detection of both, enriched **1b** and **2**, after incubation under a ^{13}CO atmosphere at all sites implies that CO "self-exchange" is indeed operative to a significant extent. To elucidate this exchange and its related mechanism in more detail, a solution of **1b** in DMF was bubbled with ^{13}CO at room temperature. Under these conditions, **2** formed rapidly as described above. To account for isostructural complexes but with ^{13}CO at different coordination sites, we will use henceforth numbers extended with characters according to Scheme 23, thus, complex cis,trans-$[ReBr_2(^{13}CO)(CO)_3]^-$ **2** with a ^{13}CO in the axis becomes **2a**.

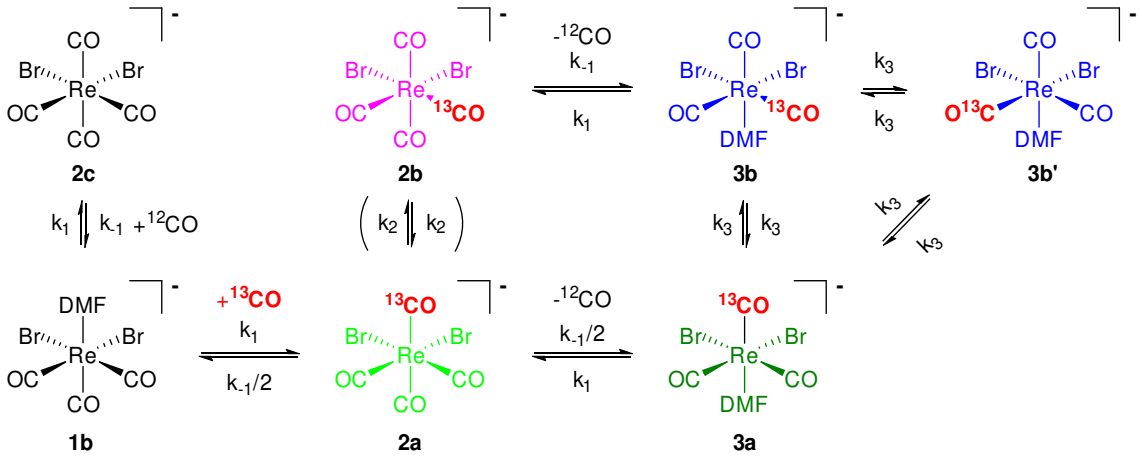

Scheme 23. Proposed model for the ^{13}CO exchange and accumulation in **1b**. Note that all complexes "**2**" and "**3**" are isostructural but the extensions "**a**" and "**b**" indicate ^{13}CO in positions with distinguishable ^{13}C NMR shifts.

After formation of **2a**, the solution was heated to 310 K and the changes monitored by ^{13}C NMR. Over time, the peak at 187.9 ppm (**2a**) decreased in intensity while three new peaks appeared at 200.4, 195.0 and 187.1 ppm (Figure 22).

Due to the excess of **1b** present at the time of the ^{13}CO addition (*pseudo* first-order conditions in [Re]), only one molecule of ^{13}CO is bound to the rhenium complexes at all time points for statistical reasons. Starting from **1b**, **2a** (187.9 ppm) forms in the first, rapid step, and three subsequent reactions can take place (Scheme 23). To prevent free CO diffusing out of the solution into the headspace, Shigemi stoppers were applied which reduce the surface area of the solvent significantly.

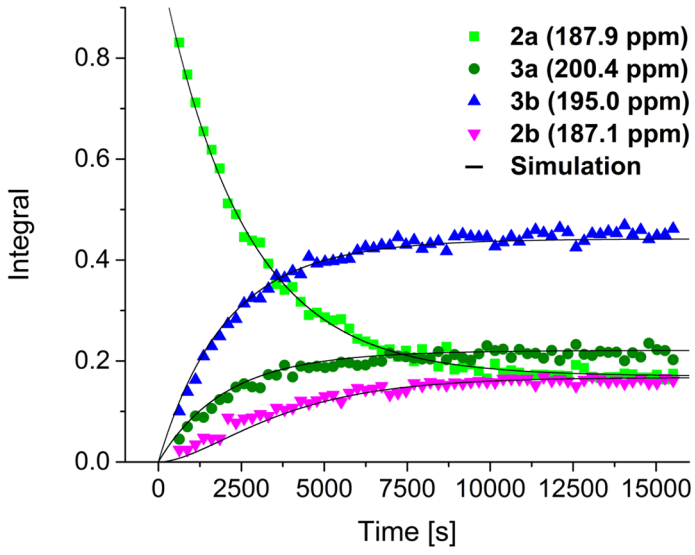

Figure 22. Time dependent change of the integrals of all species **1b** in d^7-DMF after ^{13}CO addition and upon heating to 310 K over time. Superimposed is the KinTek[178] simulation of the proposed model which corresponds to the elementary reactions depicted in Scheme 2.

In a first possible subsequent reaction, one of the two axial CO ligands is re-substituted by a solvent molecule, i.e. back reaction to **1b** or to the isostructural **3a**, containing only one ^{13}CO. Since these processes denote the same reactions, both occur with a rate constant of k_{-1} (not considering isotope effects, which are too small to be observed here). If the ^{13}CO is released in this step, **1b** is formed and the liberated ^{13}CO will rapidly react with another **1b** (in excess) to re-form **2a**. If, on the other hand, the axial ^{12}CO is replaced by a DMF molecule in this step, species **3a** forms, comprising of one ^{13}CO trans to the DMF. A signal at 200.4 ppm (Figure 17) appears, indicative for **1b** but now detectable with much higher sensitivity due to enrichment in ^{13}CO. If these reactions were the only ones to occur, we should observe a decrease of the signal at 187.9 ppm and an increase of the signal at 200.4 ppm exclusively. We note at this point that an exchange of the equatorial CO or bromide ligands would break the symmetry of the molecule and affect the signal patterns in ^{13}C NMR. Since we have found no evidence for this direct exchange of equatorial CO or bromide ligands under our conditions, we excluded this pathway from our interpretation. Starting from **2a**, an equatorial ^{12}CO and the axial ^{13}CO could change their sites with k_2 to form **2b**. The peak at 187.1 ppm accounts for this complex. In complex **3a**, the ^{13}CO trans to the DMF could exchange its position for a ^{12}CO trans to a bromido ligand with k_3 as rate constant to form **3b**, accounting for the peak at 195.0 ppm. The experimental data in Figure 22 show that the peaks of **3a** and **3b** appear first and maintain a 2:1 ratio throughout the reaction. This indicates that the replacement of the ^{13}CO from trans-DMF to trans-Br^- and vice-versa is much faster than the reaction from **2a** to **3a** (i.e. $k_3 >> k_{-1}$). By recording ^{13}C NMR spectra of a ^{13}C enriched mixture of **1b** and **2** at variable temperatures, the coalescence temperature for the exchange of **3a** and **3b** was found to be 350 ± 5 K (Figure 23). The rate constant k_3 was determined to be approximately 75 s^{-1} at 310 K, corresponding to a Gibbs energy of activation $\Delta G^{\neq} = 65 \pm 1$ kJ/mol.

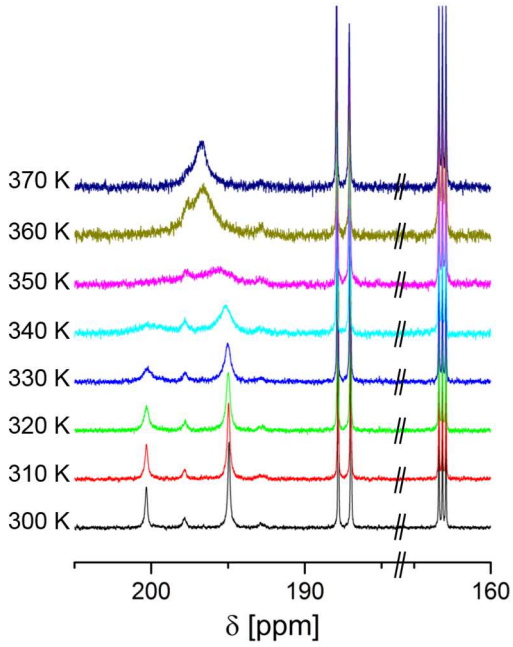

Figure 23. ^{13}C NMR spectra of ^{13}CO enriched **1b** and **2** at different temperatures (DMF-d^7, 100 mM).

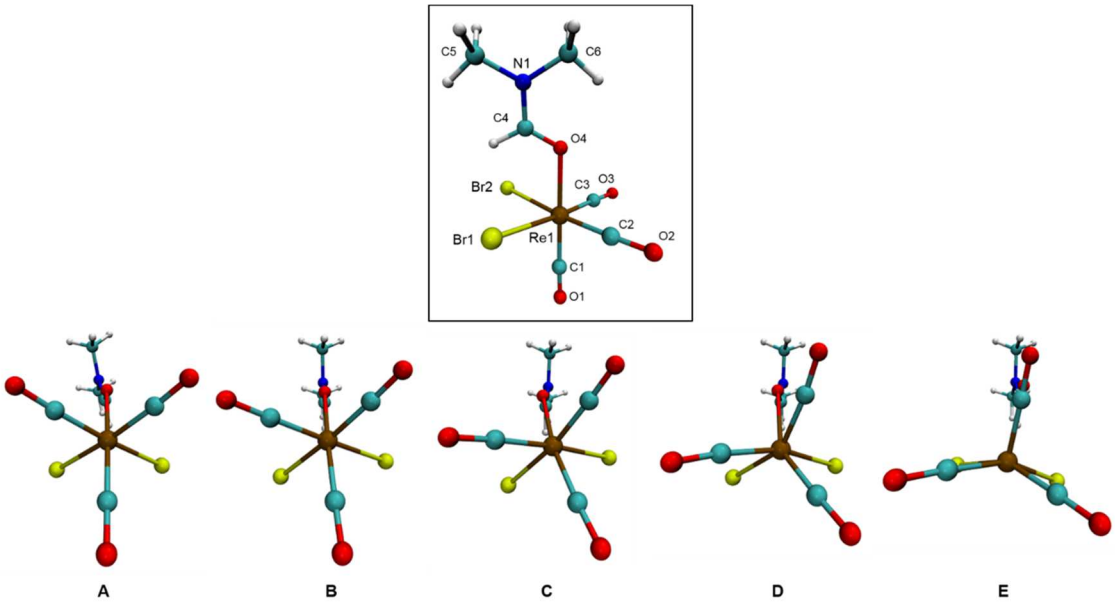

Figure 24. Optimized calculated structure of $[ReBr_2(DMF)(CO)_3]^-$ (top). Five (**A**-**E**) out of eight calculated intermediates from the NEB calculations performed to obtain the minimum energy path for the rotation in **3** (bottom).

We propose a rotation around the C_3 axis as a potential mechanism, formed by the rhenium center and the centroid of the plane formed by the three CO oxygen atoms as mechanism for **3a** - **3b** interconversion with a trigonal prismatic transition state

(Figure 24). In an attempt to support this mechanism by theory, we have performed DFT calculations (see experimental section). Eight intermediate structures (Figure 24) for a rotation in **3**(**a**/**b**) as described before were optimized to obtain a minimum energy path to the transition state (Structure **E**, Figure 24). The resulting Gibbs free energy of activation was found as $\Delta G^{\neq}$ = 56 ± 1 kJ/mol. Taking the restraints of these calculations, such as the molecule in vacuum and the limitations of DFT into account, the agreement with the experimental value $\Delta G^{\neq}$ = 65 ± 1 kJ/mol is very good and supports the hypothesis of rotation as the fundamental mechanism. It is important to note that the calculations also showed that the Re-DMF bond length is significantly elongated in the transition state E compared to the ground state (Figure 130) providing further evidence for a dissociative-interchange type mechanism for the substitution of DMF via the same transition state. For comparison, the same calculations have been performed for a rotation between **2a** and **2b** which interconverts a ^{13}CO trans to CO into the isostructure with ^{13}CO trans to a Br^- (Figure 125). The lack of a coalescence point in a ^{13}C NMR experiment between **2a** and **2b** up to 383 K (Figure 126) shows that this rotation has a significantly higher activation barrier. Indeed, the calculated value for $\Delta G^{\neq}$ = 117 ± 1 kJ/mol reveals that this rotation is a very slow, if active at all pathway at 310 K. Taken together, experimental values for both k_1 (by extrapolation of k_1 from 274 K to 310 K) and k_3 (from the variable temperature NMR experiments) could be obtained separately. The absence of a coalescence point at 383 K and the very high calculated $\Delta G^{\neq}$ indicate that k_2 is very small at 310 K and does not compete with the k_1 and k_3 pathways. By restraining our proposed model (Scheme 23) with these experimental values, the data points were fitted in KinTek™ Explorer.[178] The obtained simulated traces match the experimental data well (Figure 23) and gave a k_{-1} of 6.9 ± 0.3 × 10^{-4} $M^{-1}s^{-1}$. In agreement with this, the plot of k_{obs} vs [Re] obtained an intercept very close to zero (Figure 116 and 123). ^{13}C enriched CO allowed an in-depth look at the mechanism of CO exchange in the $[Re(CO)_3]^+$ system. Under conditions in which ^{13}CO is present in excess over starting material **1b**, the enrichment and rearrangement process would occur via continuous “cycling” between complexes **2a** and **2b** and **3a**-**3b’** species and is hence rate limited by the reverse reaction rate k_{-1}.

Conclusion

Our studies on CO exchange mechanisms and kinetics in $[ReBr_3(CO)_3]^{2-}$ in DMF showed a surprisingly high affinity for CO with the concomitant formation of the stable tetra-carbonyl complex $[NEt_4][ReBr_2(CO)_4]$ at room temperature. $[NEt_4][ReBr_2(CO)_4]$ was characterized by ^{13}C NMR, IR spectroscopy and X-ray crystallography. In experiments with $[^{99}TcCl_3(CO)_3]^{2-}$ in DMF, the behaviour was different and no evidence for the formation of $[^{99}TcCl_2(CO)_4]^-$ was obtained. Even when exchanging the chloride ligands for bromide, no tetra-carbonyl complexes formed. This distinct difference is unusual for Re^I/Tc^I since the two centers are often described as a matched-pair. Co-ligands influence substitution reactions as the two bromido ligands in **1b** are essential as no reaction with CO is observed in **1d**. Considering the experimentally determined activation parameters, the slower reaction rate in the less Lewis basic solvent MeCN and the invariance of k_{obs} with regard to the entering ligand, a dissociative-interchange type mechanism is most likely. Isotopically enriched ^{13}CO gas combined with DFT calculations enabled a comprehensive elucidation of the CO exchange mechanism in this system by ^{13}C NMR spectroscopy. The slow release of the CO ligand from **2** suggests it as a potential CO releasing molecule. Finally, the newly obtained $[NEt_4][ReBr_2(CO)_4]$ represents an interesting new symmetrical synthon for further coordination compounds.

3.5.3 Outlook

The availability of ^{13}CO enriched rhenium precursors opens up the possibility to study, in detail, very basic reaction mechanisms of these complexes with different ligands via ^{13}C-NMR. This technique is solvent-independent, possible on vast time and temperature scales and the reaction partners do not need to be labelled in any way. Investigations of this type are planned in collaboration with the group of Prof. Andreas Roodt at the University of the Free State in South Africa.

The in-depth understanding into the CO exchange behavior of the rhenium tricarbonyl synthon gained in this work has led to a fruitful collaboration with the group of Prof. Peter Hamm at the University of Zurich. By using ^{13}CO enriched $[NEt_4][ReBr_2(^{13}CO)_4]$, it was possible to prepare a known CO_2-reduction catalyst and adsorbed on a semiconductor surface. The ultrafast vibrational energy transfer between ^{13}CO-enriched and natural ^{12}CO containing complexes on the surface was then investigated by 2D-IR spectroscopy. The results of this study have resulted in a joint publication.[179] Further experiments with $^{13}C^{18}O$ enriched complexes are currently underway.

Part D: Synthesis and Characterization of Multi-Nuclear, ^{99m}Tc-containing Complexes

3.6 Pre-assembly and Self-assembly of Multinuclear Re-^{99m}Tc Complexes

3.6.1 Preface

Metal complexes containing multiple, equal or different metal centers have been known for a long time. However, in the context of nuclear imaging they have only seldom been investigated. In our continued collaboration with the Roodt group in South Africa we have studied a series of dinuclear manganese and rhenium complexes with Schiff-base ligands.[180] In a next step both ^{99}Tc and ^{99m}Tc were incorporated into dinuclear complexes with rhenium. A similar approach with simple hydroxy-clusters led to two distinct strategies when preparing radioactively labelled multi-nuclear complexes. This work led to the submission of the following manuscript.

3.6.2 Manuscript

Self-Assembled Multi-Nuclear Complexes Incorporating ^{99m}Tc

Angelo Frei,[a] Pennie P. Mokolokolo,[b] Robin Bolliger,[a] Henrik Braband,[a] Mampotso S. Tsosane,[b] Alice Brink,[b] Andreas Roodt,*[b] and Roger Alberto*,[a]

Abstract

Multinuclear complexes or clusters are rarely investigated in medicinal inorganic chemistry although they represent structural intermediates between molecules and nanomaterials. We present in this report two strategies towards ^{99m}Tc containing clusters. In a pre-assembly approach, the preformed but incomplete cluster fragment $[Re_3(\mu_2\text{-}OH)_3(\mu_3\text{-}OH)(CO)_9]^-$ reacts with a $[^{99m}Tc(CO)_3]^+$ to the highly stable $[^{99m}TcRe_3(\mu_3\text{-}OH)_4(CO)_{12}]$ cube. The same structure self-assembles when reacting the mono-nuclear Re and ^{99m}Tc precursors in one pot. Integrating the coordinating OH groups from Schiff bases in this concept leads straight to dinuclear, mixed-metal complexes of the type $[^{99m}TcRe(\mu_2\text{-}O\text{^}N\text{-}R_1)_2(CO)_6]$ in quantitative yield. Both strategies are unprecedented and open a future path towards clusters, incorporating a ^{99m}Tc radiolabel while being decorated with targeting or cytotoxic moieties.

Introduction

Research in medicinal inorganic chemistry is focused on mononuclear organometallic complexes or coordination compounds.[181-184] Their mode of action is often metal-based as in the prototypical case of cisplatin, the inspiring lead compound for many current studies. Ligand-based reactivity or, more recently, recognition of the entire complex structure according to the 3D-space occupation are conceptual extensions in this field. For the latter modality of action, the complex is chemically innocent and designed as an inhibitor for specific receptors. The topology and the functional groups mimic pharmaceutical lead structures of known activity as in the case of e.g. ferrocifen, ferroquine or protein kinase inhibitors of the staurosporine type.[185-192] Whereas most of these metal-containing drugs are based on group 8, 9 or 10 elements,[193] complexes of group 7, the manganese triad, are rarely investigated. It has recently been pointed

out that the respective chemistry is not explored to a sufficient extent and the potential behind rhenium complexes might be much brighter than previously assumed.[184, 194] Since technetium is a group 7 element, the unique possibility of combining cytotoxic, rhenium-based complexes with ^{99m}Tc molecular imaging agents of identical structure emerges. This gave rise to a new concept of molecule-based theranostics, macroscopic amounts of rhenium complexes for therapy and microscopic amounts of ^{99m}Tc homologues for diagnosis. This homology holds especially true for the low valences of the two elements in which highly robust complexes are formed. We showcased this principle recently with carbonic anhydrase inhibitors and mitochondria targeting agents.[195, 196]

A class of compounds which is rarely considered in medicinal inorganic chemistry are clusters or multinuclear compounds. An exception to this observation are polyoxometalates (POMs), which are studied for nanomedicine purposes.[197] In the context of this report, we understand clusters as polynuclear compounds in which two (or more) metal-cations are bridged by a single atom, e.g. an oxygen, which may belong to a larger ligand framework or not, and compounds with metal-metal bonds. The complexity of their syntheses might be one of the reasons for the little interest in multinuclear compounds but also the expected and even more diverse *in vivo* behaviour.

Apart from the POMs, examples have been reported, mainly with Rh_2 species exhibiting a Rh^{II}-Rh^{II} single bond,[198-200] supramolecular Ru-arene complexes[201-204] and mixed Pt-Re systems.[205, 206] Multinuclear complexes have the advantage of delivering more than one metal or bioactive moiety at a time from the coordination periphery to the target, once bound to the corresponding receptor. The difficulty is to achieve a well-defined composition and the integration of a targeting/bioactive entity. With respect to the aforementioned theranostic concept, non-invasively following the biological behaviour of such clusters or multinuclear compounds by integrating a radioelement, would be a decisive advantage. This radioelement can be an isotope of the cluster forming element or belong to the same triad as in case of ^{99m}Tc and Re. To

prepare multinuclear complexes comprising a radionuclide of the same or homologous elements, two principal pathways are compatible with a potential application on a routine base: i) preparation of an incomplete fragment of the final, multinuclear complex

followed by introduction of the radiolabel in a second step (pre-assembly strategy, path A in scheme 24) or ii) combine all components and perform the synthesis in one step (self-assembly strategy, path B in scheme 24).

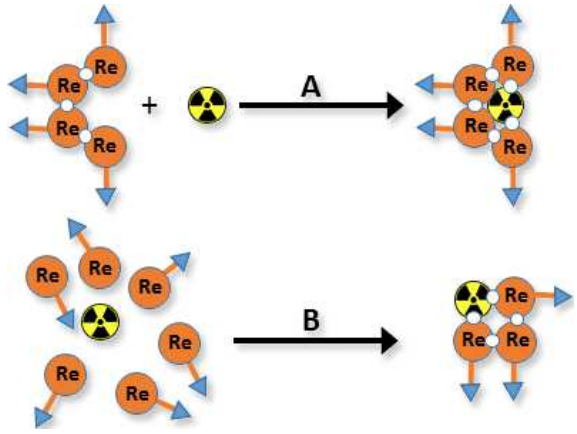

Scheme 24. Strategies to multinuclear complexes comprising ^{99m}Tc: Pre-assembling of an incomplete cluster followed by incorporation of a ^{99m}Tc fragment (Pathway A) or self-assembling of a multinuclear cluster starting from mononuclear components and ligands (Pathway B). The blue arrows indicate a bioactive moiety.

We report here on model reactions for both concepts, showing the proof-of-concept of preparing multinuclear complexes labelled with ^{99m}Tc. In a targeting scenario, both approaches allow to combine multiple targeting and/or cytotoxic agents on one single multinuclear metal complex, thereby increasing their mode of action, target finding and/or drug delivery.

Results and Discussion

The introduction of a fragment into an incomplete multinuclear framework according to path A demands a sequential relationship between precursors and final products. Such a relationship is given by the build-up of the tetranuclear complex $[Re_4(\mu_3\text{-}OH)_4(CO)_{12}]$ with cubane-like structure. Under mildly basic conditions, this tetranuclear compound forms stepwise from the precursor *fac*-$[Re(OH_2)_3(CO)_3]^+$ (**1**) via $[Re_2(\mu_2\text{-}OH)_3(CO)_6]^-$ (**2**) and $[Re_3(\mu_2\text{-}OH)_3(\mu_3\text{-}OH)(CO)_9]^-$ (**3**) or from the ^{99}Tc homologues (Scheme 25).[166, 207, 208] Similar multinuclear complexes were also obtained with alcoholato or thiolato bridges.[209-211]

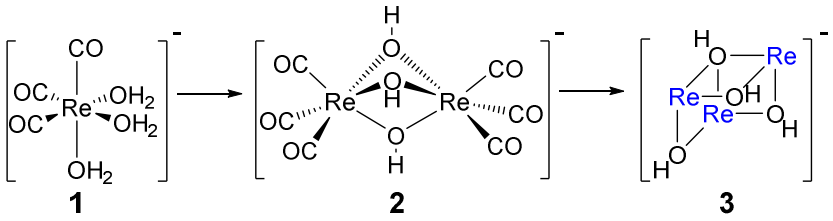

Scheme 25. Stepwise build-up of the trinuclear cluster $[Re_3(\mu_2\text{-}OH)_3(\mu_3\text{-}OH)(CO)_9]^-$ (**3**). The pre-assembly leaves a vertex for coordination to ^{99m}Tc. "Re" denominates the *fac*-$[Re(CO)_3]^+$ fragment.

As we understand multinuclear complexes in this report, the metals are bridged by single atoms, potentially bound to further organic functions, coordinating or just pendent. For the *fac*-$[Re(CO)_3]^+$ fragment, this might be an oxygen from an alcoholato group or a sulfur from a thiolate, from μ^2- or μ^3-O/SR motives. Since weakly coordinating as terminal donors, they exhibit a tendency to bridge to further metal-centres, thereby forming multinuclear clusters with a single atom bridge. Incomplete clusters such as $[Re_3(\mu_2\text{-}OH)_3(\mu_3\text{-}OH)(CO)_9]^-$ are therefore prone to coordinate to further metal centres or complex fragments and may be labelled with ^{99m}Tc.

The reaction of the incomplete, separately prepared Re_3 cluster **3** with the ^{99m}Tc precursor *fac*-$[^{99m}Tc(OH_2)_3(CO)_3]^+$ according to pathway A in Scheme 24 (pre-assembly approach) should lead to a cubane cluster incorporating ^{99m}Tc. The missing vertex is filled with the *fac*-$[^{99m}Tc(CO)_3]^+$ fragment (or another metal) to complete the cube. It has been reported earlier that **3** can be considered as a tripod ligand with the bridging three μ_2-hydroxides acting as coordinating groups. Indeed, the trinuclear cluster **3** coordinates to many 3d aqua-cations such as Co^{2+} Mg^{2+}, Ca^{2+}, Fe^{2+}, Ni^{2+}, and others.[212] Two of the clusters provide an octahedral environment and coordinate securely to the corresponding M^{2+}. Completing the cube with the $[M(CO)_3]^+$ moiety yields the extremely stable cubane complex $[Re_4(\mu_3\text{-}OH)_4(CO)_{12}]$ (**5**).

We prepared $[Re_3(\mu_2\text{-}OH)_3(\mu_3\text{-}OH)(CO)_9]^-$ and reacted it with *fac*-$[^{99m}Tc(OH_2)_3(CO)_3]^+$. In a very clean and fast reaction the mixed-metal tetranuclear cluster $[^{99m}TcRe_3(\mu_3\text{-}OH)_4(CO)_{12}]$ (**4**) formed in quantitative yields. HPLC coinjection of the homologues **4** $[^{99m}TcRe_3(\mu_3\text{-}OH)_4(CO)_{12}]$ and **5** $[Re_4(\mu_3\text{-}OH)_4(CO)_{12}]$ and comparing

the UV/vis and gamma-trace retention times confirmed the identity of the two compounds (Figure 25). The feasibility of the pre-assembly concept A is thus confirmed. Since the rhenium cluster **3** is present in large excess relative to the ^{99m}Tc complex (typically in the nanomolar range, 6h half-life time for ^{99m}Tc!), the majority of it is left unchanged after the labelling reaction.

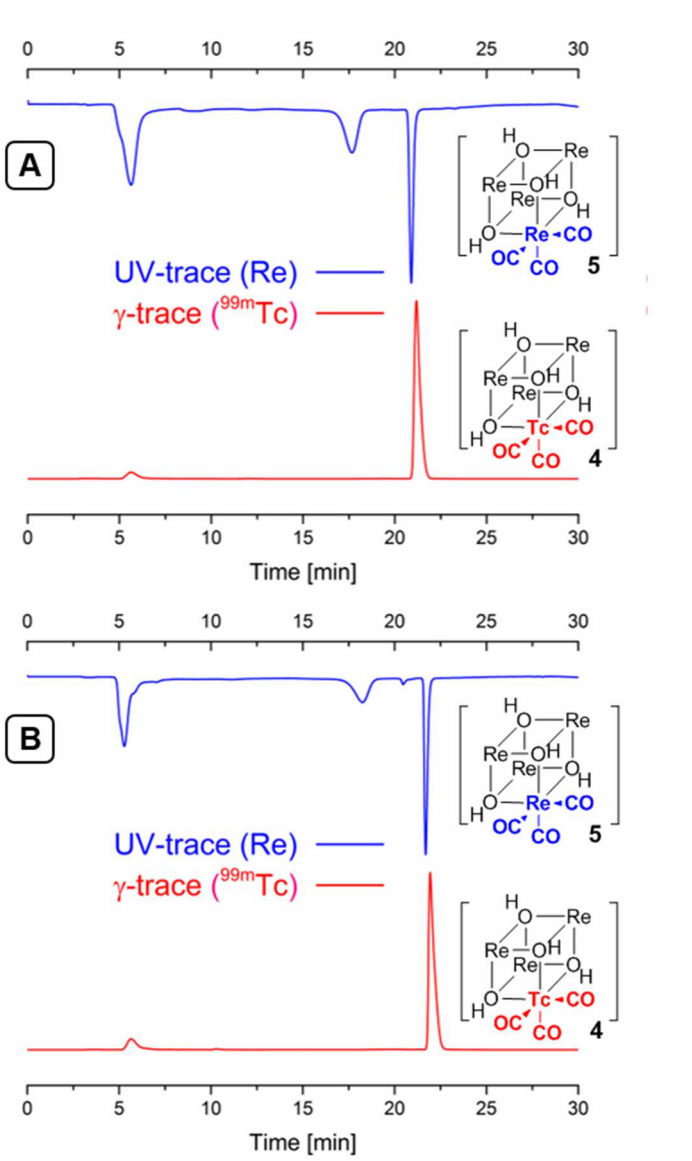

Figure 25. HPLC traces of **4** (γ-detection) and **5** (UV/vis detection) confirm the structural identity of the two homologues and feasibility of pre-assembly strategy **A** (top). *In situ* formation of the same cubane cluster **4** in one step from *fac*-$[Re(OH_2)_3(CO)_3]^+$ and *fac*-$[^{99m}Tc(OH_2)_3(CO)_3]^+$ support self-assembly strategy **B** (bottom).

The tetra-nuclear rhenium cluster **5** and its ^{99}Tc (the long-lived, macroscopic isotope of ^{99m}Tc) homologue form under mildly basic conditions by self-assembly of the mono-nuclear compounds *fac*-[Re(OH$_2$)$_3$(CO)$_3$]$^+$ and *fac*-[^{99}Tc(OH$_2$)$_3$(CO)$_3$]$^+$ respectively.[208, 213] Analogous alkoxy clusters have been prepared along the same route.[214] A self-assembly strategy should thus allow for a one-step one-pot reaction of **4** from a slightly acidic mixture of **1** and *fac*-[^{99m}Tc(OH$_2$)$_3$(CO)$_3$]$^+$. This is indeed the case (Scheme 26 and Figure 25B) and this reaction gave in one step and in quantitative yields **4** beside large amounts of **5** due to the very large excess of **1**. An HPLC trace of the crude reaction mixture (no coinjection with **5**!) is given in Figure 25B. It shows the UV-trace of **5** and the γ-trace of cluster **4**.

Extension of the self-assembly strategy as shown in scheme 26 will enable the introduction of targeting groups or bioactive moieties in such multinuclear clusters. Whereas alkoxides instead of hydroxides are principally possible, we were more interested in hydroxyl ligands with anchoring groups. In this context, Schiff base ligands comprise an aromatic hydroxyl-group which is prone to bridge two complex fragments.

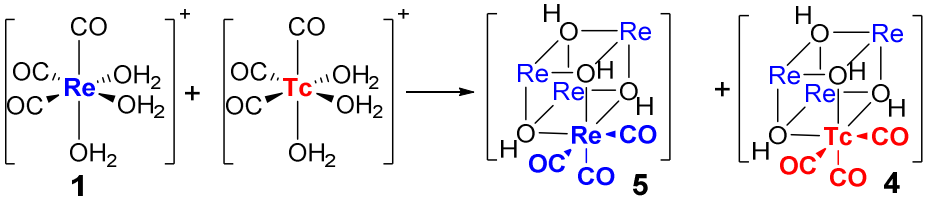

Scheme 26. Self-assembly reaction between the mono-nuclear precursors **1** and its ^{99m}Tc homologue under mildly acidic conditions yields the tetra-nuclear cubane type clusters **4** and **5**. "Re" denominates the *fac*-[Re(CO)$_3$]$^+$ fragment.

In addition, the imine parts of the Schiff bases coordinate as well and are flexible with respect to the nature of the pendent group R$_1$, i.e. they can represent a targeting moiety or another bioactive fragment. When the Schiff bases shown in Scheme 27 reacted with *fac*-[^{99}TcCl$_3$(CO)$_3$]$^{2-}$ in acetonitrile at elevated temperature, we found rapid and essentially quantitative formation of the dinuclear complex [^{99}Tc$_2$(μ$_2$-O^N-R$_1$)$_2$(CO)$_6$] (R$_1$=m-tol **6,** =cpent **7**, =EtPh **8**; R$_2$=H **6**, or Me **7**,**8**). Radio-HPLC showed one single peak after the syntheses (supporting information), and minute amounts of side products. The respective compounds could be isolated and complexes **6**-**8** were characterized by X-ray structure analysis. ORTEP diagrams are shown in Figure 26

and crystallographic details for all complexes are given in the supporting information. All three structures confirm the rigidity of the planar dinuclear frame structure and illustrates the stability induced therein. The agreement of the internal geometric parameters (such as the Tc-Tc' and O1-O1' bond distances, O1-Tc-O1'and O1-Tc-O1'angles, and not the least the Tc-O1-Tc'-O1'-planar entity) is remarkable. This confirms that the only significant variable is the substituents on the peripheral outer-sphere of the dinuclear compound, which is expected to influence the *in vivo* distribution significantly. Depending on the size of the R_n groups, molecular entities in the nanometer range may be easily obtained: for the examples described here, the dimensions of the dinuclear species when measured from the outer hydrogen atoms, already range from R_1-R_1' and R_2-R_2' 1.7 to 1.3 nm.

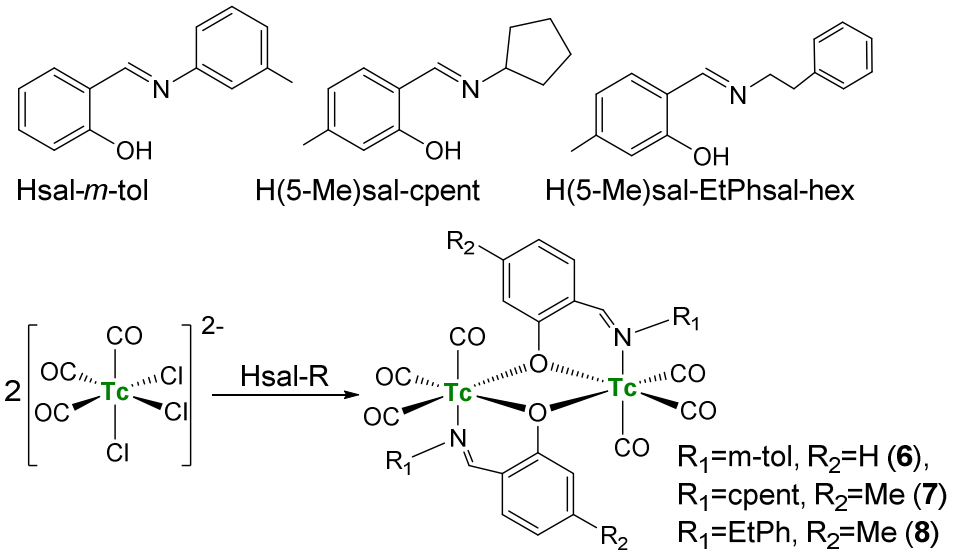

Scheme 27. Three functionalized Schiff base chelators utilized in this self-assembly study (top). Reaction sequence for either of these Schiff bases Hsal-R (bottom). In a typical reaction, $[NEt_4]_2[^{99}TcCl_3(CO)_3]$, the Schiff base ligand and NEt_3 were dissolved in acetonitrile and heated to 80 °C for 3 h.

The course of the reaction is interesting; no mononuclear intermediate was detected during the procedure. Since a mononuclear complex must exist at some stage of the reaction path as an intermediate, we conclude that its dimerization is a very rapid process under our reaction conditions, much faster than the initial coordination of one Schiff base to one $[^{99}Tc(CO)_3]^+$ moiety.

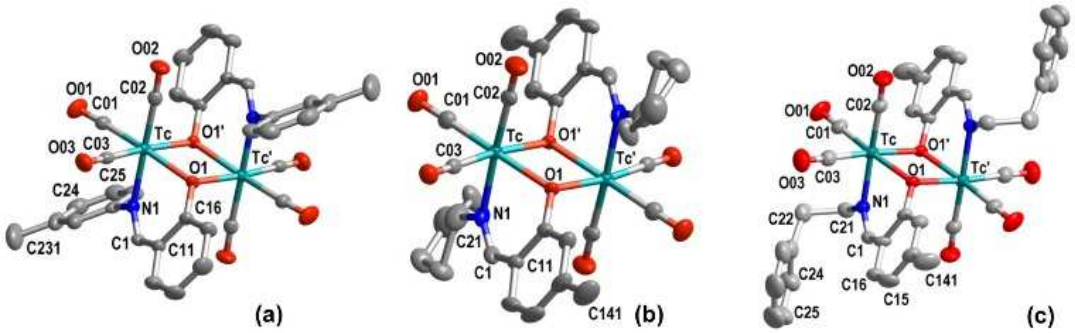

Figure 26. ORTEP diagrams (**a**)-(**c**) of **6**-**8**, with ellipsoids at 50% probability level (for **7**: only major component of disordered cpent shown). Important geometric parameters (in **6**, **7** and **8**, respectively) are: Bond distances (Å): Tc-C01: 1.899(4), 1.892(4), 1.904(4); Tc-C02 1.922(4), 1.914(4), 1.919(4); Tc-C03 1.889(4), 1.899(4), 1.896(4); Tc-O1 2.157(2), 2.158(2), 2.150(2); Tc-N1 2.188(3), 2.172(3), 2.195(3); Tc-O1' 2.189(2), 2.195(2), 2.192(2); Tc-Tc' 2.4210(5), 3.4335(3), 3.4235(5); O1-O1' 2.6821(3), 2.677(3), 2.671(3). Bond angles (°): OC-Tc-CO: 85.7(1) to 88.1(2) for nine angles; C02-Tc-N1 179.31(13), 176.18(12), 176.13(13); O1-Tc-N1 81.08(9), 82.01(9), 82.37(10); O1-Tc-O1 76.16(9), 75.87(8), 75.94(9); Tc-O1-Tc'103.81(9), 104.12(8), 104.1(1).

Aiming at the self-assembly strategy, the same reaction as described above with ^{99}Tc was done but in the presence of *fac*-[^{99m}Tc(OH$_2$)$_3$(CO)$_3$]$^+$ in acetonitrile (Scheme 28b). As expected, we observed the formation of a ^{99m}Tc compound (γ-trace) with a retention time equal to the one from the reaction of pure ^{99}Tc (β-trace). To unambiguously assess the identity of the ^{99}Tc$_2$ and the ^{99}Tc^{99m}Tc compounds, they were co-injected into HPLC and the retention times compared (Figure 27). The equal retention times confirmed the formation of [^{99}Tc^{99m}Tc (μ$_2$-O^N-Hsal-*m*-tol)$_2$(CO)$_6$].

Aiming at dinuclear compounds for application in life sciences, it is clear that a combination of ^{99}Tc and ^{99m}Tc is a "no go". As in case of the pre-assembly strategy, only a combination between Re and ^{99m}Tc is an acceptable option. Thus, dinuclear complexes like **6**-**8** must comprise one ^{99m}Tc and one Re to be potentially applicable. However, the same reactions with *fac*-[ReBr$_3$(CO)$_3$]$^{2-}$ instead of *fac*-[^{99}TcCl$_3$(CO)$_3$]$^{2-}$ with the Schiff bases as depicted in Scheme 27, in organic solvent or a water/MeOH mixture, yielded exclusively mononuclear complexes of the type *fac*-[Re(O^N-R$_1$)(CO)$_3$] (Scheme 28a). No dimerization was observed under our conditions. Previously, we isolated and fully characterized these mononuclear rhenium complexes.[215] This unequal behaviour between the two homologues Re and Tc is

rather based on a substantial different kinetics in low oxidations states than on thermodynamic features.[216]

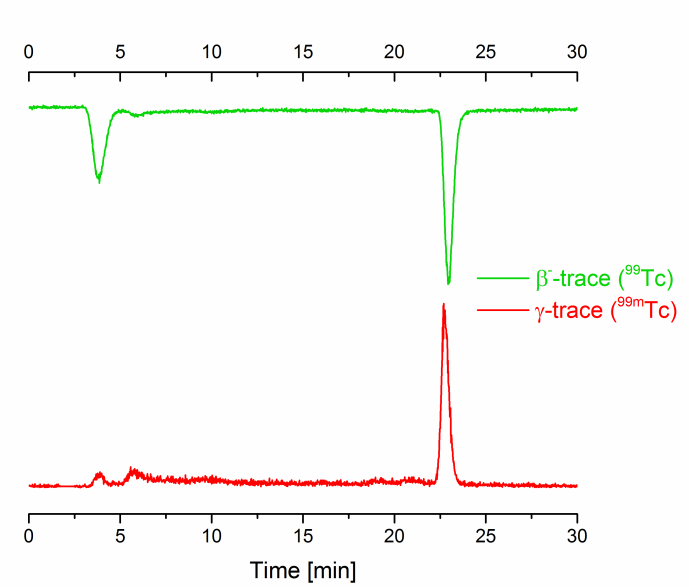

Figure 27. HPLC comparison of [$^{99}Tc_2(\mu_2$-O^N-m-tol$)_2(CO)_6$] **6** (β^--trace) and [$^{99}Tc^{99m}Tc(\mu_2$-O^N-m-tol$)_2(CO)_6$] (γ-trace).

The pivotal question is now how a mixture of *fac*-$[ReBr_3(CO)_3]^{2-}$ and *fac*-$[^{99m}(OH_2)_3(CO)_3]^+$ (prepared in water) would behave in acetonitrile in analogy to the ^{99}Tc reaction described above, and in the presence of the Schiff bases.

This reaction *c)* in Scheme 28 under identical conditions as in reaction *a)* with Hsal-*m*-tol gave the mononuclear rhenium complex **9** in quantitative yields as well as the mixed-metal dinuclear complex [^{99m}TcRe(μ_2-O^N-Hsal-*m*-tol$)_2(CO)_6$] (**10**). Due to the very low concentration of ^{99m}Tc (nanomolar) in this reaction, dimerization to yield the dinuclear ^{99m}Tc analogue of **6** is not expected for kinetic reasons. Figure 28 displays the HPLC traces of this reaction. The green and the dark red top-down traces represent the UV/vis and the β^- trace of **6** as reference. The peaks have different retention times due to the separation of the respective detectors. The red trace (bottom-up) of the ^{99m}TcRe dinuclear complex **10** has exactly the same retention time as the green β^- trace of the $^{99}Tc^{99}$Tc complex **6**. Complex **10** shows no UV/vis absorption peak (blue line) because its concentration is in the nanomolar range. It shows however a UV/Vis peak exactly at the position where the mononuclear rhenium complex **9** appears. These traces clearly demonstrate the formation of a mixed ^{99m}TcRe complex and the

mononuclear complex **9**. If this mononuclear complex **9** is the most stable form, dimerization with the ^{99m}Tc fragment and an additional ligand is not expected. It seems thus that dinuclear compound **10** is thermodynamically favoured over the monomer **9** which allows the formation of the mixed-element dinuclear complex **10** (Figure 28).

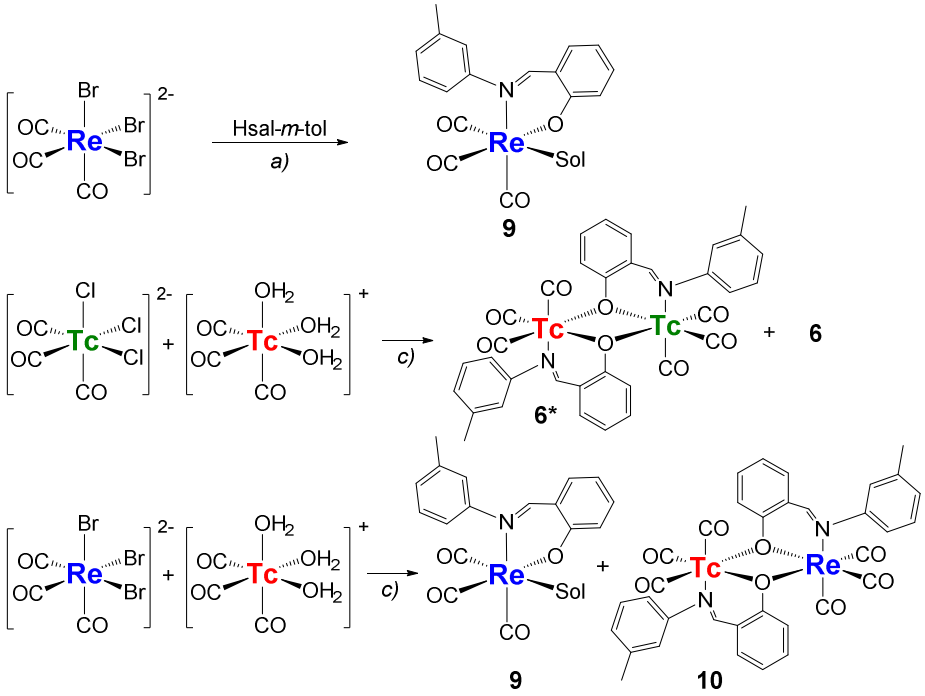

Scheme 28. Self-assembly of a dinuclear ^{99m}TcRe complex. Path *a*) rhenium (blue) only yields only mononuclear complexes. Path *b*) ^{99}Tc (green) only yields dinuclear complexes and path *c*) mixture of ^{99m}Tc (red) and Re gives mononuclear rhenium complexes and mixed ^{99m}TcRe complexes. Reaction conditions for c): $[NEt_4]_2[ReBr_3(CO)_3]$ and $[^{99m}Tc(CO)_3(H_2O)_3]^+$ where dissolved in acetonitrile. Hsal-*m*-tol and NEt_3 were added and the mixture was heated to 80 °C for 3 h.

This self-assembly reaction leads to the formation of a well-defined ^{99m}TcRe complex. We emphasize that **10** is the first of its kind. The combination of the two elements in one and the same compound may open a new path in theranostics; particularly as the residual R_n functionality in the Schiff base framework can be selected according to the purposes of the complex, i.e. a targeting molecule or a bioactive agent. For application, these compounds incorporate traces of ^{99m}Tc which allows their *in vivo* pharmacology to be tracked.

Dinuclear complexes, labelled with ^{99m}Tc can thus be prepared in one single step. In contrast to the classic labelling procedure with bifunctional ligands and a single ^{99m}Tc atom, the metals self-assemble into a dinuclear cluster since their precursors themselves act as the 'ligands'.

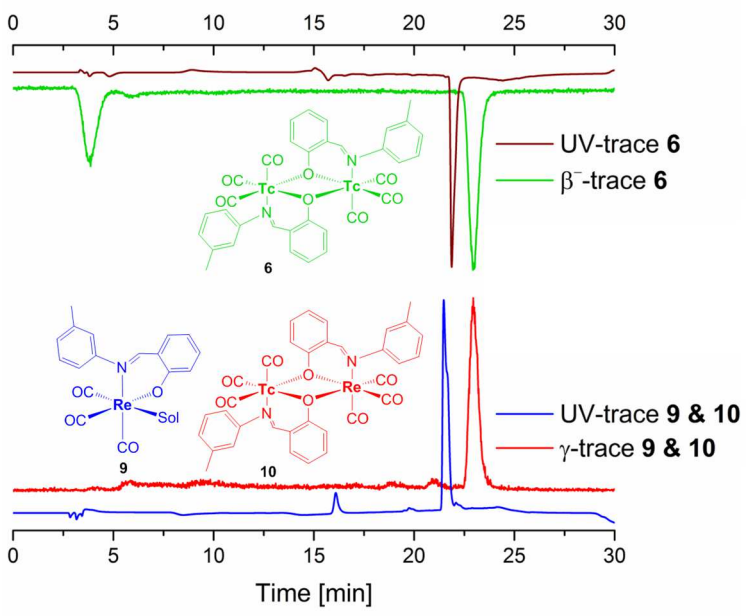

Figure 28. HPLC traces of the crude reaction mixture for the preparation of **10** (containing mostly **9** due to the large excess of rhenium present) combined with the HPLC traces (UV and β^-) of **6**: UV/vis trace **9** and **10** (blue), γ-trace **9** and **10** (red), UV-trace **6** (dark green), β⁻trace **6** (light green). For reaction conditions see Scheme 5

The product may comprise two bioactive units (R_1 and R_2 in the Schiff base ligands) and, if desired, two metal-centres to exert their respective biological functions. These compounds integrate ^{99m}Tc atoms. We emphasize that the formation of the same compound is unlikely in the exclusive presence of ^{99m}Tc since its concentration is far too low and 2nd order kinetics therefore slow. The preparation of such a dinuclear complex is unprecedented in radiopharmaceutical chemistry and might open a new view towards potential building blocks or radiopharmaceuticals. Moreover, it yields a convenient pathway to obtain pre-designed nanomaterial molecular entities, which can be varied for functionality and size.

Conclusions

Multinuclear complexes are rarely considered in medicinal inorganic chemistry. They would have the advantage of comprising more than one targeting unit or, optionally, delivering more than one bioactive moiety. As shown in this report, multinuclear complexes can be prepared along a very convenient self-assembly path form mononuclear precursors or by completing a pre-assembled cluster fragment, i.e. a fragment which serves as a ligand. If one metal in such an architecture is a □-emitter, these assemblies are of theranostic potential. We have described in here the feasibility of both synthetic strategies; firstly an incomplete and separately prepared Re_3 cluster that incorporates a $[^{99m}Tc(CO)_3]^+$ moiety to complete a cube. The bridging ligands, here hydroxide, can be replaced by functionalized alkoxides. A one pot reaction with the mononuclear precursors and, optionally a ligand, leads in one step to the identical product. The approach is not only synthetically facile, it is also highly flexible and will allow for a rapid screening of potentially useful architectures. Secondly with bridging ligands, here Schiff bases, dinuclear complexes were prepared in one step. Functionalization occurs at the ligand with a multitude of options. Both strategies exemplified in this study extend the theranostic modalities beyond mononuclear complexes and reveal the beauty of chemically combining ^{99m}Tc and Re in dinuclear complexes.

4. Conclusion & Outlook

In our group we have previously investigated Cp-ligands as potential alternative to the otherwise large and bulky chelators used to coordinate the radiometal technetium. Cp's form remarkably stable complexes with both ^{99m}Tc and Re and the possibility to functionalize the Cp's enables both the attachment of targeting and bioactive modalities as well as the integration of the Cp-metal system into biomolecules with known pharmacology. However, the synthetic strategies towards such functionalization have been rather unexplored so far.

In this work we have developed a unique Cp-ligand platform that allows for both tuning of the physico-chemical properties of the complex as well as both bis-homo and bis-heterofunctionalization with biovectors. From these ligands, both "cold" rhenium and "hot" ^{99m}Tc complexes can readily be prepared. In a next step we applied this scaffold by preparing monomeric and dimeric probes for PSMA. These results showed that dimeric probes display significantly higher affinity for PSMA overexpressing cells than the monomeric complex. Additionally, this represented a proof-of-concept of the applicability of the multimodal ligand platform. In a third project, it was shown that these ligands can be used to prepare close structural mimics of the clinically approved cancer drug pemetrexed. The therein prepared complex is a potential theranostic agent, where the rhenium complex is the therapeutic and the ^{99m}Tc the diagnostic modality.

Overall, the strength of this ligand-platform lies in its versatility, as it can be conjugated to essentially any biovector. Currently, the combination of a the PSMA-targeting unit with an additional cytotoxic payload is being explored in our group. Furthermore, the number of functionalities that can be incorporated in the Cp-ring is being expanded, which will enable more integrated approach type applications.

5. Experimental Procedures & Analytical Data

5.0 General

Materials. All chemicals were of reagent-grade quality or higher and were obtained from commercial suppliers. Solvents were used as received or dried over molecular sieves. Sodium boranocarbonate was a gift from Mallinckrodt Medical B.V. (The Netherlands). Na[$^{99m}TcO_4$] in 0.9% saline was eluted from a 99Mo/99mTc UTK FM generator purchased from Mallinckrodt Medical B.V. (The Netherlands)

Instrumentation and methods. ^{1}H and ^{13}C-NMR spectra were recorded in deuterated solvents on a Bruker DRX 400 (^{1}H: 400 MHz, ^{13}C: 100.6 MHz) or DRX 500 (^{1}H: 500 MHz ^{13}C: 125.8 MHz) MHz spectrometer at 300 K. The chemical shifts, δ, are reported in ppm (parts per million) relative to residual solvent peaks. The abbreviations for the peak multiplicities are as follows: s (singlet), d (doublet), dd (doublet of doublets), t (triplet), q (quartet), m (multiplet), br (broad). IR spectra were obtained with a PerkinElmer Spectrum Two spectrometer. Microwave reactions were performed using a Biotage Initiator+ Robot Eight or Anton Paar (AP) Monowave 200 instrument. UPLC-ESI-MS was performed on a Waters Acquity UPLC System coupled to a Bruker HCT^{TM}, using an Acquity UPLC BEH C18 1.7µm (2.1 x 50 mm) column. UPLC solvents were formic acid (0.1% in millipore water) (solvent A) and acetonitrile UPLC grade (solvent B). The temperature was regulated with a Peltier thermostatic system to the specified temperatures. High-resolution mass spectrometry (HR-MS) was performed on a Thermo DFS double-focusing system (ThermoFisher Scientific, Germany). Preparative HPLC was performed on a Varian ProStar 320 system, using a Dr. Maisch Reprosil C18 100-7 (40 x 250 mm) column (flow rate: 40.0 ml/min) or a LiChroCART RP-18e (10 x 250 mm) column. HPLC solvents were 0.1% trifluoroacetic acid (solvent A) and acetonitrile (solvent B), HPLC grade. Analytical HPLC was performed on a Merck Hitachi L7000 system, equipped with a L-7400 UV-detector and an in-line radio-detector Berthold FlowStar LB513, using an analytical Macherey-Nagel Nucleosil C18 5 μm (4.6 × 250 mm) column. Analytical UPLC was performed on a VWR Hitachi Chrommaster Ultra, using an Acquity UPLC BEH C18 1.7µm (2.1 x 50 mm) column. UPLC solvents were trifluoroacetic acid (0.1% in millipore water) (solvent A) and acetonitrile UPLC grade (solvent B).

HPLC/UPLC Methods.

UPLC-MS. The UPLC-MS runs (flow rate 0.6 mL/min) were performed with a linear gradient of A (acetonitrile (Sigma-Aldrich HPLC-grade)) and B (distilled water containing 0.1 % formic acid): *t* = 0–0.5 min, 5 % A; *t* = 4.0 min, 100 % A; *t* = 5.0 min, 100% A.

UPLC (U1). The UPLC runs (flow rate 0.5 mL/min) were performed with a linear gradient of A (acetonitrile (Sigma-Aldrich HPLC-grade)) and B (distilled water containing 0.1% TFA): *t* = 0–0.5 min, 5 % A; *t* = 4.0 min, 100 % A; *t* = 5.0 min, 100 % A.

HPLC. The HPLC runs (flow rate 0.5 mL/min) were performed with a linear gradient of A (acetonitrile (Sigma-Aldrich HPLC-grade)) and B (distilled water containing 0.1 % TFA): *t* = 0–2.1 min, 10 % A; *t* = 25 min, 100 % A; *t* = 35 min, 100% A; *t* = 37 min, 10% A; *t* = 40 min, 10% A.

radioHPLC. The radioHPLC runs (flow rate 0.5 mL/min) using a gradient of A (MeOH (Sigma-Aldrich HPLC-grade)) and B (distilled water containing 0.1 % TFA t = 0 – 3 min: 10% A; 3 – 3.1 min: 0 – 25% A; 3.1 – 9 min: 25% A; 9 – 9.1 min: 25 – 34% A; 9.1 – 18 min: 34 - 100% A; 18 – 25 min: 100% A, 25 – 25.1 min: 100 - 10% A; 25.1 – 30 min: 10% MeOH. Comparison of the HPLC retention times for the ^{99m}Tc compounds with the corresponding ^{99}Tc and Re compound confirms identity.

Preparative HPLC (Method A). The preparative HPLC runs (flow rate 40 mL/min) were performed with a linear gradient of A (acetonitrile (Sigma-Aldrich HPLC-grade)) and B (distilled water containing 0.1 % TFA): *t* = 0–2.1 min, 10 % A; *t* = 25 min, 100 % A; *t* = 40 min, 100% A.

^{99m}Tc experiments. Caution! ^{99m}Tc is a *γ*-emitter (E= 140 keV, $t_{1/2}$= 6.02 h) which should only be handled in a licensed and appropriately shielded facility. Sodium boranocarbonate releases CO gas which is highly toxic, it is recommended to be handled only in ventilated hoods.

Cell culture

Cell lines were obtained from American Type Culture Collection (ATCC). LnCap cells were maintained in RPMI 1640 medium without phenol red (Gibco) at 37 °C, 5 % CO_2. PC3 cells were maintained in DMEM/F12 medium (Gibco) at 37 °C, 5 % CO_2. Cell culture media were supplemented with 10 % fetal bovine serum (Gibco) and penicillin-streptomycin (Invitrogen).

Cell binding assay

Cells were harvested at 70% confluence, washed once with PBS and resuspended in full medium. For cell binding assays, aliquots of 5 mio cells were incubated with the indicated concentrations of the complexes in 5 ml medium for 1 hour at 4 °C. Thereafter, cells were collected by centrifugation at 100 g and 4 °C for 10 min, and washed three times with ice-cold PBS.

ICP-MS measurements

Rhenium was measured against a Re single element standard (Merck 170344.100) and verified by a control (Agilent5188-6524 PA Tuning 2). The rhenium content of the samples was determined by means of a 6 calibration standards that were produced in the range between 0 and 100 ppb in Re ($R>0.99$) with a background equivalent concentration of BEC: 9.4 ppt and a detection limit of DL: 2.6 ppt. The isotope Re185 (37.4 % abundance) Re187 (62.6 % abundance) was evaluated in “no-gas” mode and He-gas mode. Spiking the samples with untreated negative controls (to account for potential carbon content from the biological samples) resulted in equivalent values within error ranges. A solution containing indium (100 ppb) and was used as internal standard. The results are expressed as ppb Re as means ± standard deviations of three experiments.

5.1 Experimental Section Part A

5.1.1 Synthetic Procedures and Analytical Data Part 3.1

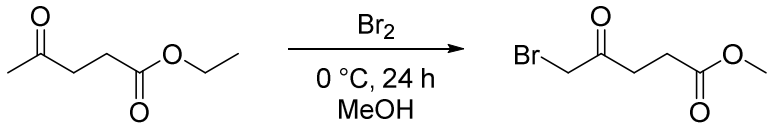

0.1. Ethyl levulinate (7.22 g, 50.0 mmol) was dissolved in MeOH (100 ml). The solution was cooled to 0 °C by means of a water-ice bath. Bromine (2.8 ml, 55 mmol) was added dropwise to the reaction mixture which turned red. Upon complete addition, the now orange solution was stirred for another 2 hours at room temperature. The solvent was removed *in vacuo* and the crude was dissolved in MTBE (50 ml) and washed with sat. $NaHCO_3$ (2 x 50 ml). The combined aqueous phases were washed with further MTBE (50 ml). The combined organic phases were dried over $MgSO_4$ and the solvent removed on a rotary evaporator. Column chromatography (silica gel, Hexane/EtOAc 3:1) yielded pure **0.1** as a yellow oil (2.42 g, 11.6 mmol, 23 %). The analytical data matched that reported previously.[217]

R_f = 0.38 (silica gel, Hexane/EtOAC 3:1). ^{1}H NMR (400 MHz, $CDCl_3$): δ (ppm) 2.64 (t, J^3 = 6.5 Hz, 2H), 2.94 (t, J = 6.5 Hz, 2H), 3.66 (s, 3H), 3.94 (s, 2H).

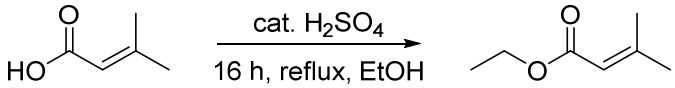

1.1. 3-methyl-2-butenoic acid (3.03 g, 30.2 mmol) was dissolved in ethanol (20 ml) and 10 drops of conc. H_2SO_4 were added under stirring. The solution was heated to reflux overnight. The next day the solution was concentrated to about 5 ml and diluted in diethyl ether (50 ml). The organic phase was washed with sat. $NaHCO_3$ (3 x 30 ml) and H_2O (2 x 30 ml). The combined organic phases were dried over $MgSO_4$ and the solvent removed on a rotary evaporator yielding **1.1** as a yellow oil (3.35 g, 26.2 mmol, 87%). The analytical data matched that reported previously.[218]

^{1}H NMR (400 MHz, $CDCl_3$): δ (ppm): 1.23 (t, J = 7.1 Hz, 1H), 1.85 (d, J = 1.3 Hz, 1H), 2.13 (d, J = 1.3 Hz, 1H), 4.10 (q, J = 7.1 Hz, 1H), 5.63 (m, J = 1.3 Hz, 1H).

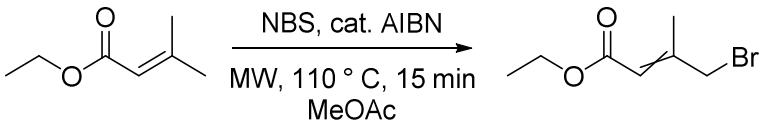

1.2. 1.1 (0.884 g, 6.9 mmol) was dissolved in MeOAc (2 ml) in a Biotage microwave vial (2 – 5 ml). N-Bromosuccinimide (1.24 g, 7.0 mmol) and Azobisiobutyronitrile (25 mg, 0.15 mmol) were added. The resulting suspension was heated by microwave to 110 °C for 15 min (low absorbance settings). The reaction mixture was diluted with DCM (50 ml) and washed with sat. Na_2SO_3 (2 x 50 ml). The organic phase was dried over $MgSO_4$ and the solvent removed on a rotary evaporator, yielding **1.2** as a yellowish oil (1.18 g, 5.7 mmol, 83 %). The product was determined to be a 1.4:1 mixture of the *cis-* and *-trans* isomer by comparison of the ^{1}H-NMR with the literature references.[219] The crude product was used in the next step without further purification.
^{1}H NMR (400 MHz, $CDCl_3$): δ (ppm) 1.24 – 1.30 (m, 2 x 3H), 2.02 (d, *J* = 1.4 Hz, 3H), 2.25 (d, *J* = 1.3 Hz, 3H), 3.92 (d, *J* = 0.6 Hz, 2H) 4.12 – 4.22 (m, 2 x 2H), 4.53 (s, 2H), 5.75 (d, *J* = 1.4 Hz, 1H), 5.93 (t, *J* = 0.6 Hz, 1H).

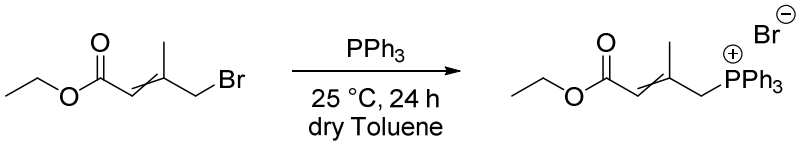

1.3. 1.3 was synthesized according to a modified procedure published by Richmond *et al.*[220] Triphenylphosphine (2.63 g, 10.0 mmol) was dissolved in dry toluene (80 ml). To this solution **1.2** (1.89 g, 9.13 mmol) in dry toluene (20 ml) was added. The mixture was stirred for 24 h at room temperature under nitrogen. The precipitate was collected by filtration (frit) and washed with cold toluene. The white solid was dried *in vacuo* yielding **1.3** as an off-whiteish powder (3.60 g, 7.70 mmol, 84 %). The crude product was used in the next step without further purification.
^{1}H NMR (400 MHz, $CDCl_3$): δ (ppm) 1.03 (t, *J* = 7.1 Hz, 3H), 1.18 (t, *J* = 7.1 Hz, 3H), 1.99 (m, 2H), 2.12 (m, 2H), 3.76 (m, 2H), 4.05 (q, *J* = 7.1 Hz, 3H), 4.49 (m, 2H), 5.07 (m, 2H), 5.61 (m, 2H), 5.78 (m, 1H), 6.28 (m, 1H), 7.64 – 7.79 (m, 30H).

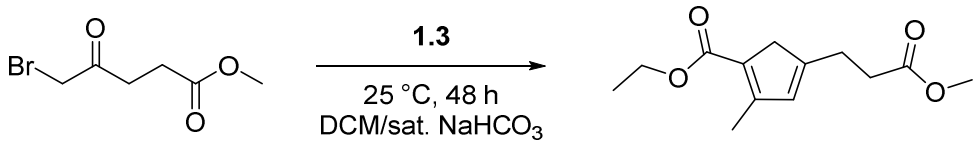

1a. A solution of **1.3** (0.815 g, 1.7 mmol) in DCM (25 ml) was layered with sat. $NaHCO_3$ (25 ml) and then stirred vigorously for 5 min under nitrogen atmosphere. The mixture turned bright orange. A solution of **0.1 (**0.33 g, 1.6 mmol) in DCM (15 ml) was added dropwise to the biphasic mixture. The mixture was stirred vigorously for 48 h at room temperature under nitrogen atmosphere. The organic phase was then separated from the aqueous phase. The aqueous phase was further washed with DCM (2 x 30 ml). The combined organic phases were dried over $MgSO_4$ and the solvent removed on a rotary evaporator. Column chromatography (silica gel, Hexane/Et_2O 3:1) yielded pure **1a** as a colorless oil (0.248 g, 1.0 mmol, 66 %).

R_f = 0.17 (silica gel, Hexane/Et_2O 3:1). UPLC (gradient U1): RT = 2.89 min. ^1H NMR (400 MHz, $CDCl_3$): δ (ppm) 1.18 (t, *J* = 7.1 Hz, 3H), 2.18 (t, *J* = 2.5 Hz, 3H), 2.45 (m, 2H), 2.62 (m, 2H), 3.12 (m, 2H), 3.56 (s, 3H), 4.08 (q, *J* = 7.1 Hz, 2H), 5.98 (s, 1H). ^{13}C NMR (101 MHz, $CDCl_3$): δ (ppm). 14.33, 15.26, 25.84, 33.15, 44.20, 51.49, 59.19, 126.97, 132.39, 152.85, 155.38, 164.76, 172.97. HR-ESI mass spectrum (MeOH): found 261.10961 calcd. for [$C_{13}H_{18}O_4$+Na_+] 261.10973.

.

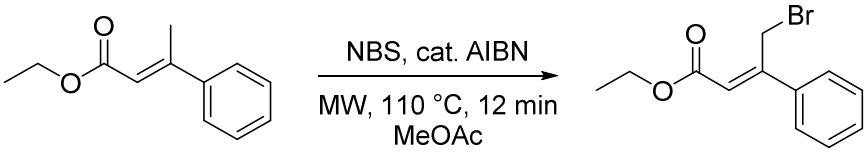

4.1. Ethyl trans-β-methylcinnamate (0.504 ml, 2.8 mmol) was dissolved in MeOAc (2 ml) in a Biotage microwave vial (2 – 5 ml). N-Bromosuccinimide (500 mg, 2.8 mmol) and Azobisiobutyronitrile (25 mg, 0.15 mmol) were added. The resulting suspension was heated by microwave to 110 °C for 12 min (low absorbance settings). The reaction mixture was diluted with DCM (50 ml) and washed with sat. Na_2SO_3 (2 x 50 ml). The organic phase was dried over $MgSO_4$ and the solvent removed on a rotary evaporator, yielding **4.1** as a yellowish oil (734 mg, 2.7 mmol, 97 %). The analytical data matched that reported previously.[221] The product was used in the next step without further purification.

^{1}H NMR (500 MHz, $CDCl_3$): δ (ppm) 1.34 (t, ^3J = 7.2 Hz, 3H), 4.27 (q, J^3 = 7.1 Hz, 2H), 4.98 (s, 3H), 6.21 (s, 1H), 7.41 – 7.42 (m, 3H), 7.54 – 7.56 (m, 2H).

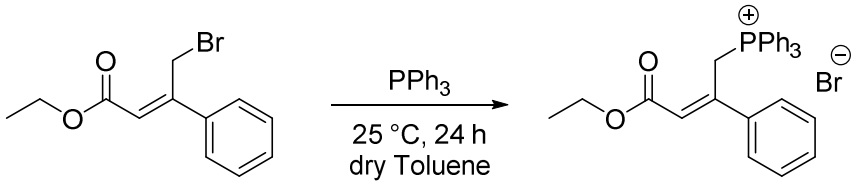

4.2. To a stirred solution of **4.1** (2.50 g, 9.29 mmol) in dry toluene (100 ml), triphenylphosphine (2.56 g, 9.75 mmol) was added. The mixture was stirred for 24 h at room temperature under nitrogen. The precipitate was collected by filtration (frit) and washed with cold toluene. The white solid was dried *in vacuo* yielding **4.2** as a white powder (3.21 g, 6.04 mmol, 65 %). The analytical data matched that reported previously.[95] The product was used in the next step without further purification.
^{1}H NMR (400 MHz, $CDCl_3$): δ (ppm) 1.11 (t, J^3 = 7.1 Hz, 3H), 3.89 (q, J^3 = 7.1 Hz, 2H), 6.06 (d, J = 5.3 Hz, 1H), 6.13 (d, J = 17.5 Hz, 2H), 7.21 -7.26 (m, 3H), 7.52 – 7.57 (m, 7H), 7.66 – 7.77 (m, 10H).

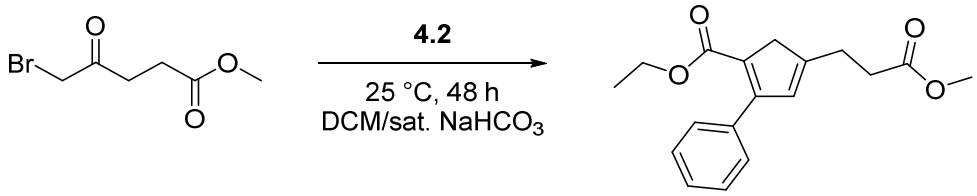

4a. A solution of **4.2** (2.56 g, 4.8 mmol) in DCM (50 ml) was layered with sat. $NaHCO_3$ (50 ml) and then stirred vigorously for 5 min under nitrogen atmosphere. The mixture turned bright orange. A solution of **0.1 (**0.958 g, 4.6 mmol) in DCM (10 ml) was added dropwise to the biphasic mixture. The mixture was stirred vigorously for 48 h at room temperature under nitrogen atmosphere. The organic phase was then separated from the aqueous phase. The aqueous phase was further washed with DCM (2 x 30 ml). The combined organic phases were dried over $MgSO_4$ and the solvent removed on a rotary evaporator. Column chromatography (silica gel, Hexane/EtOAc 5:1) yielded pure **4a** as a yellowish oil, that solidified upon cooling (0.379 g, 1.3 mmol, 27 %).
R_f = 0.66 (silica gel, Hexane/EtOAc 3:1). UPLC (gradient U1): RT = 3.20 min. ^{1}H NMR (400 MHz, $CDCl_3$): δ (ppm) 1.18 (t, ^3J = 7.1 Hz, 3H), 2.62 (m, J = 7.8 Hz, 2H), 2.81 (m, J = 3.9 Hz, 2H), 3.48 (s, 2H), 3.69 (s, 3H), 4.12 (q, ^3J = 7.1 Hz, 2H), 6.33 (s, 1H), 7.33-

7.39 (m, 3H), 7.47-7.49 (m, 2H). ^{13}C NMR (125 MHz, $CDCl_3$): δ (ppm): 14.29, 26.16, 33.46, 445..83, 51.89, 59.833, 12.., 117.78, 128.33, 18.88, 132.01, 135.81, 153.11, 155.76, 164.39, 173.26. HR-ESI mass spectrum (MeOH): found 301.14358; calcd. for [$C_{18}H_{21}O_4$] 301.14344.

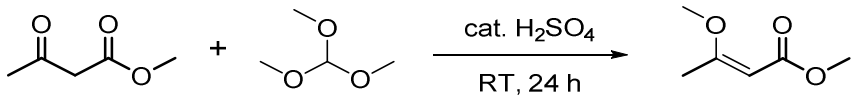

6.1. 6.1 was synthesized following a previously published procedure.[222] Methyl acetoacetonate (18.6 ml, 172 mmol), trimethylorthoformate (19.2 ml, 175 mmol) and concentrated H_2SO_4 (12 drops) were stirred at room temperature under a nitrogen atmosphere. After 24 h, isoquinoline (20 drops) was added. The reaction mixture was distilled (190 mBar, 140 °C) to give **6.1** (18.38 g, 141 mmol, 82%) as a colorless liquid. The analytical data matched that reported previously.[222]

^{1}H NMR (400 MHz, $CDCl_3$): δ (ppm): 2.23 (s, 3H), 3.57 (s, 3H), 3.61 (s, 3H), 4.96 (s, 1H).

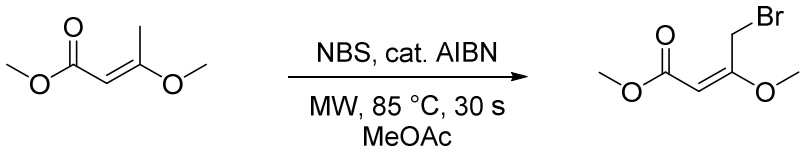

6.2. 6.1 (0.763 g, 5.9 mmol) was dissolved in MeOAc (3 ml) in an Anton Paar microwave vial (10 ml). N-Bromosuccinimide (1.1 g, 6.2 mmol) and Azobisiobutyronitrile (45 mg, 0.3 mmol) were added. The resulting suspension was heated by microwave to 85 °C for 30 s. The reaction mixture was diluted with DCM (75 ml) and washed with sat. Na_2SO_3 (2 x 75 ml). The organic phase was dried over $MgSO_4$ and the solvent removed on a rotary evaporator, yielding **6.1** as a yellow oil (0.892 mg, 4.3 mmol, 73 %). The analytical data matched that reported previously.[223] The product was used in the next step without further purification.

^{1}H NMR (400 MHz, $CDCl_3$): δ (ppm): 3.69 (s, 3H), 3.71 (s, 3H), 4.51 (s, 2H), 5.12 (s, 1H).

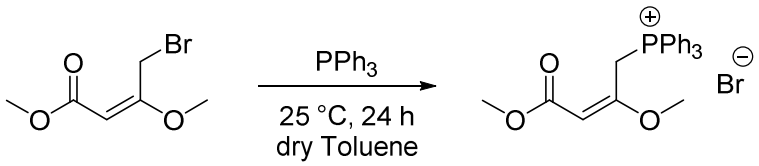

6.3. To a stirred solution of **6.2** (2.68 g, 12.8 mmol) in dry toluene (100 ml), triphenylphosphine (3.70 g, 14.1 mmol) was added. The mixture was stirred for 24 h at room temperature under nitrogen. The precipitate was collected by filtration (frit) and washed with cold toluene. The white solid was dried *in vacuo* yielding **6.3** as a white powder (3.23 g, 6.9 mmol, 54 %). The product was used in the next step without further purification.

^{1}H NMR (400 MHz, $CDCl_3$): δ (ppm) 3.48 (s, 3H), 3.53 (s, 3H), 5.06 (1H), 5.75 (d, J = 15.5 Hz, 2H) 7.65 – 7.87 (m, 15H).

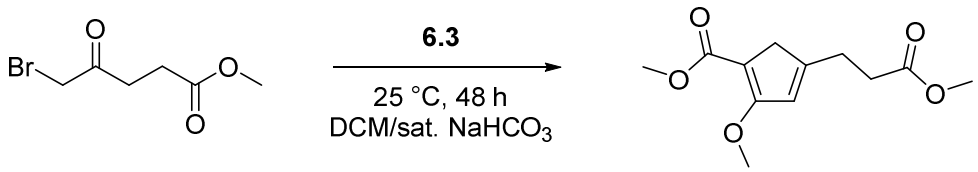

6a. A solution of **6.3** (1.63 g, 3.5 mmol) in DCM (50 ml) was layered with sat. $NaHCO_3$ (50 ml) and then stirred vigorously for 5 min under nitrogen atmosphere. The mixture turned bright orange. A solution of **0.1 (**0.655 g, 3.1 mmol) in DCM (10 ml) was added dropwise to the biphasic mixture. The mixture was stirred vigorously for 48 h at room temperature under nitrogen atmosphere. The organic phase was then separated from the aqueous phase. The aqueous phase was further washed with DCM (2 x 30 ml). The combined organic phases were dried over $MgSO_4$ and the solvent removed on a rotary evaporator. Column chromatography (silica gel, Hexane/EtOAc 2:1) yielded pure **7a** as a yellowish oil (0.170 g, 0.7 mmol, 23 %).

R_f = 0.12 (silica gel, Hexane/EtOAc 3:1). UPLC (gradient U1): RT = 2.18 min. ^{1}H NMR (500 MHz, $CDCl_3$): δ (ppm): 2.52 (t, ^{3}J = 7.46 Hz, 2H), 2.70 (t, ^{3}J = 7.42 Hz, 2H), 3.15 (s, 2H), 3.63 (s, 3H), 3.66 (s, 3H), 3.89 (s, 3H) 6.27 (s, 1H). ^{13}C NMR (125 MHz, $CDCl_3$): δ (ppm): 26.69, 32.99, 40.60, 50.67, 51.77, 58.62, 103.66, 120.55, 156.25, 164.21,

168.11, 172.84. HR-ESI mass spectrum (MeOH): found 241.10702; calcd. for [$C_{12}H_{16}O_5$+H^+] 241.10705.

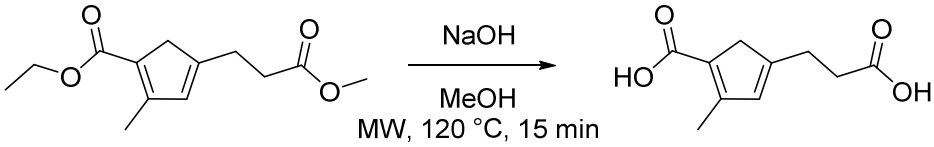

2a. 1a (31 mg, 0.13 mmol) was dissolved in MeOH (1 ml) in an Anton Paar microwave vial (10 ml) equipped with a stirring bar. 1 M NaOH was added (0.4 ml) and the solution was heated by microwave to 120 °C for 15 min. UPLC measurement showed complete consumption of the starting material. The reaction solution was diluted with H_2O (5 ml) and neutralized to pH = 3 by dropwise addition of 1 M HCl. **2a** was obtained by evaporating the solvent *in vacuo* and was used without further purification.
UPLC (gradient U1): RT = 1.91 min.

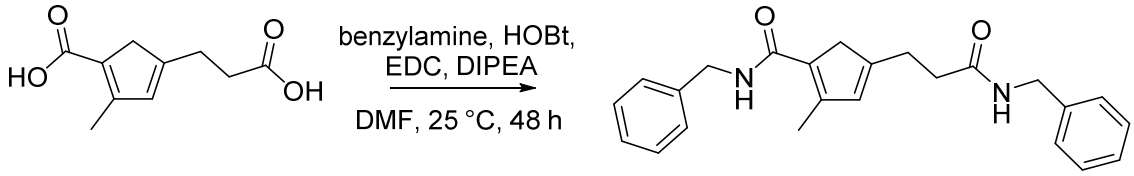

3a. **2a** (48 mg, 0.21 mmol) was dissolved in DMF (2 ml). Benzylamine (0.53 ml, 0.49 mmol) and HOBt (66 mg, 0.49 mmol) were added under stirring. After 5 min, EDC (93 mg, 0.49 mmol) and DIPEA (0.170 ml, 0.98 mmol) were added and the solution was stirred at room temperature for 48 h. The solvent was removed *in vacuo* and the crude was purified by preparative HPLC (Method A) and **3a** was obtained as a yellowish powder (30 mg, 0.08 mm, 38 %).
UPLC (gradient U1): RT = 2.65 min. ^{1}H NMR (400 MHz, $CDCl_3$): δ (ppm) 2.25 (m, 3H), 2.49 (m, 2H), 2.72 – 2.75 (m, 2H), 3.25 – 3.26 (m, 2H), 4.34 (s, 2H), 4.46 (s, 2H), 6.11 (s, 1H), 7.19 – 7.30 (m, 10H). ^{13}C NMR (125 MHz, $CDCl_3$): δ (ppm) 15.39, 27.54, 36.51, 43.78, 44.05, 44.69, 127.99, 128.18, 128.40, 128.48, 129.45, 129.52, 130.64, 133.87, 139.95, 140.68, 152.27, 152.95, 168.03, 174.92. HR-ESI mass spectrum (MeOH): found 375.20669; calcd. for [$C_{24}H_{27}O_2N_2$] 375.20670.

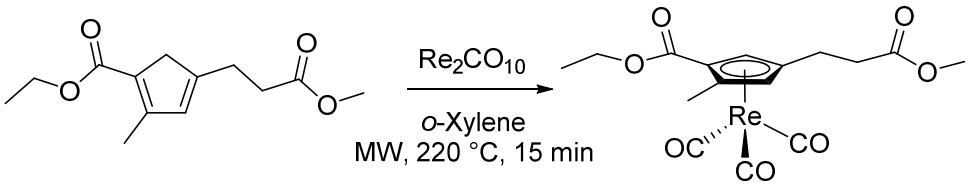

1b. A solution of **1a** (59 mg, 0.25 mmol) and $Re_2(CO)_{10}$ (82 mg, 0.13 mmol) in *o*-Xylene (2 ml) in a Anton Paar microwave vial (10 ml) equipped with a stirring bar was heated to 220 °C for 15 min (Careful, toxic CO gas is released during the reaction, take appropriate precautions). The solvent was evaporated *in vacuo*, yielding pure **1b** (97 mg, 0.19 mmol, 76 %) as a dark brown oil.

UPLC (gradient U1): RT = 3.40 min. ^{1}H NMR (400 MHz, $CDCl_3$): δ (ppm) 1.31 (t, J = 7.1 Hz, 3H), 2.50 (s, 3H), 2.49 – 2.53 (m, 2H), 2.63 – 2.82 (m, 2H), 3.71 (s, 3H), 4.18 – 4.34 (m, 2H), 5.22 (d, J = 2.0 Hz, 1H), 5.77 (d, J = 2.0 Hz, 1H). ^{13}C NMR (126 MHz, $CDCl_3$): δ (ppm) 13.89, 14.27, 23.31, 35.60, 52.11, 61.12, 84.65, 85.58, 86.02, 107.08, 110.77, 164.92, 172.55, 193.40. IR bands (Golden Gate, cm^{-1}): 2024, 1921. HR-ESI mass spectrum (MeOH): found 509.06060; calcd. for [$C_{16}H_{18}O_7Re+H^+$] 509.06046.

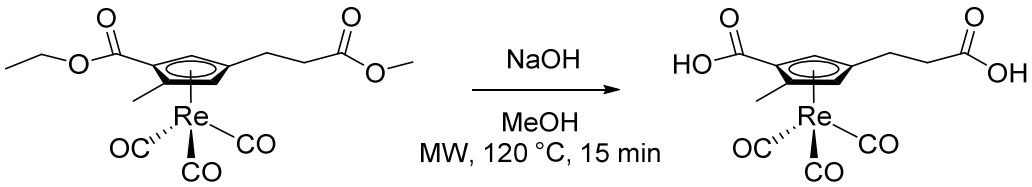

2b. A solution of **1b** (40 mg, 0.079 mmol) in MeOH (1 ml) and 1 M NaOH (0.5 ml) in a Anton Paar microwave vial (10 ml) was heated by microwave to 120 °C for 15 min. The crude was diluted with 1 M HCl (20 ml) and washed with DCM twice (2 x 20 ml). The combined organic phase was washed once with water (20 ml) dried over $MgSO_4$ and the solvent removed *in vacuo* yielding **2b** as a pale yellow solid (25 mg, 0.054 mmol, 68 %). Single crystals were obtained by slow evaporation of a MeOH solution. The product was used in the next step without further purification.

UPLC (gradient U1): RT = 2.51 min. ^{1}H NMR (400 MHz, CD_3OD): δ (ppm) 2.49 (s, 3H), 2.50 – 2.80 (m, 4H), 5.53 (d, J^3 = 2.0 Hz, 1H), 5.93 (d, J^3 = 2.1 Hz, 1H). ^{13}C NMR (126 MHz, CD_3CO): δ (ppm) 13.97, 24.29, 36.55, 85.94, 87.53, 88.00, 109.12, 112.11, 167.99, 175.72, 194.97. IR bands (Golden Gate, cm^{-1}): 2024, 1920. HR-ESI mass spectrum (MeOH): found 464.99870; calcd. for [$C_{13}H_{10}O_7Re^-$] 464.99895.

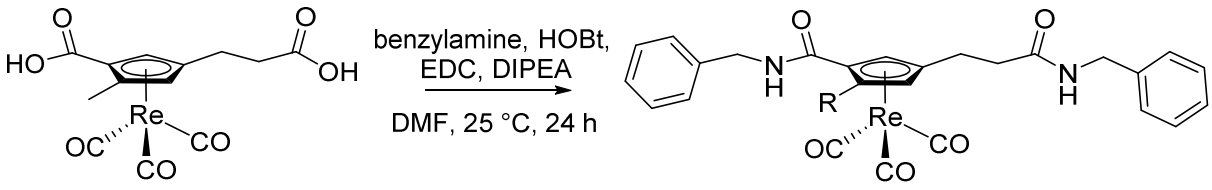

3b. 2b (47 mg, 0.1 mmol) was dissolved in DMF (5 ml). Benzylamine (0.023 ml, 0.21 mmol) and HOBt (29 mg, 0.21 mmol) were added under stirring. After 5 min, EDC (41 mg, 0.21 mmol) and DIPEA (0.073 ml, 0.42 mmol) were added and the solution was stirred for 24 h. The solvent was removed *in vacuo* and the crude was purified by preparative HPLC (Method A) and **3a** was obtained as a pale yellow powder (10 mg, 0.016 mmol, 16 %). Single crystals were obtained by slow evaporation of a MeOH solution.

UPLC (gradient U1): RT = 3.20 min. ^{1}H NMR (400 MHz, $CDCl_3$): δ (ppm) 2.45 (t, ^{3}J = 7.2 Hz, 2H), 2.48 (s, 3H), 2.64 – 2.78 (m, 2H), 4.32 – 4.51 (m, 4H), 5.40 (d, J^{3} = 2.0 Hz, 1H), 5.97 (d, J^{3} = 2.0 Hz, 1H) 7.21 – 7.30 (m, 10H) 8.40 – 8.44 (m, 2H). ^{13}C NMR (125 MHz, $CDCl_3$): δ (ppm) 14.17, 25.30, 38.73, 43.98, 44.12, 49.00, 84.82, 86.78, 90.93, 108.57, 111.42, 128.14, 128.26, 128.38, 128.56, 129.50, 129.57, 139.85, 139.99, 166.28, 173.85, 195.29. IR bands (Golden Gate, cm^{-1}): 2017, 1906. HR-ESI mass spectrum (MeOH): found 645.13941; calcd. for [$C_{27}H_{26}O_5N_2Re+H^+$] 645.13937.

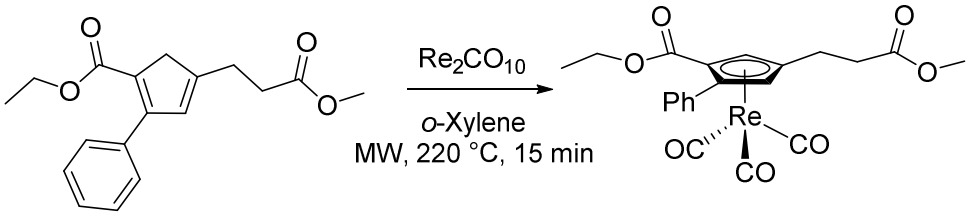

4b. 4a (96 mg,, 0.32 mmol) was dissolved in *o*-Xylene (2 ml) in a Anton Paar microwave vial (10 ml). $Re_2(CO)_{10}$ (104 mg, 0.16 mmol) was added and the mixture was heated by microwave to 220 °C for 15 min (Careful, toxic CO gas is released during the reaction, take appropriate precautions). The solvent was evaporated *in vacuo* and the crude was purified by column chromatography (silica gel, Hexane/EtOAc 5:1) yielding pure **4b** as a yellowish oil (83%).

R_f = 0.59 (silica gel, Hexane/EtOAc 3:1). UPLC (gradient U1): RT = 3.55 min. ^{1}H NMR (500 MHz, $CDCl_3$): δ (ppm) 1.20 (t, ^{3}J = 7.1 Hz, 3H), 2.56 (t, ^{3}J = 7.5 Hz, 2H), 2.74 – 2.89 (m, 2H), 3.73 (s, 3H), 4.13 – 4.25 (m, 2H), 5.51 (d, ^{3}J = 2.1 Hz, 1H), 5.91 (d, ^{3}J =

2.1 Hz, 1H), 7.32-7.33 (m, 3H), 7.42-7.44 (m, 2H). ^{13}C NMR (126 MHz, $CDCl_3$): δ (ppm) 14.05, 23.32, 35.70, 52.13, 61.35, 85.57, 87.00, 87.26, 106.95, 114.56, 127.94, 129.10, 130.69, 131.02, 163.97, 172.44, 193.09. IR bands (Golden Gate, cm^{-1}): 2023, 1920. HR-ESI mass spectrum (MeOH): found 571.07646; calcd. for [$C_{21}H_{19}O_7Re+H^+$] 571.07611.

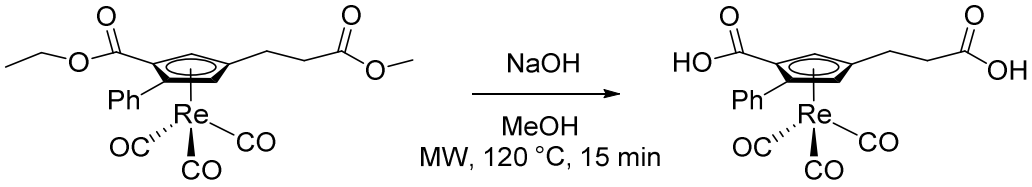

5b. A solution of **4b** (82 mg, 0.144 mmol) in MeOH (2 ml) and 1 M NaOH (0.25 ml) in a Anton Paar microwave vial (10 ml) was heated by microwave to 120 °C for 15 min. The crude was diluted with 1 M HCl (20 ml) and washed with DCM twice (2 x 20 ml). The combined organic phase was washed once with water (20 ml) dried over $MgSO_4$ and the solvent removed *in vacuo* yielding **5b** as a pale yellow oil (70 mg, 0.133 mmol, 92 %). The product was used in the next step without further purification.

UPLC (gradient U1): RT = 2.75 min. ^{1}H NMR (400 MHz, CD_3OD): δ (ppm) 2.59-2.63 (m, 2H), 2.71 – 2.88 (m, 2H), 5.78 (d, J = 2.2 Hz, 1H), 6.07 (d, J = 2.2 Hz, 1H), 7.30-7.32 (m, 3H), 7.47-7.49 (m, 2H). ^{13}C NMR (125 MHz, CD_3OD): δ (ppm): 24.27, 36.61, 86.75, 89.06, 89.11, 109.13, 115.67, 128.73, 129.74, 131.96, 132.31, 167.00, 175.74, 194.66. IR bands (Golden Gate, cm^{-1}): 2024, 1918.

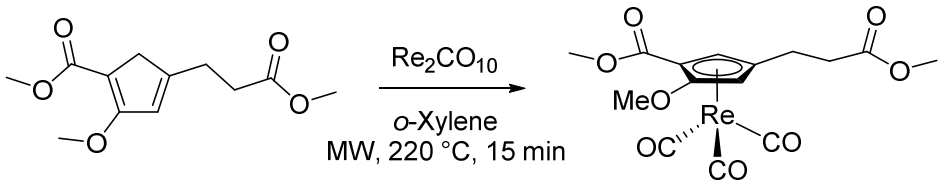

6b. 6a (64 mg,, 0.27 mmol) was dissolved in *o*-Xylene (3 ml) in a Anton Paar microwave vial (10 ml). $Re_2(CO)_{10}$ (87 mg, 0.13 mmol) was added and the mixture was heated by microwave to 220 °C for 15 min (Careful, toxic CO gas is released during the reaction, take appropriate precautions). The solvent was evaporated *in vacuo* and the crude was purified by column chromatography (silica gel, Hexane/EtOAc 2:1) yielding pure **6b** as

a yellow oil (64 mg, 0.12 mmol, 44 %). R_f = 0.14 (silica gel, Hexane/EtOAc 3:1). UPLC (gradient U1): RT = 2.97 min.

^{1}H NMR (500 MHz, $CDCl_3$): δ (ppm): 2.47 – 2.51 (m, 2H), 2.59 – 2.85 (m, 2H), 3.71 (s, 3H), 3.73 (s, 3H), 3.80 (s, 3H), 5.11 (d, J = 2.3 Hz, 1H), 5.58 (d, J = 2.2 Hz, 1H). ^{13}C NMR (125 MHz, $CDCl_3$): δ (ppm): 23.85, 35.31, 52.07, 52.12, 59.00, 66.31, 72.52, 80.02, 100.80, 145.14, 164.47, 172.39, 192.70. IR bands (Golden Gate, cm^{-1}): 2024, 1921. HR-ESI mass spectrum (MeOH): found 511.03967; calcd. for [$C_{15}H_{15}O_8Re+H^+$] 511.03972.

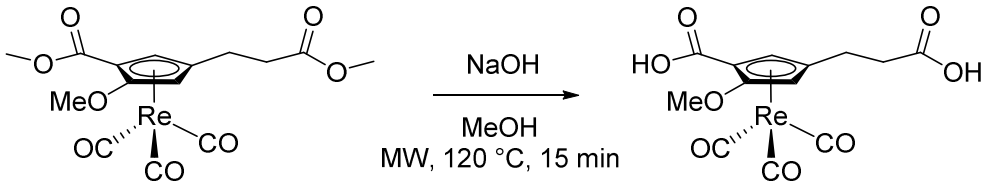

7b. A solution of **6b** (51 mg, 0.101 mmol) in MeOH (3 ml) and 1 M NaOH (0.4 ml) in an Anton Paar microwave vial (10 ml) was heated by microwave to 120 °C for 15 min. The crude was diluted with 1 M HCl (10 ml) and washed with DCM twice (2 x 10 ml). The combined organic phase was washed once with water (10 ml) dried over $MgSO_4$ and the solvent removed *in vacuo* yielding **7b** as a pale yellow solid (23 mg, 0.048 mmol, 48 %). The product was used in the next step without further purification.

UPLC (gradient U1): RT = 2.34 min. ^{1}H NMR (500 MHz, CD_3OD): δ (ppm): 2.46 – 2.83 (m, 4H), 3.72 (s, 3H), 5.58 (s, 1H), 5.73 (s, 1H). ^{13}C NMR (125 MHz, CD_3OD): δ (ppm): 24.95, 30.75, 36.35, 59.36, 68.49, 81.75, 103.04, 147.10, 167.45, 175.74, 194.49. IR bands (Golden Gate, cm^{-1}): 2025, 1923. HR-ESI mass spectrum (MeOH+NaOH): found 504.99033; calcd. for [$C_{13}H_{11}O_8Re+Na^+$] 504.99037.

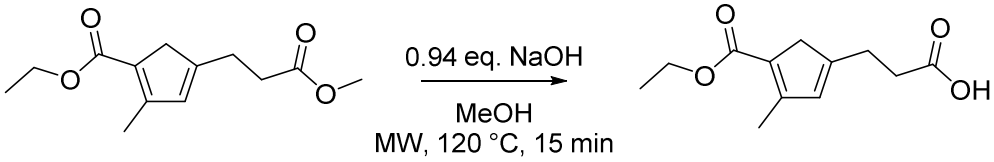

8a. 1a (38 mg, 0.16 mmol) was dissolved in MeOH (1 ml) in an Anton Paar microwave vial (10 ml) equipped with a stirring bar. 1 M NaOH was added (0.150 ml, 0.150 mmol) and the solution was heated to 120 °C for 15 min. UPLC measurement showed complete consumption of the starting material. The reaction solution was diluted with

H_2O (5 ml) and neutralized to pH = 3 by dropwise addition of 1 M HCl. **8a** was obtained by evaporating the solvent *in vacuo* and was used without further purification.
UPLC (gradient U1): RT = 2.49 min.

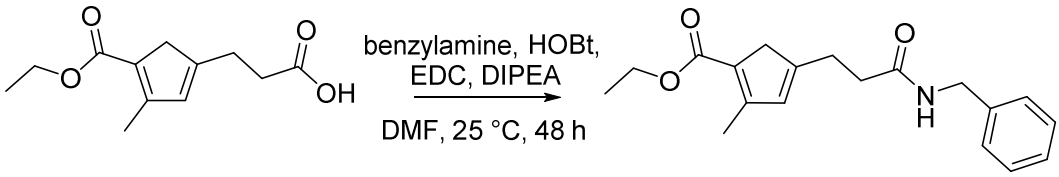

9a. 8a (59 mg, 0.26 mmol) was dissolved in DMF (4 ml). Benzylamine (0.031 ml, 0.29 mmol) and HOBt (39 mg, 0.29 mmol) were added under stirring. After 5 min, EDC (55 mg, 0.29 mmol) and DIPEA (0.100 ml, 0.57 mmol) were added and the solution was stirred for 48 h. The solvent was removed *in vacuo* and the crude was purified by preparative HPLC (Method A) and **9a** was obtained as a yellow oil (57 mg, 0.18 mmol, 69 %).
UPLC (gradient U1): RT = 2.76 min. ^{1}H NMR (400 MHz, $CDCl_3$): δ (ppm): 1.29 (t, J^3 = 7.1 Hz, 3H), 2.27 (t, J^3 = 2.3 Hz, 3H), 2.48 (t, J^3 = 7.5 Hz, 2H), 2.76 (t, J^3 = 7.5 Hz, 2H), 3.21 (m, 2H), 4.18 (q, J^3 = 7.1 Hz, 2H), 4.42 (d, J = 5.7 Hz, 2H), 6.08 (s, 1H), 6.13 (t, J = 5.3 Hz, 1H), 7.20 – 7.33 (m, 5H). ^{13}C NMR (126 MHz, $CDCl_3$): δ (ppm): 14.57, 15.59, 26.73, 35.89, 43.93, 44.42, 59.63, 127.20, 127.79, 127.89, 128.88, 133.07, 137.86, 153.11, 155.85. 165.26, 172.61. HR-ESI mass spectrum (MeOH): found 314.17497; calcd. for [$C_{19}H_{23}NO_3$+H^+] 314.17507.

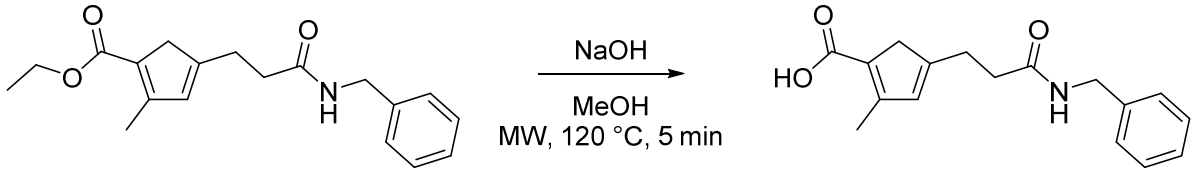

10a. 9a (50 mg, 0.16 mmol) was dissolved in MeOH (2 ml) in an Anton Paar microwave vial (10 ml) equipped with a stirring bar. 1 M NaOH (1 ml) was added and the solution was heated to 120 °C for 5 min. UPLC measurement showed complete consumption of the starting material. The reaction solution was diluted with H_2O (5 ml) and neutralized to pH = 3 by dropwise addition of 1 M HCl. **10a** was obtained by evaporating the solvent *in vacuo* and was used without further purification.
UPLC (gradient U1): RT = 2.33 min.

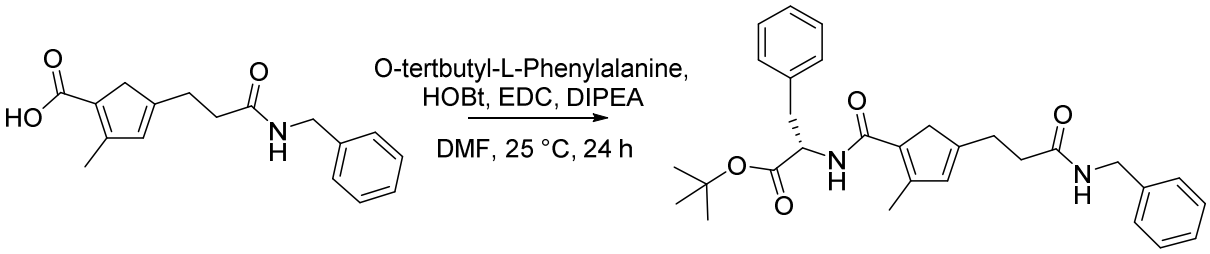

11a. The crude of **10a** obtained from **9a** (36 mg, 0.115 mmol) was dissolved in DMF (3 ml). O-tertbutyl-L-Phenylalanine (33 mg, 0.13 mmol) and HOBt (17 mg, 0.13 mmol) were added under stirring. After 5 min, EDC (24 mg, 0.13 mmol) and DIPEA (0.044 ml, 0.25 mmol) were added and the solution was stirred for 24 h. The solvent was removed *in vacuo* and the crude was purified by preparative HPLC (Method A) and **11a** was obtained as a yellow oil (15 mg, 0.03 mmol, 26 % from **9a**).

UPLC (gradient U1): RT = 3.19 min. ^{1}H NMR (500 MHz, $CDCl_3$) δ (ppm) 1.41 (s, 9H), 2.22 (t, J^3 = 2.2 Hz, 3H), 2.43 (t, J^3 = 7.6 Hz, 3H), 2.75 (t, J^3 = 7.6 Hz, 2H), 3.12 – 3.16 (m, 4H), 4.44 (d, J^3 = 5.7 Hz, 2H), 4.86 (m, 1H), 5.80 (m, 1H), 5.98 (d, J^3 = 7.5 Hz, 1H), 6.04 (s, 1H), 7.15 – 7.33 (m, 10H). ^{13}C NMR (126 MHz, $CDCl_3$): δ (ppm): 15.37, 26.50, 28.13, 35.98, 38.35, 43.83, 53.40, 76.90, 77.16, 77.41, 82.48, 127.05, 127.73, 127.94, 128.46, 128.60, 128.89, 129.57, 129.74, 133.12, 136.54, 138.26, 150.68, 151.24, 164.70, 171.23, 171.79. HR-ESI mass spectrum (MeOH): found 489.27518; calcd. for [$C_{30}H_{35}N_2O_4$+H^+] 489.27478.

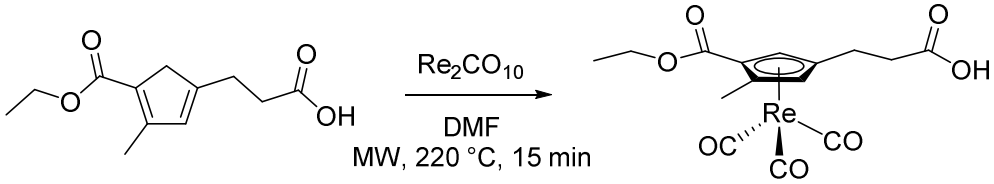

8b. 8a (80 mg, 0.34 mmol) was dissolved in DMF (4 ml) in an Anton Paar microwave vial (10 ml). $Re_2(CO)_{10}$ (110 mg, 0.17 mmol) was added and the mixture was heated by microwave to 220 °C for 15 min (Careful, toxic CO gas is released during the reaction, take appropriate precautions). UPLC showed complete consumption of the starting material. The crude solution was dried in vacuo and used without further purification in the next step.

UPLC (gradient UMS1): RT = 2.88 min.

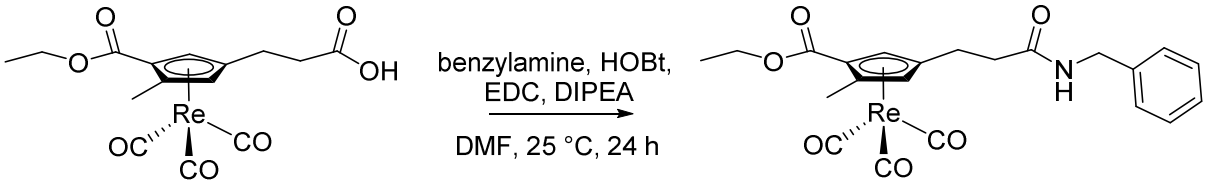

9b. 8b (154 mg, 0.31 mmol) was dissolved in DMF (5 ml). Benzylamine (0.037 ml, 0.34 mmol) and HOBt (46 mg, 0.34 mmol) were added under stirring. After 5 min, EDCI (66 mg, 0.34 mmol) and DIPEA (0.120 ml, 0.69 mmol) were added and the solution was stirred for 24 h. The solvent was removed *in vacuo* and the crude was purified by preparative HPLC (Method A) and **9b** was obtained as an orange oil (45 mg, 0.08 mmol, 26%).

UPLC (gradient U1): RT = 3.23 min. ^{1}H NMR (400 MHz, $CDCl_3$): δ (ppm): 1.31 (t, J^3 = 7.1 Hz, 3H), 2.40 (m, J = 3.3 Hz, 2H), 2.48 (s, 3H) 2.68 – 2.88 (m, 2H), 4.17 – 4.34 (m, 2H), 4.45 (d, J = 5.7, 2 H), 5.20 (d, J = 2.1 Hz, 1H), 5.77 (d, J = 2.2 Hz, 1H), 5.85 (t, 1 H), 7.25 – 7.36 (m, 5H). ^{13}C NMR (125 MHz, $CDCl_3$): δ (ppm): 13.87, 14.28, 23.75, 38.07, 44.10, 61.13, 84.61, 85.73, 86.06, 107.58, 110.76, 127.95, 128.04, 128.99, 137.78, 164.92, 171.19, 193.56. IR bands (Golden Gate, cm^{-1}): 2021, 1918. HR-ESI mass spectrum (MeOH): found 584.10780; calcd. for [$C_{22}H_{23}O_6NRe+H^+$] 584.10774.

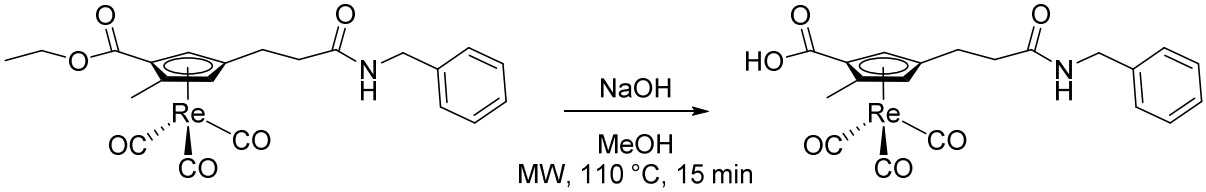

10b. A solution of **9b** (43 mg, 0.074 mmol) in MeOH (2 ml) and 1 M NaOH (0.15 ml) in an Anton Paar microwave vial (10 ml) was heated by microwave to 110 °C for 15 min. The crude was diluted with 1 M HCl (10 ml) and washed with DCM twice (2 x 10 ml). The combined organic phase was washed once with water (10 ml) dried over $MgSO_4$ and the solvent removed *in vacuo* yielding **10b** as an orange solid (32 mg, 0.058 mmol, 78 %). The product was used in the next step without further purification.

UPLC (gradient U1): RT = 2.81 min. ^{1}H NMR (400 MHz, CD_3OD): δ (ppm): 2.45 (s, 3H), 2.45 (m, 2H), 2.61 – 2.68 (m, 1H), 2.75 – 2.82 (m, 1H), 4.37 (m, 2H), 5.42 (d, J^3

= 2.1 Hz, 1H), 5.89 (d, J^3 = 2.2 Hz, 1H), 7.21 – 7.32 (m, 5H). ^{13}C NMR (101 MHz, CD_3OD): δ (ppm): 12.63, 23.71, 37.17, 42.77, 84.60, 86.65, 107.46, 110.82, 126.87, 127.26, 128.18, 138.49, 166.58, 172.44, 193.60. IR bands (Golden Gate, cm^{-1}): 2021, 1917. HR-ESI mass spectrum (MeOH): found 554.06196; calcd. for [$C_{20}H_{18}O_6NRe$-H^+] 554.06189.

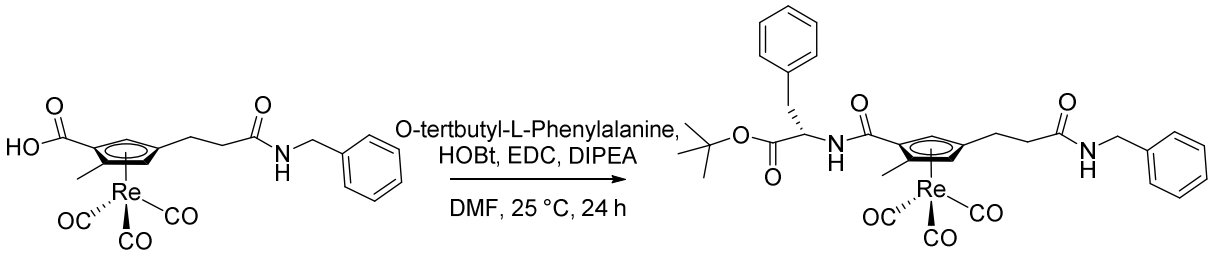

11b. 10b (181 mg, 0.326 mmol) was dissolved in DMF (2 ml). O-tertbutyl-L-Phenylalanine (93 mg, 0.36 mmol) and HOBt (49 mg, 0.36 mmol) were added under stirring. After 5 min, EDCI (69 mg, 0.36 mmol) and DIPEA (0.125 ml, 0.72 mmol) were added and the solution was stirred for 24 h. The solvent was removed *in vacuo* and the crude was purified by preparative HPLC (Method A) and **11b** was obtained as a pale red solid and directly used for the next step (112.8 mg, 0.149 mmol, 46%).
UPLC (gradient U1): RT = 3.68 min.

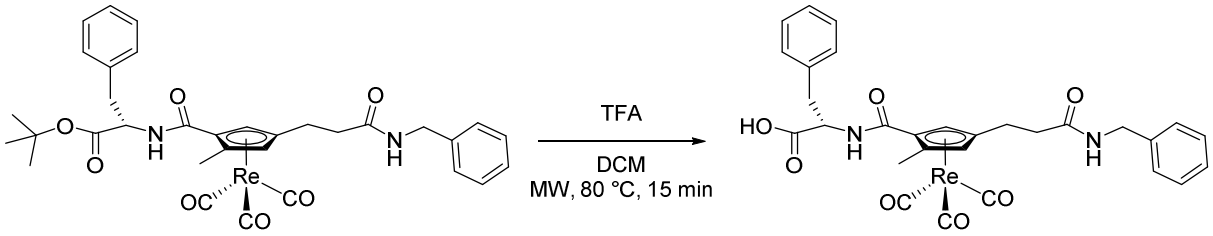

12b. 11b (15 mg, 0.02 mmol**)** was dissolved in DCM (2 ml) in an Anton Paar microwave vial (10 ml). TFA (0.5 ml) was added and the solution was heated to 80 °C by microwave for 15 min. The solvent was evaporated and the crude was purified by preparative HPLC (Method A) and **12b** was obtained as an orange oil (15 mg, 0.16 mmol, 80 %).
UPLC (gradient U1): RT = 3.08 min, 3.13 min. ^{1}H NMR (500 MHz, CD_3OD): δ (ppm): 2.31 (s, 3 H), 2.37 (s, 3H), 2.42 – 2.45 (m, 4H), 2.61 – 2.67 (m, 2H), 2.72 – 2.79 (m, 2H), 3.04 – 3.09 (m, 2H), 3.25 – 3.29 (m, 2H), 4.34 – 4.35 (m, 4H), 4.71 – 4.75 (m, 2H), 5.35 (d, J^3 = 2.0 Hz, 1H), 5.38 (d, J^3 = 2.0 Hz, 1H), 5.95 (d, J^3 = 2.0 Hz, 1H), 5.96 (d, J^3 = 2.0 Hz, 1H), 7.16 – 7.32 (m, 20H). ^{13}C NMR (101 MHz, CD_3OD): 13.98, 25.21,

25.25, 37.90, 38.07, 38.62, 38.78, 44.17, 44.19, 55.16, 55.23, 85.50, 85.65, 86.61, 87.26, 90.94, 91.47, 107.56, 108.37, 110.41, 110.74, 127.81, 128.27, 128.36, 128.65, 128.67, 129.53, 129.59, 130.15. 130.25, 138.46, 138.49, 139.84, 165.84, 166.12, 173.85, 173.88, 174.37, 174.56, 195.12. IR bands (Golden Gate, cm^{-1}): 2021, 1921. HR-ESI mass spectrum (MeOH): found 725.12675; calcd. for [$C_{29}H_{27}N_2O_7Re+Na^+$] 725.12680.

[^{99m}Tc(OH$_2$)$_3$(CO)$_3$]$^+$

A Biotage microwave vial (2 – 5 ml) was charged with sodium boranocarbonate (4 mg, 38.5 *µ*mol), sodium tartrate dihydrate (7 mg, 30.4 *µ*mol) and sodium tetraborate decahydrate (7 mg, 18.5 *µ*mol). The vial was sealed and flushed with N_2 for 5 min before adding [$^{99m}TcO_4$]$^-$ eluate (1-2 ml) from a commercial generator. The solution was heated by microwave to 110 °C for 7 min. In order to normalize the overpressure, evolving gases were released with a 1 ml disposable syringe. Excess sodium boranocarbonate was quenched *via* dropwise addition of 1 M HCl to pH = 2 and the solution was subsequently basified by addition of 1 M NaOH to pH = 8.

General procedure for the labelling of Cp-Ligands 1a, 4a, 6a, 3a and 12a.

Generally, 0.5 ml of a 5 mM stock solution of the respective ligand in MeOH was added to a Biotage microwave vial (2 – 5 ml). The vial was sealed, and the solvent was removed by passing a stream of N_2 through the vial *via* two syringe needles for 30 min.

Method A (**1a**, **4a**, **6a**). [^{99m}Tc(OH$_2$)$_3$(CO)$_3$]$^+$ (0.5 ml, pH = 8) was added to the dried ligand and the pH adjusted to 12 by addition of 1 M NaOH. The solution was heated by microwave to 120 °C for 30 min. In order to normalize the overpressure, evolving gases were released with a 1 ml disposable syringe-needle.

Method B “one pot” (**1a**, **4a**, **6a**, **3a**, **12a**). The vial with the dried ligand was opened and sodium boranocarbonate (4 mg, 38.5 *µ*mol), sodium tartrate dihydrate (7 mg, 30.4 *µ*mol) and sodium tetraborate decahydrate (7 mg, 18.5 *µ*mol). The vial was sealed again and flushed with N_2 for 5 min before adding [$^{99m}TcO_4$]$^-$ eluate (1-2 ml) from a commercial generator. The solution was heated by microwave to 120 °C for 30 min (**1a**, **4a**, **6a**) or 140 °C for 30 min (**3a**) or 2 x 30 min (**12a**). Complexes **2c**, **5c**, **7c** and **3c** were obtained in radiochemical puritiy > 95%. For **12c**, some [$^{99m}TcO_4$]$^-$ and

$[^{99m}Tc(OH_2)_3(CO)_3]^+$ was observed (< 20 %). **12c** was purified by loading the reaction mixture onto a Chromafix C18 cartridge and washing it with H_2O (2 ml). Pure **12c** could be eluted by washing the cartridge with MeOH (2 ml).

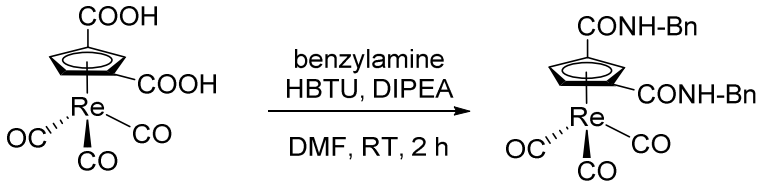

13. S2b (140 mg, 0.33 mmol), benzylamine (0.072 ml, 0.66 mmol), HBTU (251 mg, 0.66 mmol) and DIPEA (0.115 ml, 0.66 was dissolved in DMF (6 ml) and stirred at room temperature for 2 h. H_2O (4 ml) was added to the reaction solution and an off-white precipitate was observed. The precipitate was collected by centrifugation, washed with water (2 x 5 ml) and dried *in vacuo* yielding **13** (no yield was determined).
^1H NMR (400 MHz, CD_3OD): δ (ppm) 4.47 (s, 4H), 6.21 (d, J^3 = 1.8 Hz, 2H), 6.82 (t, J^3 = 1.8 Hz, 1H), 7.24 – 7.32 (m, 10H).

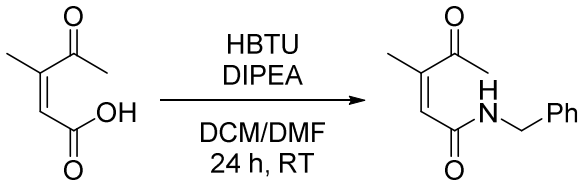

15. **14** (1.34 g, 10.5 mmol) was dissolved in a DCM/DMF mixture (55 ml, 10:1 DCM/DMF). HBTU (8 g, 21 mmol) and DIPEA (3.7 ml, 21 mmol) were added and the mixture was stirred for 24 h at room temperature. The solvent was evaporated *in vacuo* and the crude was purified by column chromatography on silica (3:2, Hexane/EtOAc) yielding pure **15** (0.62 g, 2.9 mmol, 28 %).
R_f: 0.4 (silica gel, Hexane/EtOAc 3:2). ^1H NMR (400 MHz, CD_3OD): δ (ppm) 2.14 (d, J^3 = 1.4 Hz, 3H), 2.39 (s, 3H), 4.48 (s, 2H), 6.87 (q, J^3 = 1.4 Hz, 1H), 7.26 – 7.38 (m, 5H).

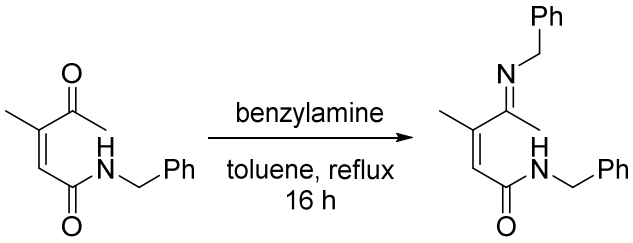

AFX045

16. 15 (0.295 g, 1.4 mmol) and benzylamine (0.164 ml, 1.5 mmol) were dissolved in toluene (10 ml). The solution was refluxed through a Dean-Stark apparatus overnight. The next day the solvent was evaporated *in vacuo* and the crude was purified by column chromatography on silica (3:2, Hexane/EtOAc) yielding pure **16** (0.171 g, 0.56 mmol, 40 %).

R_f: 0.34 (silica gel, Hexane/EtOAc 3:2). ^{1}H NMR (400 MHz, $CDCl_3$): δ (ppm) 1.25 (s, 3H), 1.96 (d, J^3 = 1.6 Hz, 3H), 3.06 (m, 2H), 4.43 – 4.61 (m, 2H), 5.98 (q, J^3 = 1.6 Hz, 1H), 7.04 – 7.28 (m, 10H).

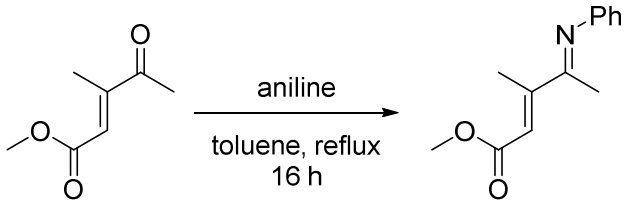

19. **18** (83 mg, 0.58 mmol) and aniline (0.06 ml, 0.64 mmol) were dissolved in toluene (15 ml). The solution was refluxed through a Dean-Stark apparatus overnight. The next day the solvent was evaporated *in vacuo* yielding **19**.

^{1}H NMR (400 MHz, $CDCl_3$): δ (ppm) 2.00 (s, 3H), 2.45 (s, 3H), 3.79 (s, 3H, 6.39 (s, 1H), 6.69 (d, J^3 = 7.4 Hz, 2H), 7.08 (t, J^3 = 7.4 Hz, 1H), 7.33 (t, J^3 = 7.4 Hz, 2H).

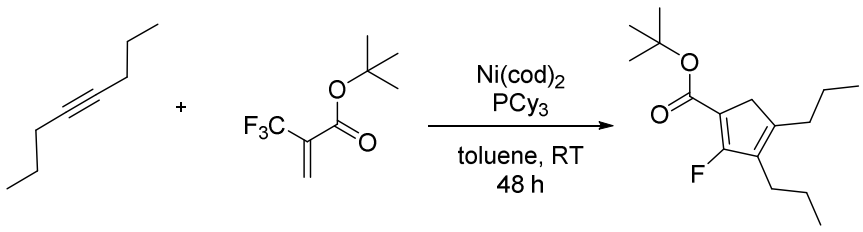

20. 4-ocytne (0.1 ml, 0.7 mmol), α-trifluoromethylacrylic acid t-butyl ester (0.1 ml), $Ni(cod)_2$ (186 mg, 0.7 mmol), and tricyclohexylphosphine (192 mg, 0.7 mmol) were dissolved in toluene (5 ml) in a glove-box. The solution was stirred at room temperature

for 48 h. The crude was filtered through a pad of silica with EtOAc (10 ml), concentrated *in vacuo* and purified by column chromatography on silica (20:1 Hexane/EtOAc) yielding pure **20.**

^{1}H NMR (400 MHz, $CDCl_3$): δ (ppm) 0.90 (m, 6H), 1.42 – 1.53 (m, 13H), 2.22 (t, J^3 = 7.5 Hz, 2H), 2.31 (t, J^3 = 7.5 Hz, 2H), 3.07 (d, J^3 = 7.5 Hz, 2H).

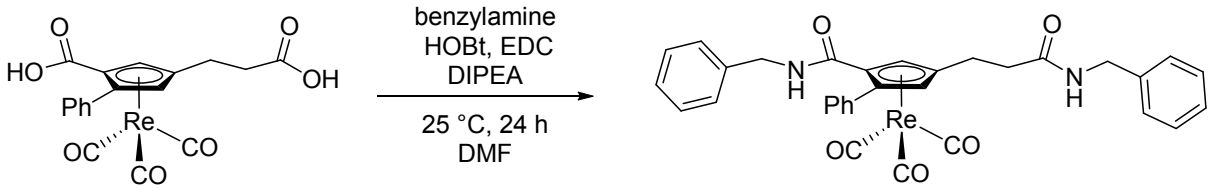

21. 5b (28 mg, 0.053 mmol) was dissolved in DMF (2 ml). Benzylamine (0.013 ml, 0.12 mmol) and HOBt (16 mg, 0.12 mmol) were added under stirring. After 5 min, EDC (22 mg, 0.12 mmol) and DIPEA (0.040 ml, 0.23 mmol) were added and the solution was stirred for 24 h. The solvent was removed *in vacuo* and the crude was purified by preparative HPLC (Method A) and **21** was obtained as a pale orange oil (18 mg, 0.026 mmol, 49 %).

UPLC (gradient U1): RT = 3.37 min. ^{1}H NMR (400 MHz, $CDCl_3$): δ (ppm) 2.44 (t, J^3 = 7.24 Hz, 2H), 2.26 – 2.93 (m, 2H), 4.36 (d, J^3 = 5.7 Hz, 2H), 4.44 (d, J^3 = 5.68 Hz, 2H), 5.46 (d, J^3 = 2.7 Hz, 2H) 5.66 (d, J^3 = 5.5 Hz, 2H), 5.91 (m, 2H), 7.04 – 7.06 (m, 2H), 7.24 - 7.29 (m, 13H). ^{13}C NMR (125 MHz, $CDCl_3$): δ (ppm): 23.64, 38.10, 44.05, 44.12, 77.36, 86.00, 87.15, 107.04, 109.81, 127.74, 127.84, 128.02, 128.81, 128.94, 129.09, 129.57, 130.31, 131.10, 137.20, 137.90, 162.81, 170.91, 193.55. IR bands (Golden Gate, cm^{-1}): 2021, 1919. HR-ESI mass spectrum (MeOH): found 729.13591; calcd. for [$C_{32}H_{27}N_2O_5Re+Na^+$] 729.13697.

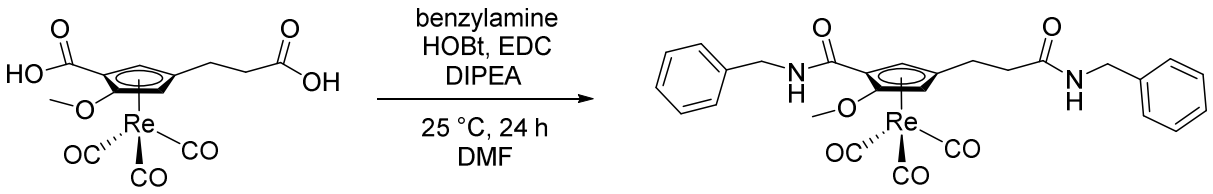

22. 7b (23 mg, 0.048 mmol) was dissolved in DMF (2 ml). Benzylamine (0.011 ml, 0.11 mmol) and HOBt (14 mg, 0.11 mmol) were added under stirring. After 5 min, EDC (20 mg, 0.11 mmol) and DIPEA (0.037 ml, 0.21 mmol) were added and the solution was stirred for 24 h. The solvent was removed *in vacuo* and the crude was purified by preparative HPLC (Method A) and **22** was obtained as a pale orange solid (8 mg, 0.012 mmol, 25 %).

UPLC (gradient U1): RT = 3.13 min. ^{1}H NMR (400 MHz, $CDCl_3$): δ (ppm): 2.33 – 2.42 (m, 2H) 2.62 – 2.69 (m, 1H), 2.85 – 2.97 (m, 1H), 3.68 (s, 3H), 4.44 – 4.46 (m, 2H), 4.55 – 4.57 (m, 2H), 5.16 (d, J^3 = 2.3 Hz, 1H), 5.77 (d, 2.2 Hz, 1H), 5.80 (m, 1H), 6.88 (m, 1H), 7.26 – 7.34 (m, 10H). ^{13}C NMR (126 MHz, $CDCl_3$): δ (ppm): 24.18, 29.86, 37.88, 43.28, 43.96, 59.34, 66.68, 80.47, 100.71, 127.42, 127.55, 127.97, 128.87, 128.95, 138.05, 138.47, 141.29, 162.98, 170.73, 193.16. IR bands (Golden Gate, cm^{-1}): 2020, 1919. HR-ESI mass spectrum (MeOH): found 683.11702; calcd. for $[C_{27}H_{25}N_2O_6Re+Na^+]$ 683.11623.

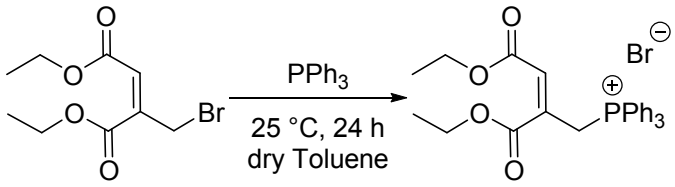

26. 25 (800 mg, 3.0 mmol) was dissolved in dry toluene (60 ml) and kept under a nitrogen atmosphere. To this solution triphenylphosphine (870 mg, 3.3 mmol) was added. The solution was stirred at room temperature and under nitrogen for 24 h. The precipitate was collected by filtration (frit) and washed with cold toluene. The white solid was dried *in vacuo* yielding **26** as an off-whiteish powder (no yield was determined).

^{1}H NMR (400 MHz, $CDCl_3$): δ (ppm) 1.04 (t, J^3 = 7.16 Hz, 3H), 1.23 (t, J^3 = 7.14 Hz, 3H), 3.74 (q, J^3 = 7.14 Hz, 2H), 4.12 (t, J^3 = 7.14 Hz, 2H), 5.30 – 5.33 (m, 2H), 7.04 – 7.05 (m, 1H), 7.63 – 7.93 (m, 15H).

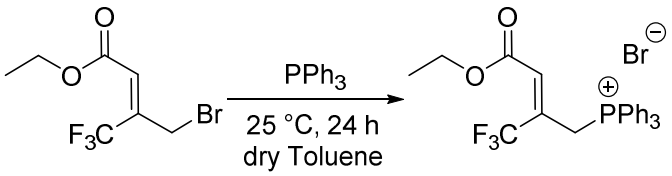

28. 27 (482 mg, 1.85 mmol) was dissolved in dry toluene (50 ml) and kept under a nitrogen atmosphere. To this solution triphenylphosphine (0.5 mg, 1.9 mmol) was added. The solution was stirred at room temperature and under nitrogen for 24 h. The precipitate was collected by filtration (frit) and washed with cold toluene. The white solid was dried *in vacuo* yielding **28** as a white powder (no yield was determined).
^{1}H NMR (400 MHz, $CDCl_3$): δ (ppm) 1.05 (t, J^3 = 8 Hz, 3H), 3.87 (q, J^3 = 8 Hz, 2H), 5.55 - 5.60 (m, 2H), 6.37 – 6.38 (m, 1H), 7.63 – 7.73 (m, 15H).

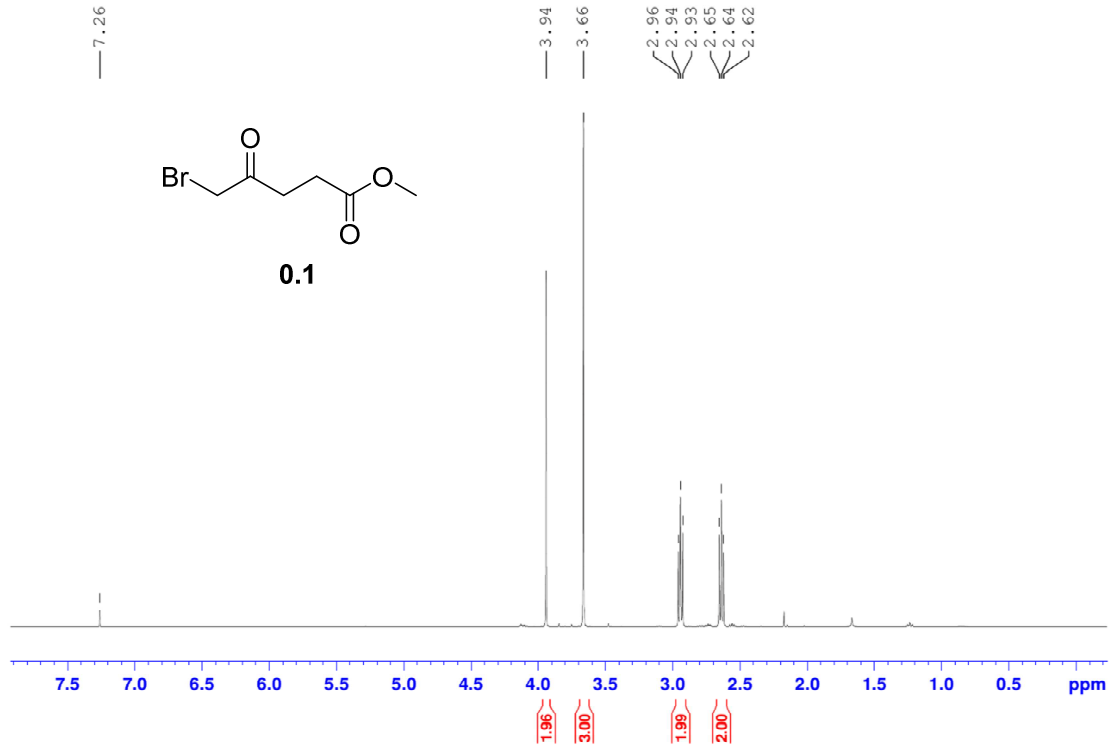

Figure 29.^{1}H NMR of **0.1** in $CDCl_3$.

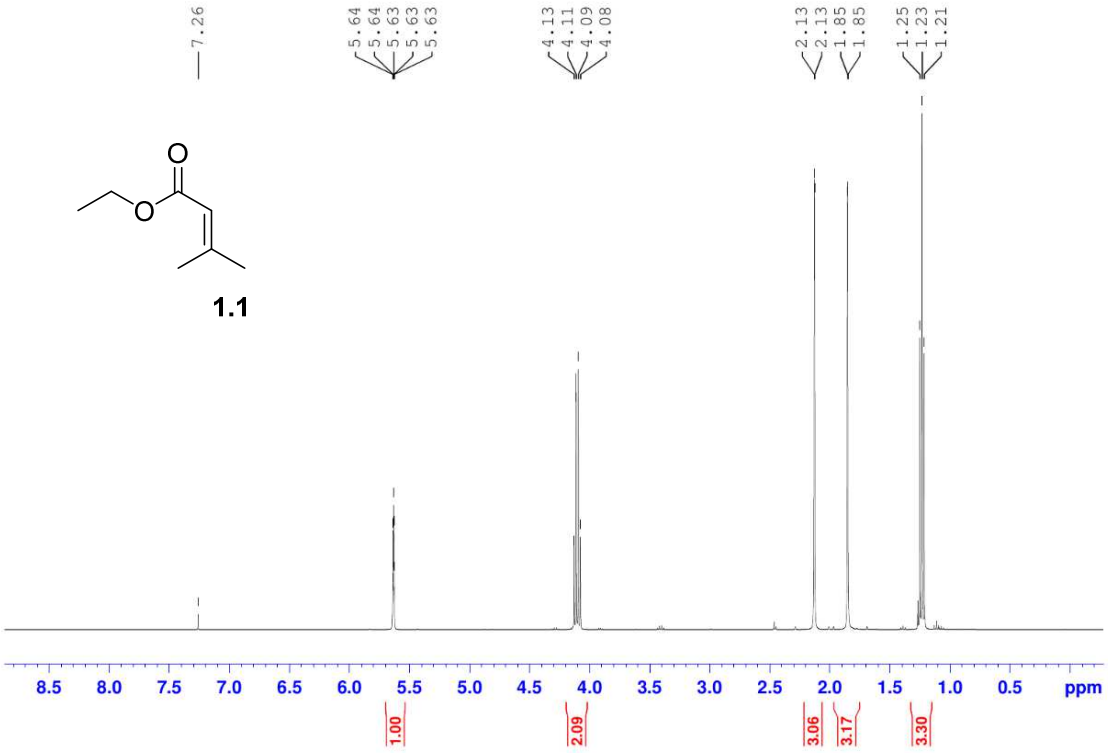

Figure 30. ^{1}H NMR of **1.1** in $CDCl_3$.

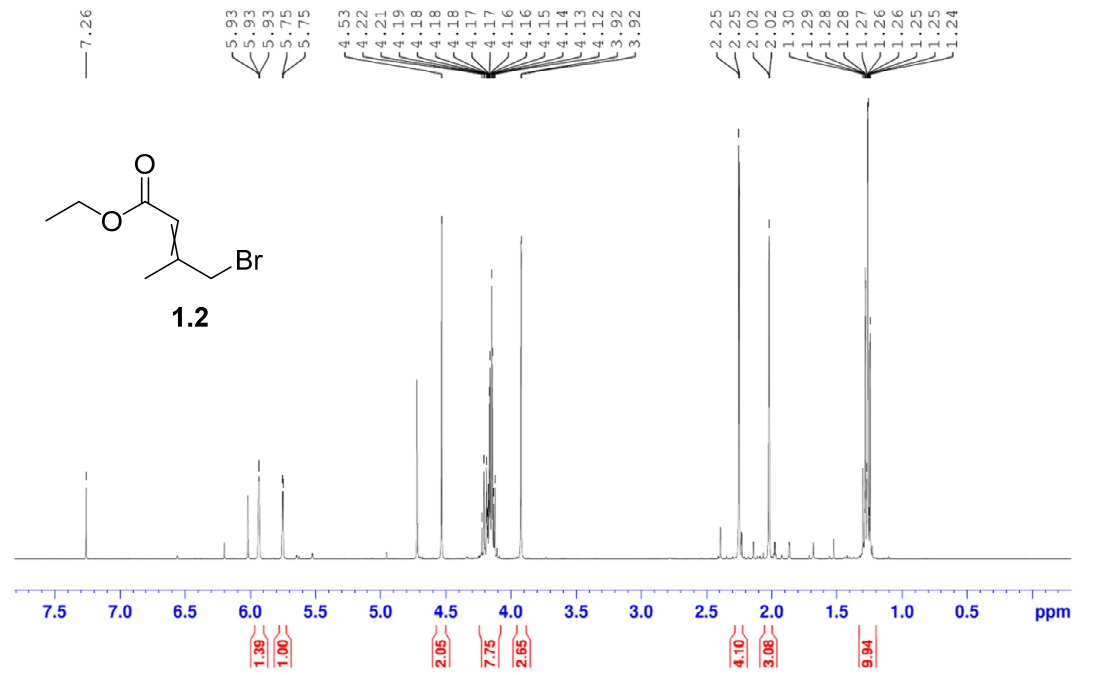

Figure 31. ^{1}H NMR of **1.2** in $CDCl_3$.

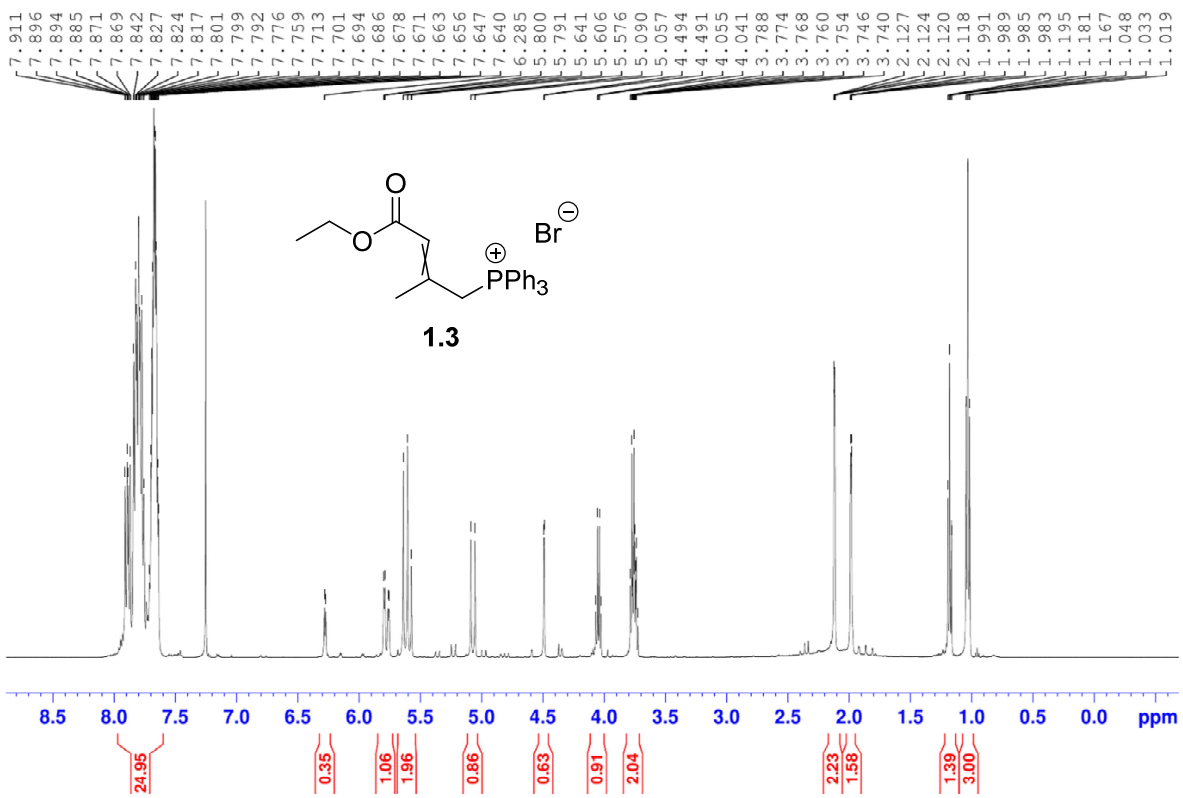

Figure 32. ^{1}H NMR of **1.3** in $CDCl_3$.

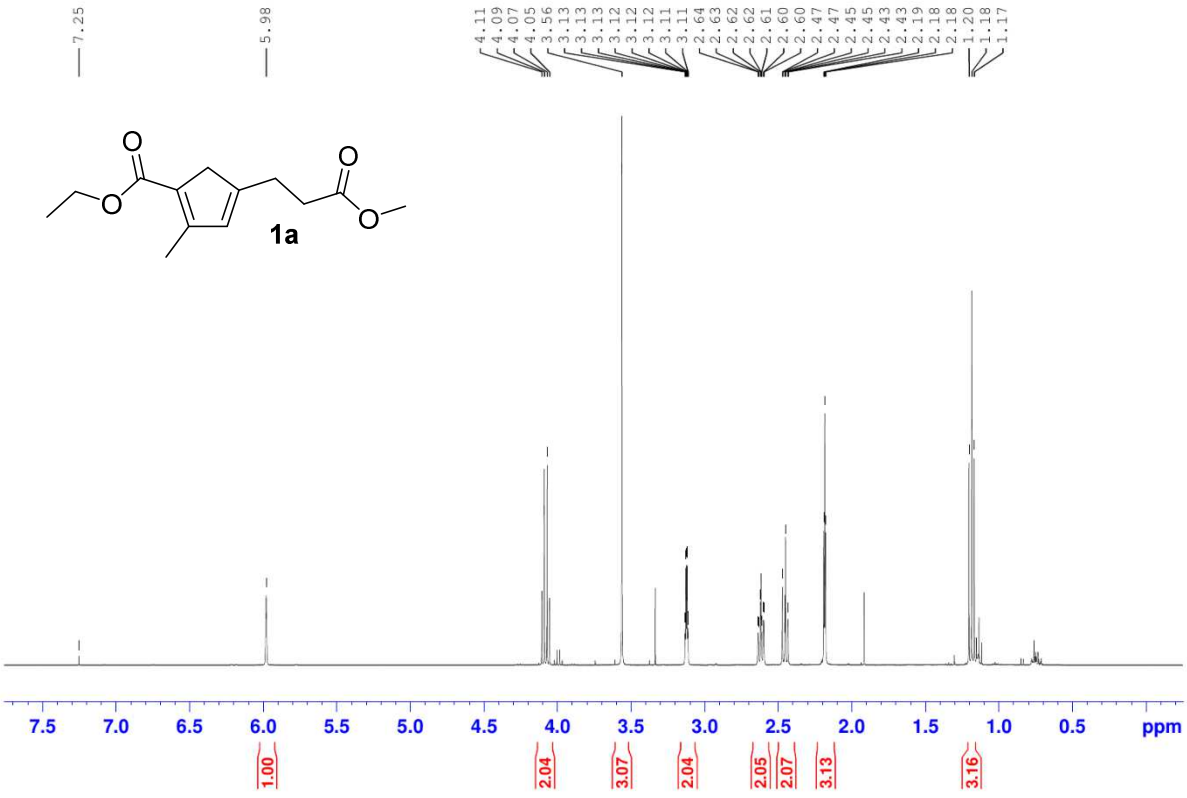

Figure 33. ^{1}H NMR of **1a** in $CDCl_3$.

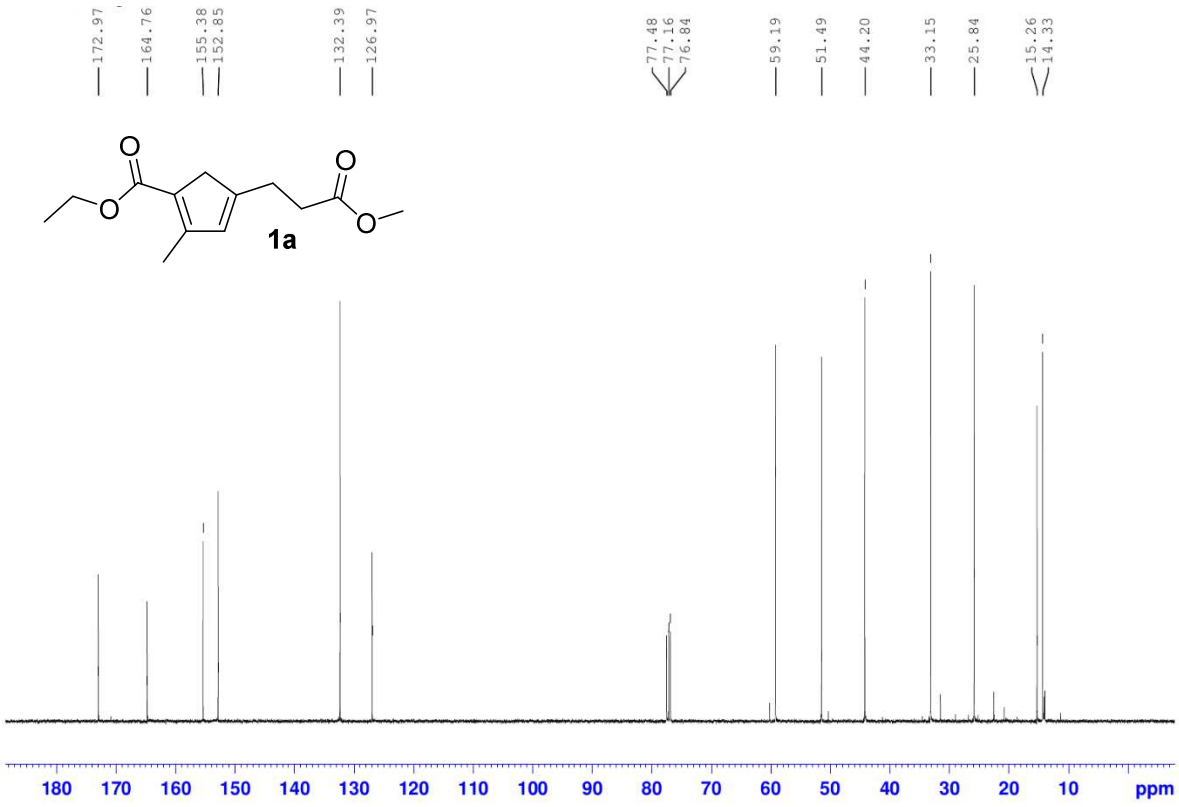

Figure 34. ^{13}C NMR of **1a** in $CDCl_3$.

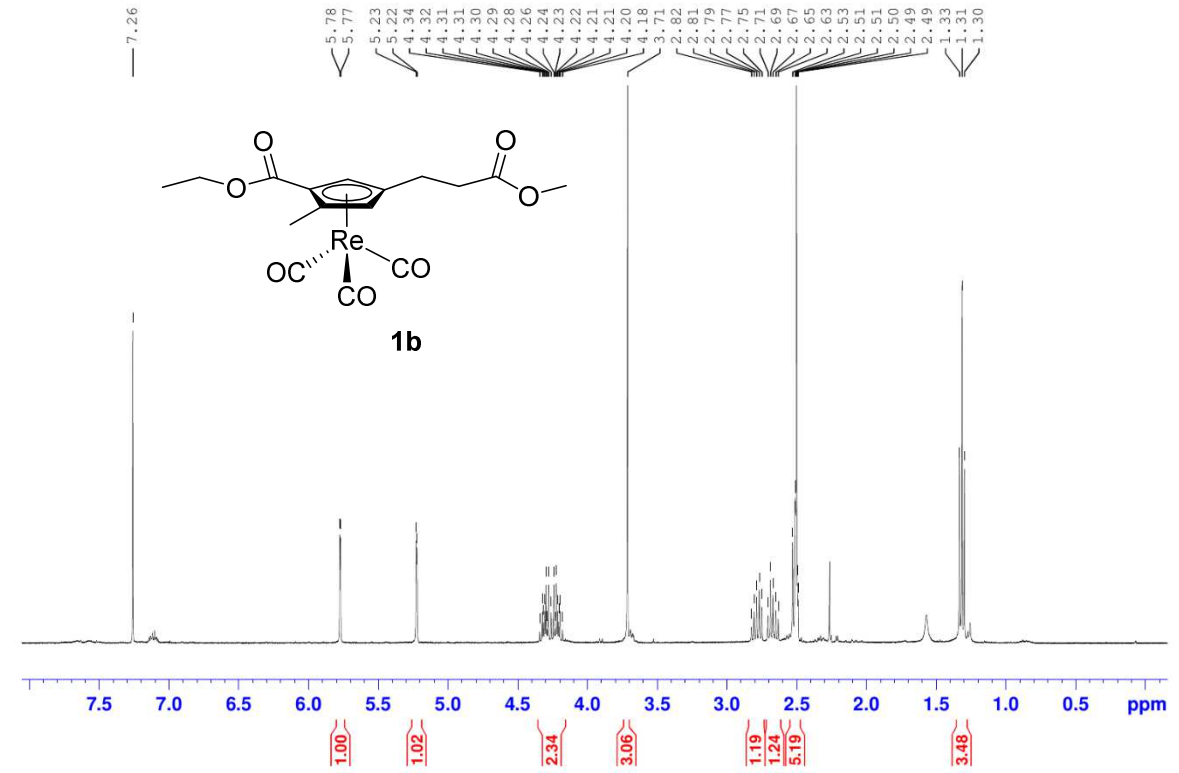

Figure 35. ^{1}H NMR of **1b** in $CDCl_3$.

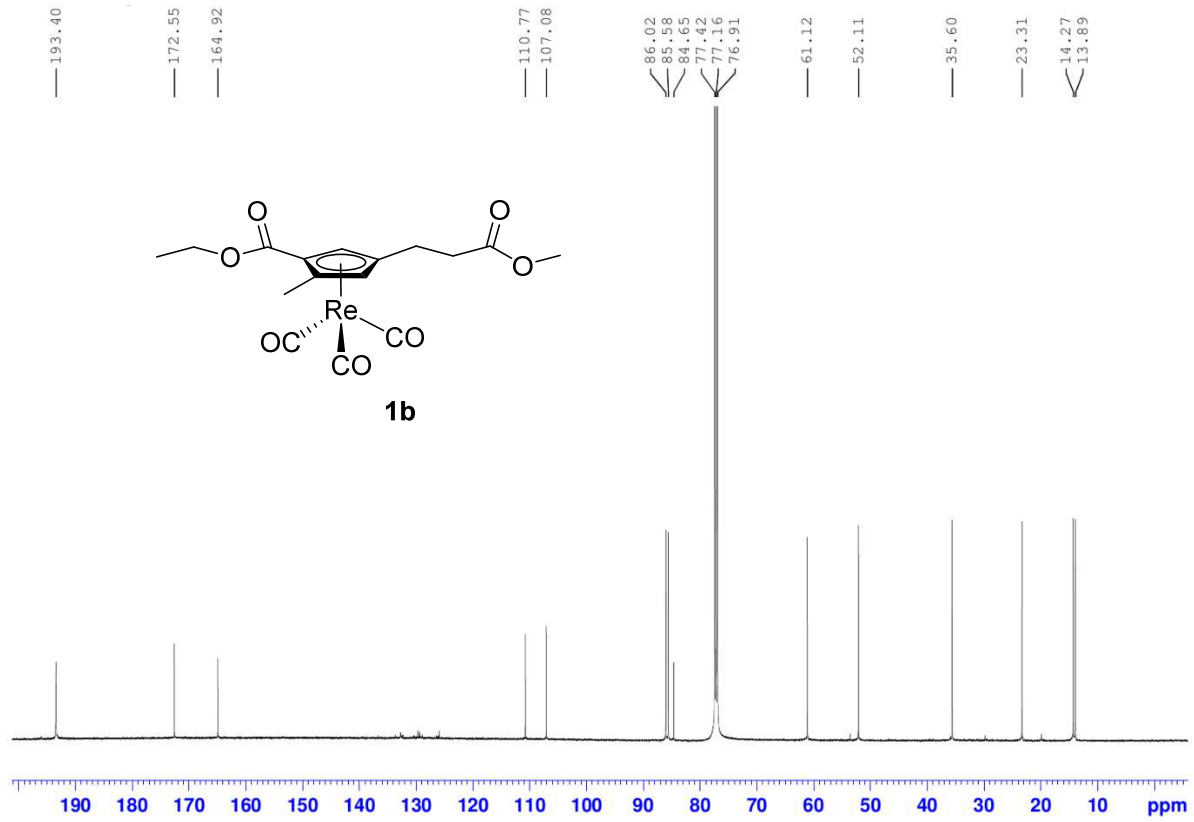

Figure 36. ^{13}C NMR of **1b** in $CDCl_3$.

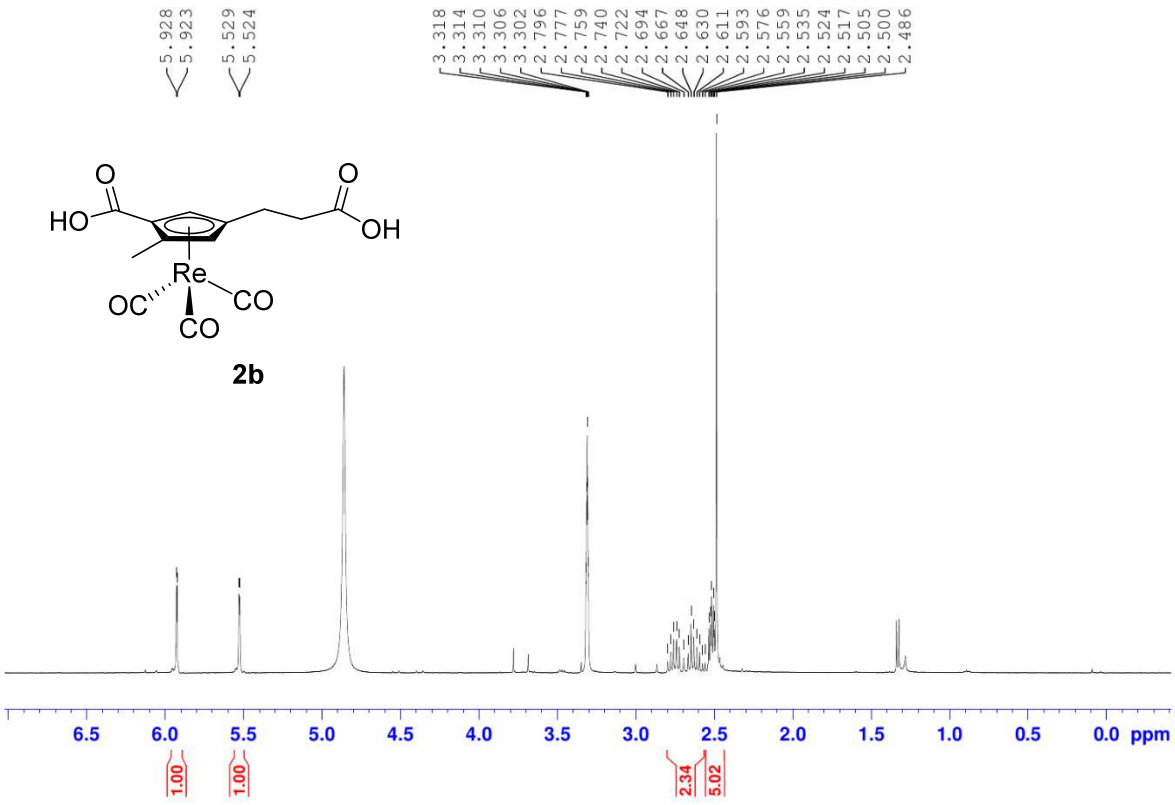

Figure 37. ^{1}H NMR of **2b** in CD_3OD.

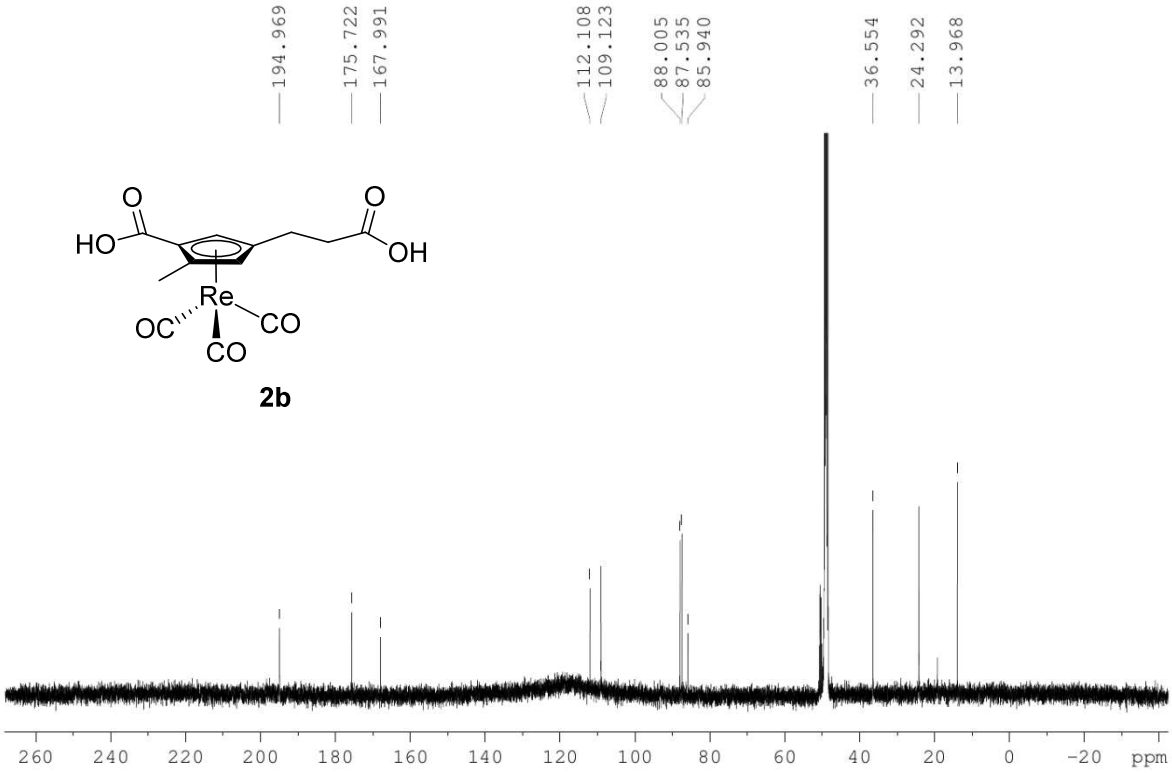

Figure 38. ^{13}C NMR of **2b** in CD_3OD.

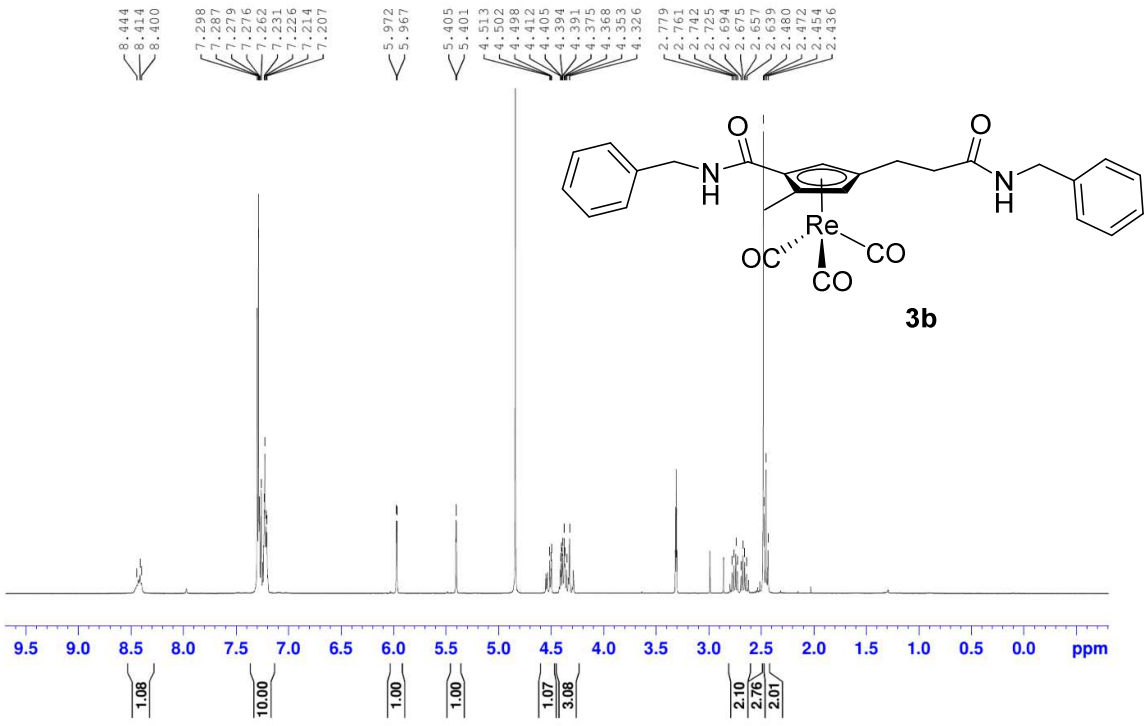

Figure 39. ^{1}H NMR of **3b** in $CDCl_3$.

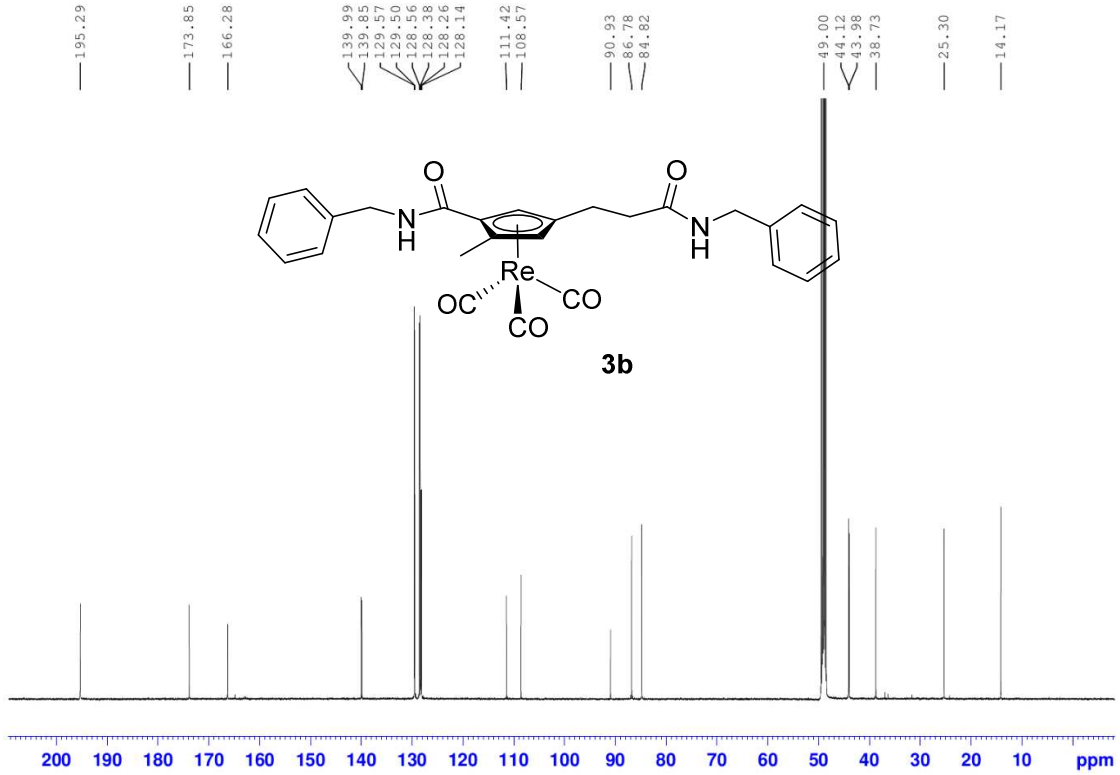

Figure 40. ^{13}C NMR of **3b** in $CDCl_3$.

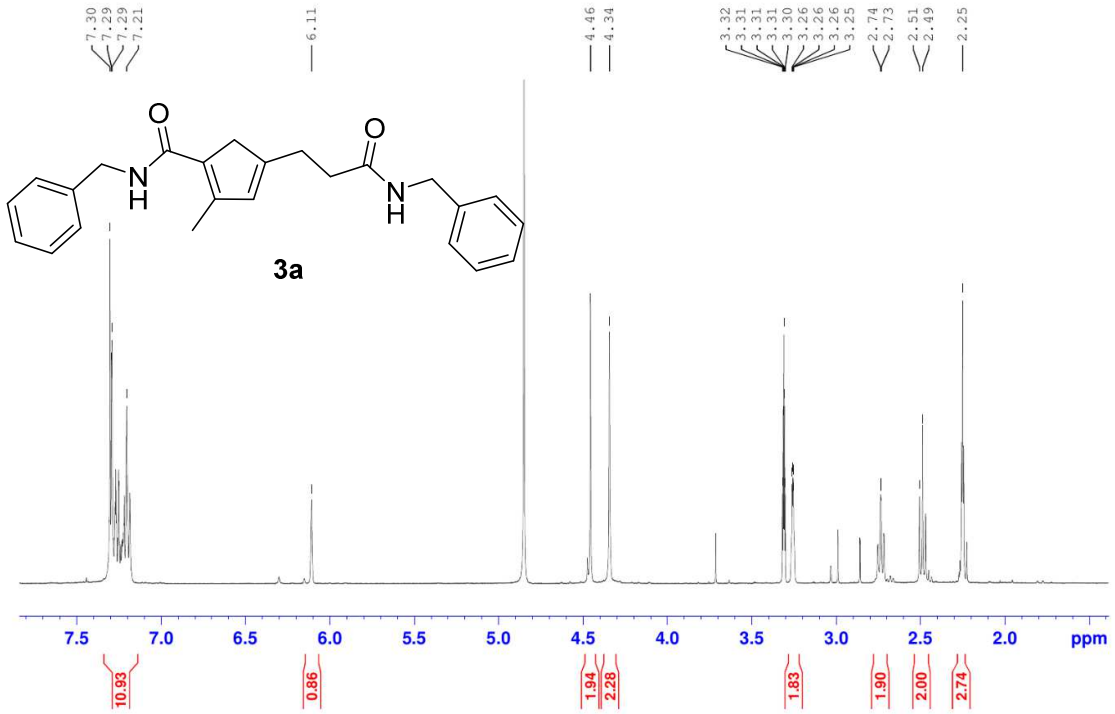

Figure 41. ^{1}H NMR of **3a** in CD_3OD.

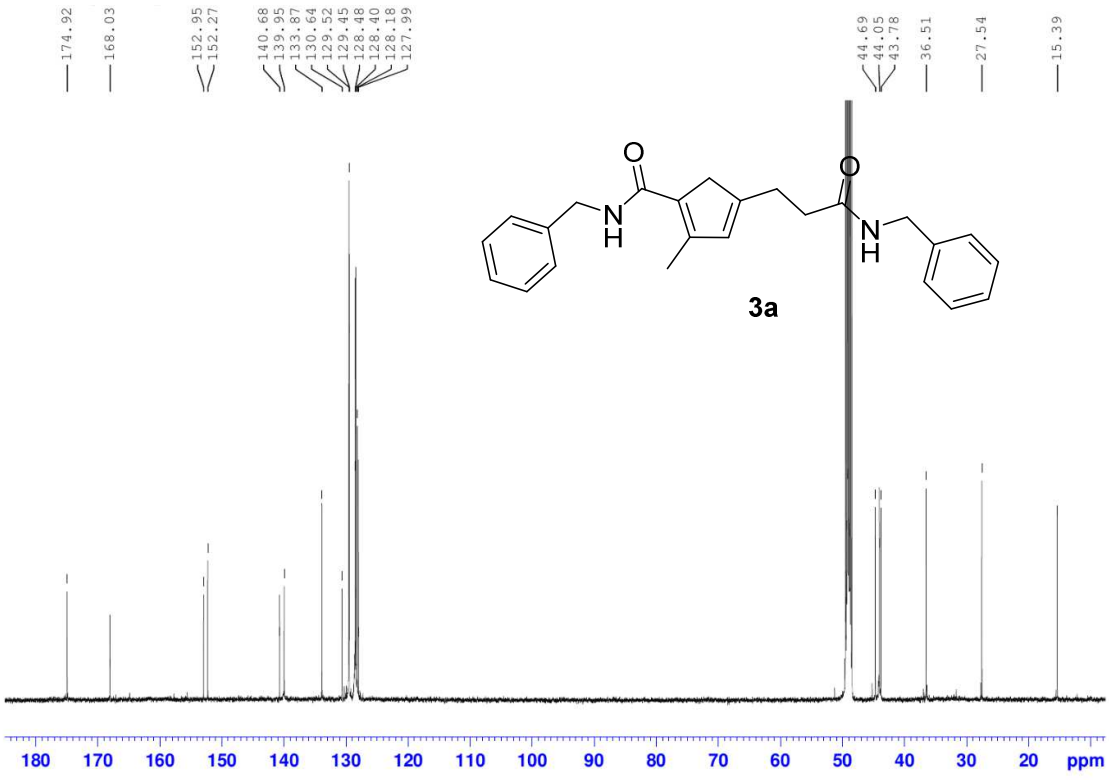

Figure 42. ^{13}C NMR of **3a** in CD_3OD.

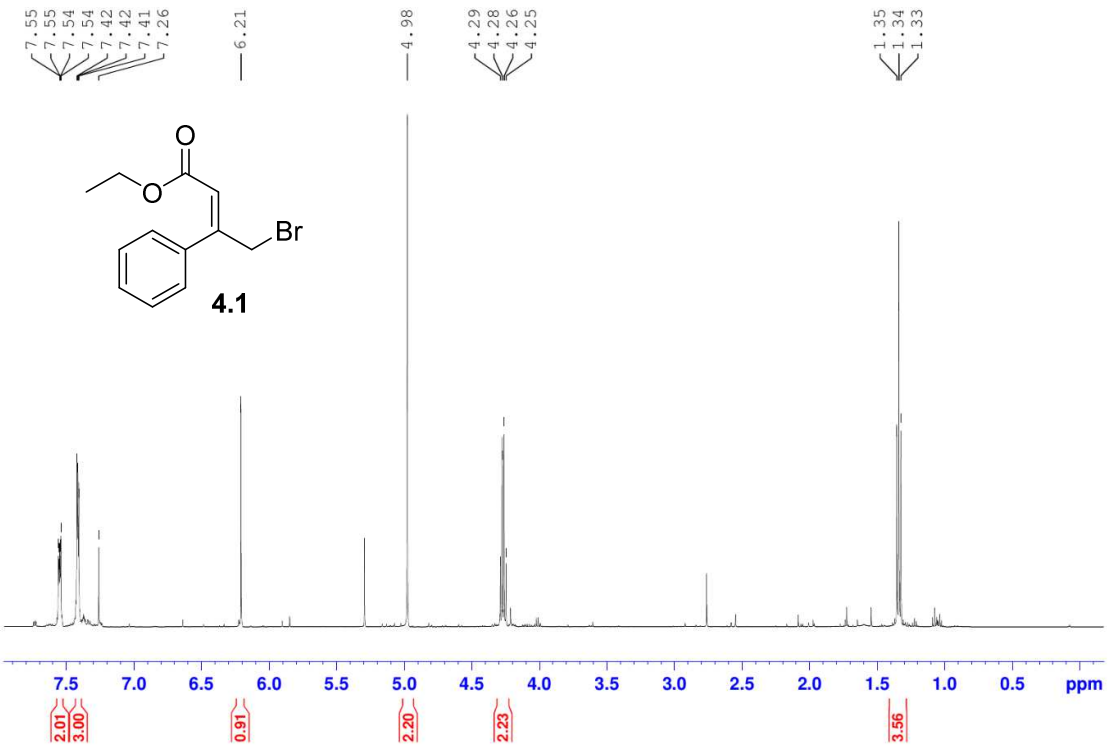

Figure 43.^{1}H NMR of **4.1** in $CDCl_3$.

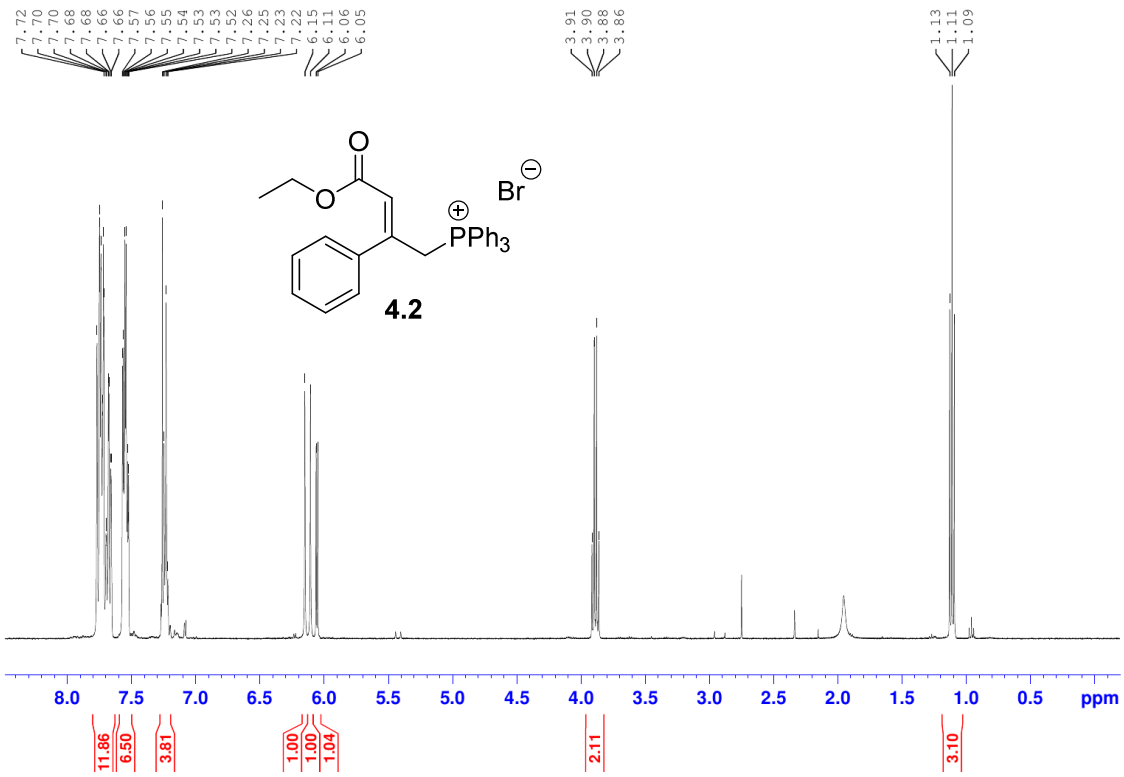

Figure 44. ^{1}H NMR of **4.2** in $CDCl_3$.

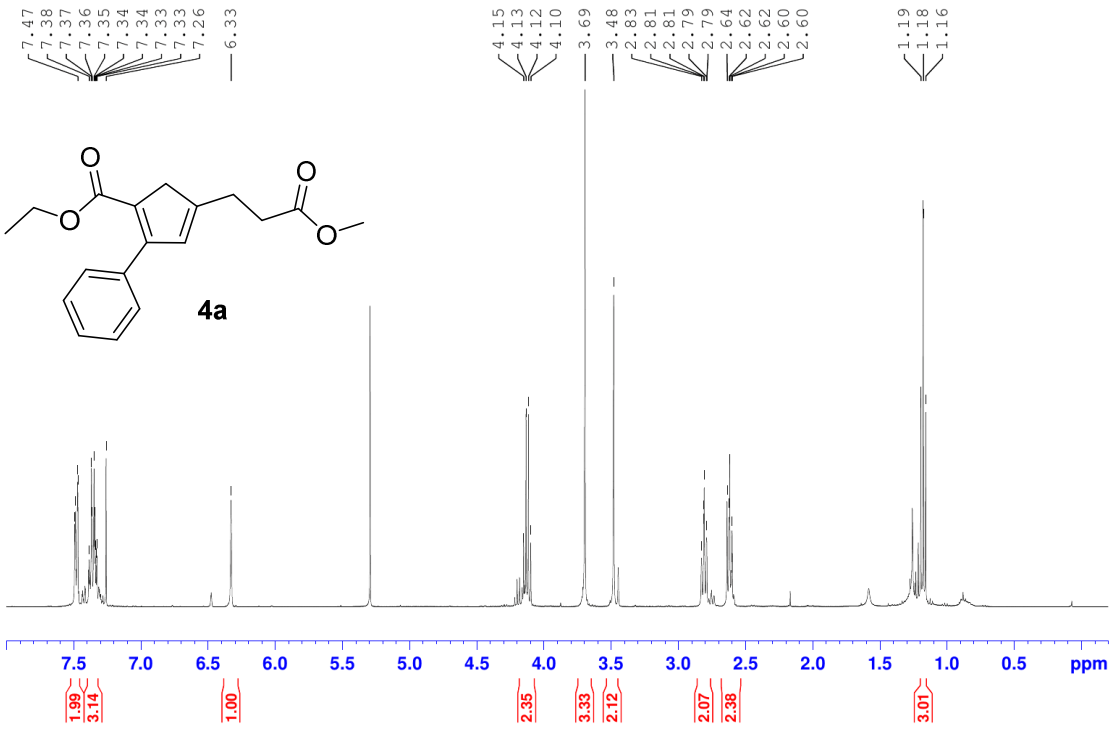

Figure 45. ^{1}H NMR of **4a** in $CDCl_3$.

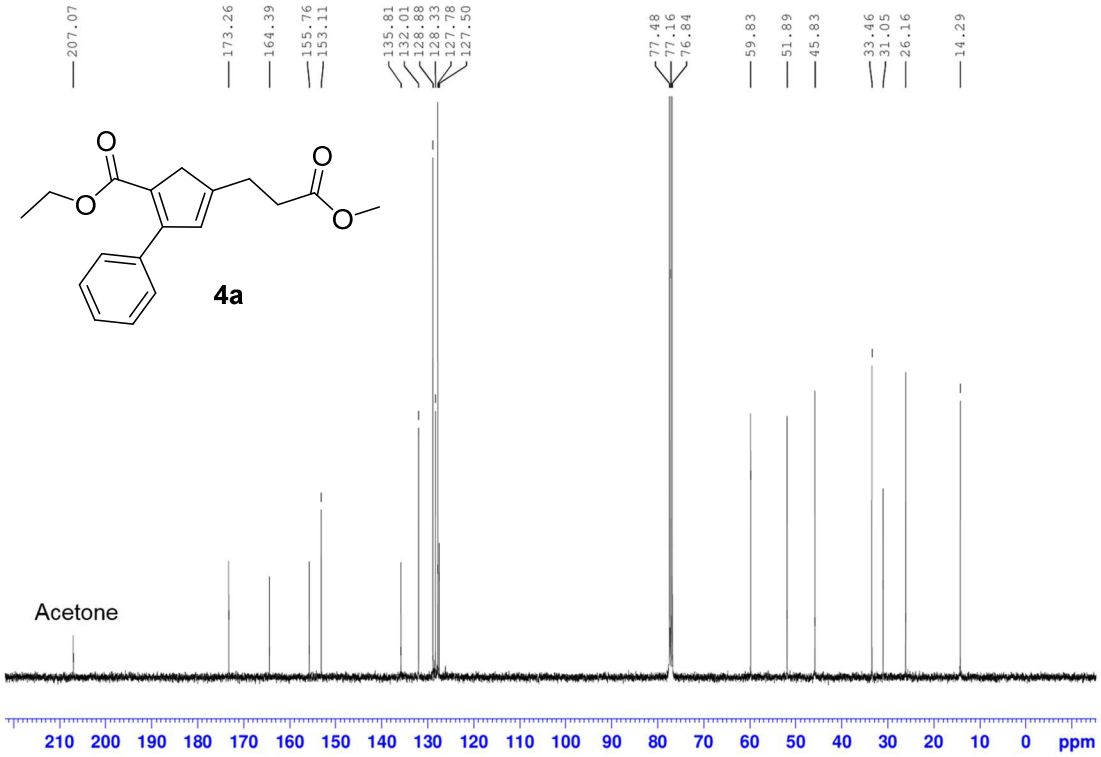

Figure 46. ^{13}C NMR of **4a** in $CDCl_3$.

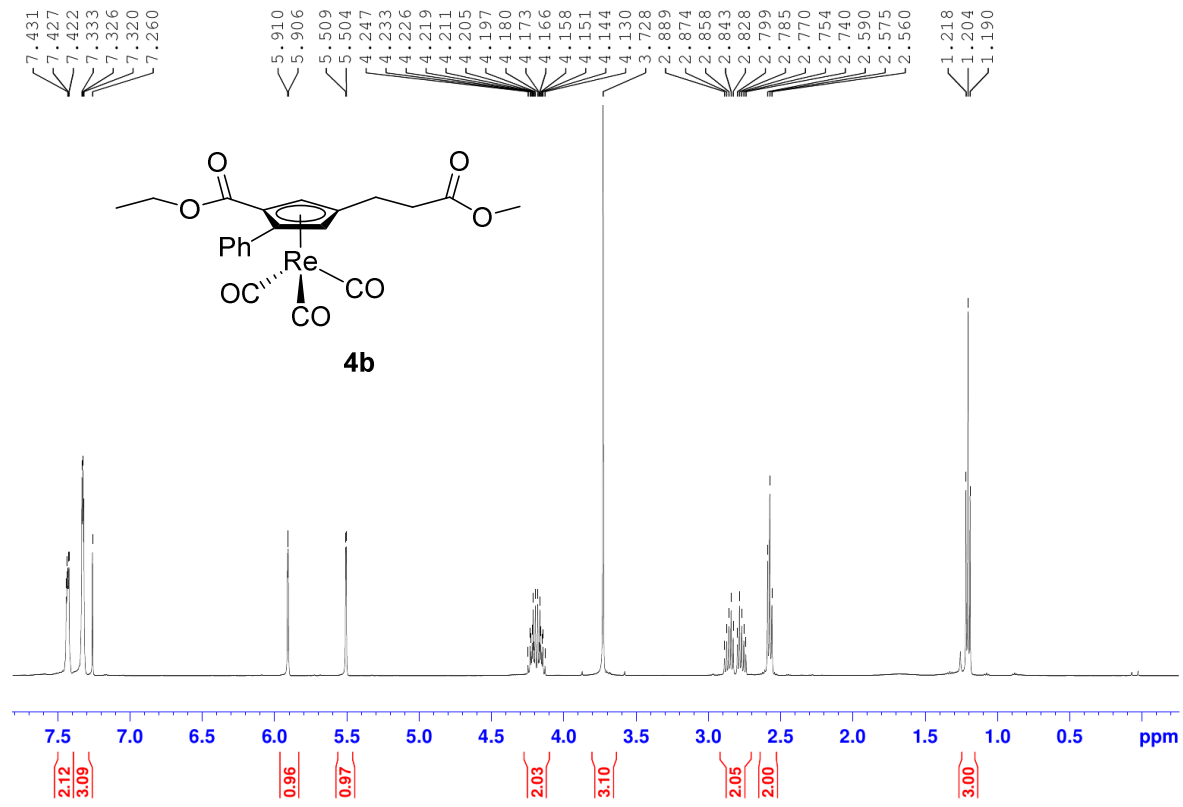

Figure 47. ^{1}H NMR of **4b** in $CDCl_3$.

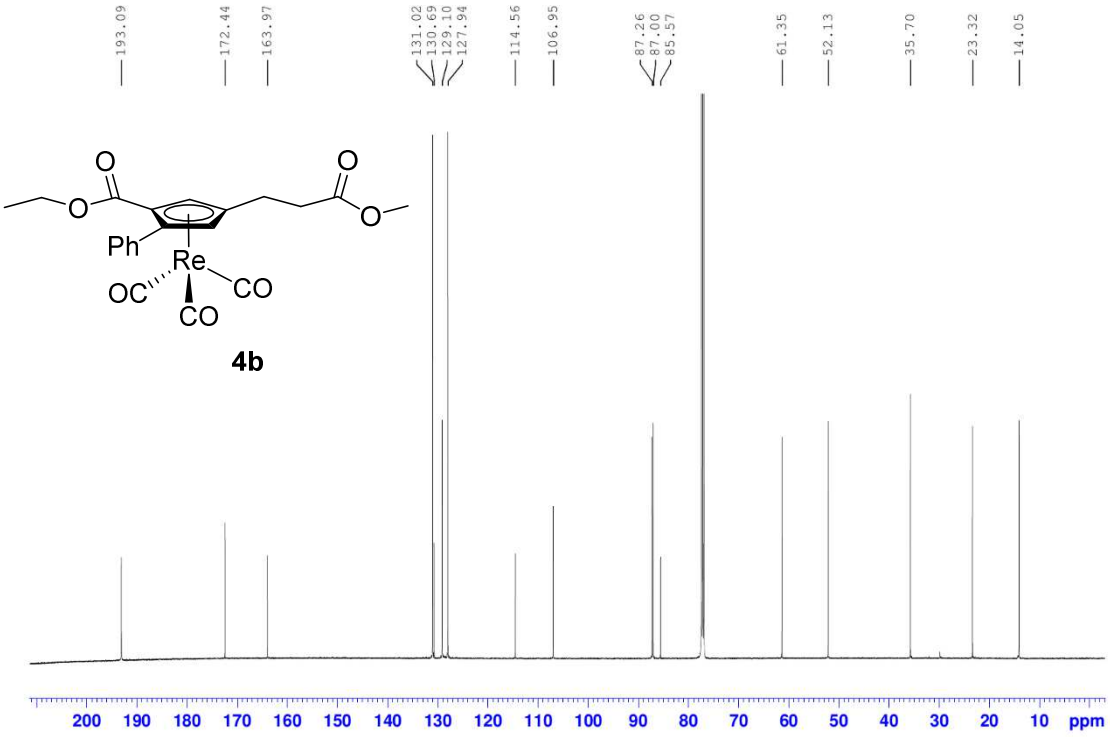

Figure 48. ^{13}C NMR of **4a** in $CDCl_3$.

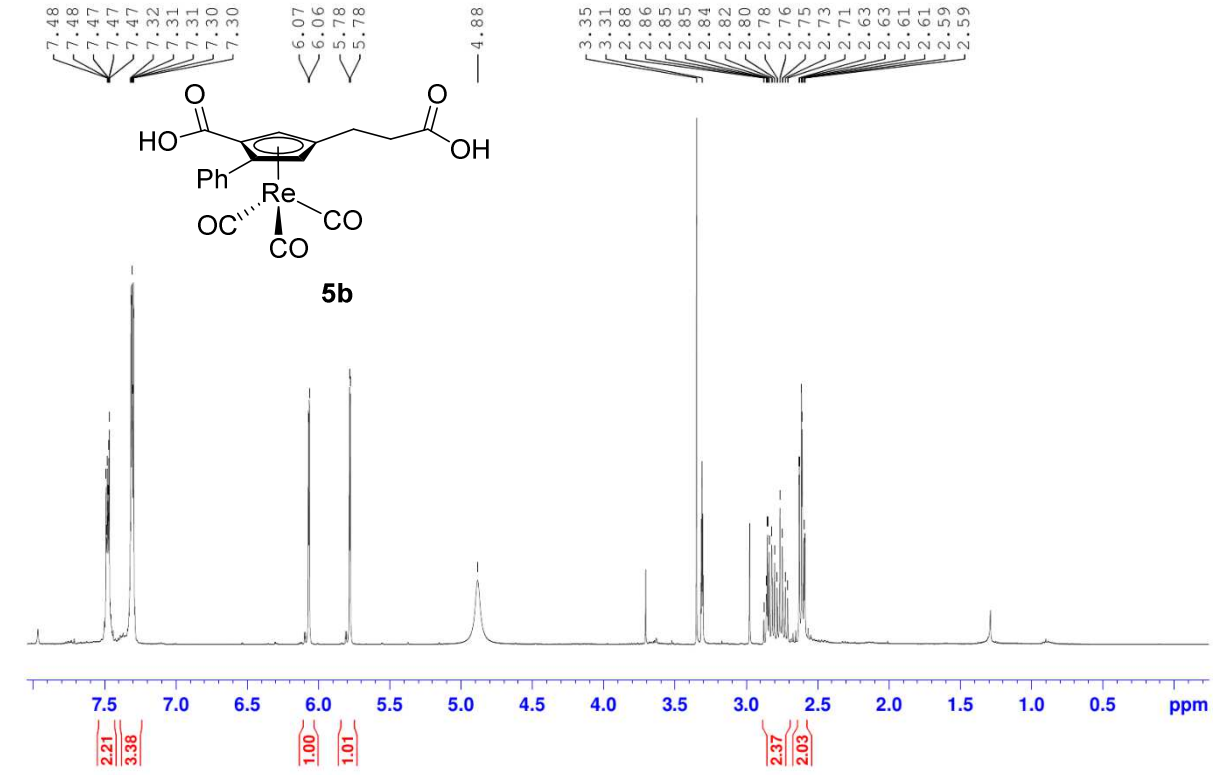

Figure 49. ^{1}H NMR of **5b** in CD_3OD.

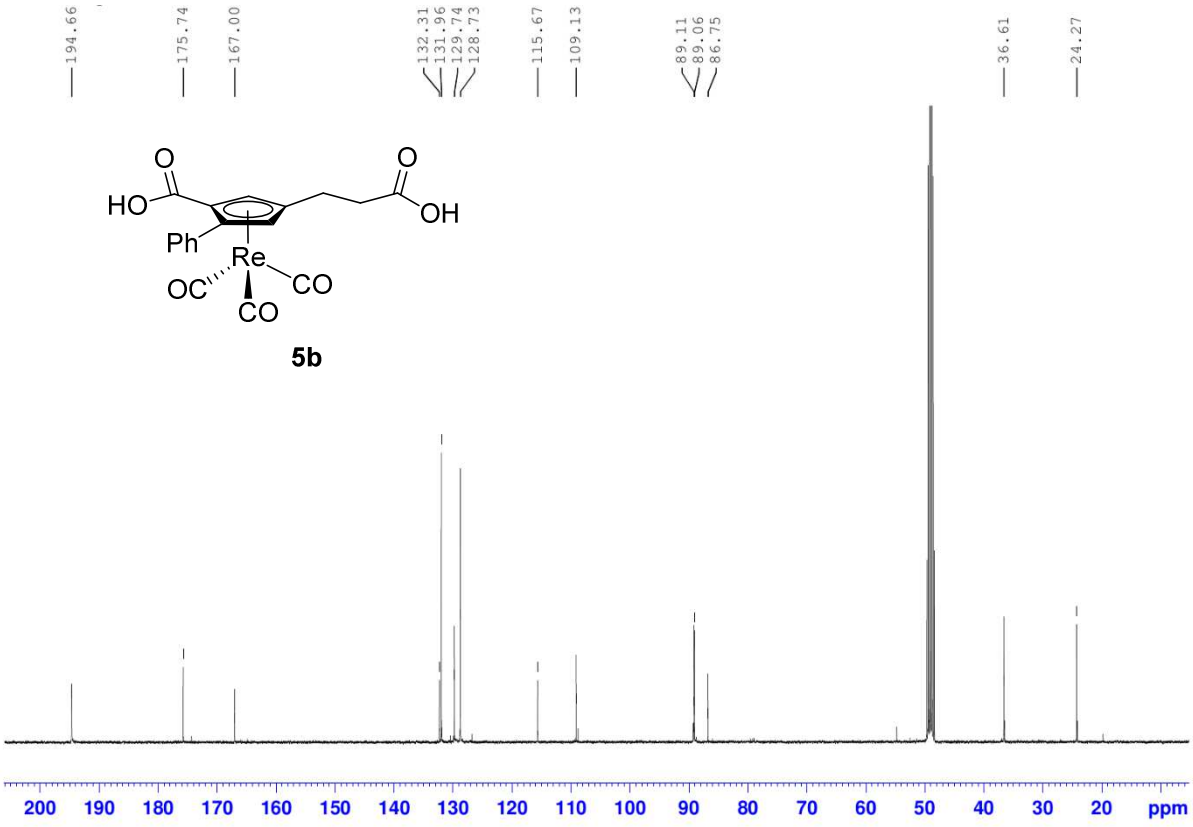

Figure 50. ^{13}C NMR of **5b** in CD_3OD.

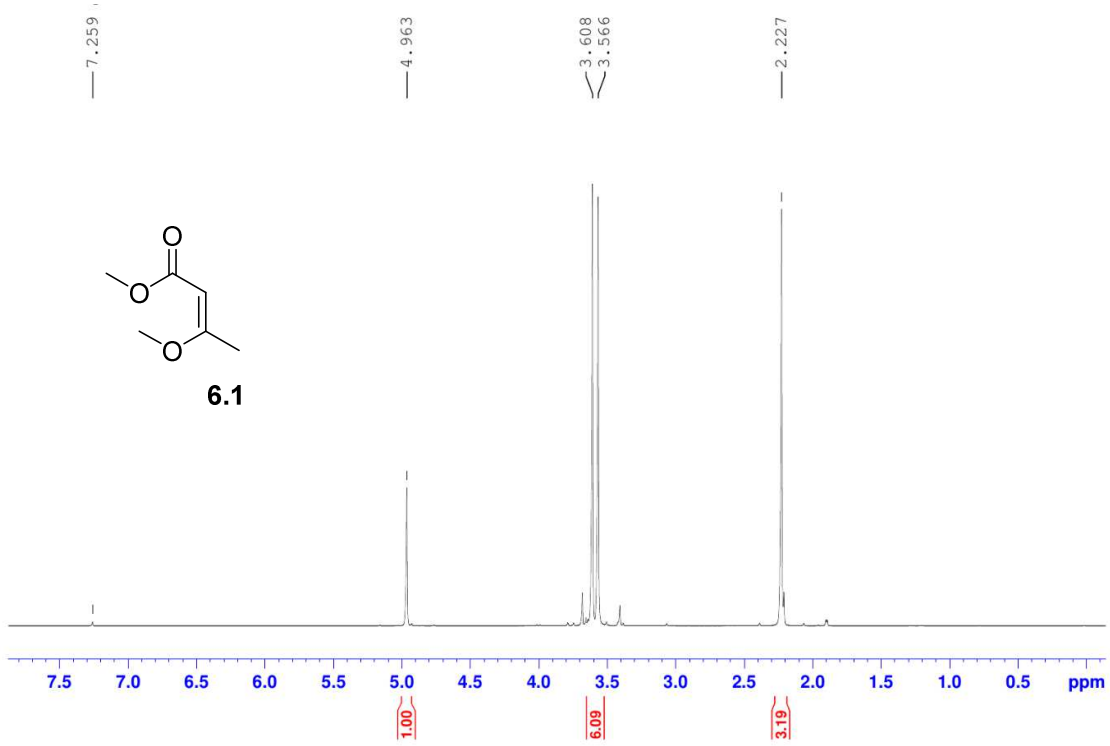

Figure 51. ^{1}H NMR of **6.1** in $CDCl_3$.

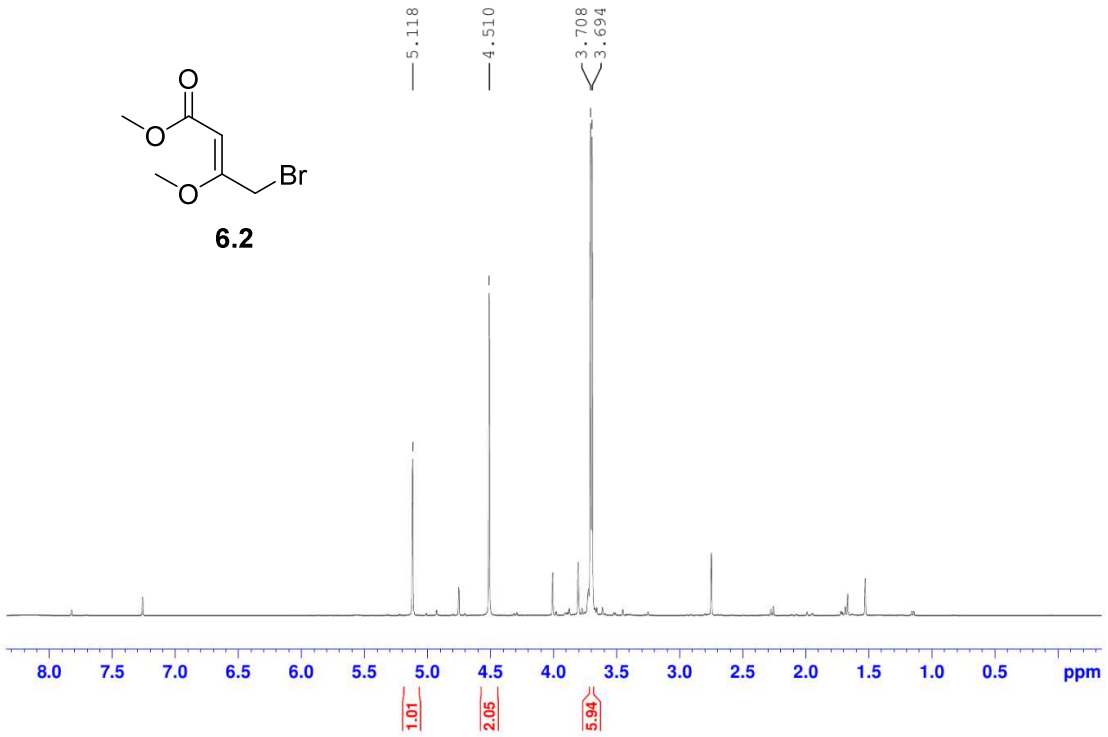

Figure 52.[1]H NMR of **6.2** in $CDCl_3$.

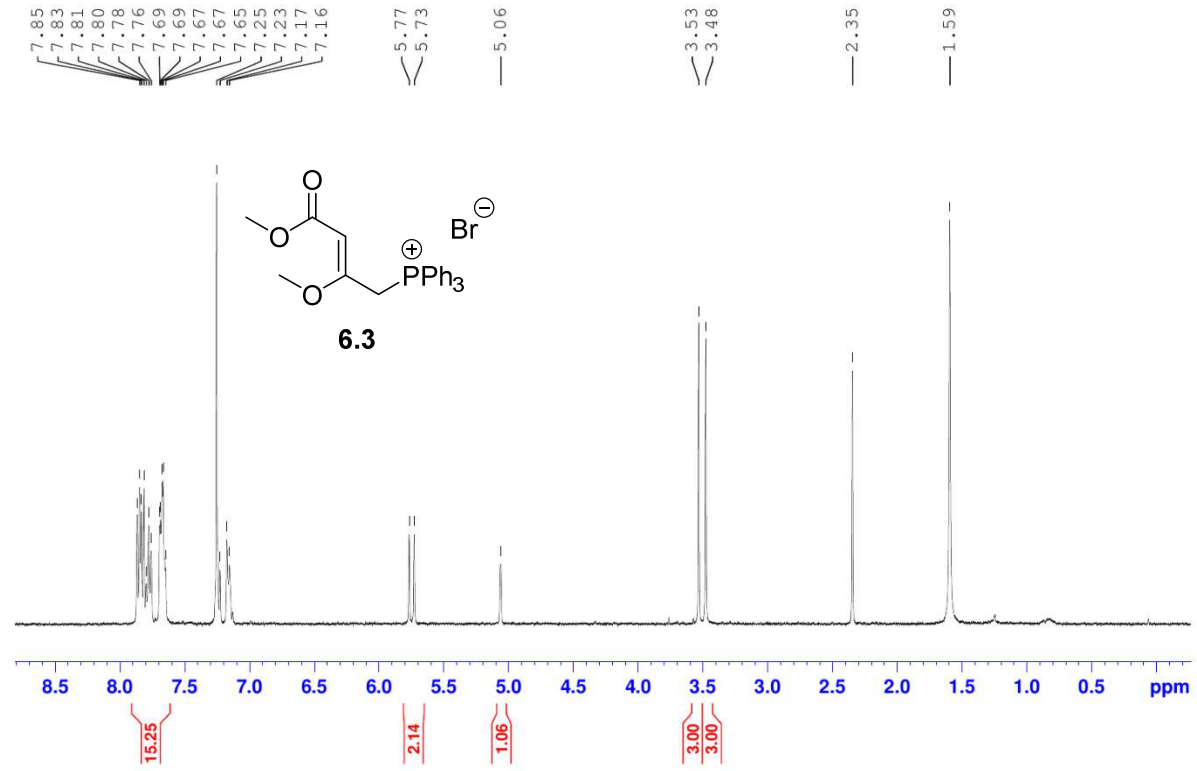

Figure 53.[1]H NMR of **6.3** in $CDCl_3$.

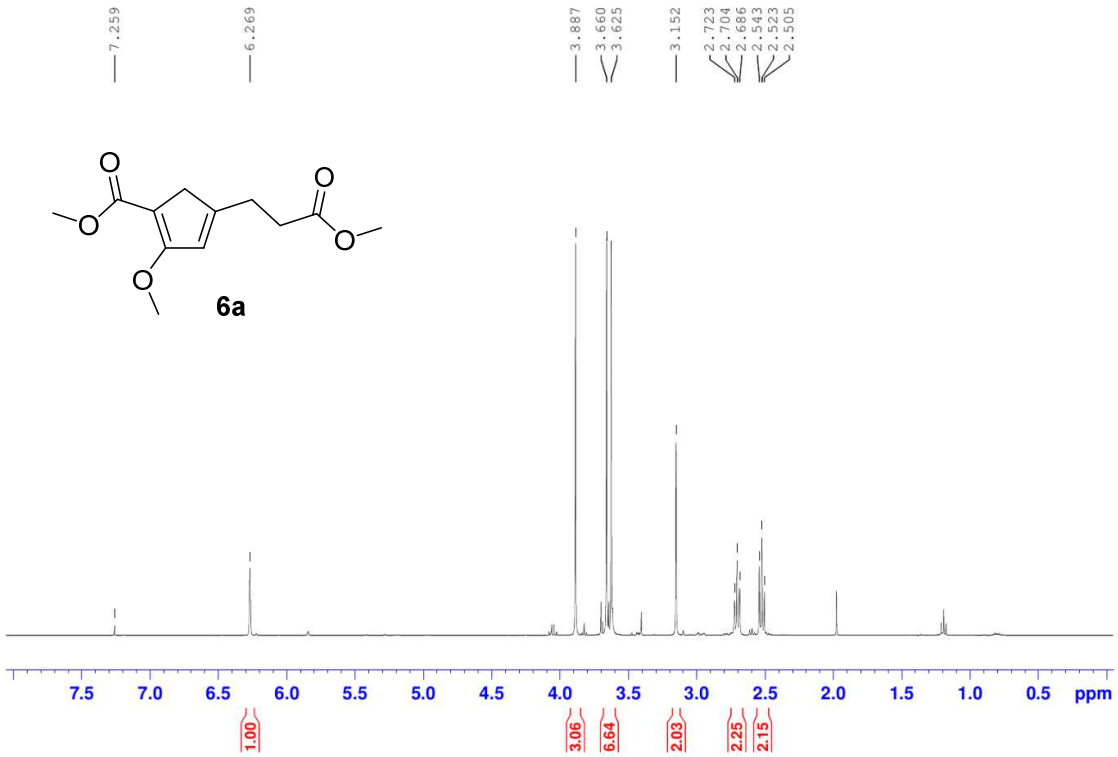

Figure 54. ^{1}H NMR of **6a** in $CDCl_3$.

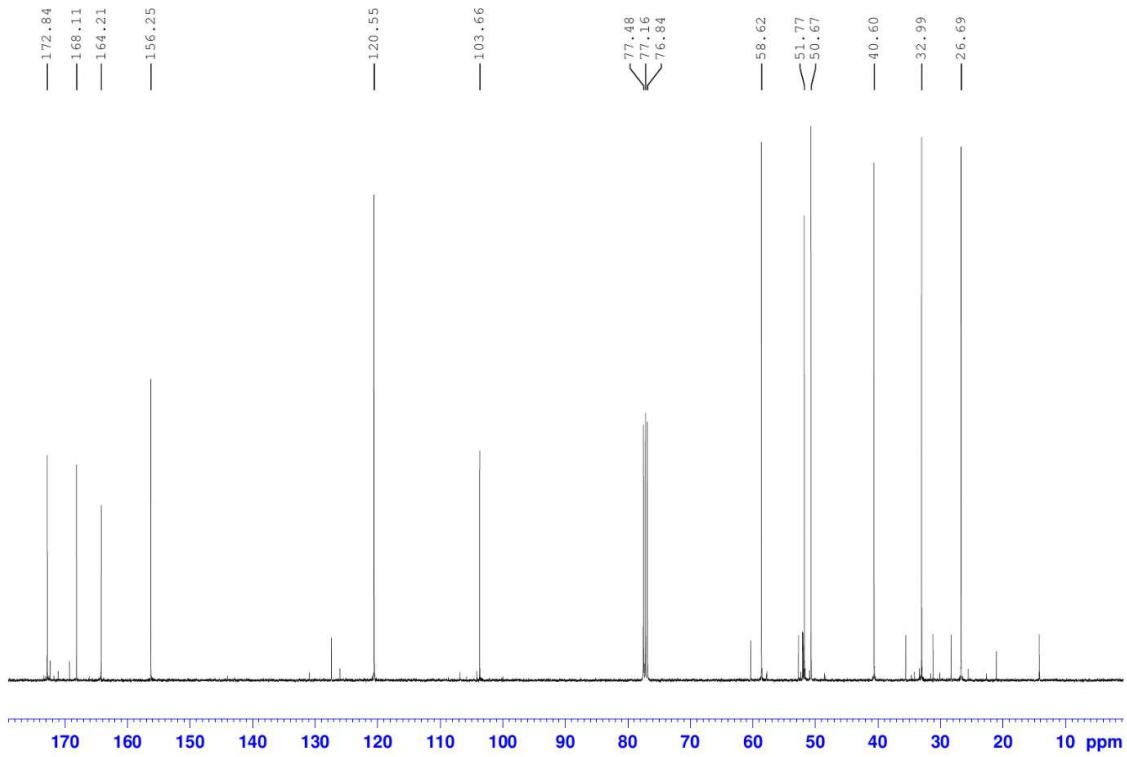

Figure 55. ^{13}C NMR of **6a** in $CDCl_3$.

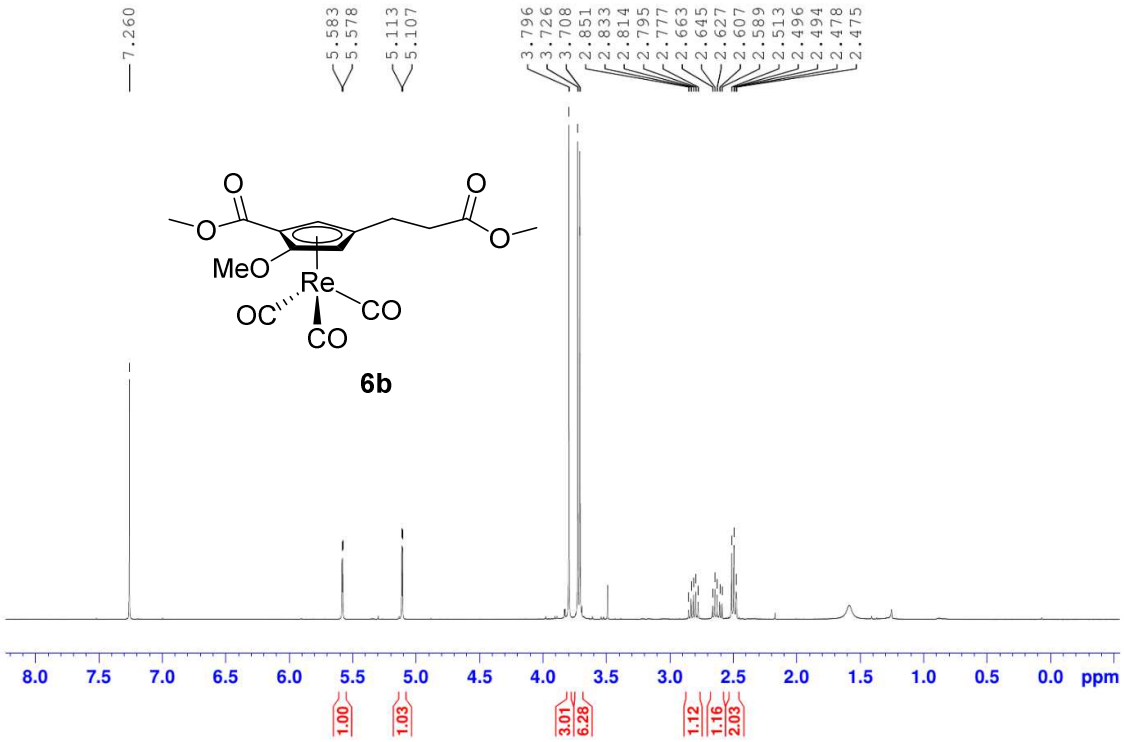

Figure 56. ^{1}H NMR of **6b** in $CDCl_3$.

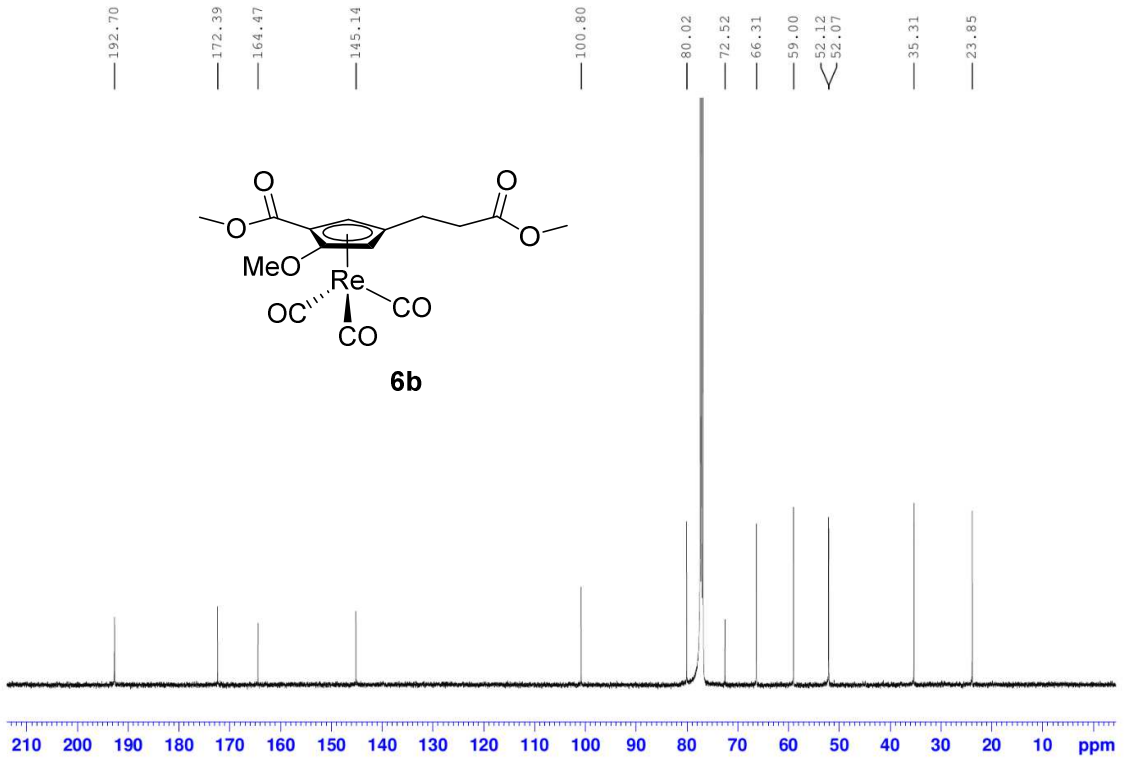

Figure 57. ^{13}C NMR of **6b** in $CDCl_3$.

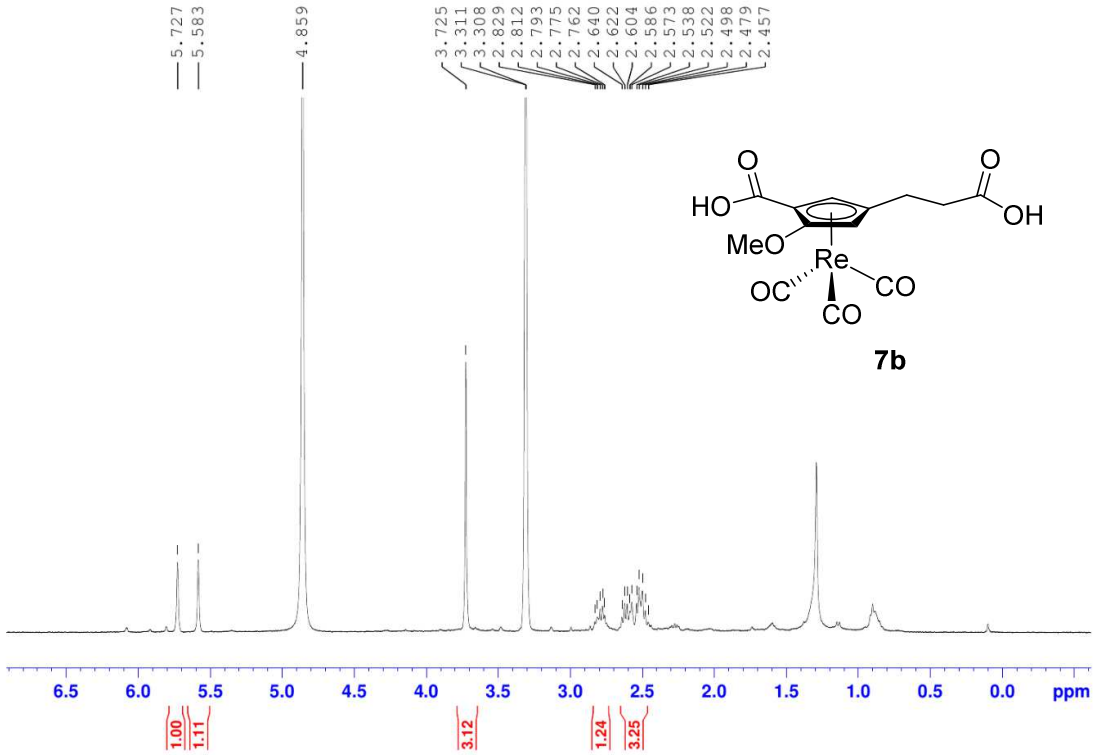

Figure 58. ^{1}H NMR of **7b** in CD_3OD.

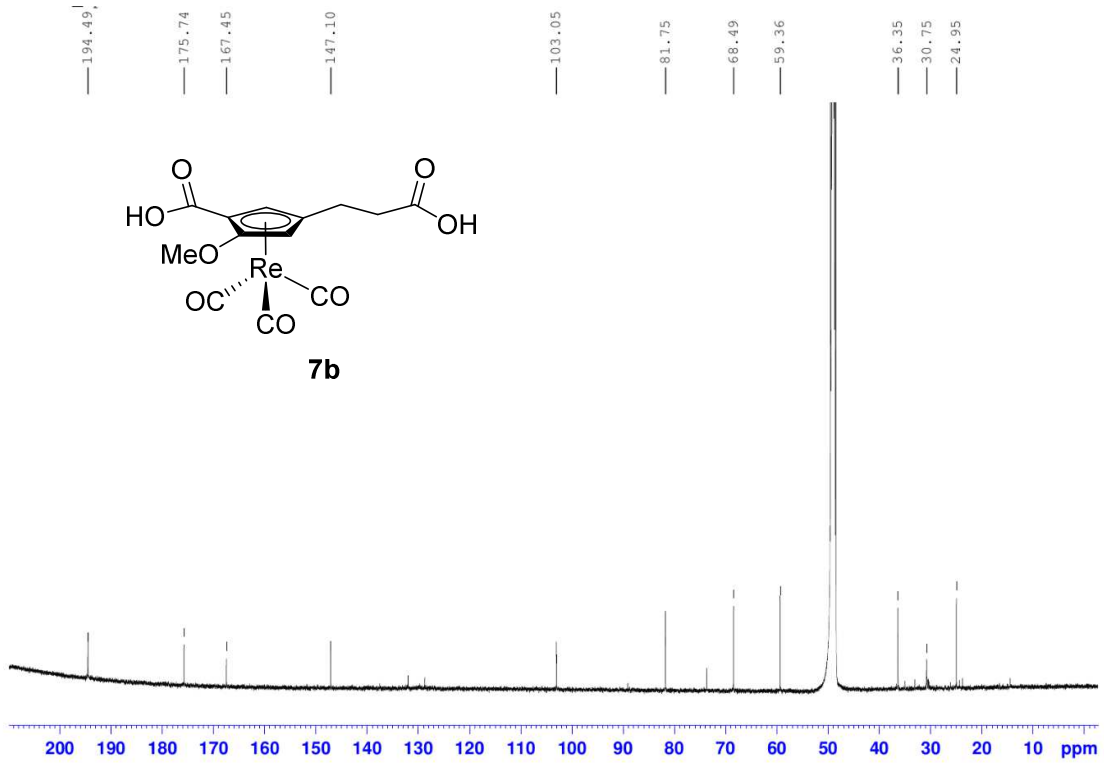

Figure 59. ^{13}C NMR of **7b** in CD_3OD.

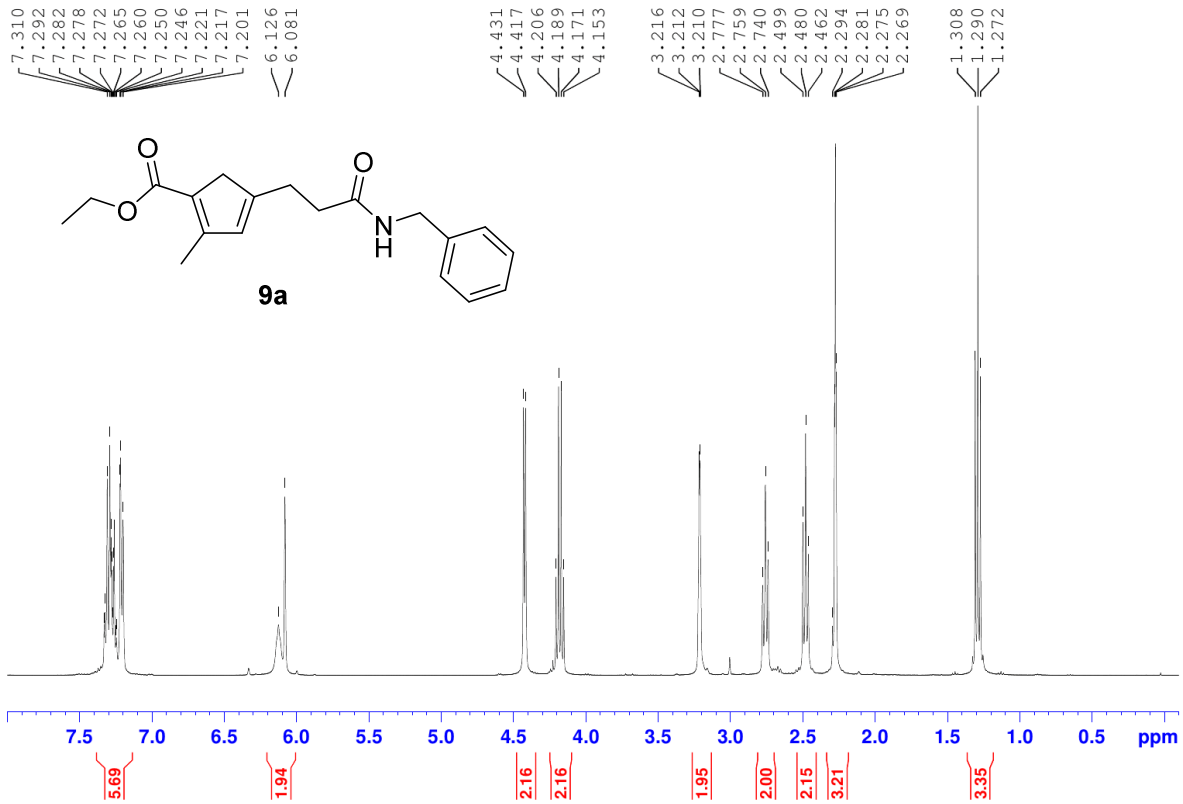

Figure 60. ^{1}H NMR of **9a** in $CDCl_3$.

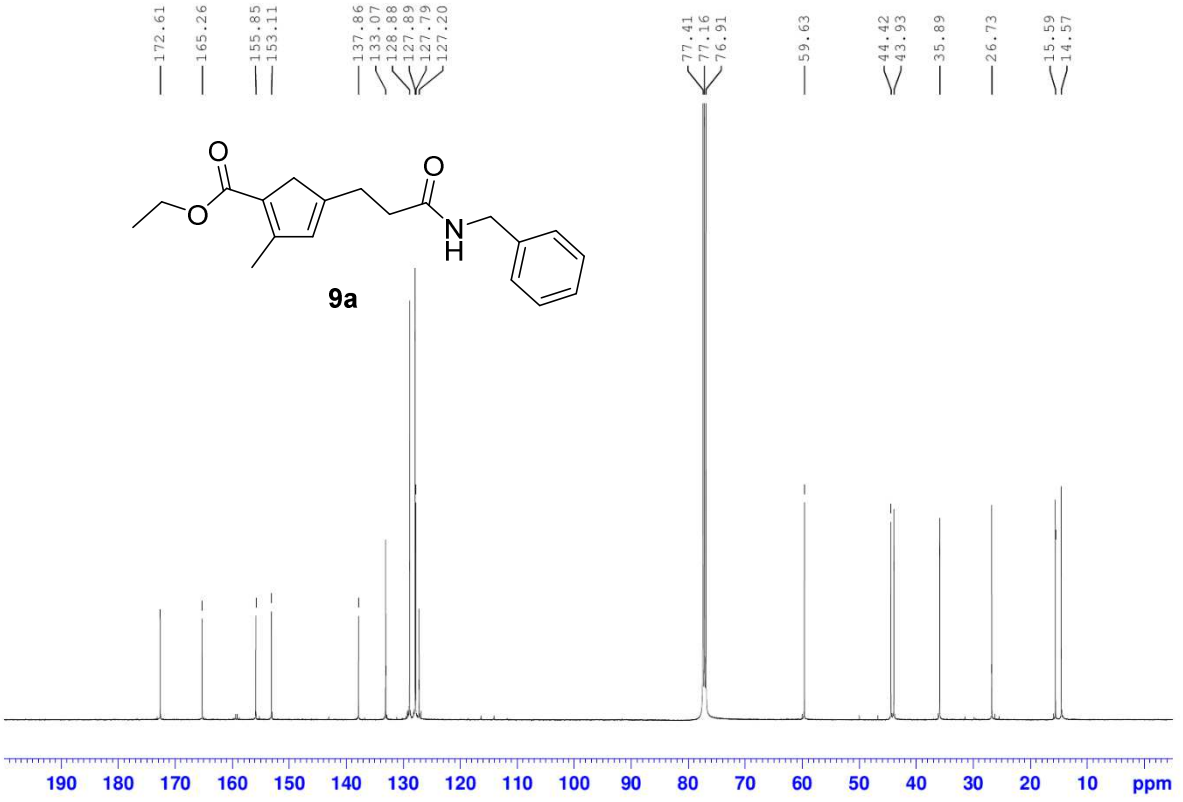

Figure 61. ^{13}C NMR of **9a** in $CDCl_3$.

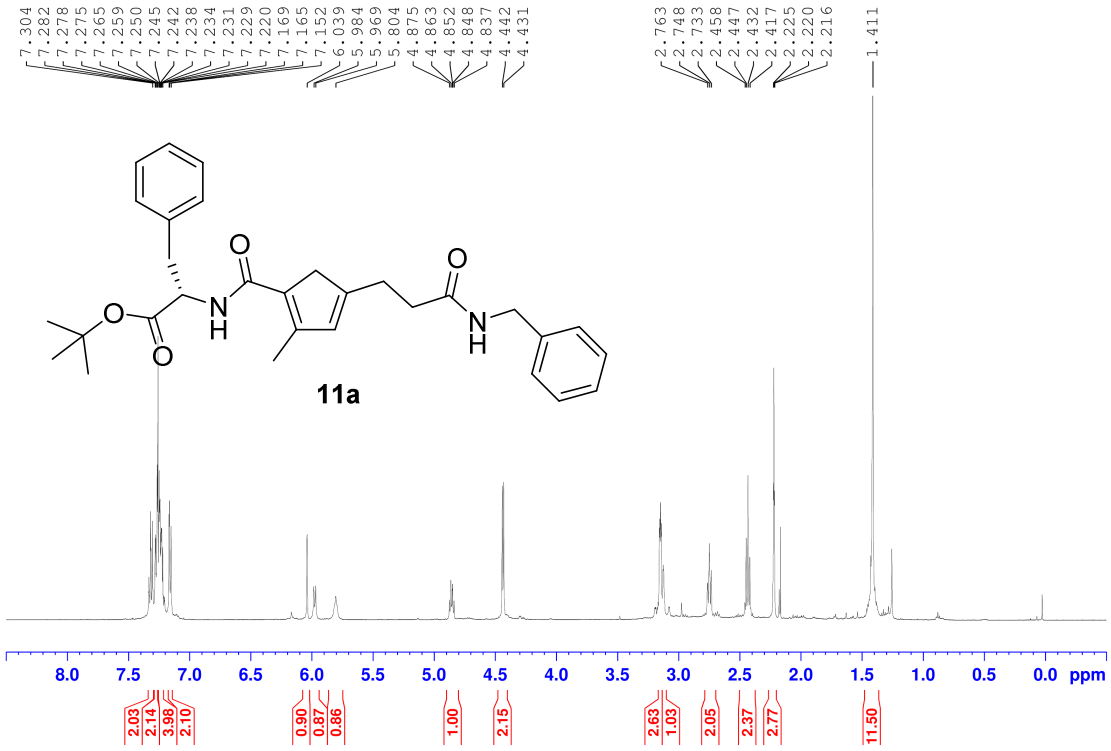

Figure 62. ^{1}H NMR of **11a** in $CDCl_3$.

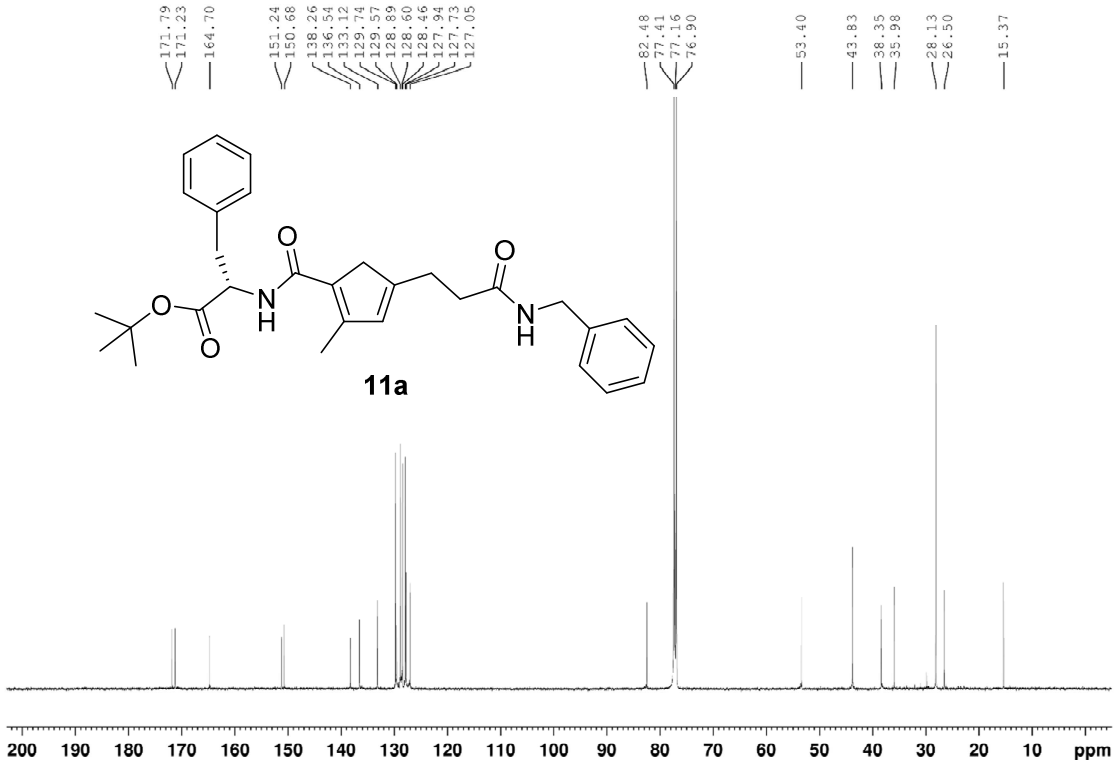

Figure 63. ^{13}C NMR of **11a** in $CDCl_3$.

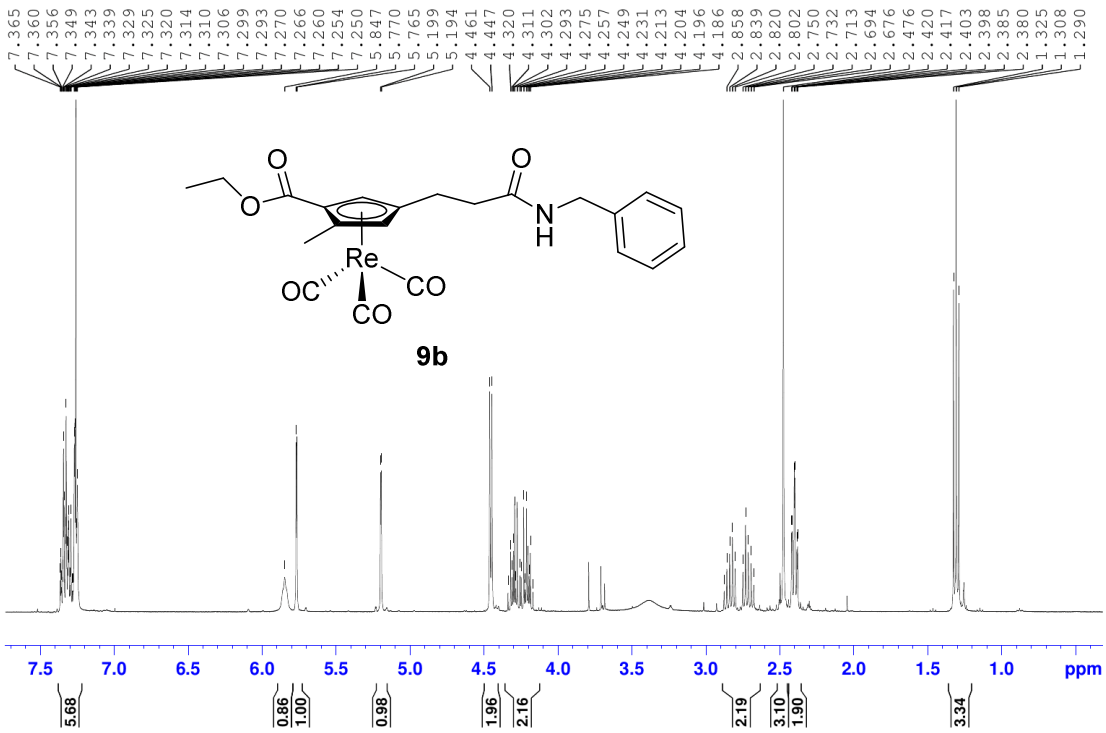

Figure 64. ^{1}H NMR of **9b** in $CDCl_3$.

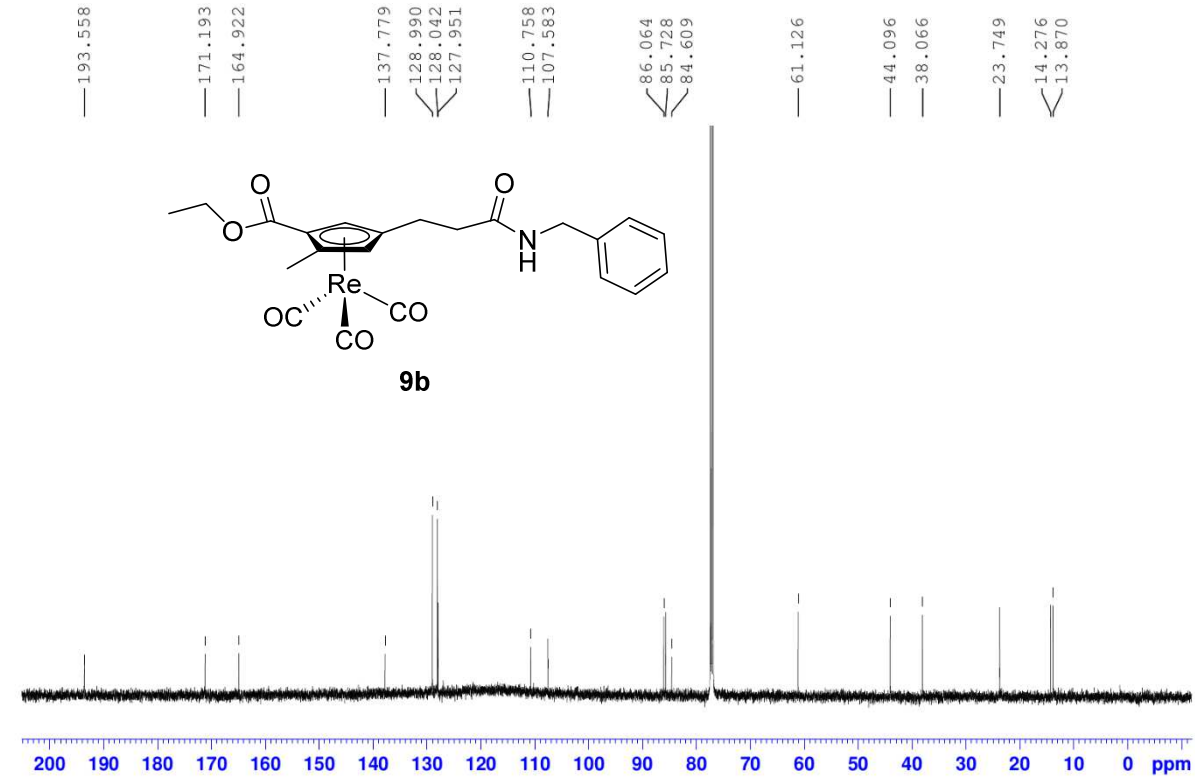

Figure 65. ^{13}C NMR of **9b** in $CDCl_3$.

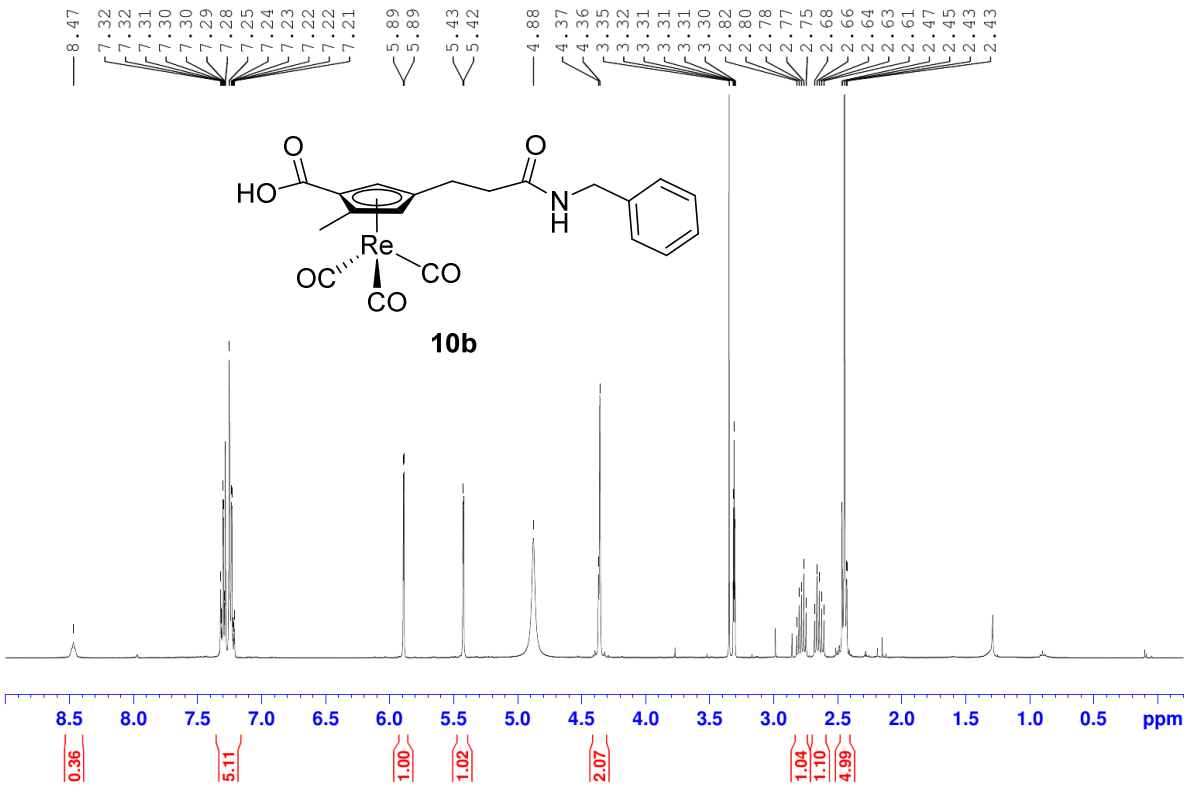

Figure 66. ^{1}H NMR of **10b** in CD_3OD.

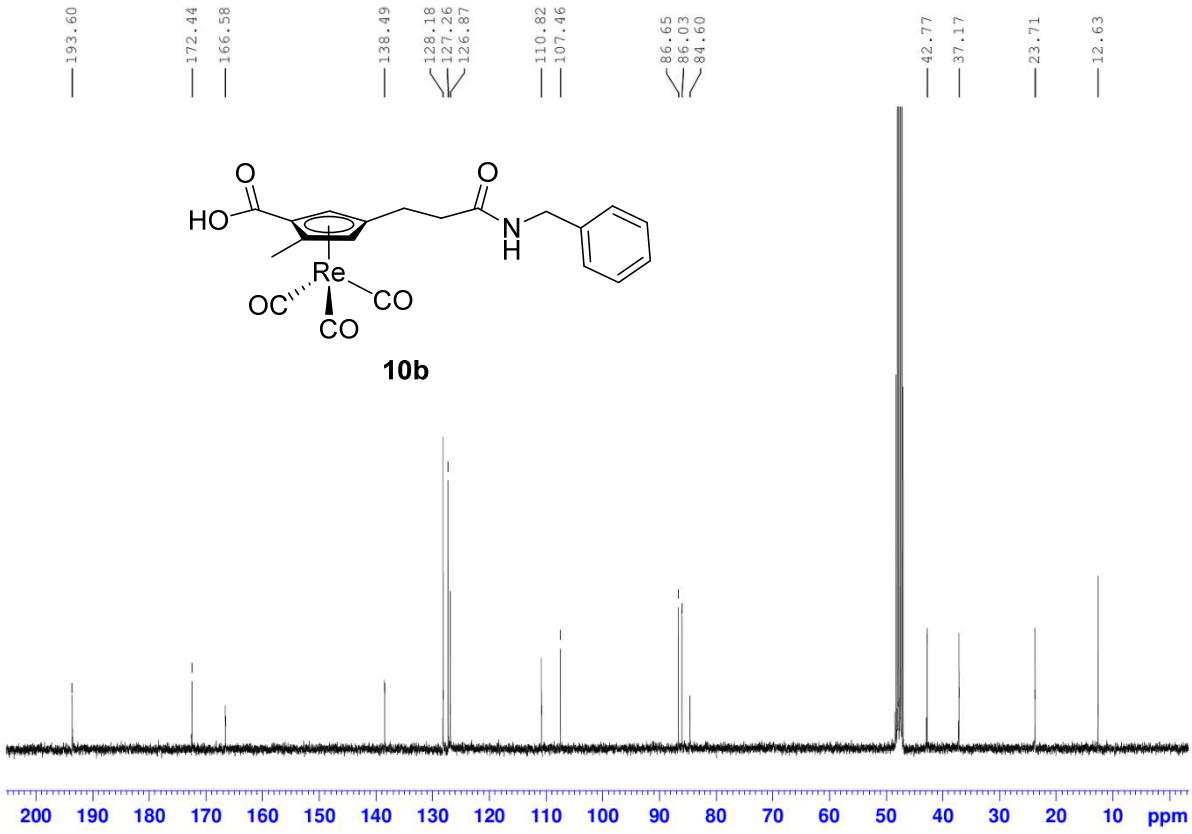

Figure 67. ^{1}H NMR of **10b** in CD_3OD.

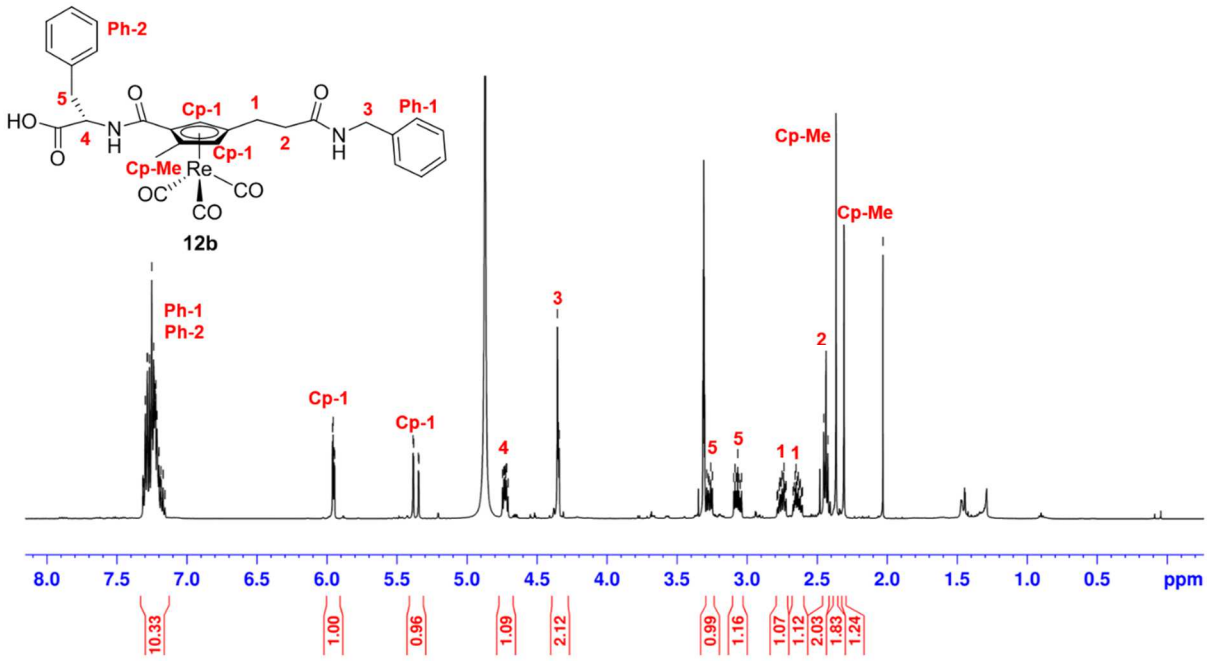

Figure 68. ^{1}H NMR-shift assignments for **12b** in CD_3OD (Amide and Carboxylic protons are not visible due to deuterium exchange).

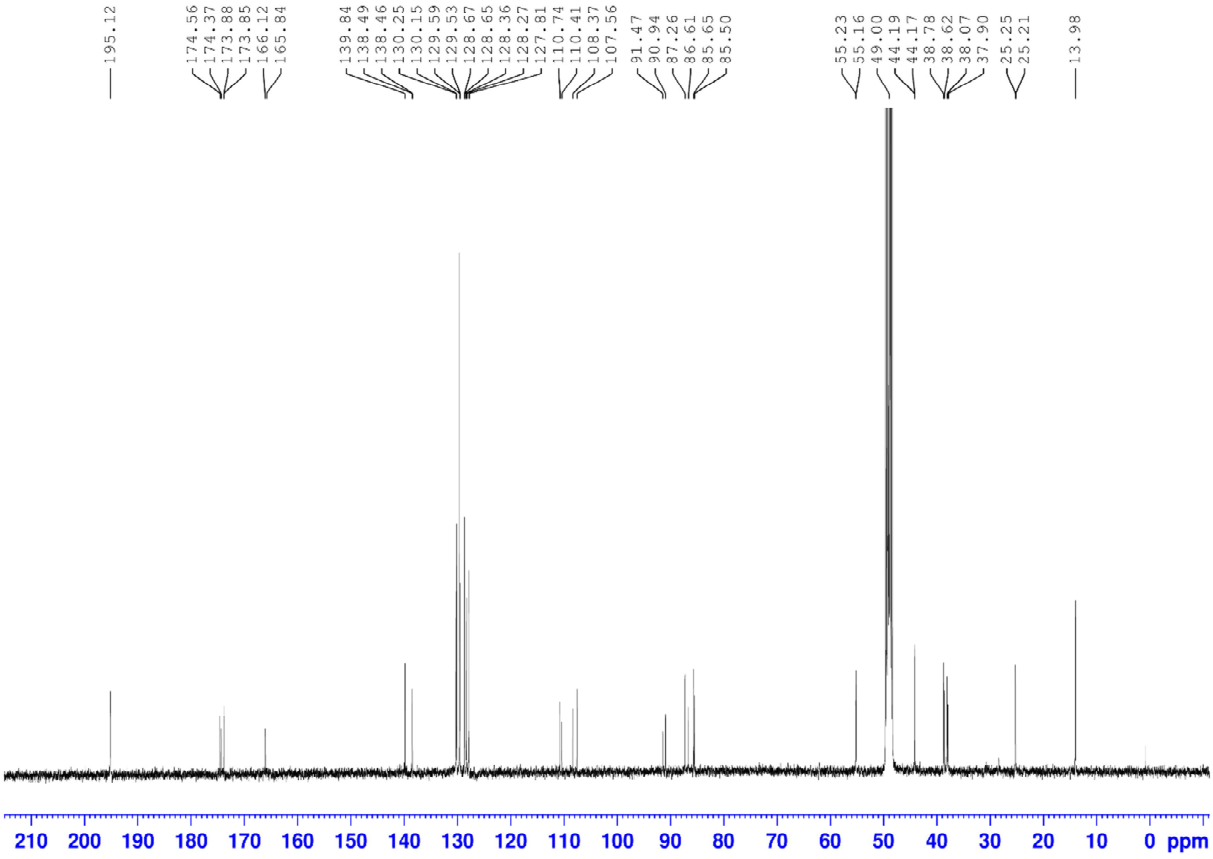

Figure 69.^{13}C NMR of **12b** in CD_3OD.

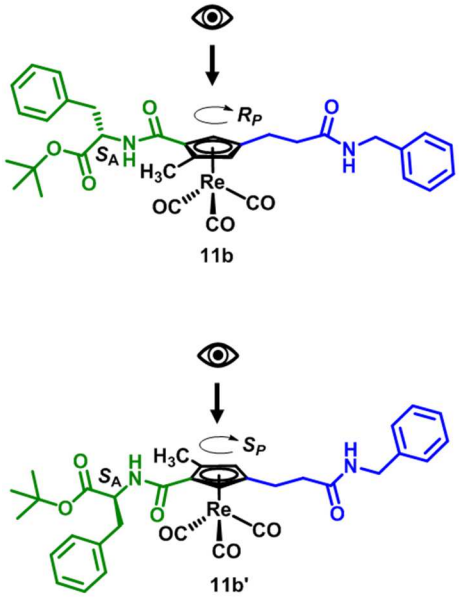

Figure 70. The two possible diastereoisomers of **11b** formed due to the planar chirality of the Cp-ligand combined with the chiral center at the attached aminoacid.

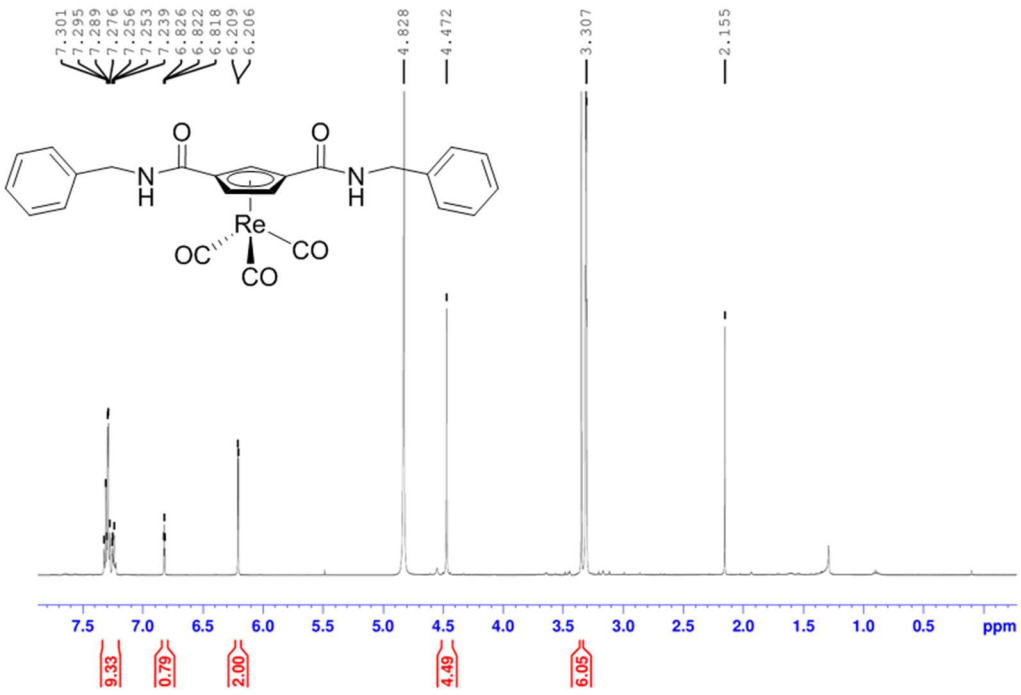

Figure 71. ^{1}H NMR of **13** in MeOD.

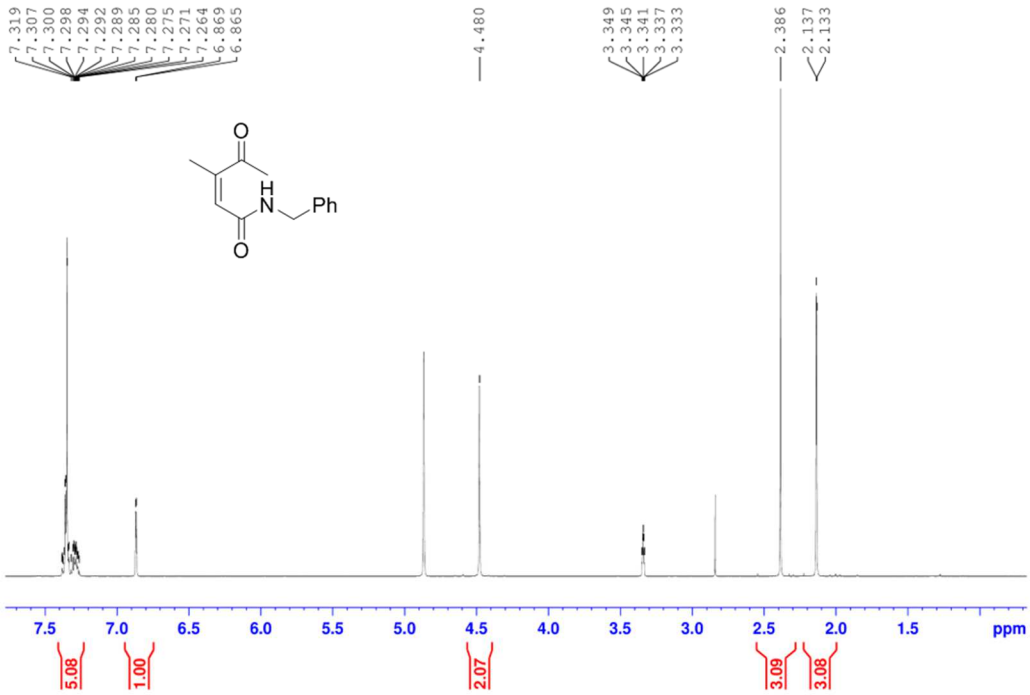

Figure 72. ^{1}H NMR of **15** in $CDCl_3$.

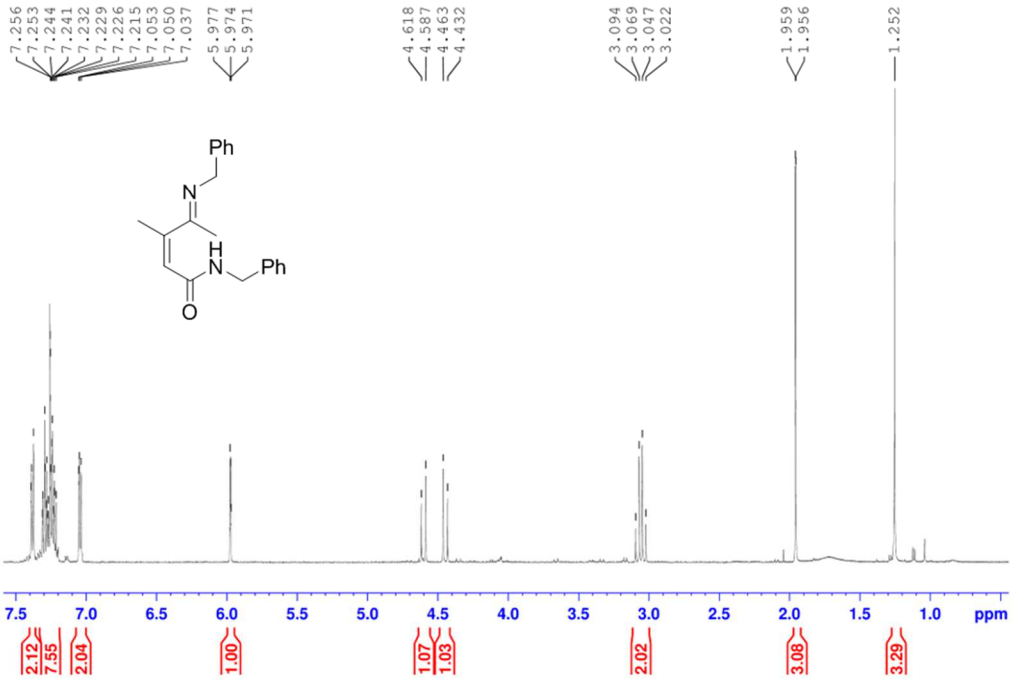

Figure 73. ^{1}H NMR of **16** in $CDCl_3$.

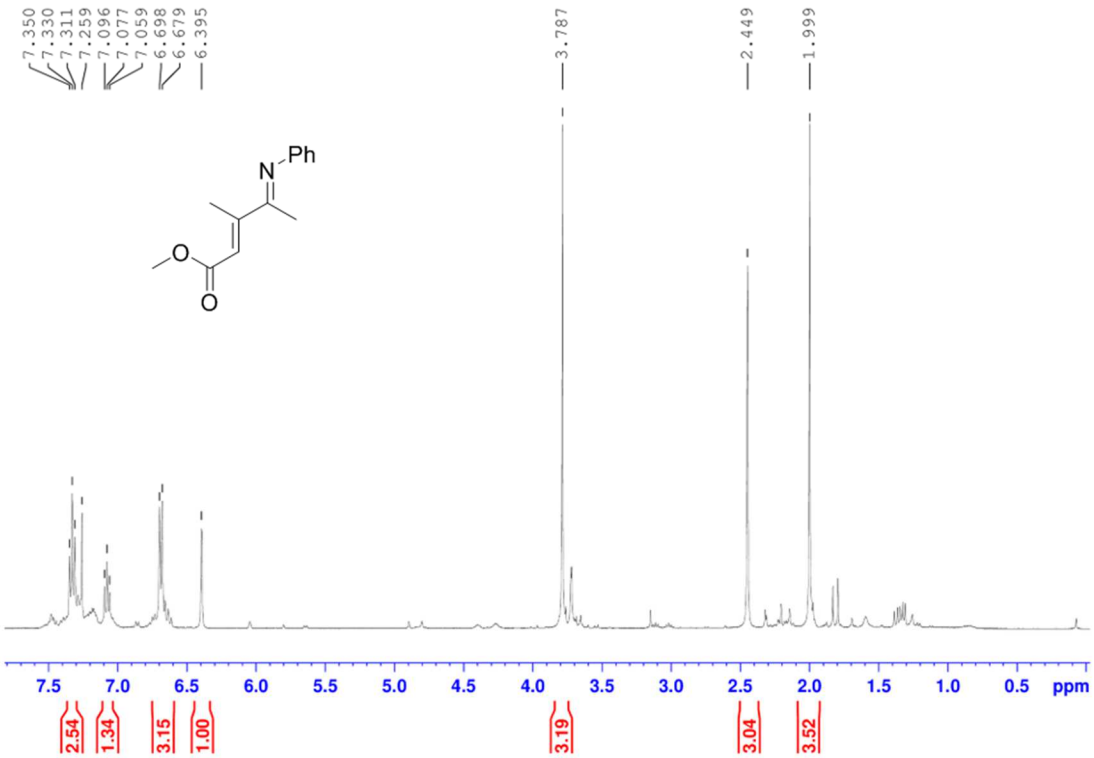

Figure 74. ^{1}H NMR of **19** in $CDCl_3$.

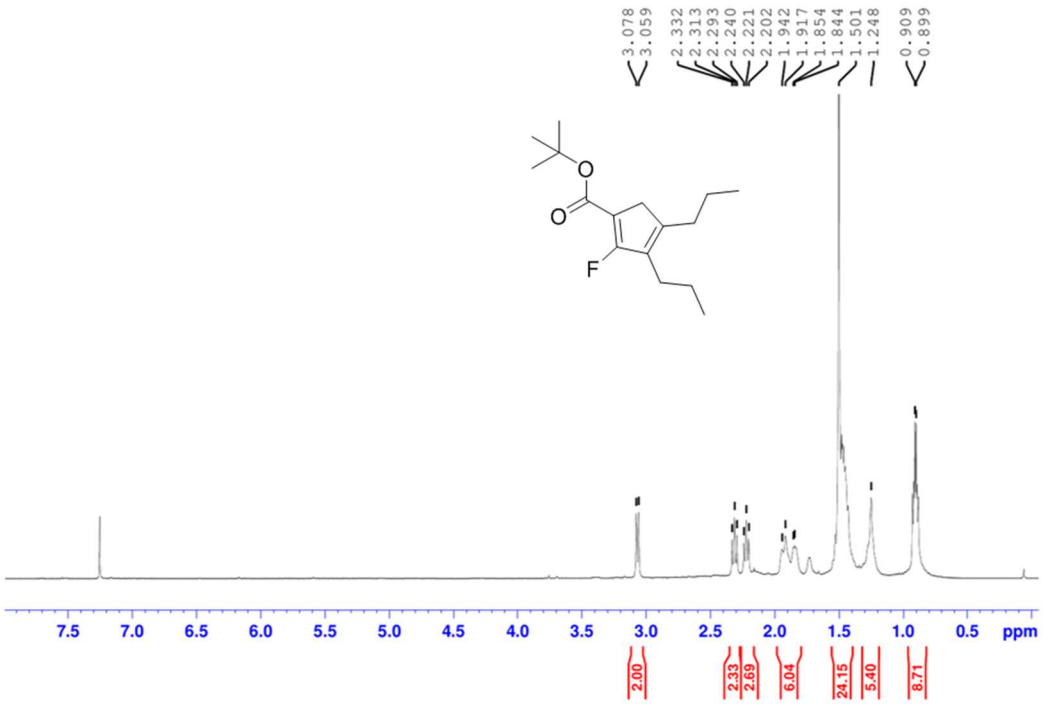

Figure 75. ^{1}H NMR of **20** in $CDCl_3$.

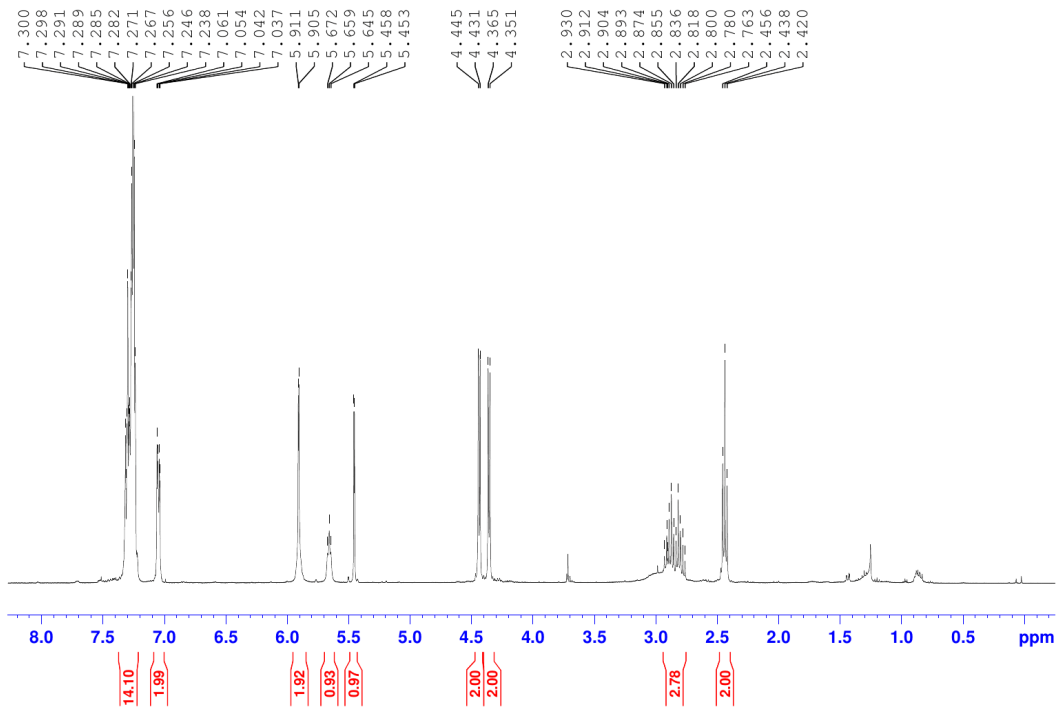

Figure 76. ^{1}H NMR of **21** in $CDCl_3$.

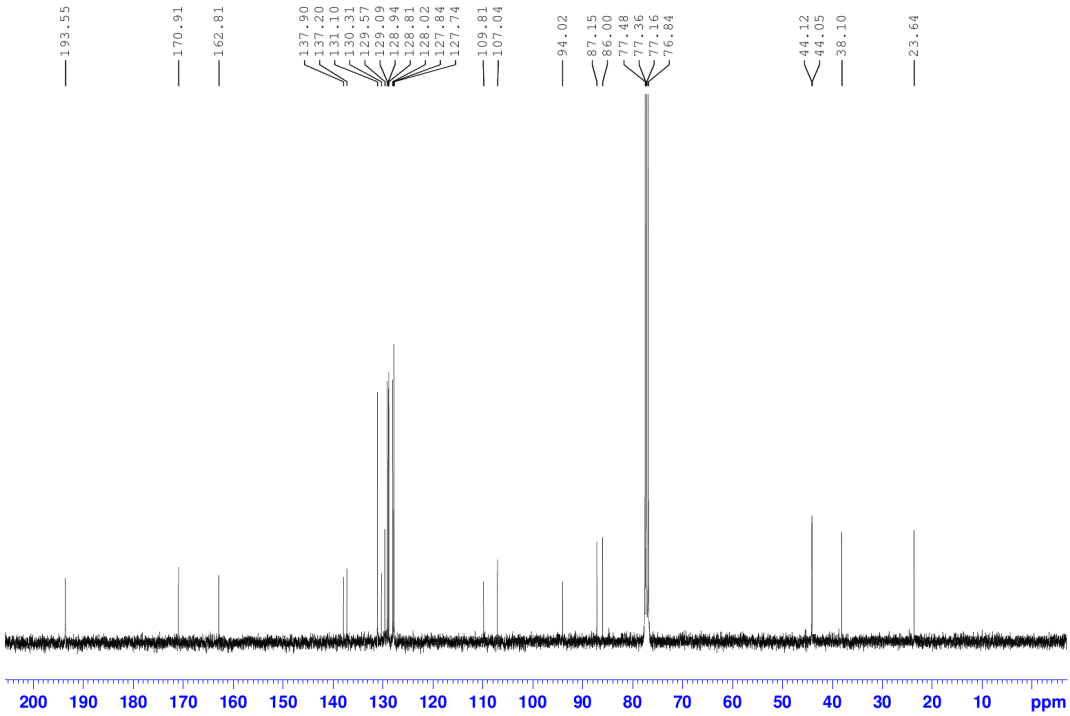

Figure 77. ^{13}C NMR of **21** in $CDCl_3$.

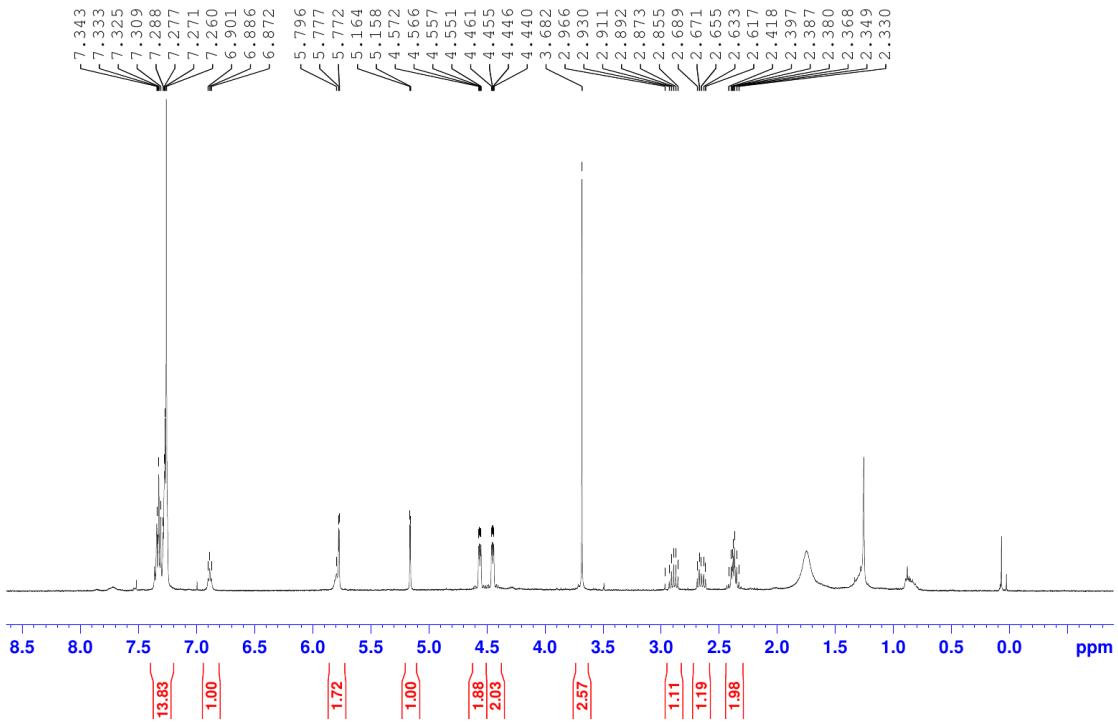

Figure 78. ^{1}H NMR of **22** in $CDCl_3$.

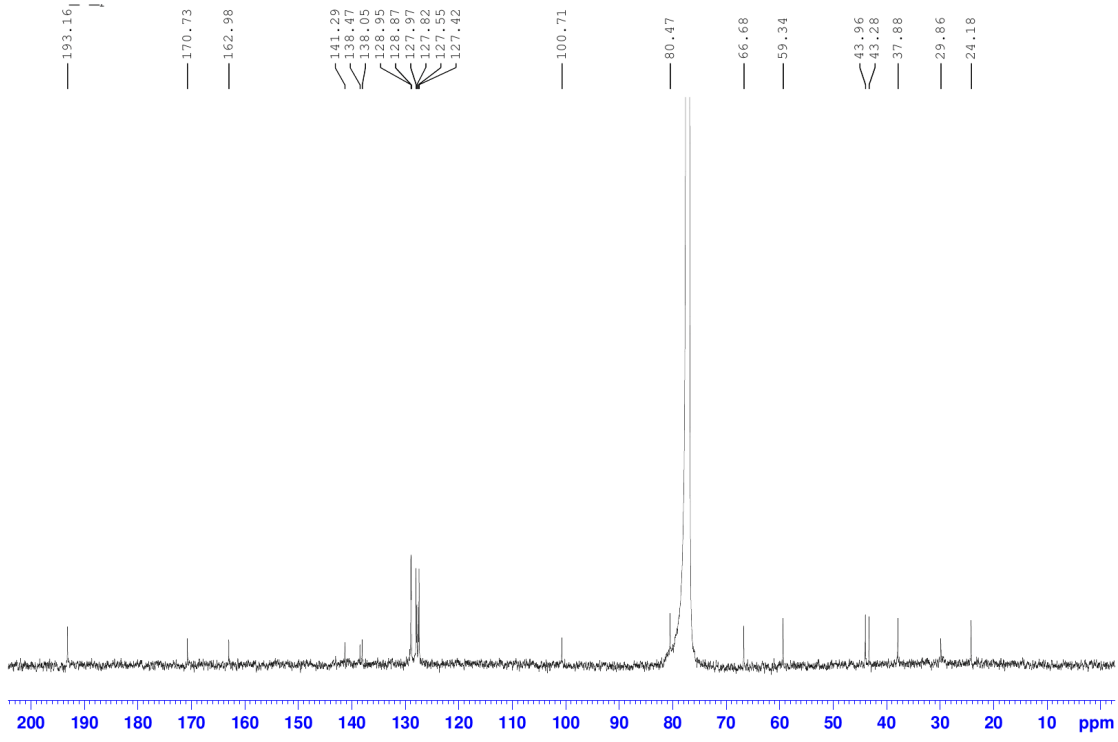

Figure 79. ^{13}C NMR of **22** in $CDCl_3$.

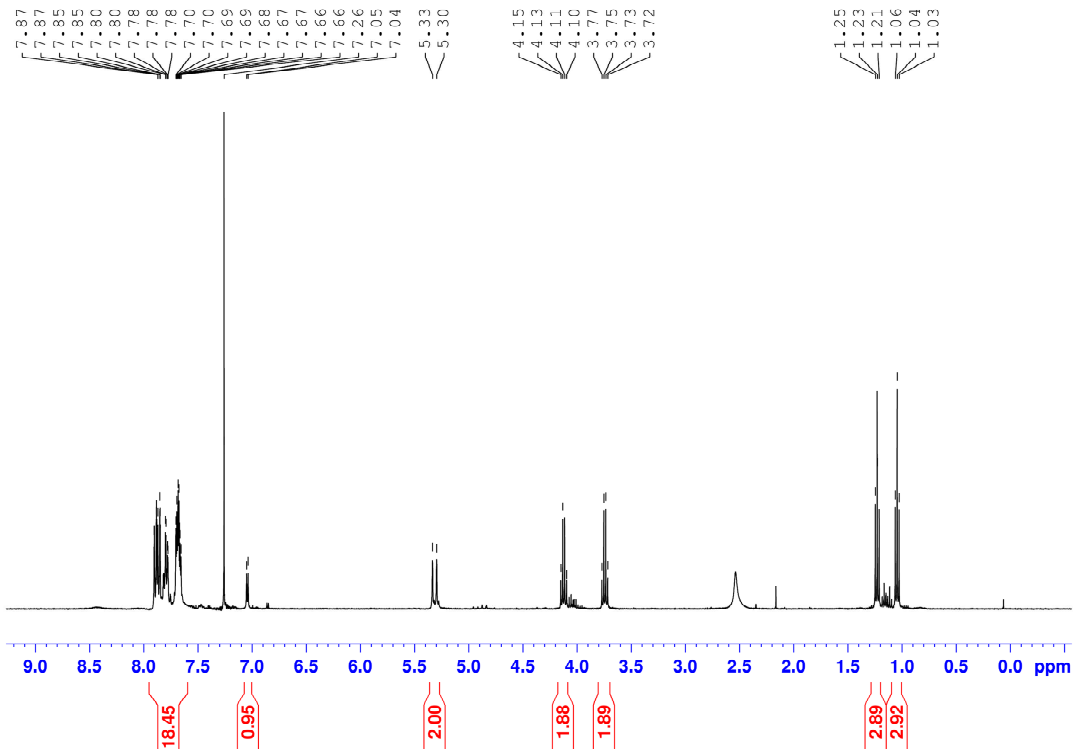

Figure 80. ^{1}H NMR of **26** in $CDCl_3$.

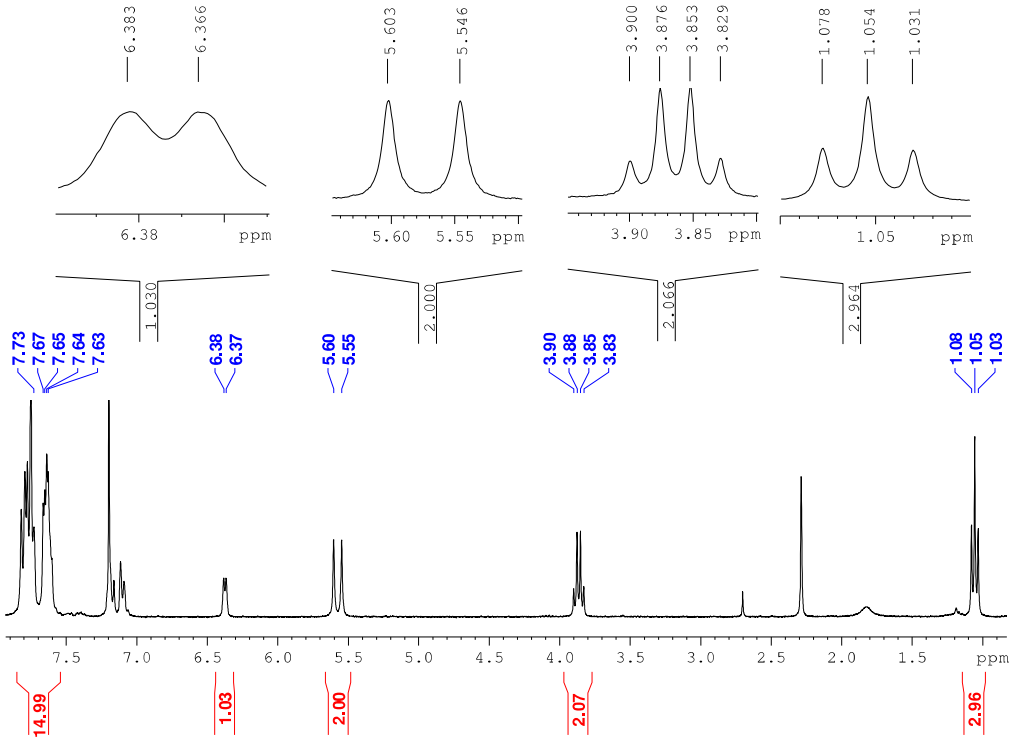

Figure 81. ^{1}H NMR of **28** in $CDCl_3$.

Table 2. Crystal data and structure refinement for **2b**.

Empirical formula	$C_{13}H_{11}O_7Re$
Diffractometer	Xcalibur Ruby
Wavelength [Å]	0.71073
Formula weight	465.42
Crystal system	Triclinic
Space group	P-1
a [Å]	7.9181(4)
b [Å]	8.2128(4)
c [Å]	12.5431(6)
a [°]	92.787(4)
b [°]	103.453(5)
g [°]	117.593(5)
Volume [$Å^3$]	691.40(7)
Z	2
Density (calculated) [Mg/m^3]	2.236
Absorption coefficient [mm^{-1}]	8.818
F(000)	440
Crystal size [mm^3]	0.270 x 0.110 x 0.090
Crystal description	colourless prism
Theta range for data collection [°]	2.846 to 32.886
Index ranges	-11<=h<=11, -12<=k<=12, -18<=l<=18
Reflections collected	13095
Independent reflections	4680 [R(int) = 0.0416]
Reflections observed	4283
Criterion for observation	I > 2(I)
Completeness to theta	100.0 % to 25.242°
Absorption correction	Semi-empirical from equivalents
Max. and min. transmission	1.00000 and 0.37184
Data / restraints / parameters	4680 / 0 / 195
Goodness-of-fit on F^2	1.023
Final R indices [I>2sigma(I)]	R1 = 0.0256, wR2 = 0.0482
R indices (all data)	R1 = 0.0300, wR2 = 0.0499
Extinction coefficient	n/a
Largest diff. peak and hole [$e.Å^{-3}$]	1.312 and -1.135

Table 3. Crystal data and structure refinement for **3b**.

Empirical formula	$C_{27}H_{25}N_2O_5Re$
Diffractometer	Xcalibur Ruby
Wavelength [Å]	0.71073
Formula weight	643.69
Crystal system	Orthorhombic
Space group	Fdd2
a [Å]	36.3108(13)
b [Å]	23.5876(8)
c [Å]	11.6762(4)
a [°]	90
b [°]	90
g [°]	90
Volume [$Å^3$]	10000.5(6)
Z	16
Density (calculated) [Mg/m^3]	1.710
Absorption coefficient [mm^{-1}]	4.900
F(000)	5056
Crystal size [mm^3]	0.280 x 0.200 x 0.100
Crystal description	colourless prism
Theta range for data collection [°]	2.244 to 32.788
Index ranges	-29<=h<=54, -14<=k<=34, -17<=l<=11
Reflections collected	13972
Independent reflections	6394 [R(int) = 0.0283]
Reflections observed	5853
Criterion for observation	I > 2(I)
Completeness to theta	99.9 % to 25.242°
Absorption correction	Semi-empirical from equivalents
Max. and min. transmission	1.00000 and 0.52864
Data / restraints / parameters	6394 / 1 / 317
Goodness-of-fit on F^2	1.043
Final R indices [I>2sigma(I)]	R1 = 0.0318, wR2 = 0.0846
R indices (all data)	R1 = 0.0359, wR2 = 0.0878
Absolute structure parameter	-0.009(12)
Extinction coefficient	n/a
Largest diff. peak and hole [$e.Å^{-3}$]	1.333 and -1.093

5.1.2 Synthetic Procedures and Analytical Data Part 3.2

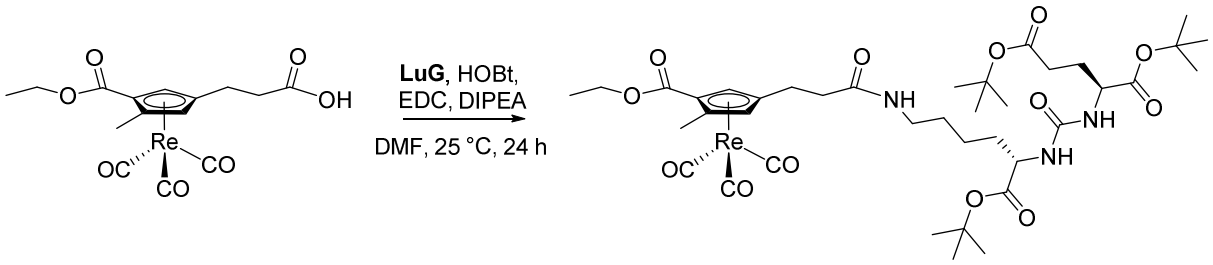

29. 8b (136 mg, 0.275 mmol) was dissolved in DMF (5 ml). **LuG** (148 mg, 0.3 mmol) and HOBt (41 mg, 0.3 mmol) were added under stirring. After 5 min, EDC (58 mg, 0.3 mmol) and DIPEA (0.105 ml, 0.61 mmol) were added and the solution was stirred for 24 h at 25 °C. The solvent was removed *in vacuo* and the crude was purified by preparative HPLC (Method A) and **29** was obtained as a pale-yellow oil (79 mg, 0.082 mmol, 30 % overall yield from **1a**).

UPLC (gradient U1): RT = 3.81 min. ^{1}H NMR (500 MHz, $CDCl_3$): δ (ppm) 1.28 – 1.34 (m, 5H), 1.42 – 1.43 (m, 9H), 1.43 – 1.44 (m, 9H), 1.46 (m, 9H), 1.46 – 1.59 (m, 3H), 1.72 – 1.80 (m, 1H), 1.81 – 1.88 (m, 1H), 2.03 – 2.11 (m, 1H). 2.29 – 2.35 (m, 2H), 2.36 - 2.41 (m, 2H), 2.47 – 2.48 (m, 3H), 2.63 – 2.70 (m, 1H), 2.78 – 2.89 (m, 1H), 3.07 – 3.39 (m, 2H), 4.17 – 4.34 (m, 4H), 5.26 (d, J^3 = 2.1 Hz, 1H), 5.38 (t, J^3 = 7.9 Hz, 1H), 5.53 (t, J^3 = 7.4 Hz, 1H), 5.78 (d, J^3 = 2.1 Hz, 0.5H), 5.84 (d, J^3 = 2.1 Hz, 0.5H), 6.53 – 6.58 (m, 1H). ^{13}C NMR (125 MHz, $CDCl_3$): δ (ppm) 13.91. 13.96, 14.24, 14.28, 22.61, 22.82, 22.87, 23.79, 23.87, 27.98, 28.11, 28.14, 28.15, 28.18, 28.68, 28.82, 29.84, 31.74, 31.82, 32.48, 32.59, 37.31, 37.67, 39.10, 39.22, 53.31, 53.34, 53.39, 53.54, 61.03, 61.23, 80.81, 80.83, 81.82, 81.87, 82.50, 82.58, 84.39, 84.46, 85.81, 85.97, 86.04, 86.09, 108.19, 108.26, 110.46, 110.64, 157.37, 157.42, 165.06, 165.40, 171.41, 171.43, 172.41, 172.43, 172.47, 173.27, 173.39, 193.69. HR-ESI mass spectrum (MeOH): found 964.36010; calcd. for [$C_{39}H_{58}N_3O_{13}Re+H^+$] 946.35999.

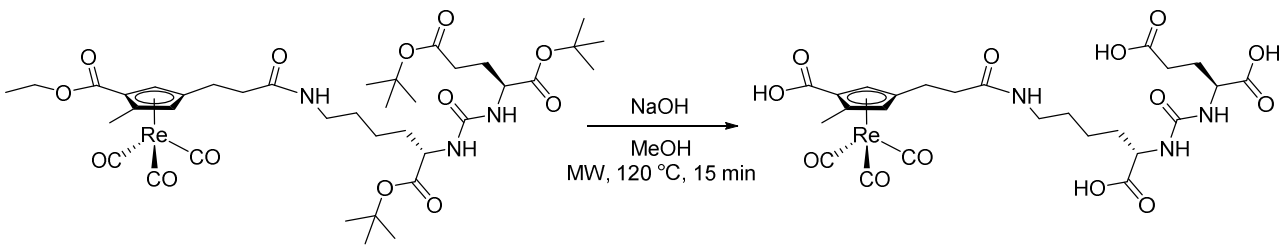

30. 3 (16 mg, 0.017 mmol) was dissolved in MeOH (2 ml) in an Anton Paar microwave vial (10 ml) and 1 M NaOH was added. The solution was heated by microwave to 120 °C for 15 min. The crude was diluted with H_2O (5 ml) and neutralized to pH = 3 by dropwise addition of 1 M HCl. The solvent was evaporated *in vacuo* and the crude was purified by preparative HPLC, yielding **30** as a yellowish oil (10 mg, 0.013 mmol, 76 %). UPLC (gradient U1): RT = 2.35 min. ^{1}H NMR (400 MHz, $CDCl_3$): δ (ppm) 1.38 – 1.57 (m, 4H), 1.62 – 1.74 (m, 1H), 1.78 – 1.98 (m, 2H), 2.10 – 2.20 (m, 1H), 2.36 – 2.46 (m, 4H), 2.49 (s, 3H), 2.59 – 2.81 (m, 2H), 3.16 – 3.21 (m, 2H), 4.23 – 4.34 (m, 2H), 5.49 (d, J^3 = 1.96 Hz, 1H), 5.90 (d, J^3 = 1.96 Hz, 1H). ^{13}C NMR (125 MHz, $CDCl_3$): δ (ppm) 14.02, 23.95, 25.10, 28.85, 28.95, 29.89, 29.95, 31.09, 31.11, 33.05, 33.18, 38.57, 40.15, 40.19, 53.56, 53.58, 54.04, 86.11, 87.44, 87.94, 108.95, 112.15, 159.98, 160.12, 168.14, 174.04, 175.90, 176.02, 176.48, 176.56, 176.59, 195.02. HR-ESI mass spectrum (MeOH): found 766.12671; calcd. for [$C_{25}H_{29}N_3O_{13}Re+H^+$] 766.12634.

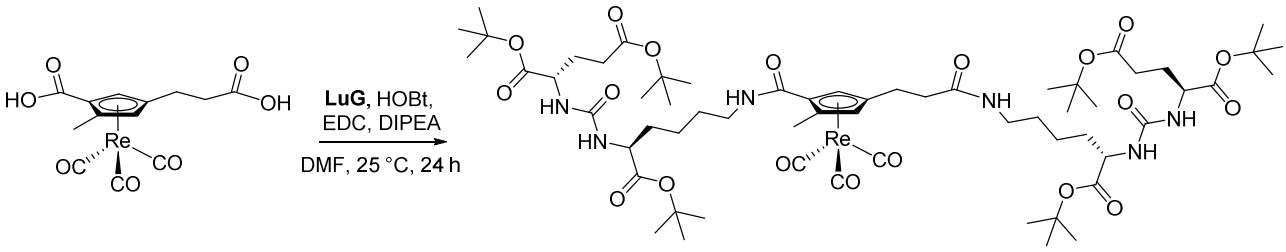

31. 2b (78 mg, 0.168 mmol) was dissolved in DMF (5 ml). **LuG** (164 mg, 0.34 mmol) and HOBt (50 mg, 0.37 mmol) were added under stirring. After 5 min, EDC (71 mg, 0.37 mmol) and DIPEA (0.129 ml, 0.74 mmol) were added and the solution was stirred for 24 h at 25 °C. The solvent was removed *in vacuo* and the crude was purified by preparative HPLC (Method A) and the two diastereoisomers of **31** (**31a** and **31b**) were obtained as a pale-yellow oil (**31a**, 38.3 mg, 0.027 mmol; **31b**, 35.9 mg**,** 0.026 mmol; yield: 31 %).

31a. UPLC (gradient U1): RT = 4.11 min. ^{1}H NMR (500 MHz, $CDCl_3$): δ (ppm) 1.35 – 1.50 (m, 58H), 1.50 – 1.64 (m, 5H), 1.72 – 1.96 (m, 5H), 2.01 – 2.14 (m, 2H), 2.25 – 2.43 (m, 6H), 2.49 (s, 3H), 2.57 – 2.68 (m, 1H), 2.83 – 2.93 (m, 1H), 3.09 – 3.20 (m, 1H), 3.27 – 3.38 (m, 3H), 4.23 – 4.38 (m, 4H), 5.19 (s, 1H), 5.33 – 5.39 (m, 1H), 5.45 – 5.51 (m, 1H), 5.54 – 5.60 (m, 1H), 5.66 – 5.71 (m, 1H), 5.89 (s, 1H), 6.59 – 6.63 (m, 1H), 6.68 – 6.74 (m, 1H). ^{13}C NMR (126 MHz, $CDCl_3$): δ (ppm) 13.93, 22.16, 22.58,

23.92, 28.16, 28.18, 28.22, 28.45, 28.80, 31.69, 31.82, 32.66, 32.78, 37.50, 38.98, 39.42, 53.20, 53.25,53.35, 53.48, 77.16, 80.84, 80.88, 81.89, 82.01, 82.42, 82.45, 82.95, 85.19, 90.93, 107.85, 109.04, 157.45, 157.71, 164.47, 171.62, 172.53, 172.59, 172.63, 172.65, 172.87, 173.21, 194.31, 194.39. HR-ESI mass spectrum (MeOH): found 1405.64555; calcd. for [$C_{61}H_{97}N_6O_{19}Re+H^+$] 1405.64388.

31b. UPLC (gradient U1): RT = 4.13 min. ^{1}H NMR (500 MHz, $CDCl_3$): δ (ppm) 1.35 – 1.50 (m, 58H), 1.50 – 1.64 (m, 5H), 1.72 – 1.96 (m, 5H), 2.01 – 2.14 (m, 2H), 2.25 – 2.43 (m, 6H), 2.49 (s, 3H), 2.64 – 2.76 (m, 2H), 3.09 – 3.20 (m, 1H), 3.27 – 3.38 (m, 3H), 4.23 – 4.38 (m, 4H), 5.16 (m, 1H), 5.58 – 5.62 (m, 2H), 5.73 (m, 1H), 5.89 – 5.91 (m, 2H), 6.77 – 6.82 (m, 2H). ^{13}C NMR (126 MHz, $CDCl_3$): δ (ppm) 13.41, 13.73, 18.03, 22.13, 22.30, 22.90, 23.55, 27.41, 27.61, 27.63, 27.65, 27.70, 28.11, 28.97, 29.04, 29.24, 29.27, 29.32, 29.35, 31.19, 31.26, 31.54, 32.19, 32.51, 33.06, 37.19, 38.73, 38.82, 52.60, 52.73, 52.94, 80.24, 80.34, 81.30, 81.64, 81.87, 81.98, 82.97, 84.32, 90.32, 106.62, 108.70, 157.18, 163.90, 171.14, 171.87, 171.97, 172.21, 172.33, 172.37, 172.88, 193.77. HR-ESI mass spectrum (MeOH): found 1405.64572; calcd. for [$C_{61}H_{97}N_6O_{19}Re+H^+$] 1405.64388.

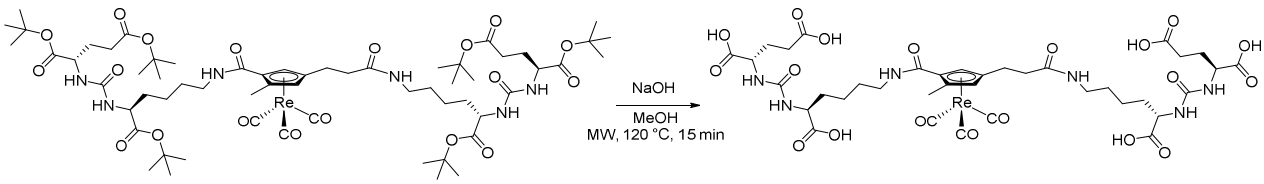

32. A 1:1 mixture of **31** (60 mg, 0.043 mmol) was dissolved in MeOH (2 ml) and 1 M NaOH (1 ml) in an Anton Paar microwave vial (10 ml) and was heated by microwave to 120 °C for 15 min. The solution was adjusted to pH = 3 by addition of 1 M HCl. The solvent was evaporated *in vacuo* and the crude was purified by preparative HPLC (Method A), yielding **32** as a yellowish oil (25.7 mg, 0.024 mmol, 56 %).

UPLC (gradient U1): RT = 2.24 min. ^{1}H NMR (500 MHz, CD_3OD): δ (ppm) 1.39 – 1.74 (m, 10H), 1.79 – 1.96 (m, 4H), 2.10 - 2.19 (m, 2H), 2.36 – 2.46 (m, 6H), 2.50 (s, 3H), 2.62 – 2.74 (m, 2H), 3.15 – 3.27 (m, 4H), 4.23 – 4.28 (m, 2H), 4.30 – 4.35 (m, 2H), 5.43 (m, 1H), 5.99 (m, 1H). HR-ESI mass spectrum (MeOH): found 1067.25684; calcd. for [$C_{37}H_{48}N_6O_{19}Re-H^+$] 1067.25372.

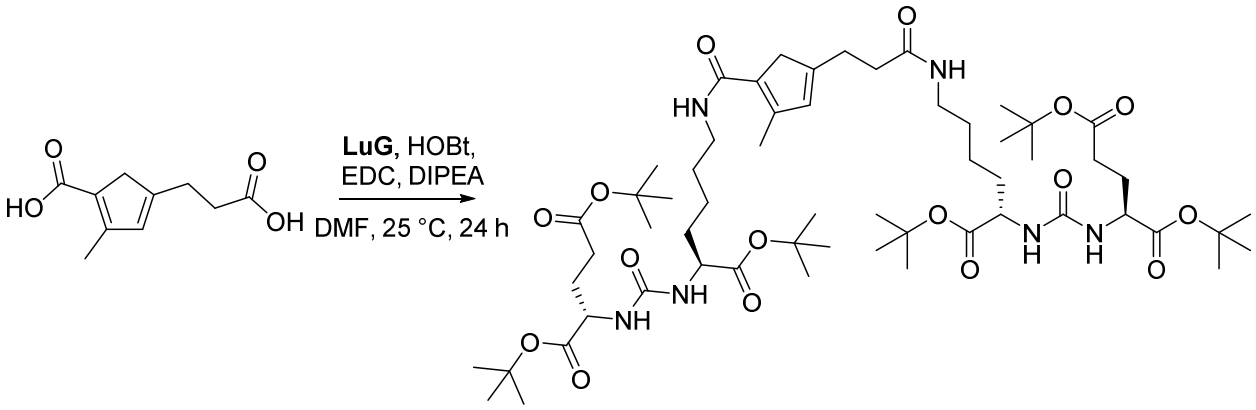

33. 2a(41 mg, 0.210 mmol) was dissolved in DMF (5 ml). **LuG** (225 mg, 0.462 mmol) and HOBt (62 mg, 0.462 mmol) were added under stirring. After 5 min, EDC (89 mg, 0.462 mmol) and DIPEA (0.161 ml, 0.924 mmol) were added and the solution was stirred for 24 h at 25 °C. The solvent was removed *in vacuo* and the crude was purified by preparative HPLC (Method A) and **33** was obtained as a pale-yellow oil (36 mg, 0.032 mmol, 15 % overall yield from **1a**).

UPLC (gradient U1): RT = 3.78 min. ^{1}H NMR (400 MHz, $CDCl_3$): δ (ppm) 1.18 – 1.29 (m, 4H), 1.31 – 1.38 (m, 54H), 1.38 - 1.57 (m, 6H), 1.60 – 1.80 (m, 4H), 1.92 – 2.03 (m, 2H), 2.12 (s, 3H), 2.17 – 2.28 (m, 4H), 2.28 – 2.40 (m, 2H), 2.51 – 2.60 (m, 1H), 2.67 – 2.75 (m, 1H), 2.83 – 2.96 (m, 2H), 3.03 – 3.11 (m, 1H), 3.19 – 3.32 (m, 3H), 4.14 – 4.27 (m, 4H), 5.30 – 5.36 (m, 1H), 5.36 - 5.40 (m, 1H), 5.49 – 5.56 (m, 1H), 5.86 – 5.93 (m, 1H), 5.95 (s, 1H), 5.97 – 6.00 (m, 1H), 6.50 – 6.57 (m, 1H). ^{13}C NMR (125 MHz, $CDCl_3$): δ (ppm) 15.73, 22.41, 23.21, 27.50, 28.38, 28.60, 28.62, 28.67, 28.68, 29.01, 29.80, 30.29, 32.21, 32.37, 32.89, 33.11, 36.57, 39.17, 39.60, 44.15, 53.55, 53.62, 53.81, 54.02, 81.14, 81.16, 82.05, 82.20, 82.53, 82.63, 131.41, 133.78, 149.43, 151.01, 157.76, 158.13, 166.96, 172.89, 172.92, 173.01, 173.04, 173.12, 173.15, 173.96 HR-ESI mass spectrum (MeOH): found 1135.71147; calcd. for [$C_{58}H_{99}N_6O_{16}Re+H^+$] 1135.71121.

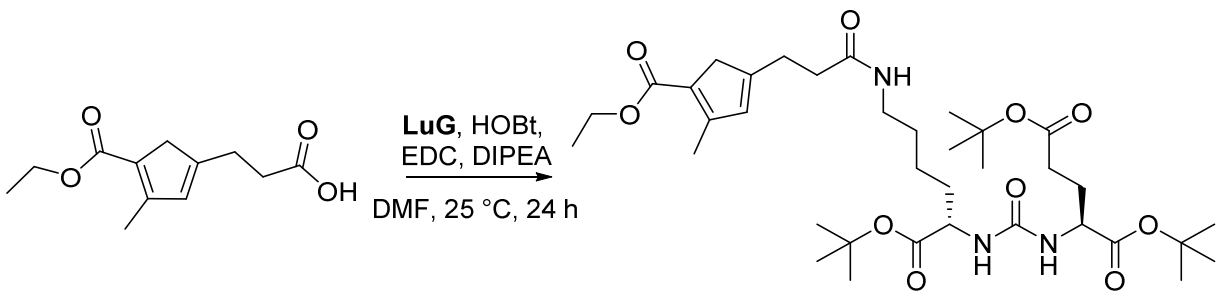

35. 8a (57 mg, 0.253 mmol) was dissolved in DMF (5 ml). **LuG** (136 mg, 0.278 mmol) and HOBt (38 mg, 0.278 mmol) were added under stirring. After 5 min, EDC (53 mg, 0.278 mmol) and DIPEA (0.097 ml, 0.557 mmol) were added and the solution was stirred for 24 h at 23 °C. The solvent was removed *in vacuo* and the crude was purified by preparative HPLC (Method A) and **35** was obtained as a pale-yellow oil (30 mg, 0.043 mmol, 17 % overall yield from **1a**).

UPLC (gradient U1): RT = 3.48 min. ^{1}H NMR (500 MHz, $CDCl_3$): δ (ppm) 1.27 – 1.40 (m, 3H), 1.38 – 1.53 (m, 31H), 1.74 – 1.92 (m, 3 H), 2.03 – 2.11 (m, 1H), 2.27 (s, 3H), 2.32 – 2.38 (m, 2H), 2.40 – 2.53 (m, 2H), 2.65 - 2.72 (m, 1H), 2.81 – 2.88 (m, 1H), 2.97 – 3.05 (m, 1H), 3.16 – 3.25 (m, 1H), 3.36 – 3.45 (m, 2H), 4.19 – 4.36 (m, 4H), 5.30 – 5.36 (m, 1H), 5.58 – 5.64 (m, 1H), 6.12 (s, 1H), 6.39 – 6.44 (m, 1H). ^{13}C NMR (125 MHz, $CDCl_3$): δ (ppm) 14.53, 15.70, 22.28, 27.02, 27.92, 28.08, 28.11, 28.16, 28.66, 31.82, 32.45, 35.63, 38.88, 44.17, 53.21, 53.36, 59.83, 80.78, 81.72, 82.29, 127.05, 133.14, 154.08, 155.91, 157.52, 165.84, 172.40, 172.52, 172.56, 173.35. HR-ESI mass spectrum (MeOH): found 694.42714; calcd. for $[C_{36}H_{59}N_3O_{10}+H^+]$ 694.42732.

General procedure for the labelling of Cp-Ligands 33 and 35.

Generally, 0.5 ml of a 5 mM stock solution of the respective ligand in MeOH was added to a Biotage microwave vial (2 – 5 ml). The vial was sealed, and the solvent was removed by passing a stream of N_2 through the vial *via* two syringe needles for 30 min. $[^{99m}Tc(OH_2)_3(CO)_3]^+$ (0.5 ml, pH = 13) was added to the dried ligand and the solution was heated by microwave to 140 °C for 10 (**35**) or 15 (**33**) min. In order to normalize the overpressure, evolving gases were released with a 1 ml disposable syringe-needle.

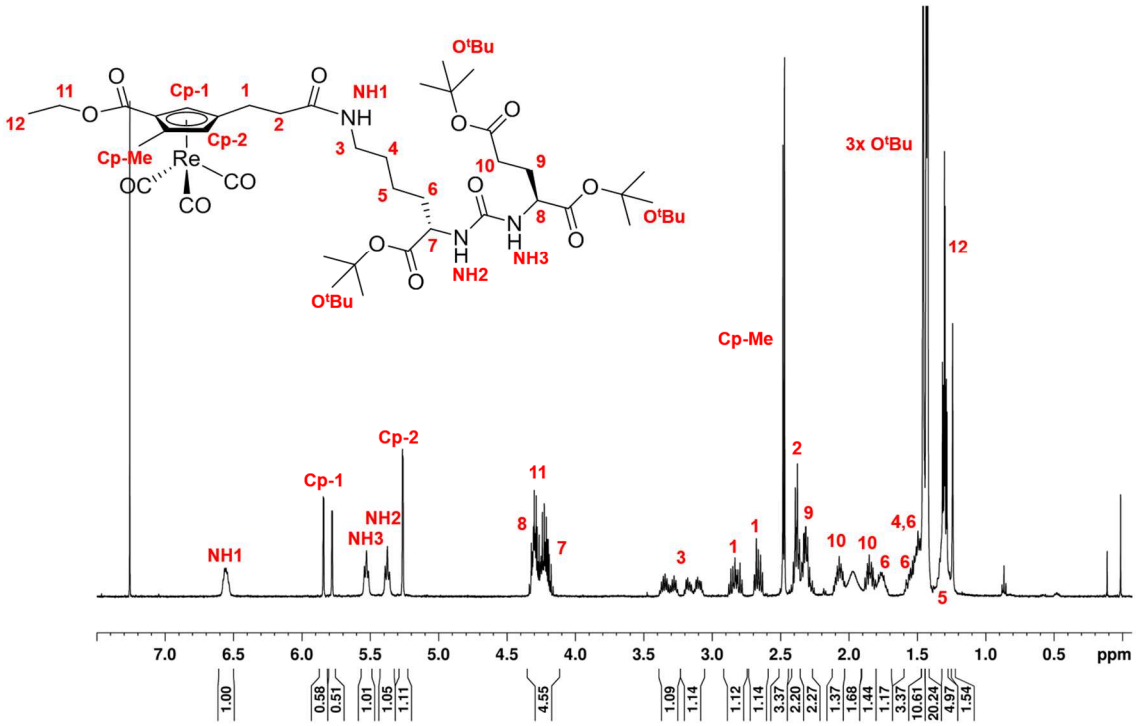

Figure 82. ^{1}H NMR of **29** in $CDCl_3$ with assigned proton signals.

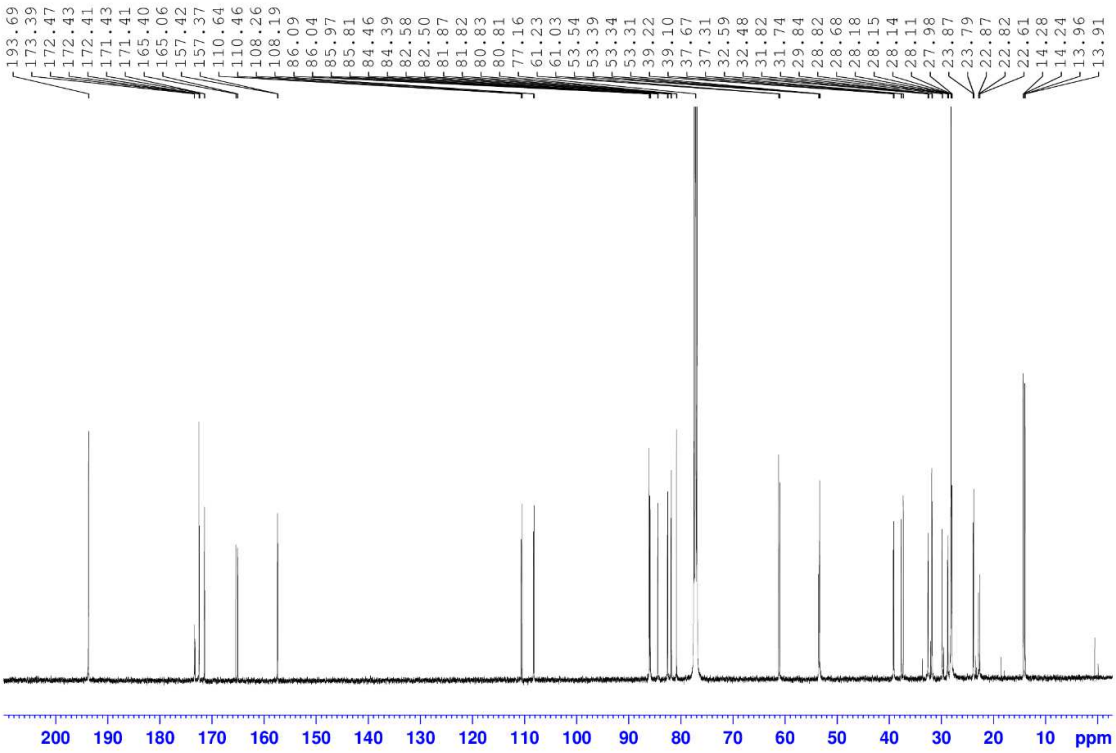

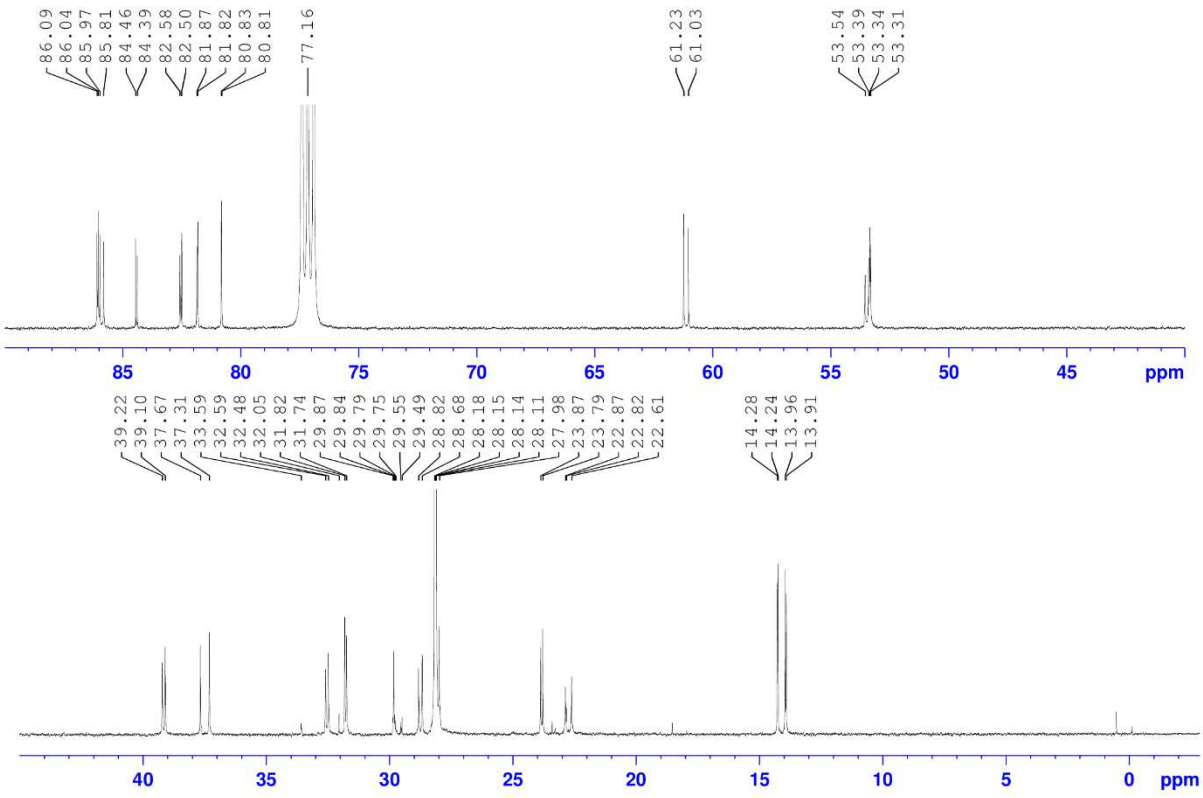

Figure 83. ^{13}C NMR of **29** in $CDCl_3$.

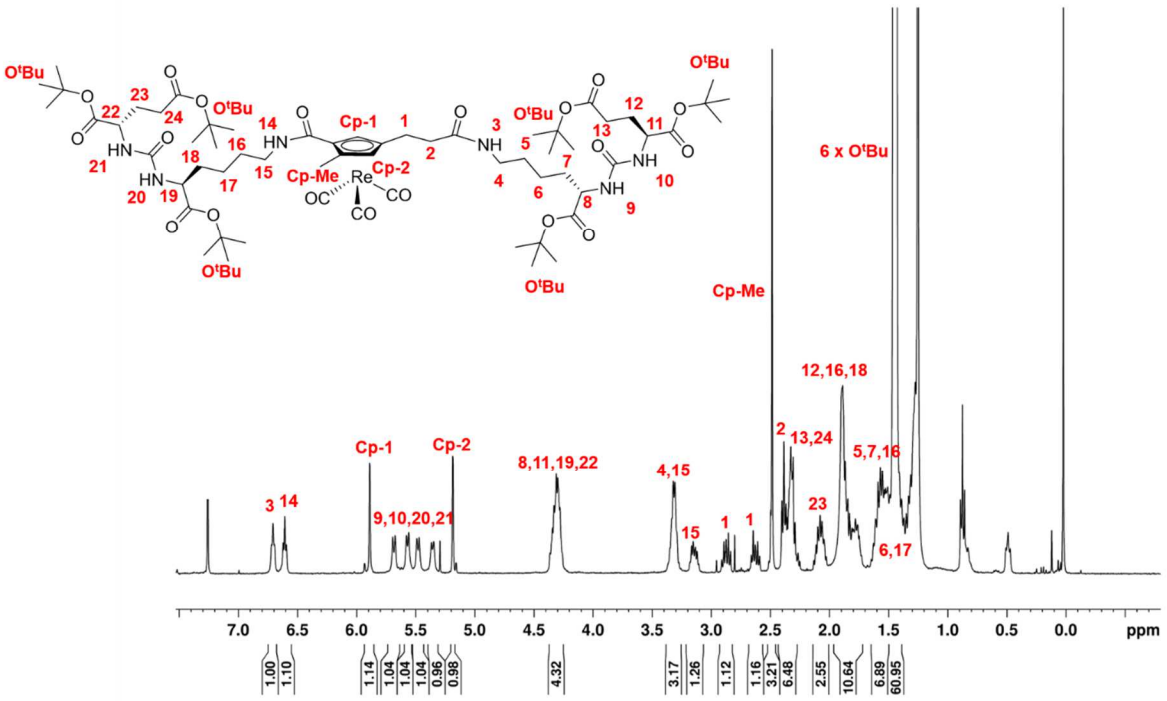

Figure 84. ^{1}H NMR of **31** in $CDCl_3$ with assigned proton signals.

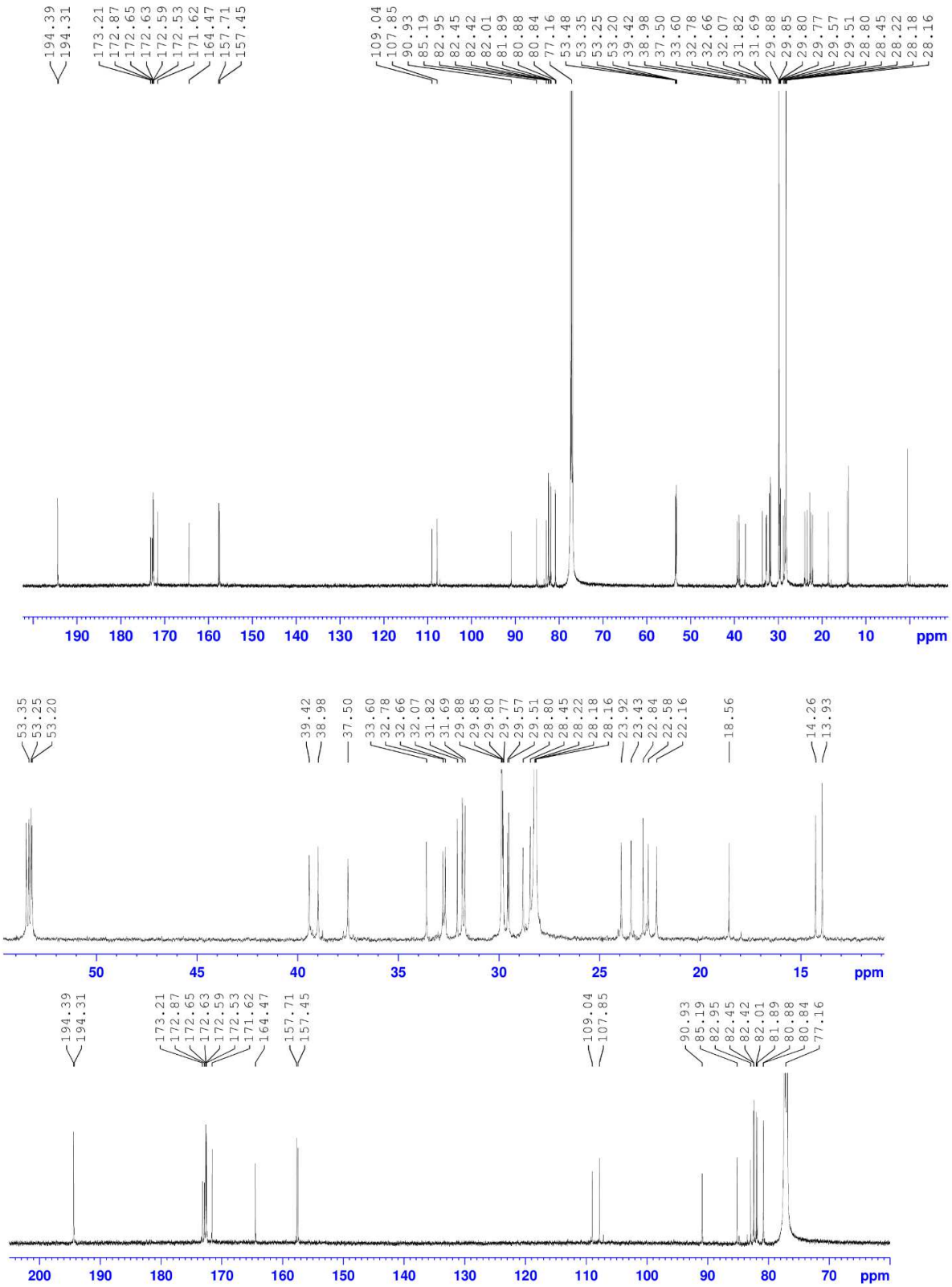

Figure 85. ^{13}C NMR of **31** in $CDCl_3$.

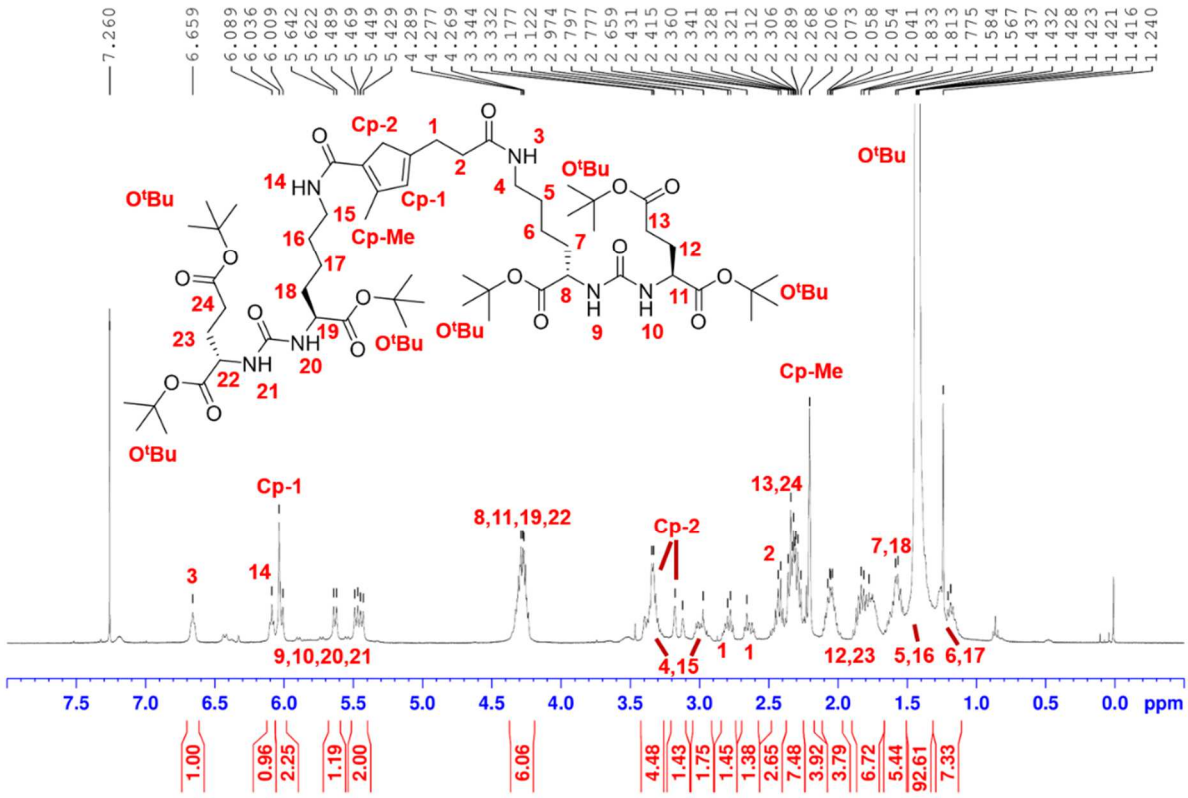

Figure 86. ^{1}H NMR of **33** in $CDCl_3$ with assigned proton signals.

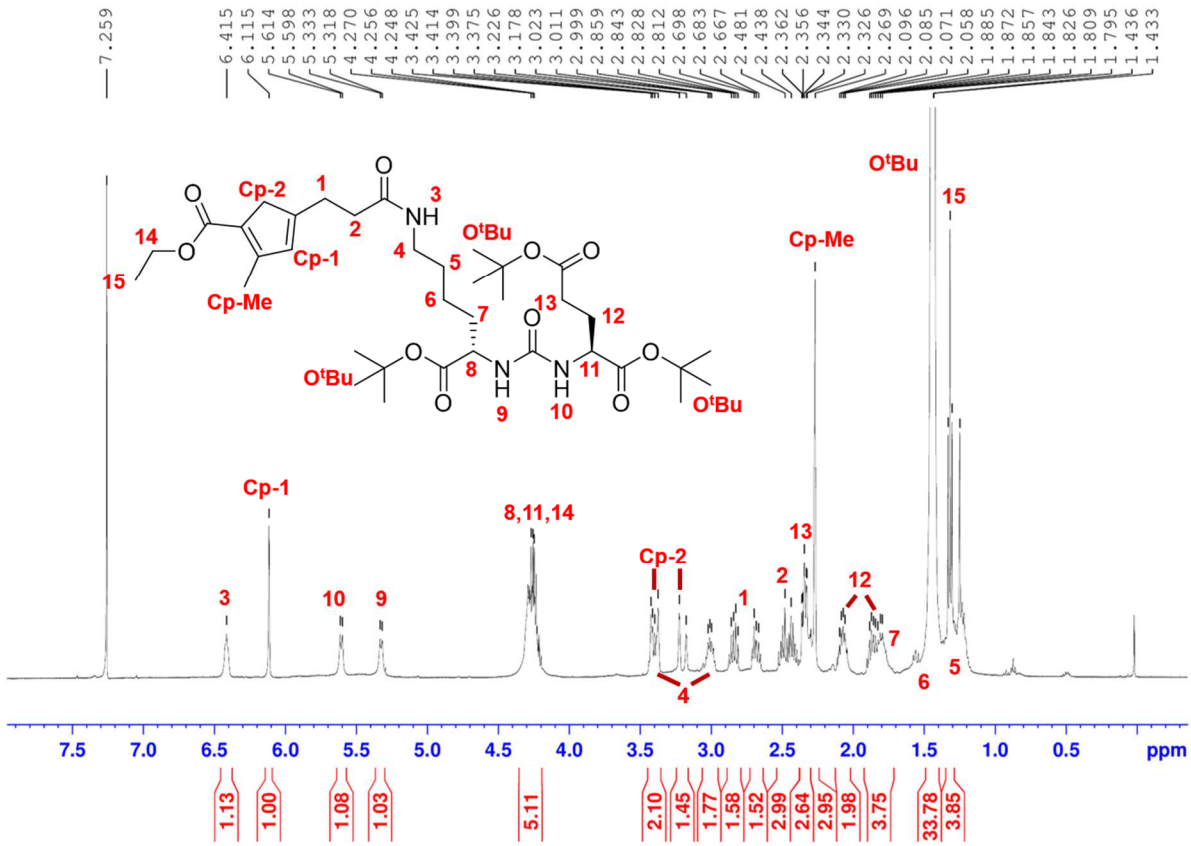

Figure 87. ^{1}H NMR of **35** in $CDCl_3$ with assigned proton signals.

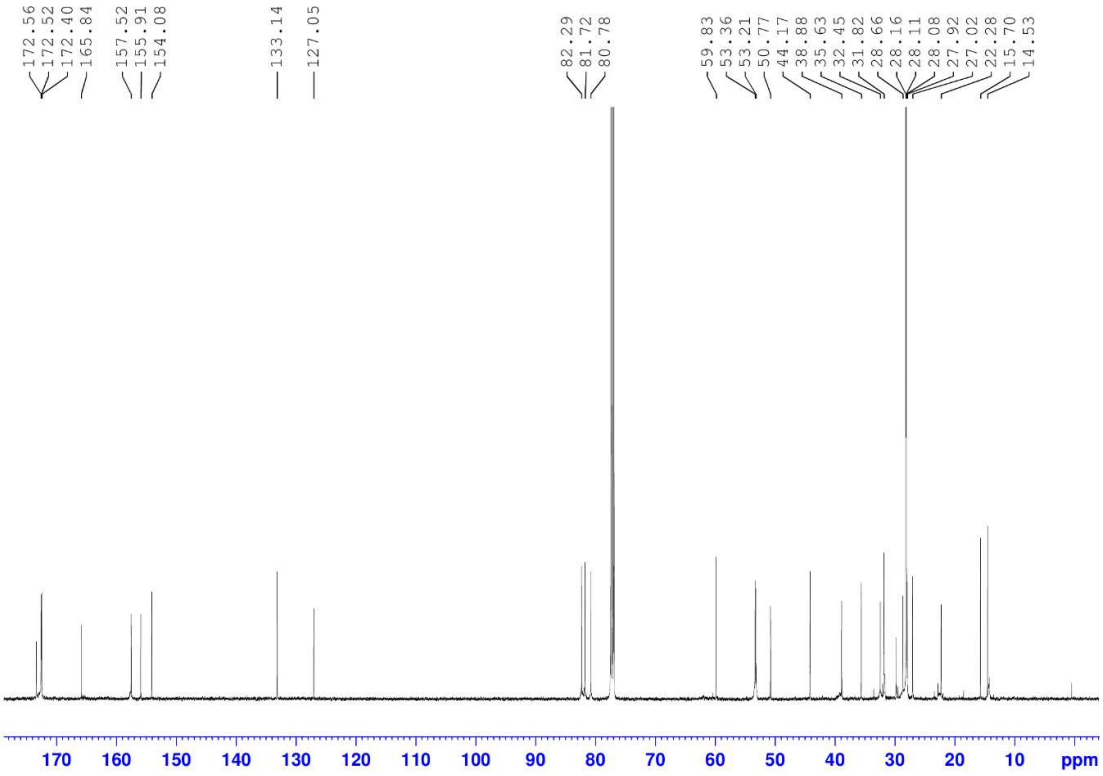

Figure 88. ^{13}C NMR of **35** in $CDCl_3$.

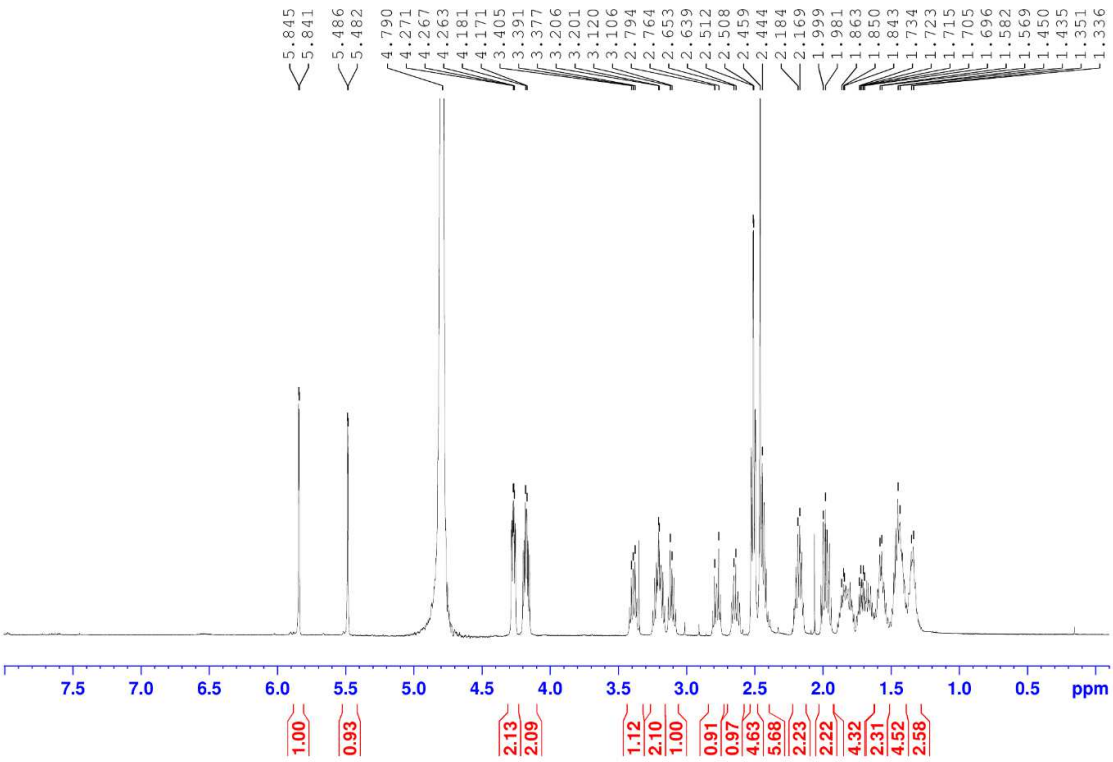

Figure 89. ^{1}H NMR of **32** in D_2O.

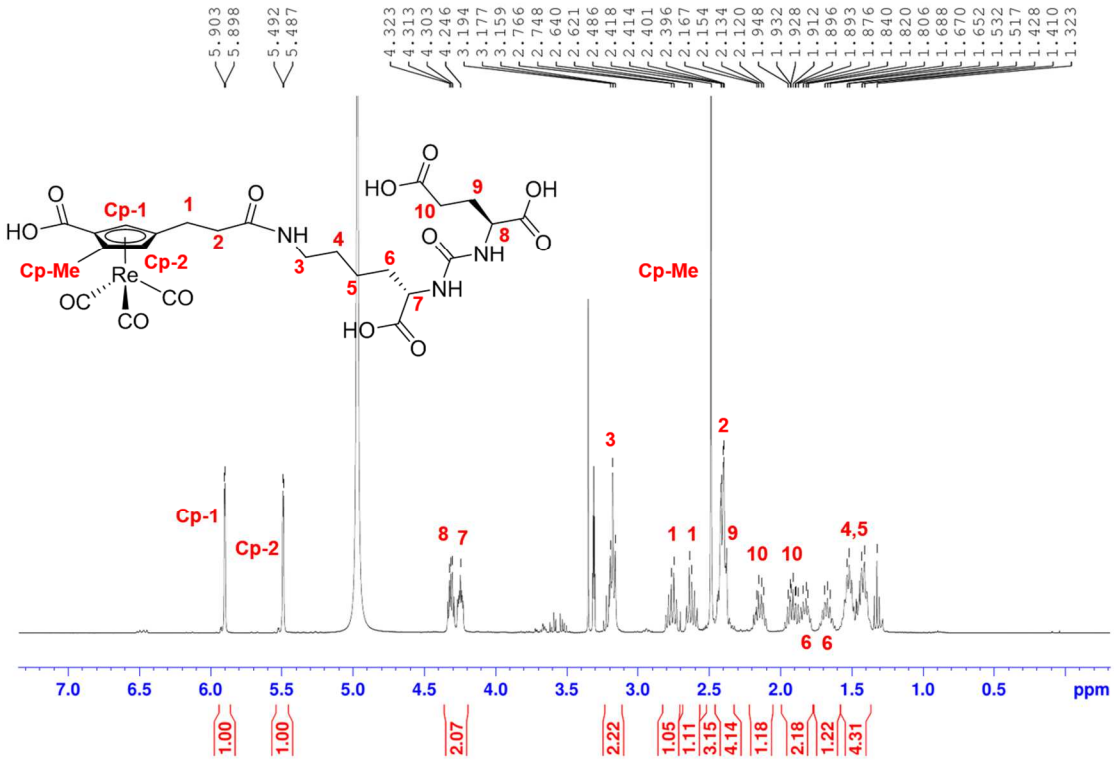

Figure 90. ^{1}H NMR of **30** in MeOD with assigned proton signals.

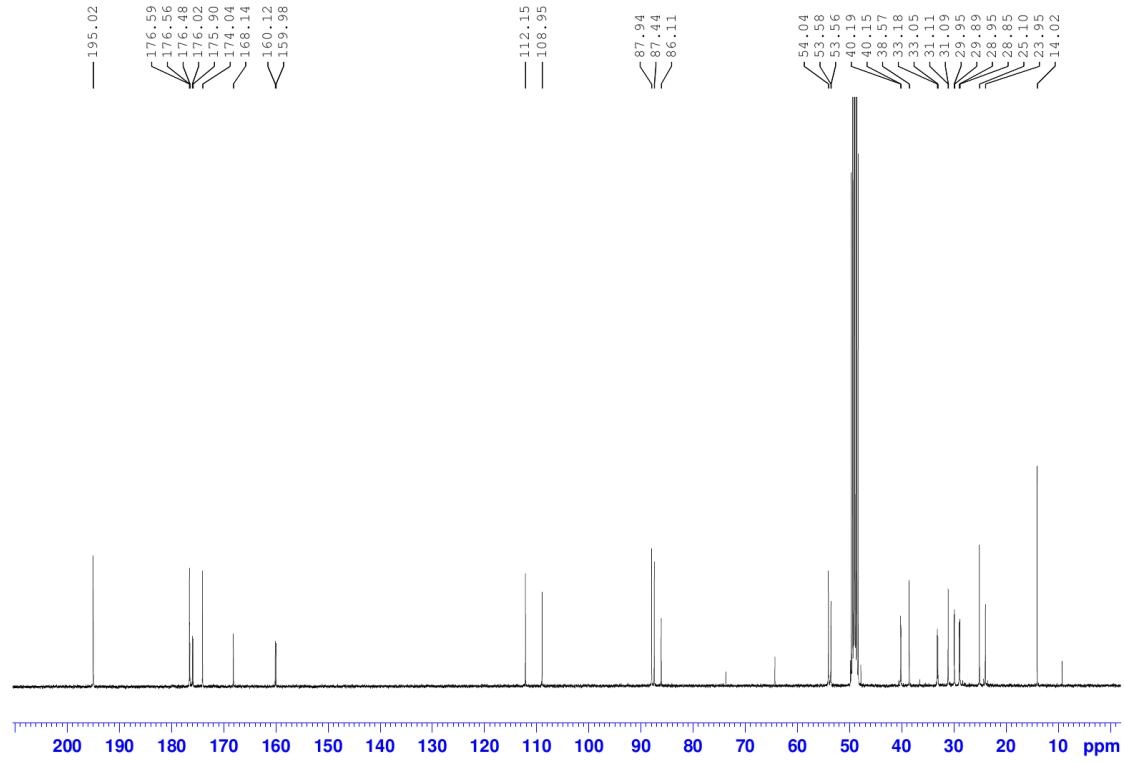

Figure 91. ^{13}C NMR of **30** in MeOD.

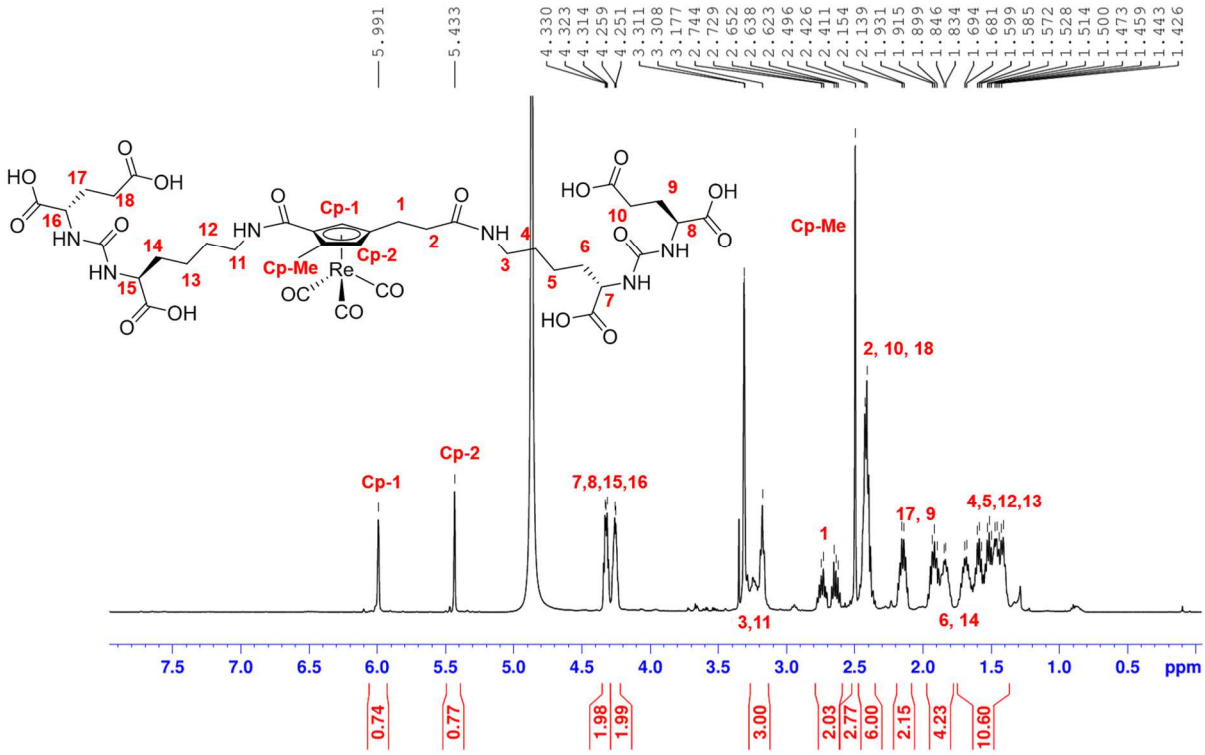

Figure 92. ^{1}H NMR of **32** in MeOD with assigned proton signals.

5.1.3 Synthetic Procedures and Analytical Data Part 3.3

37 was prepared according to a previously described procedure.[134, 224]

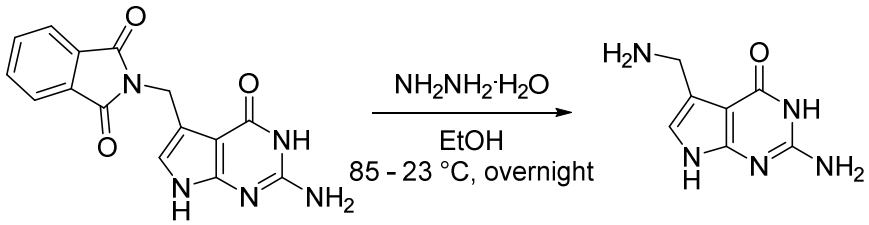

39. 38 (75 mg, 0.242 mmol) was dissolved in EtOH (10 ml) and hydrazine hydrate (0.13 ml (50 wt%), 2.09 mmol) was added. The mixture was heated to reflux for 2 h and then stirred at room temperature overnight. The solvent was evaporated *in vacuo* and the obtained crude **39** was used in the next step without furher purification.

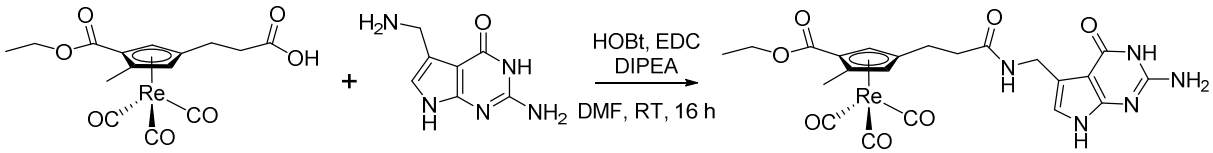

40. Crude **39** (ca. 0.242 mmol) and crude **8b** (ca. 0.285 mmol) were dissolved in DMF (3 ml) and HOBt (42 mg, 0.31 mmol) was added. After 5 min, EDC (60 mg, 0.31 mmol) and DIPEA (0.109 ml, 0.63 mmol) were added and the solution was stirred at room temperature for 16 h. The solvent was removed *in vacuo* and the crude was purified by preparative HPLC (Method A) and **40** was obtained as a yellow oil (32.3 mg, 0.049 mmol, 20 % overall yield from **38**).

UPLC (gradient U1): RT = 2.59 min. ^{1}H NMR (400 MHz, CD_3CN): δ (ppm) 1.22 (t, ^{3}J = 7.2 Hz, 3H), 2.35 – 2.41 (m, 5H), 2.55 – 2.76 (m, 2H), 3.29 (s, 4H), 4.09 – 4.25 (m, 2H), 4.39 – 4.40 (m, 2H), 5.36 (d, ^{3}J = 2 Hz, 2H), 5.76 (d, ^{3}J = 2 Hz, 2H), 6.65 (s, 1H), 7.45 (s, 1H), 7.60 – 7.88 (m, 2H), 10.50 (1H). ^{13}C NMR (126 MHz, CD_3CN): δ (ppm) 13.90, 14.40, 24.56, 35.80, 38.25, 49.90, 61.78, 85.46, 87.27, 87.43, 99.96, 109.23, 111.79, 117.28, 117.87, 152.40, 158.97, 165.59, 172.74, 195.13. HR-ESI mass spectrum (MeOH): found 656.11514; calcd. for [$C_{22}H_{22}N_5O_7Re+H^+$] 656.11495.

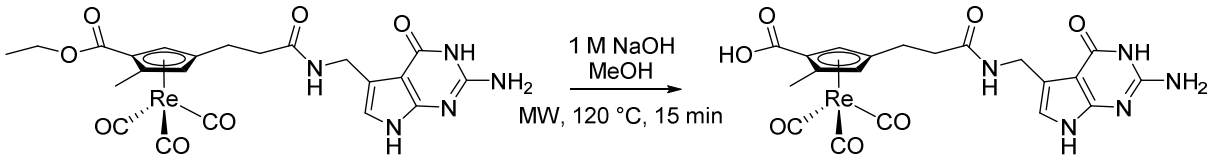

41. 40 (32.3 mg, 0.049 mmol) was dissolved in MeOH (2 ml) in an Anton Paar microwave vial (10 ml) and 1 M NaOH (1 ml) was added. The solution was heated by microwave to 120 °C for 15 min. The crude was diluted with H_2O (5 ml) and neutralized to pH = 3 by dropwise addition of 1 M HCl. The solvent was evaporated *in vacuo* and the crude was used in the next step without further purification.
UPLC (gradient U1): RT = 2.25 min.

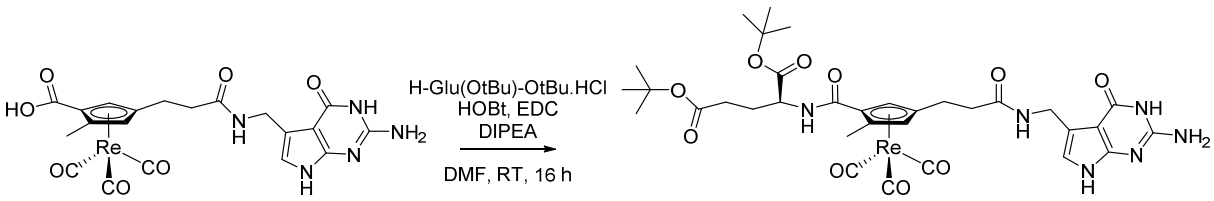

42. 41 (Assume 0.049 mmol), H-Glu(OtBu)-OtBu.HCl (16 mg, 0.054 mmol) and HOBt (8 mg, 0.06 mmol) were dissolved in DMF (3 ml). After 5 min, EDC (11 mg, 0.06 mmol) and DIPEA (0.020 ml, 0.11 mmol) were added and the solution was stirred at room temperature for 16 h. The solvent was removed *in vacuo* and the crude was purified by preparative HPLC (Method A) and **42** was obtained as a mixture of two diastereoisomers as a clear oil (26.5 mg, 0.031 mmol, 62 % overall yield from **40**).
UPLC (gradient U1): RT = 2.59 min. ^{1}H NMR (400 MHz, CD_3OD): δ (ppm) 1.44 – 1.45 (m, 9H), 1.47 – 1.49 (m, 9H), 1.87 – 2.22 (m, 2H), 2.33 – 2.45 (m, 7H), 2.59 – 2.82 (m, 2H), 4.43 – 4.49 (m, 3H), 5.34 – 5.36 (m, 1H), 6.05 – 6.07 (m, 1H), 6.66 (s, 1H).
^{13}C NMR (126 MHz, CD_3OD): δ (ppm) 13.99, 14.05, 25.22, 25.36, 27.44, 27.60, 32.65, 36.52, 36.55, 28.86, 53.80, 54.16, 81.92, 81.97, 83.17, 83.19, 84.82, 85.28, 86.66, 86.90, 90.14, 90.59, 100.08, 100.10, 108.29, 108.83, 111.09, 111.68, 116.45, 116.50, 116.62, 116.68, 117.04, 150.82, 150.87, 153.75, 161.51, 161.53, 166.45, 166.44, 172.52, 172.76, 173.47, 173.98, 195.24, 195.34. HR-ESI mass spectrum (MeOH): found 869.25262; calcd. for [$C_{33}H_{41}N_6O_{10}Re+H^+$] 869.25144.

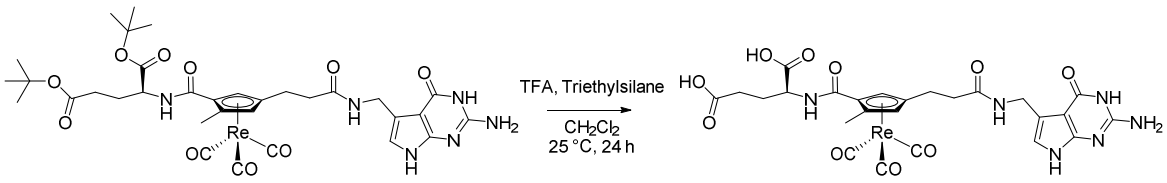

43. 42 (10 mg, 0.010 mmol) was dissolved in CH_2Cl_2 (3 ml). TFA (0.1 ml) and triethylsilane (0.05 ml) were added and the solution was stirred at 25 °C for 24 h. The

solvent was evaporated *in vacuo* and the crude was purified by preparative HPLC (method A) and **43** was obtained as a mixture of two diastereoisomers as a reddish solid (3 mg, 0.004 mmol, 38 %).

UPLC (gradient U1): RT = 2.21 min. ^{1}H NMR (400 MHz, CD_3OD): δ (ppm) 1.99 – 2.10 (m, 1H), 2.18 – 2.31 (m, 1H), 2.35 (s, 1.5 H), 2.40 (s, 1.5H), 2.39 – 2.50 (m, 4H), 2.56 – 2.85 (m, 2H), 4.34 – 4.54 (m, 3H), 5.29 – 5.32 (m, 1H), 6.05 – 6.08 (m, 1H), 6.64 (s, 1H). ^{13}C NMR (126 MHz, CD_3OD): δ (ppm) 13.83, 14.02, 25.13, 25.49, 26.50, 27.41, 27.46, 31.32, 31.41, 36.46, 36.53, 38.80, 39.09, 49.85, 53.28, 53.32, 68.87, 84.66, 85.10, 86.67, 86.77, 90.21, 90.32, 100.08, 100.12, 108.62, 108.73, 111.35, 111.70, 116.72, 116.81, 117.05, 117.17, 150.20, 153.66, 161.33, 161.35, 166.42, 166.56, 173.47, 175.25, 175.44, 176.71, 176.73, 195.13, 195.32. HR-ESI mass spectrum (MeOH): found 757.12671; calcd. for [$C_{25}H_{26}N_6O_{10}Re+H^+$] 757.12624.

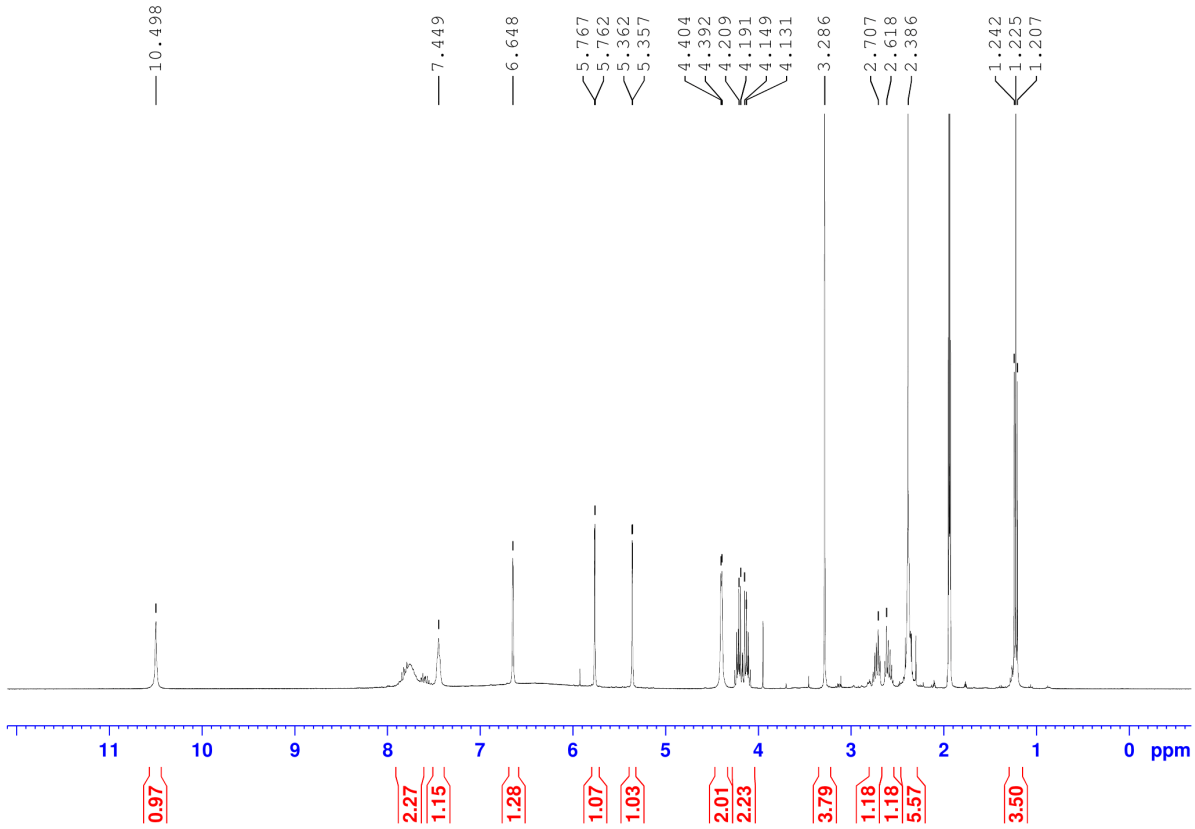

Figure 93. ^{1}H NMR of **40** in CD_3CN.

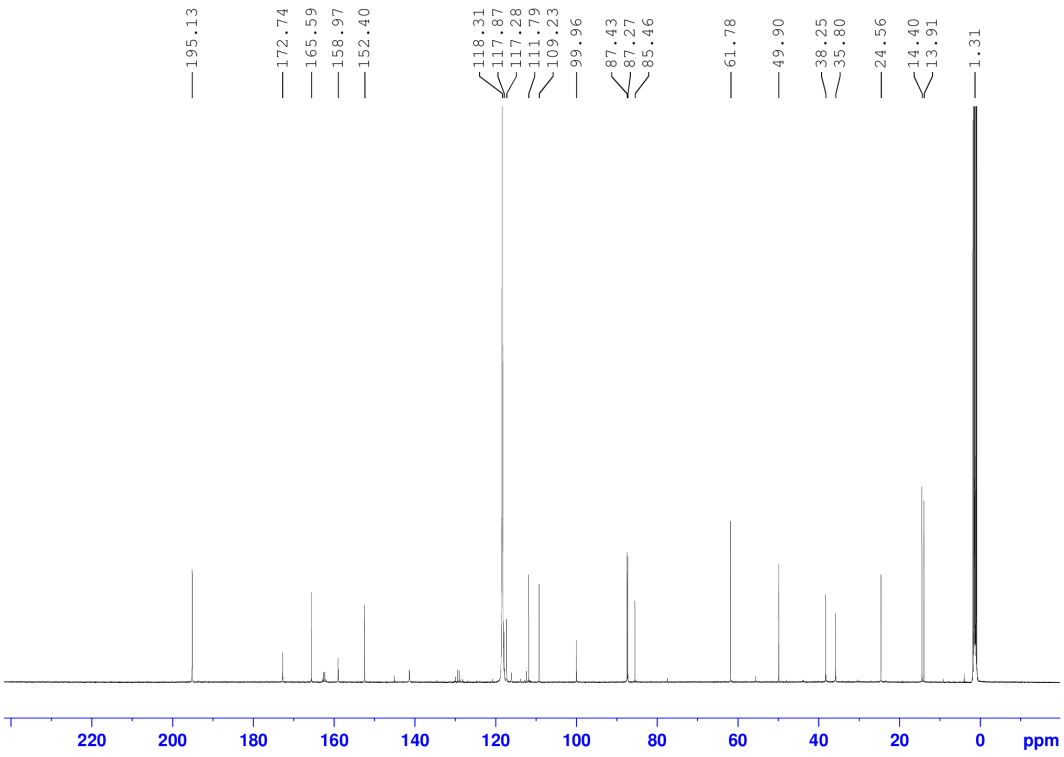

Figure 94. ^{13}C NMR of **40** in CD_3CN.

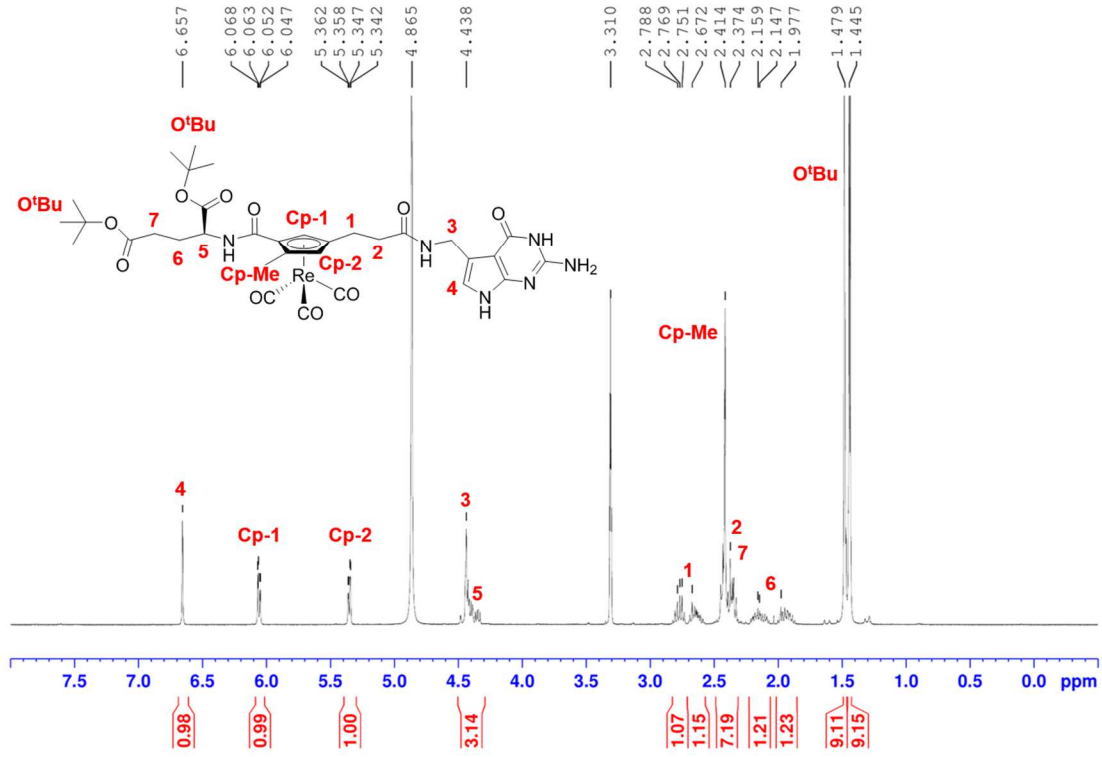

Figure 95. ^1H NMR of **42** in CD_3OD with assigned proton signals.

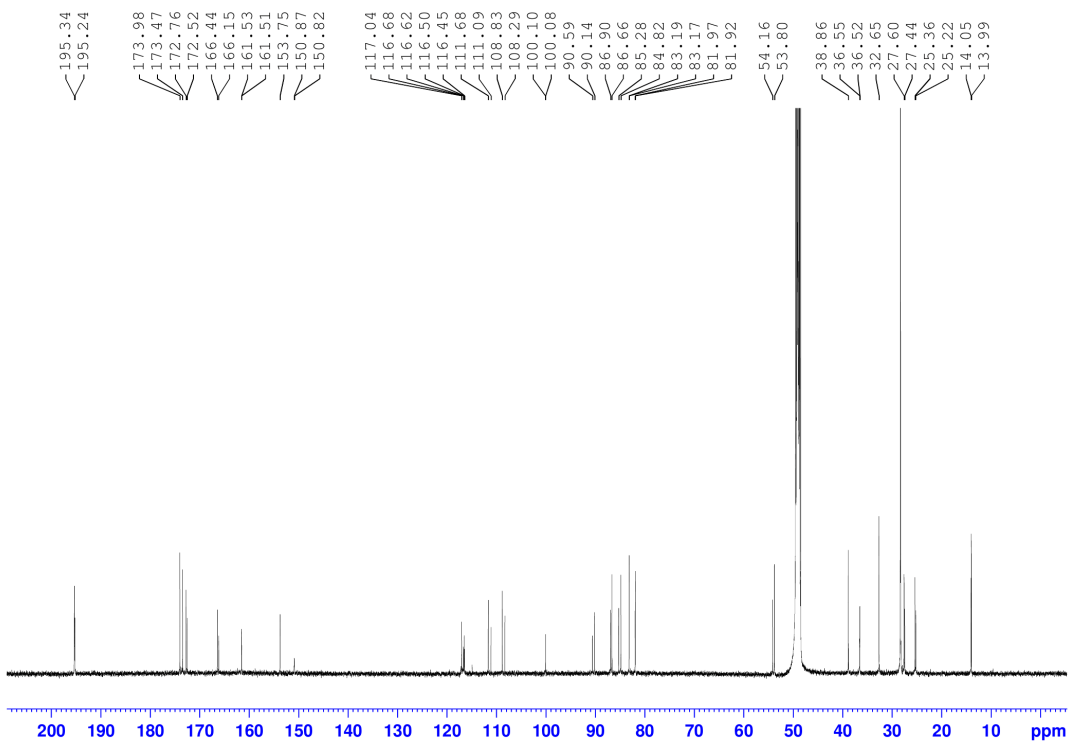

Figure 96. ^{13}C NMR of **42** in CD_3OD.

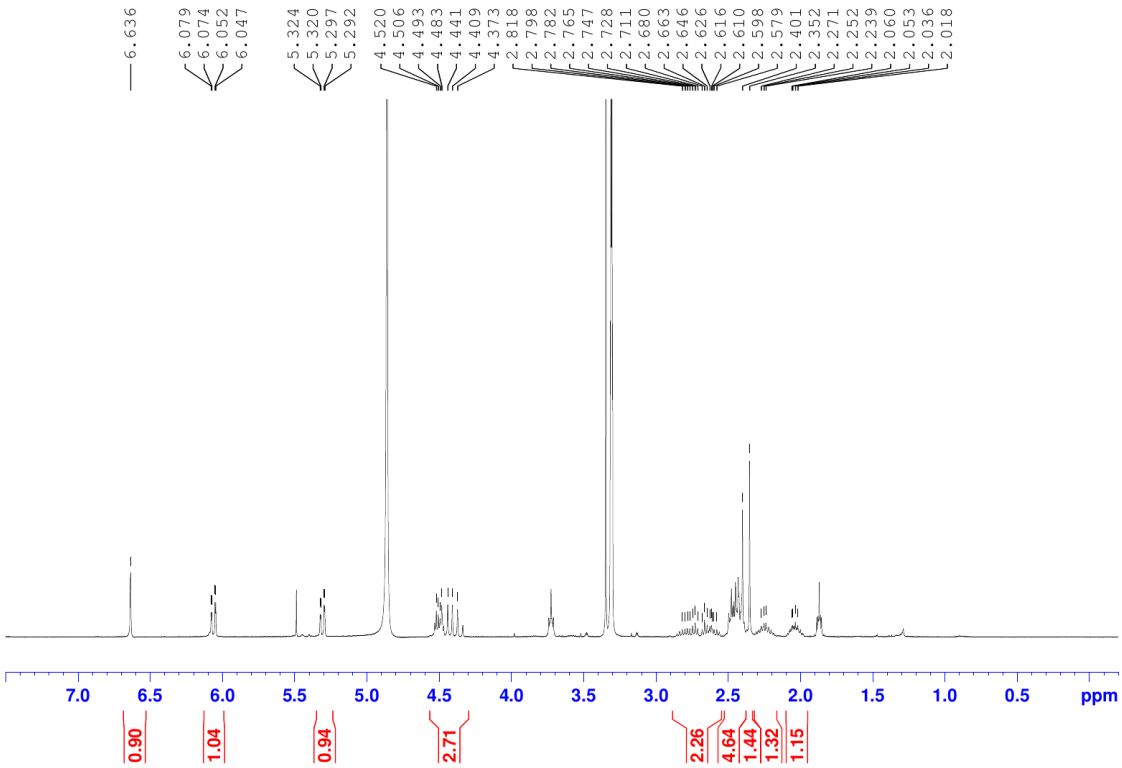

Figure 97. ^{1}H NMR of **43** in CD_3OD.

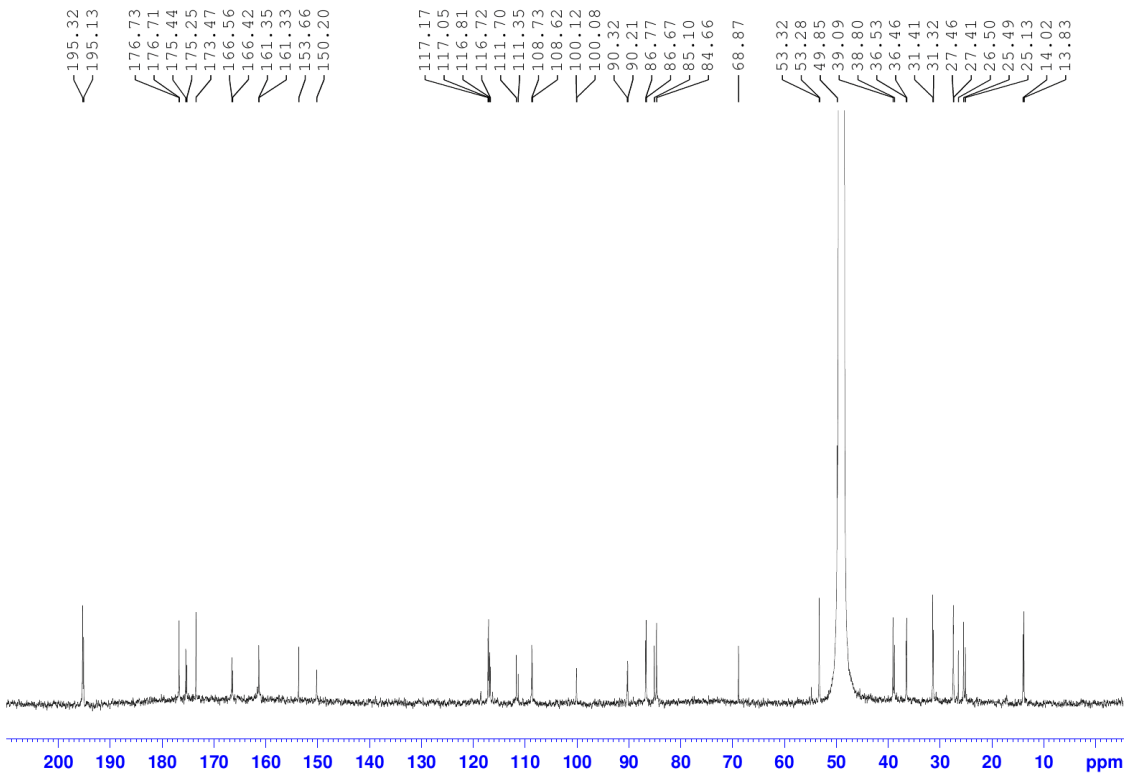

Figure 98. ^{13}C NMR of **43** in CD_3OD.

5.2 Experimental Section Part B

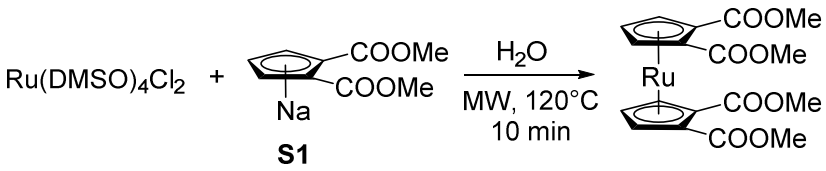

49. $Ru(DMSO)_2Cl_2$ (73 mg, 0.15 mmol) and **S1** (62 mg, 0.3 mmol) were dissolved in H_2O (2 ml) in a Biotage microwave vial and the mixture was heated by microwave to 120 °C for 10 min. The crude was diluted with H_2O (10 ml) and extracted with DCM (2 x 10 ml). The combined organic phases were dried over anhydrous $MgSO_4$, filtered and the solvents evaporated *in vacuo* yielding **49** as a light brown solid (35 mg, 0.1 mmol, 67%).

^1H NMR (400 MHz, $CDCl_3$): δ (ppm) 3.77 (s, 6H), 4.85 (t, J^3 = 2.6 Hz, 1H), 5.22 (d, J^3 = 2.6 Hz, 2H). ^{13}C NMR (101 MHz, $CDCl_3$): δ (ppm) 52.35, 75.92, 78.28, 80.86, 167.25.

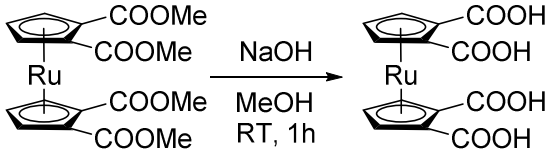

50. 49 (48 mg, 0.104 mmol) was suspended in MeOH (10 ml) and 1 M NaOH (1.04 ml) was added. The mixture was stirred at room temperature for 1 h. The precipitate was collected by filtration and dried *in vacuo* yielding **5** (23 mg, 0.056 mml, 54%).

^1H NMR (400 MHz, $CDCl_3$): δ (ppm) 7.16 (s, 1H), 7.50 (s, 2H).

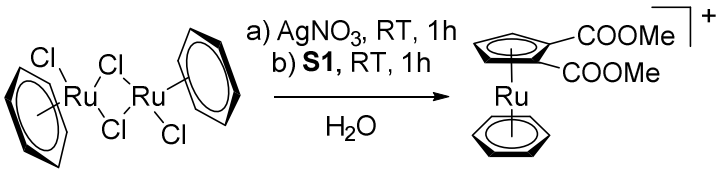

45. 44 (61 mg, 0.12 mmol) was suspended in H_2O (2 ml) and $AgNO_3$ (83 mg, 0.49 mmol) was added and the mixture was stirred at room temperature for 1 h. The dark precipitate was removed by filtration and **S1** (52 mg, 0.26 mmol) was added to the filtrate and the solution was stirred for another hour at room temperature. The solvent was evaporated *in vacuo* and the crude was re-dissolved in the minimal amount of H_2O required. NH_4PF_6 was added until no more precipitate formed. The mixture was cooled

overnight and the next day the precipitate was collected by centrifugation and dried *in vacuo* yielding **2** as a brown precipitate (36 mg, 0.1 mmol, 41%).

^{1}H NMR (400 MHz, CD_3CN): δ (ppm) 3.84 (s, 6H), 5.49 (t, J^3 = 2.6 Hz), 5.78 (d, J^3 = 2.6 Hz, 2H), 6.24 (s, 6H). ^{13}C NMR (126 MHz, CD_3CN): δ (ppm) 54.21, 82.38, 83.26, 90.07, 96.07, 164.90.

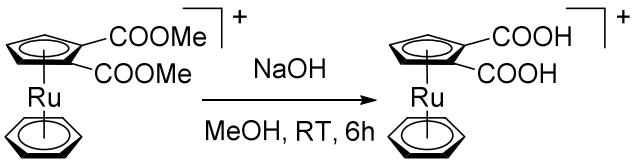

46. 45 (25 mg, 0.06 mmol) was dissolved in MeOH (3 ml) and 1 M NaOH (0.2 ml) was added. The mixture was stirred at room temperature for 6 h. The solution was diluted with H_2O (5 ml) was neutralized to pH = 7 by addition of 1 M HCl and the crude was purified by filtration through a short 18C (2 x 10 ml H_2O, 2 x 10 ml MeOH). The solvent was evaporated, yielding **46** (3.6 mg, 0.011 mmol, 18 %).

^{1}H NMR (400 MHz, D_2O): 5.80 (s, 1H), 6.11 (s, 2H), 6.40 (s, 6H).

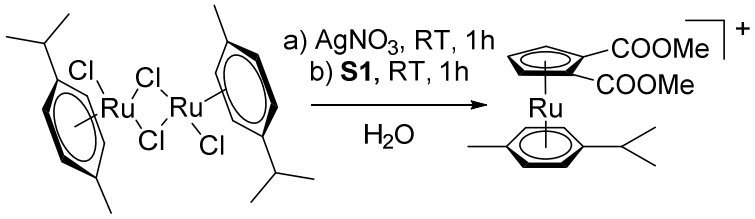

48. 47 (66 mg, 0.11 mmol) was suspended in H_2O (2 ml) and $AgNO_3$ (73 mg, 0.43 mmol) was added and the mixture was stirred at room temperature for 1 h. The dark brown precipitate was removed by filtration and **S1** (46 mg, 0.23 mmol) was added to the filtrate and the solution was stirred for another hour at room temperature. The solvent was evaporated *in vacuo* and the crude was re-dissolved in the minimal amount of H_2O required. NH_4PF_6 was added until no more precipitate formed. The mixture was cooled overnight and the next day the precipitate was collected by centrifugation, washed with H_2O (3 x 5 ml dried *in vacuo* yielding **2** as a brown precipitate (67 mg, 0.16 mmol, 73%).

^{1}H NMR (400 MHz, CD_3CN): δ (ppm) 1.22 (s, 3H), 1.23 (s, 3H), 2.22 (s, 3H), 2.71 (m, 1H), 3.83 (s, 6H), 5.44 (t, J^3 = 2.62 Hz, 1H), 5.70 (d, J^3 = 2.64 Hz, 2H), 6.11 – 6.18 (m, 4H).

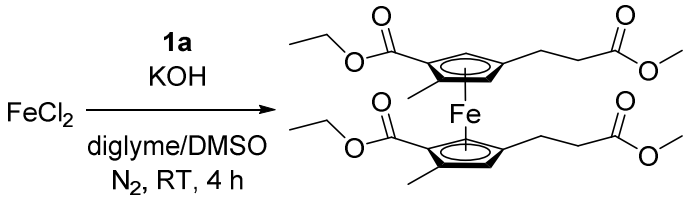

51. 1a (28 mg, 0.12 mmol) was dissolved in diglyme (4 ml) and bubbled with N_2 for 15 min. Finely grounded KOH (42 mg) was added to this solution and kept under nitrogen atmosphere and the solution turned yellow immediately. In a separate beaker, $FeCl_2$ (8 mg, 0.06 mmol) was dissolved in previously degassed DMSO (4 ml). The **1a** containing solution was slowly added to the $FeCl_2$ solution and stirred at room temperature for 4 h. The reaction mixture was neutralized by adding 1 M HCl until a yellow precipitate could be observed. The precipitate was collected by filtration and washed with H_2O (2 x 10 ml) and dried *in vacuo* (no yield was determined).

^{1}H NMR (400 MHz, CD_3Cl): 1.36 – 1.41 (m, 3H), 2.15 – 2.16 (m, 3H), 2.50 – 2.64 (m, 4H), 3.70 (m, 3H), 4.00 (m, 1H), 5.25 – 4.32 (m, 2H), 4.42 (m, 0.5H), 4.49 (m, 0.5H).

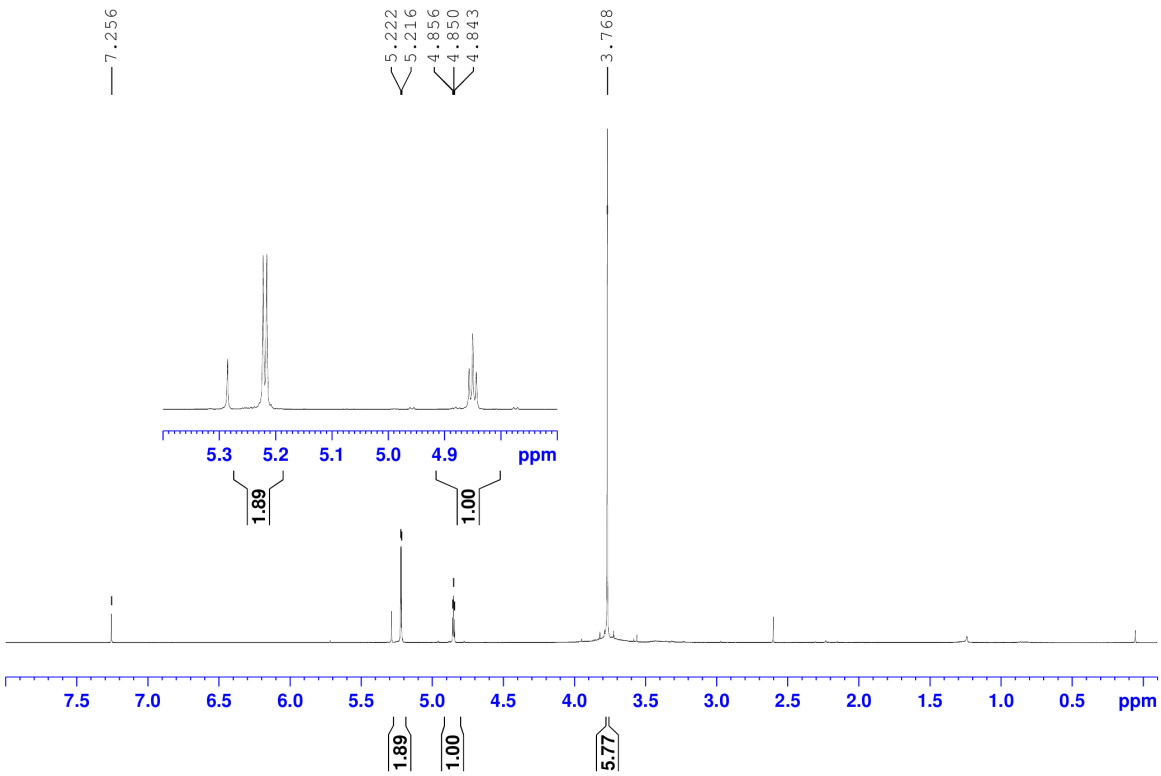

Figure 99. ^{1}H NMR of **49** in $CDCl_3$.

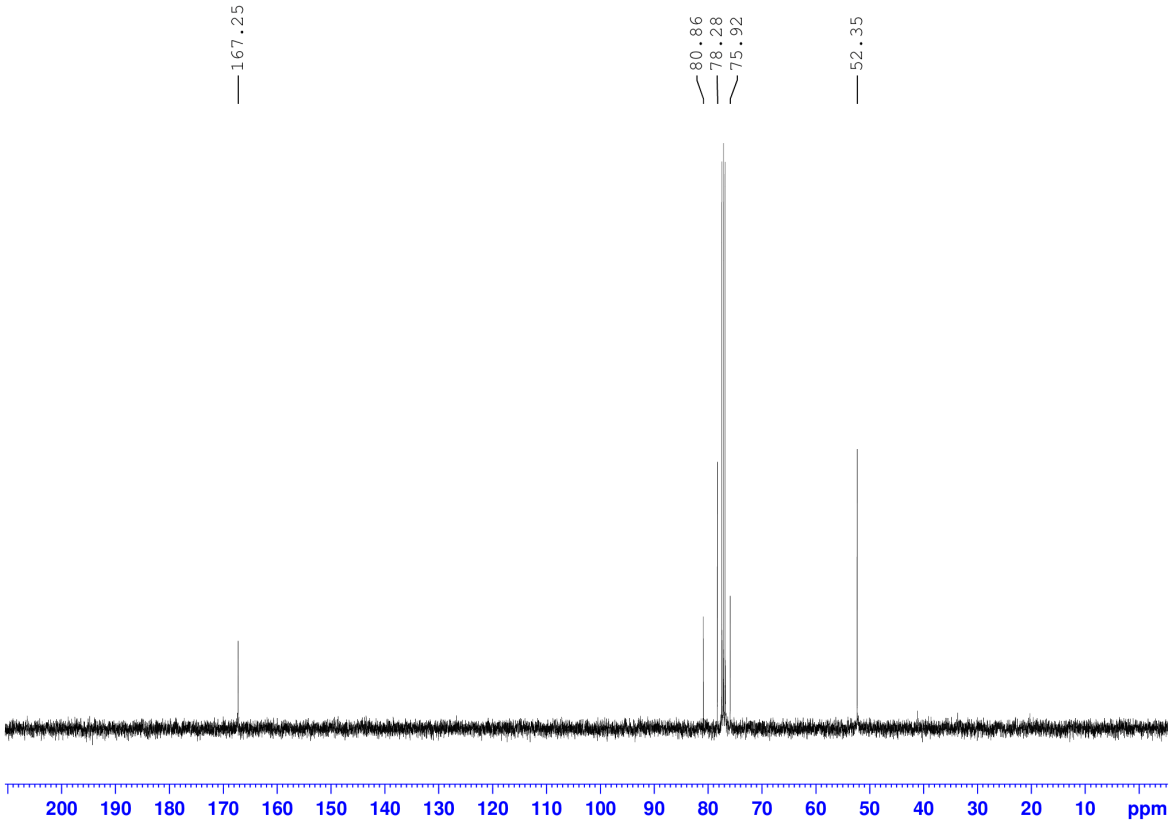

Figure 100. ^{13}C NMR of **49** in $CDCl_3$.

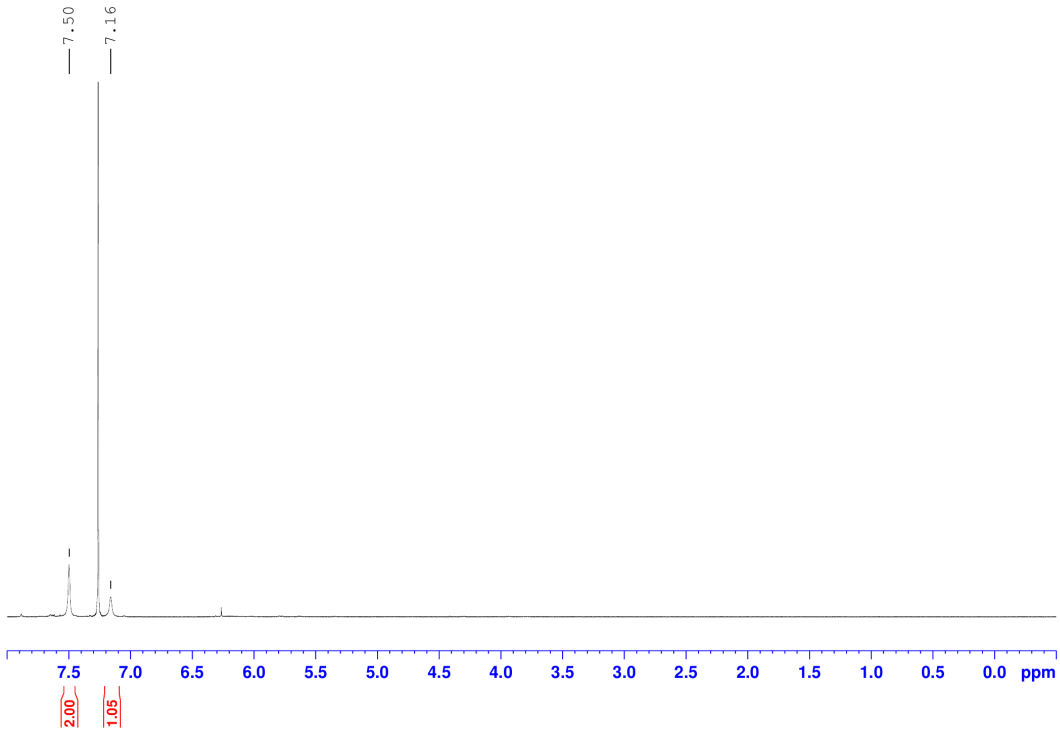

Figure 101. ^{1}H NMR of **50** in $CDCl_3$.

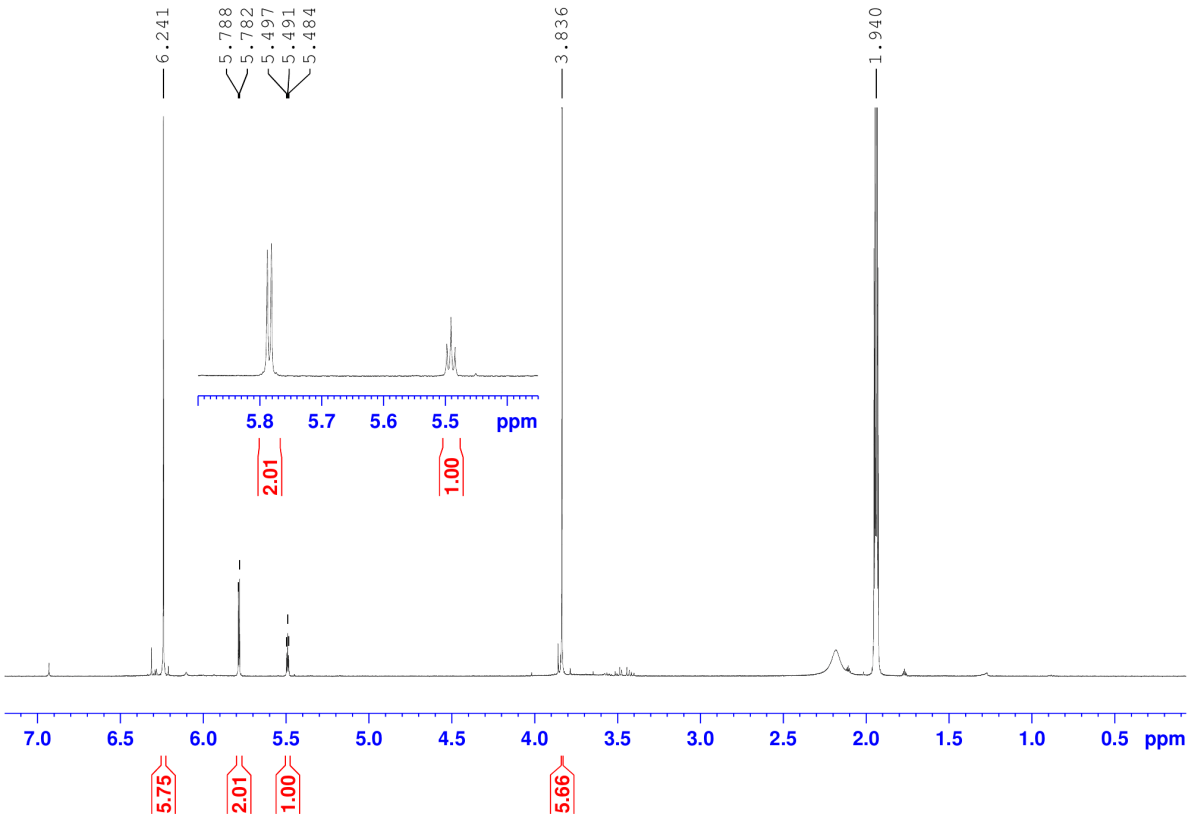

Figure 102. ^{1}H NMR of **45** in CD_3CN.

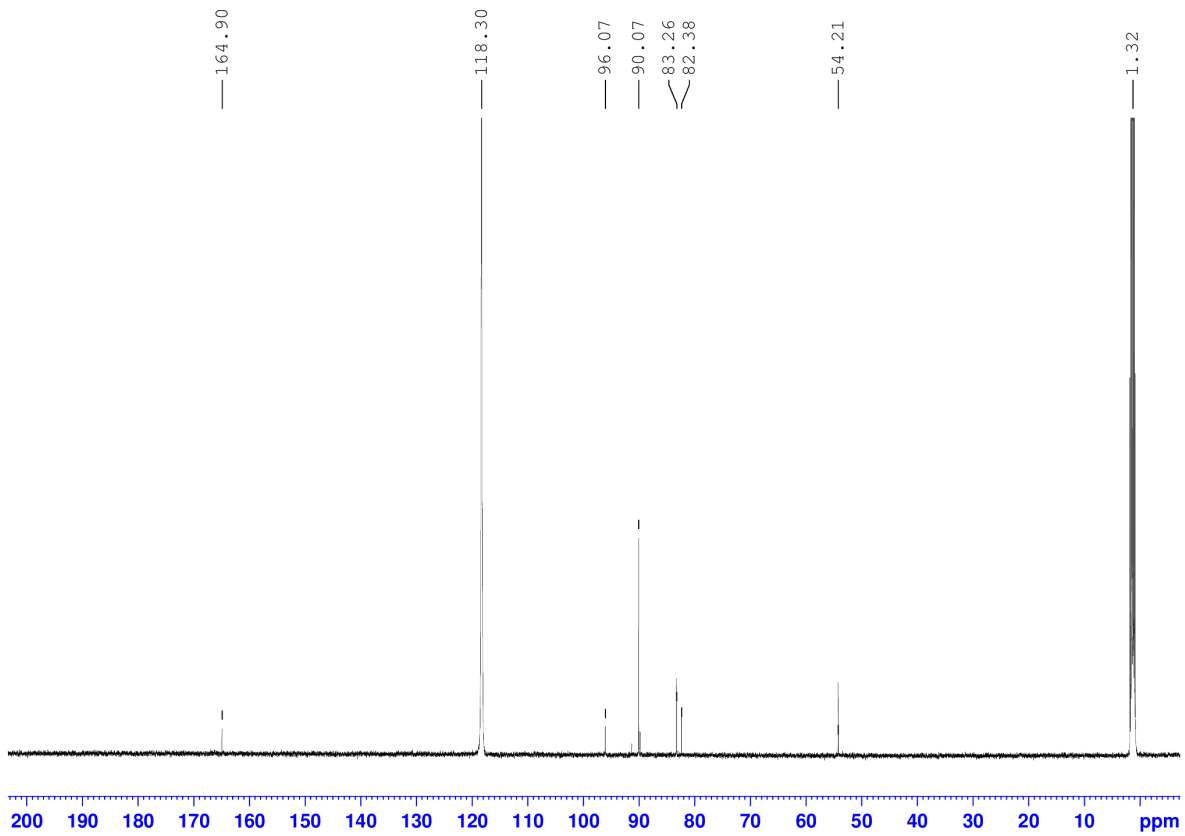

Figure 103. ^{13}C NMR of **45** in CD_3CN.

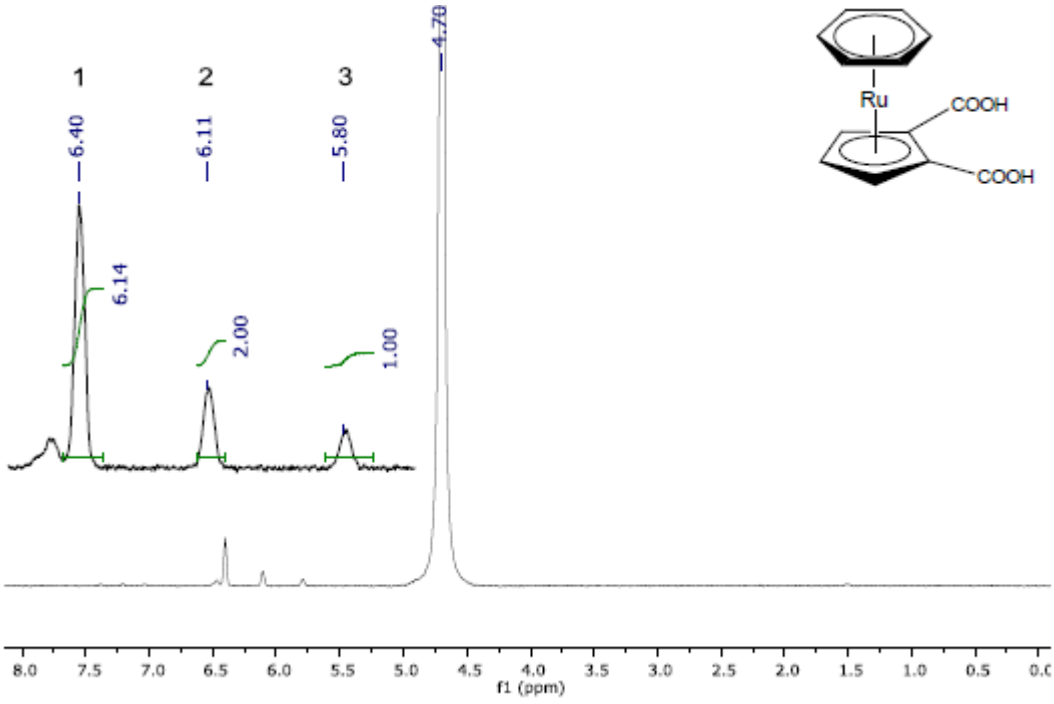

Figure 104. ^{1}H NMR of **46** in D_2O.

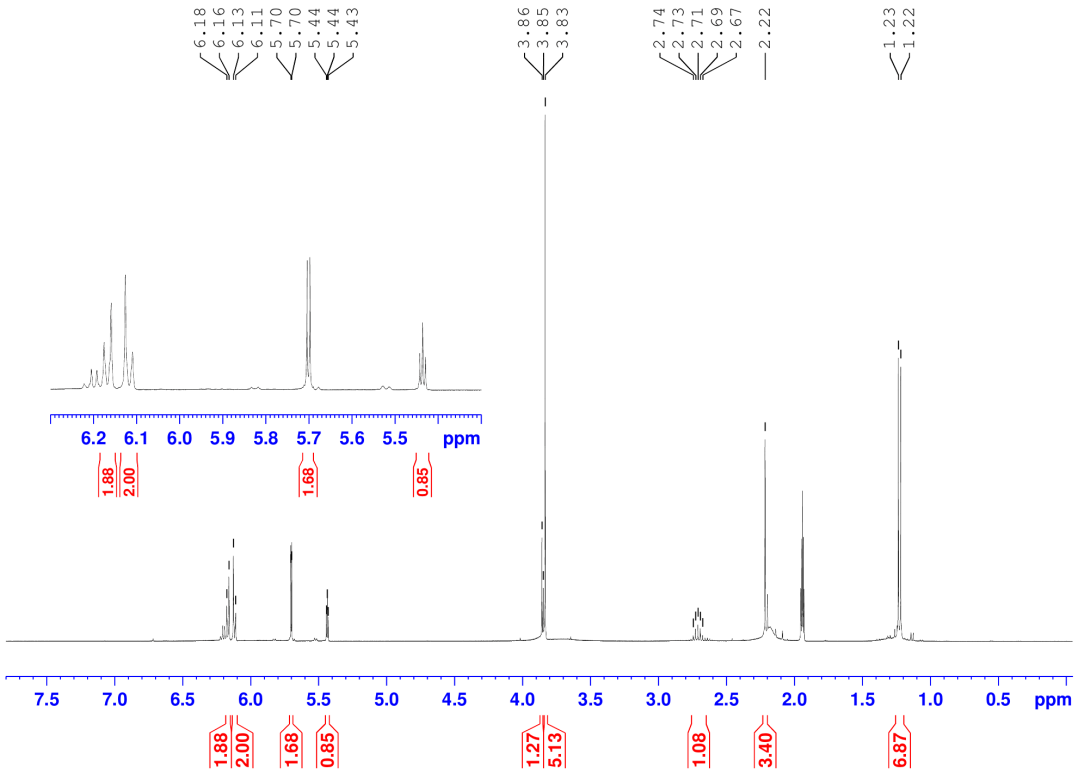

Figure 105. ^{1}H NMR of **48** in CD_3CN.

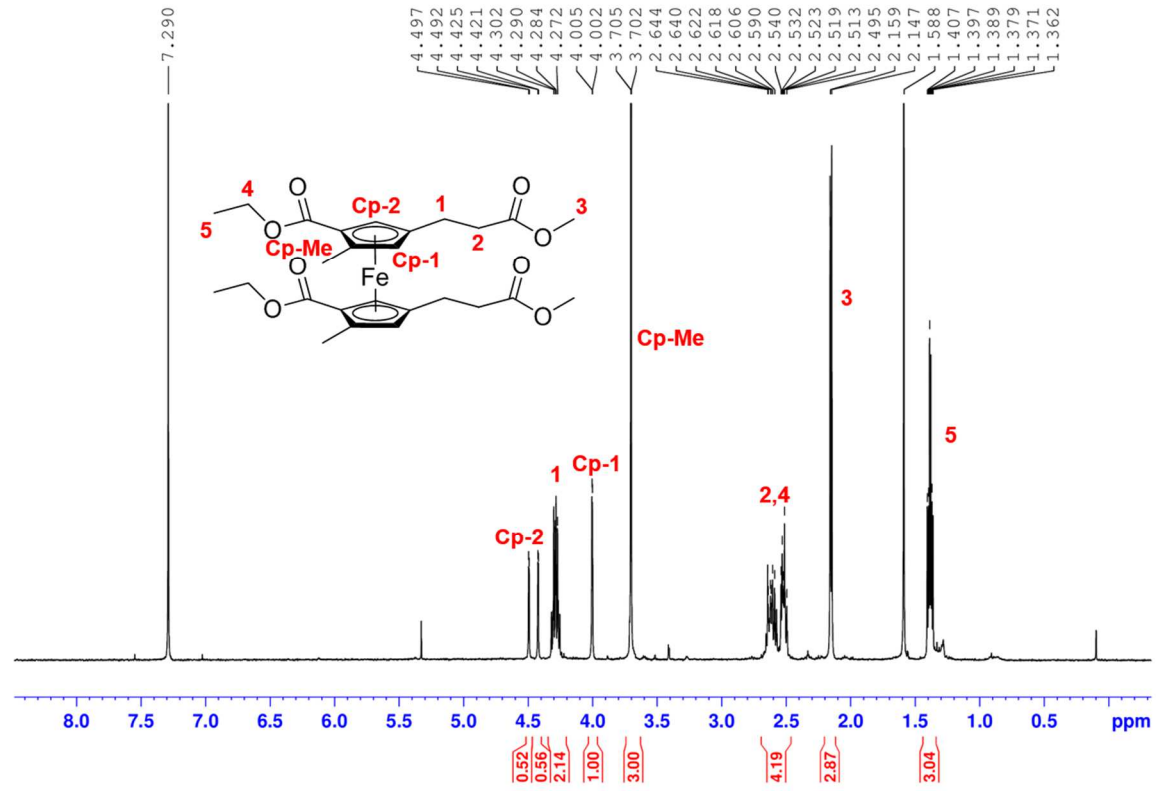

Figure 106.^{1}H NMR of **51** in $CDCl_3$ assigned proton signals.

Table 4. Crystal data and structure refinement for **45**.

Empirical formula	C_{15} H_{15} F_6 O_4 P Ru
Diffractometer	Xcalibur, Ruby
Wavelength [Å]	0.71073
Formula weight	505.31
Crystal system	Monoclinic
Space group	P 1 21/n 1
a [Å]	11.5596(5)
b [Å]	12.6616(5)
c [Å]	12.4950(6)
α [°]	90
β [°]	109.789(5)
γ [°]	90
Volume [$Å^3$]	1720.81(14)
Z	4
Density (calculated) [Mg/m^3]	1.950
Absorption coefficient [mm^{-1}]	1.086
F(000)	1000
Crystal size [mm^3]	0.23 x 0.14 x 0.06
Crystal description	colourless plate
Theta range for data collection [°]	2.469 to 32.907
Index ranges	-17<=h<=17, -19<=k<=17, -19<=l<=18
Reflections collected	17987
Independent reflections	5881 [R(int) = 0.0455]
Reflections observed	4653
Criterion for observation	I > 2(I)
Completeness to theta	99.9 % to 25.242°
Absorption correction	Semi-empirical from equivalents
Max. and min. transmission	1.00000 and 0.75543
Data / restraints / parameters	5881 / 0 / 246
Goodness-of-fit on F^2	1.048
Final R indices [I>2sigma(I)]	R1 = 0.0375, wR2 = 0.0802
R indices (all data)	R1 = 0.0546, wR2 = 0.0904
Extinction coefficient	n/a
Largest diff. peak and hole [$e.Å^{-3}$]	1.433 and -0.526

Table 5. Crystal data and structure refinement for **49**.

Empirical formula	C_{18} H_{18} O_8 Ru
Diffractometer	Xcalibur, Ruby
Wavelength [Å]	0.71073
Formula weight	463.39
Crystal system	Monoclinic
Space group	P 1 21/c 1
a [Å]	8.1481(5)
b [Å]	14.3423(6)
c [Å]	14.8462(9)
α [°]	90
β [°]	92.831(6)
γ [°]	90
Volume [$Å^3$]	1732.85(16)
Z	4
Density (calculated) [Mg/m^3]	1.776
Absorption coefficient [mm^{-1}]	0.951
F(000)	936
Crystal size [mm^3]	0.15 x 0.12 x 0.04
Crystal description	colourless plate
Theta range for data collection [°]	2.747 to 30.508
Index ranges	-10<=h<=11, -20<=k<=18, -21<=l<=20
Reflections collected	12171
Independent reflections	5291 [R(int) = 0.0536]
Reflections observed	3739
Criterion for observation	I > 2(I)
Completeness to theta	99.9 % to 25.242°
Absorption correction	Analytical
Max. and min. transmission	0.968 and 0.904
Data / restraints / parameters	5291 / 0 / 257
Goodness-of-fit on F^2	1.046
Final R indices [I>2sigma(I)]	R1 = 0.0507, wR2 = 0.0995
R indices (all data)	R1 = 0.0808, wR2 = 0.1164
Extinction coefficient	n/a
Largest diff. peak and hole [$e.Å^{-3}$]	1.958 and -1.224

Table 6. Crystal data and structure refinement for **51**.

Empirical formula	C_{26} H_{34} Fe O_8
Diffractometer	XtaLAB Synergy, Dualflex, Pilatus 200K
Wavelength [Å]	0.71073
Formula weight	530.38
Crystal system	Monoclinic
Space group	P 1 2/c 1
a [Å]	13.4268(3)
b [Å]	7.67030(10)
c [Å]	13.2464(3)
α [°]	90
β [°]	115.275(3)
γ [°]	90
Volume [$Å^3$]	1233.62(5)
Z	2
Density (calculated) [Mg/m^3]	1.428
Absorption coefficient [mm^{-1}]	0.660
F(000)	560
Crystal size [mm^3]	0.11 x 0.08 x 0.06
Crystal description	clear red cube
Theta range for data collection [°]	2.655 to 32.974
Index ranges	-19<=h<=20, -11<=k<=11, -19<=l<=19
Reflections collected	38307
Independent reflections	4274 [R(int) = 0.0287]
Reflections observed	3854
Criterion for observation	I > 2(I)
Completeness to theta	100.0 % to 25.242°
Absorption correction	Semi-empirical from equivalents
Max. and min. transmission	1.00000 and 0.94524
Data / restraints / parameters	4274 / 0 / 162
Goodness-of-fit on F^2	1.061
Final R indices [I>2sigma(I)]	R1 = 0.0260, wR2 = 0.0704
R indices (all data)	R1 = 0.0299, wR2 = 0.0720
Extinction coefficient	n/a
Largest diff. peak and hole [$e.Å^{-3}$]	0.477 and -0.231

5.3 Experimental Section Part C

Materials. All chemicals were of reagent-grade quality or higher. Solvents were used as received or dried over molecular sieves. Deuterated NMR solvents were obtained from ARMAR chemicals. Carbon-^{13}C monoxide (<5 atom % ^{18}O, 99 atom % ^{13}C) was obtained from Sigma Aldrich. 2,6-dimethylphenyl isocyanide (>98%) was obtained from Fluka.

Instrumentation and methods. ^{13}C-NMR spectra were recorded in deuterated solvents on a Bruker AV2 and DRX 500 (^{13}C: 125.8 MHz) MHz spectrometer at the specified temperatures and concentrations. The chemical shifts, δ, are reported in ppm (parts per million) relative to residual solvent peaks. IR spectra were obtained with a PerkinElmer Spectrum Two spectrometer. UV/Vis spectra were measured on a Varian Cary 50 Scan UV/Vis spectrophotometer. The temperature was regulated with a Peltier thermostatic system to the specified temperatures.

Synthesis of [NEt$_4$][ReBr$_2$(CO)$_4$] (2). [NEt$_4$]$_2$[ReBr$_3$(CO)$_3$] (100 mg g, 0.13 mmol) was dissolved in DMF (5 ml). The clear solution was bubbled with ~1 atm of CO gas through a canula for 6 h, resulting in a pale yellow crystals suitable for X-ray diffraction analysis. Dissolution of the crystals in d^8-THF and subsequent filtration yielded a solution of pure **2**. ^{13}C NMR (125.8 MHz, d^8-THF) δ 188.5, 187.1. IR bands (neat cm^{-1}): ν_{CO} = 2110, 1995, 1968, 1909.

Synthesis of [NEt$_4$][ReBr(CO)$_3$(Xyl-NC)] (4). [NEt$_4$]$_2$[ReBr$_3$(CO)$_3$] (65.0 mg, 0.084 mmol) was dissolved in d^7-DMF (0.250 ml) and added to a solution of 2,6-dimethylphenyl isocyanide (10.8 mg, 0.082 mmol) in d^7-DMF (0.450 ml) in an NMR tube. After one hour at room temperature, complete consumption of the free isocyanide was observed. Slow evaporation of the solution yielded single crystals of **4** suitable for X-ray diffraction analysis (^{13}C NMR and IR spectra of free 2,6-dimethylphenyl isocyanide and **4** are reported in the SI (Figure 119-120 and 127)). ^{13}C NMR (125.8 MHz, d^7-DMF) δ 191.1, 136.6, 130.5, 129.2,19.0. IR bands (neat cm^{-1}): ν_{CO} = 2008, 1925, 1882, ν_{CN} = 2171.

Synthesis of [ReBr(DMF)$_2$(CO)$_3$] (1c). ReBr(CO)$_5$ (30 mg, 0.074 mmol) was dissolved in d^7-DMF (1 ml) and heated to 130 °C for one day. ^{13}C NMR showed complete consumption of ReBr(CO)$_5$ and quantitative formation of **1c** (^{13}C NMR spectra of **1c** and ReBr(CO)$_5$ are reported above (Figure 17) and in the SI (Figure 128) respectively). ^{13}C NMR (125.8 MHz, d^7-DMF) δ 198.0, 193.1, 169.6 (*t*).

^{99}Tc experiments. Caution: ^{99}Tc is a weak β$^-$ emitter (E_{max} = 0.292 MeV, half-life time = 2.12 × 10^5 y. It should be handled only in appropriately equipped laboratories.

[^{99}TcCl$_3$(CO)$_3$]$^{2-}$. [NEt$_4$]$_2$[^{99}TcCl$_3$(CO)$_3$] (4.5 mg, 8.2 µmol) was dissolved in DMF (1 ml) and a ^{99}Tc NMR spectrum was recorded (Figure 113). Bubbling of this solution with ~1 atm of CO gas through a canula for 6 h resulted in no significant changes in the ^{99}Tc NMR.

[Tc(CO)$_3$(DMF)$_3$]$^+$. [NEt$_4$]$_2$[^{99}TcCl$_3$(CO)$_3$] (4.4 mg, 8.0 µmol) was dissolved in DMF (1 ml) and AgPF$_6$ (6.07 mg, 24.0 µmol) were added. Formation of a precipitate was observed immediately. The suspension was left standing for 24 h, filtered and a ^{99}Tc NMR spectrum was recorded (Figure 114). Bubbling of this solution with ~1 atm of CO gas through a canula for multiple hours resulted in no significant changes in the ^{99}Tc NMR.

[TcBr$_n$(CO)$_3$(DMF)$_{3-n}$]$^+$. [NEt$_4$]$_2$[^{99}TcCl$_3$(CO)$_3$] (5.3 mg, 9.6 µmol) was dissolved in DMF (1 ml) and AgPF$_6$ (6.07 mg, 24.0 µmol) were added. To this solution, three equivalents of NaBr (3.0 mg, 29.2 µmol) were added and a ^{99}Tc NMR spectrum was recorded (Figure 115). Bubbling of this solution with ~1 atm of CO gas through a canula for multiple hours resulted in no significant changes in the ^{99}Tc NMR.

Kinetic Studies.

Formation kinetics of [NEt$_4$][ReBr$_2$(CO)$_4$]. All the kinetic runs were performed under *pseudo* first-order conditions with the metal complex in excess. Depending on the concentration of **1b** required for the measurement, one of two experimental procedures was followed. For concentrations smaller than 75 mM, the respective quantity of **1a** was dissolved in a small volume of the respective deuterated solvent. An NMR tube containing (typically 0.5 ml) of deuterated solvent and 20 µl of *p*-Xylene was bubbled

steadily with ^{13}CO via a 20 ml syringe equipped with a needle long enough to reach the bottom of the NMR tube. Measurement of the ^{13}C-NMR spectrum of this solution allowed the determination of the ^{13}CO concentration in solution by comparison of the integral (and taking into account the relative abundance of ^{13}C) with both the solvent peak as well as the quaternary carbon peak of *p*-Xylene, which was used as a second internal standard. The NMR sample was then cooled down to the required temperature and the experiment started upon addition of **1b**. The number of scans per experiment was adjusted depending on the starting concentration and temperature to maintain a reasonable balance between time resolution and signal to noise ratio. NMR spectra were measured until the signal of free ^{13}CO disappeared. For the measurements at concentrations higher than 75 mM it was not possible to dissolve **1a** in a small enough volume so a different procedure was followed. Starting compound **1a** was dissolved in (typically 0.5 ml) the respective solvent together with 20 μl *p*-Xylene. The sample was locked and shimmed in the NMR spectrometer at the respective measuring temperature. The ^{13}CO was then added to the sample, which was cooled to 5-10 °C below the measurement temperature. After the addition was complete the sample was placed in the NMR machine and the measurement was started upon stabilization of the shim. The first experiment was used to estimate the initial ^{13}CO concentration analogously to the first method.

Treatment of NMR data. From the NMR measurements, two curves were obtained from each run by integrating the peaks of the free and coordinated ^{13}CO respectively. The data points were computer fitted via least square to a single exponential in Origin to obtain the respective observed pseudo first-order rate constant (k_{obs}). Both the plot for the determination of k_1 as well as the Eyring plots were linearly fitted in Origin.[52] Global fits of the kinetic data to evaluate the activation parameters using the exponential form of the Eyring equation were done as previously described.[55, 176]

^{13}CO exchange experiments. In a typical experiment, the appropriate amount of **1a** was weighed in and dissolved in (typically 0.5 ml) d^7-DMF together with 20 μl *p*-Xylene in a 5 mm diameter NMR tube. The solution was bubbled with ^{13}CO as described above and sealed with a Shigemi glass stopper to ensure minimal “out-diffusion” of CO. The sample was placed into the NMR at 300 K. The temperature was then raised to 310 K and the measurement started.

UV/vis Kinetics. All the kinetic runs were performed in DMF and under *pseudo* first-order conditions with the metal complex in excess. In a typical experiment an aliquot of a 100 mM stock solution of **1b** in DMF was added to 2.5 ml of DMF in a quartz cuvette ([**1b**] = 0.2 – 1.6 mM) at room temperature (25 ± 1 °C). A constant aliquot of an 8 mM stock solution of Xyl-NC was then added to this solution and spectra were recorded every 15 seconds until no more significant changes were observed in the UV/vis spectrum ([Xyl-NC] = 0.04 mM).

Kinetic Simulations. The experimental NMR data displayed in Figure 22 were fit by simulation to a single kinetic model (Scheme 2) using the computer program KinTek Explorer (KinTek Corp, Austin, Texas, USA).[178] This program simulates experimental results by using direct numerical integration of the rate equations for the full model.

X-ray Crystallography. Crystallographic data were collected at 183(2) K with Mo K_α radiation (λ = 0.71073 Å) that was graphite-monochromated on an Oxford Diffraction CCD Xcalibur system with a Ruby detector. Suitable crystals were covered with oil (Infineum V8512, formerly known as Paratone N), placed on a nylon loop that is mounted in a CrystalCap Magnetic™ (Hampton Research) and immediately transferred to the diffractometer. The program suite CrysAlis^{Pro} was used for data collection, multi-scan absorption correction and data reduction.[62] The structures were solved with direct methods using SIR97[225] and were refined by full-matrix least-squares methods on F^2 with SHELXL-97.[226] All four ethyl groups of the disordered tetraethylammonium cation in compound **4** were located on two positions each (ratio 85:15). Due to the disorder, all carbon atoms of the minor component were refined isotropically. (CCDC numbers 1484435 and 1484436)

DFT Calculations. DFT calculations on the level of generalized gradient approximation are carried out with Perdew-Burke-Ernzerhof exchange and correlation functional.[227] All calculations are performed using the mixed Gaussian- and Plane Wave algorithm implemented in the CP2K software.[176] The core electrons are approximated on the basis of GTH pseudopotentials.[228-230] For elements C, O, H, and N only the valence electrons are treated explicitly. For Re the outermost 15 electrons are treated explicitly. The electron density is expanded in a double zeta basis set.[231]

Plane waves are cut off at 350 Ry. All calculations are done in singlet state and in vacuum.

First, the structures are optimized. From the optimized structure, the minimum energy path for the rotation of the $(CO)_3$ unit is found using the climbing image nudged elastic band method (CI-NEB).[232] The path is represented by 8 structures for $[Re(CO)_3Br_2(DMF)]^-$ and by 5 structures for $[Re(CO)_4Br_2]^-$, respectively.

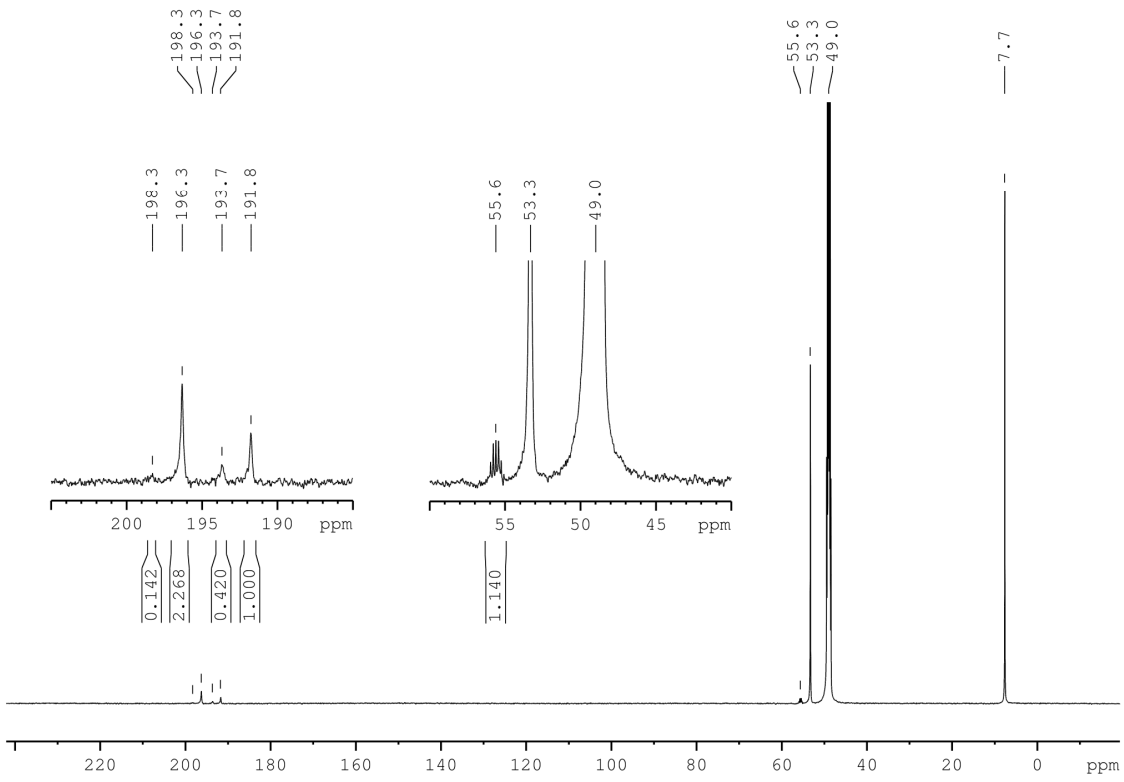

Figure 107. ^{13}C NMR of $[NEt_4]_2[ReBr_3(CO)_3]$ in MeOD (300 K).

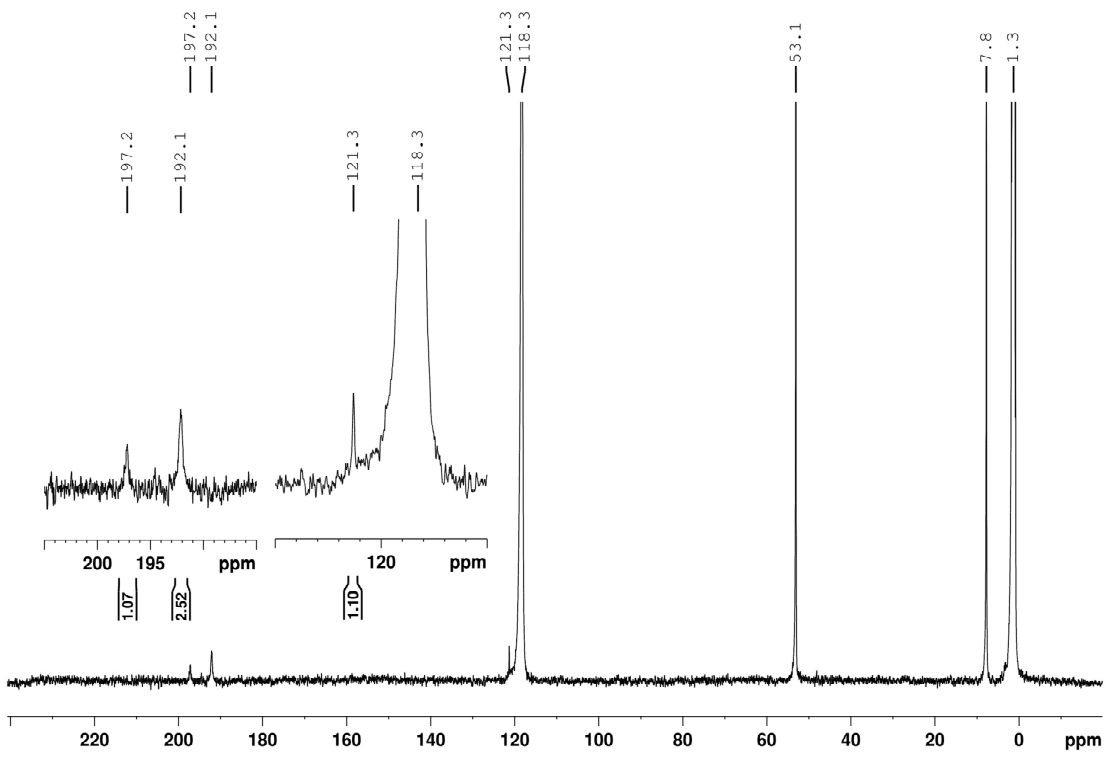

Figure 108. ^{13}C NMR of $[NEt_4]_2[ReBr_3(CO)_3]$ in CD_3CN (300 K).

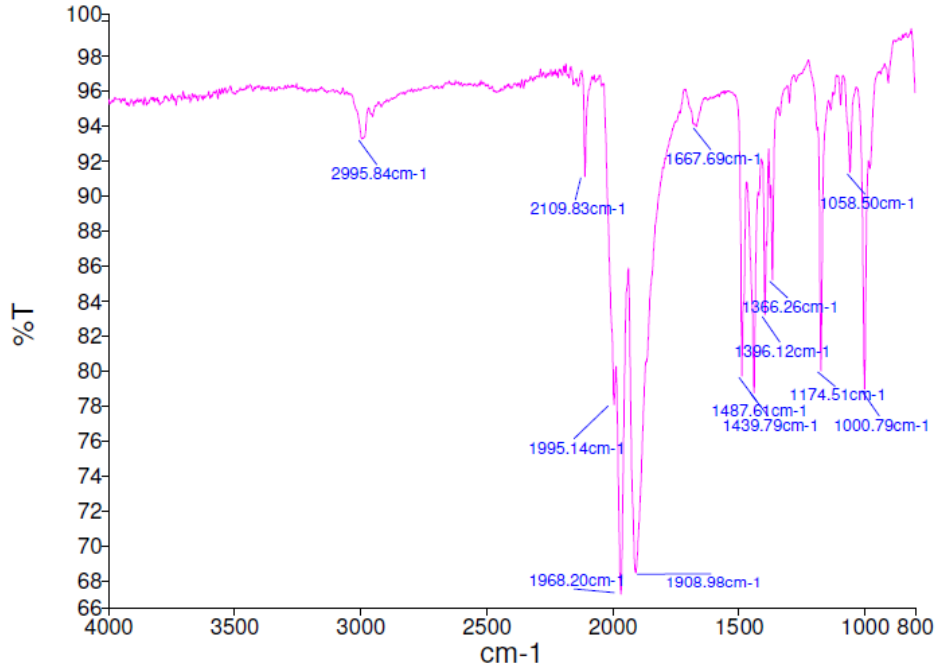

Figure 109. IR spectrum of **2** (neat).

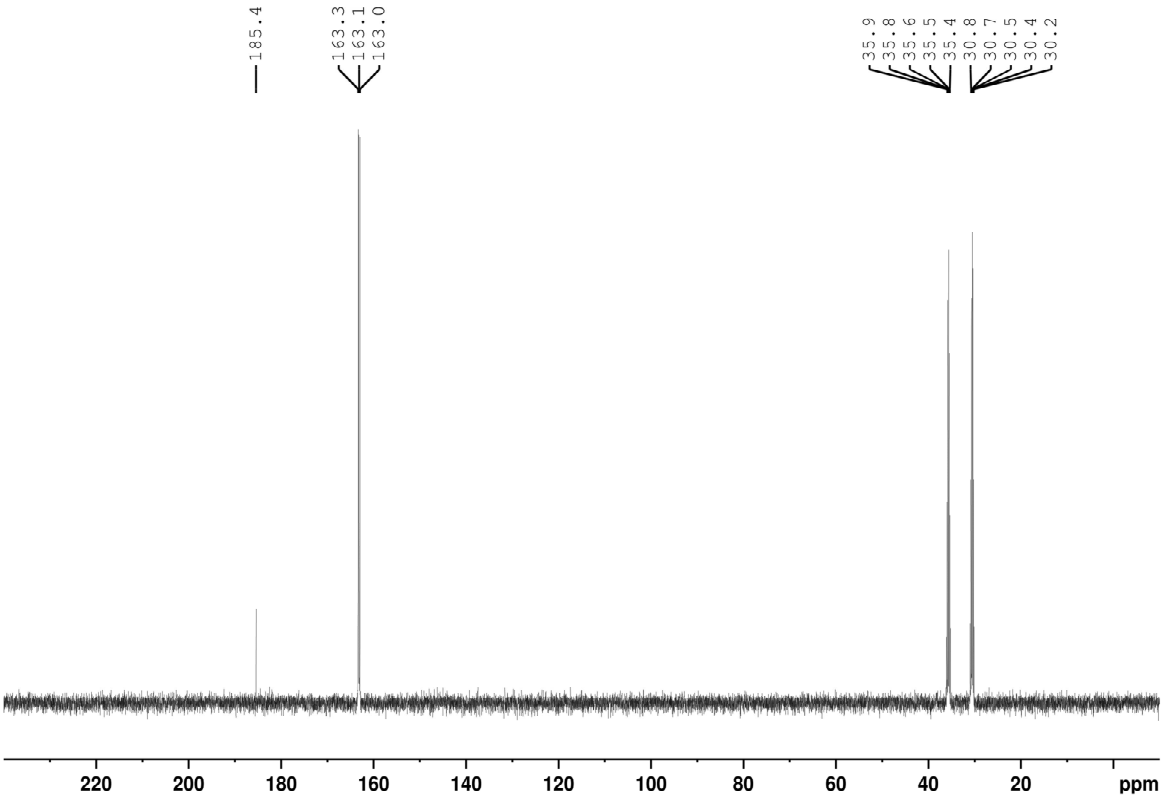

Figure 110. ^{13}C NMR of ^{13}CO in d^7-DMF (300 K).

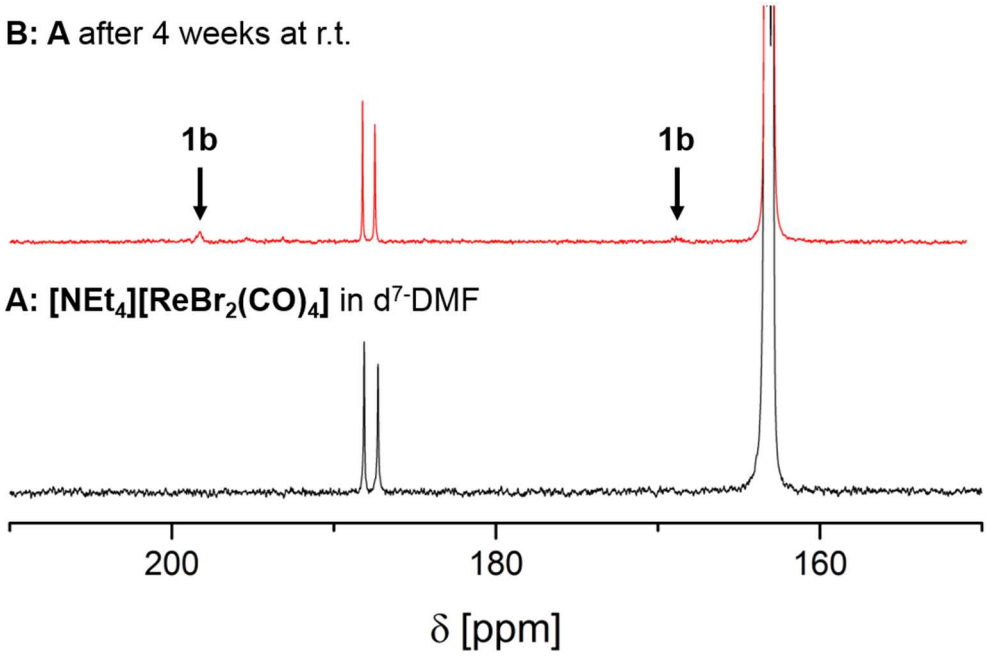

Figure 111. ^{13}C NMR of $[NEt_4][ReBr_2(CO)_4]$ (**2**) in d^7-DMF (70 mM, 300 K).

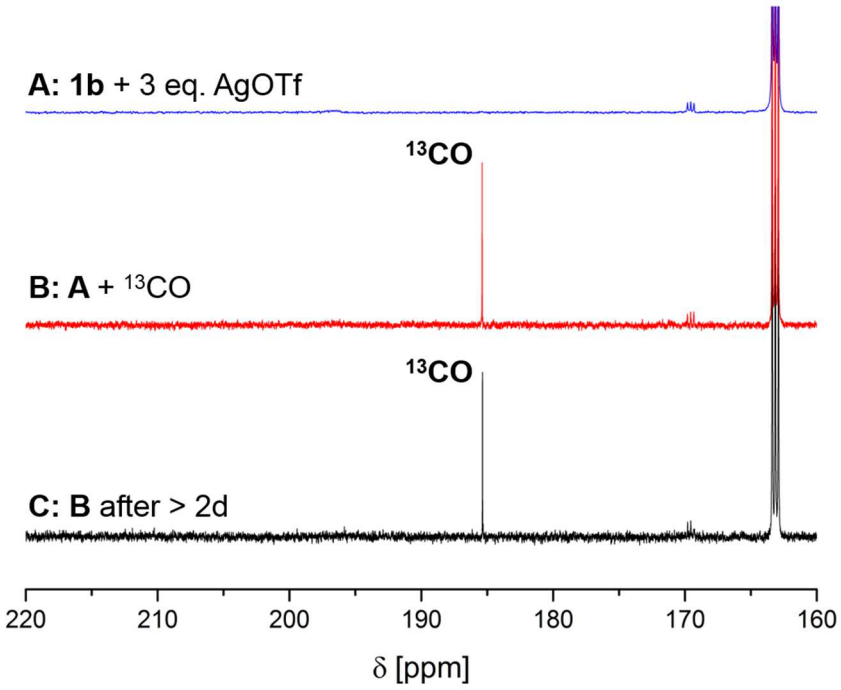

Figure 112. A: ^{13}C NMR of **1b** (22.19 mg, 0.029 mmol) and silver trifluoromethane-sulfonate (22.17 mg, 0.086 mmol) in d^{7}-DMF (0.6 ml, 300 K). **B**: ^{13}C NMR of **A** bubbled with ^{13}CO (2x ~20 ml) at 274 K. **C**: ^{13}C NMR of **B** after >2d (and heating to 300 K after 6 h).

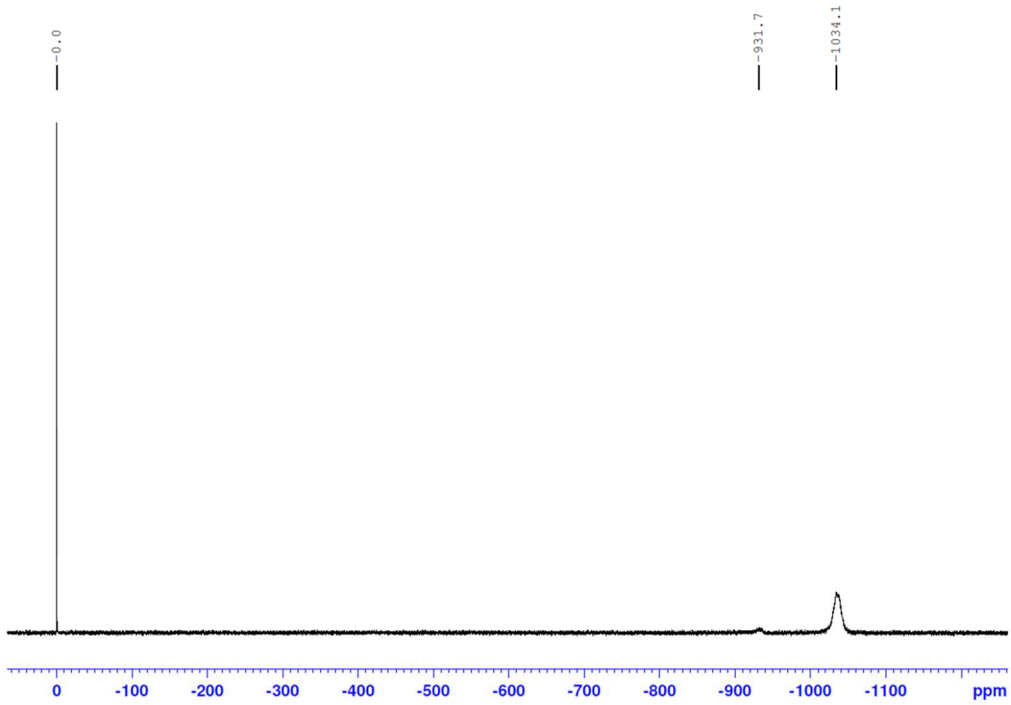

Figure 113. ^{99}Tc NMR of $[^{99}TcCl_3(CO)_3]^{2-}$ in DMF (8.2 mM, 300 K).

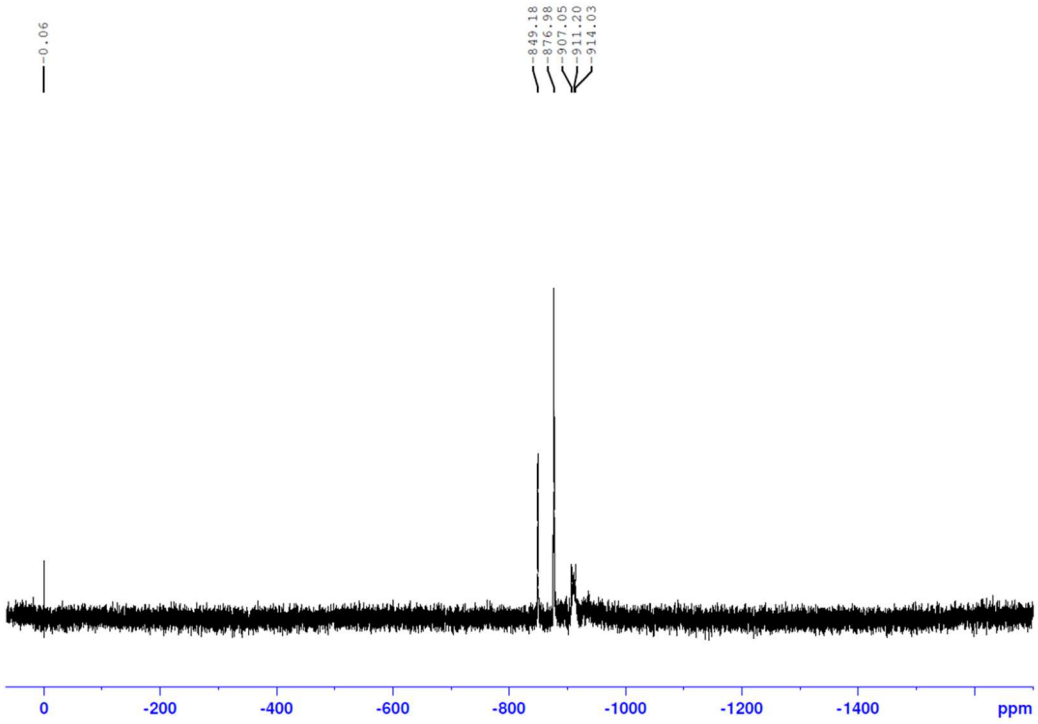

Figure 114. ^{99}Tc NMR of $[^{99}Tc(CO)_3(DMF)_3]^+$ in DMF (8.0 mM, 300 K).

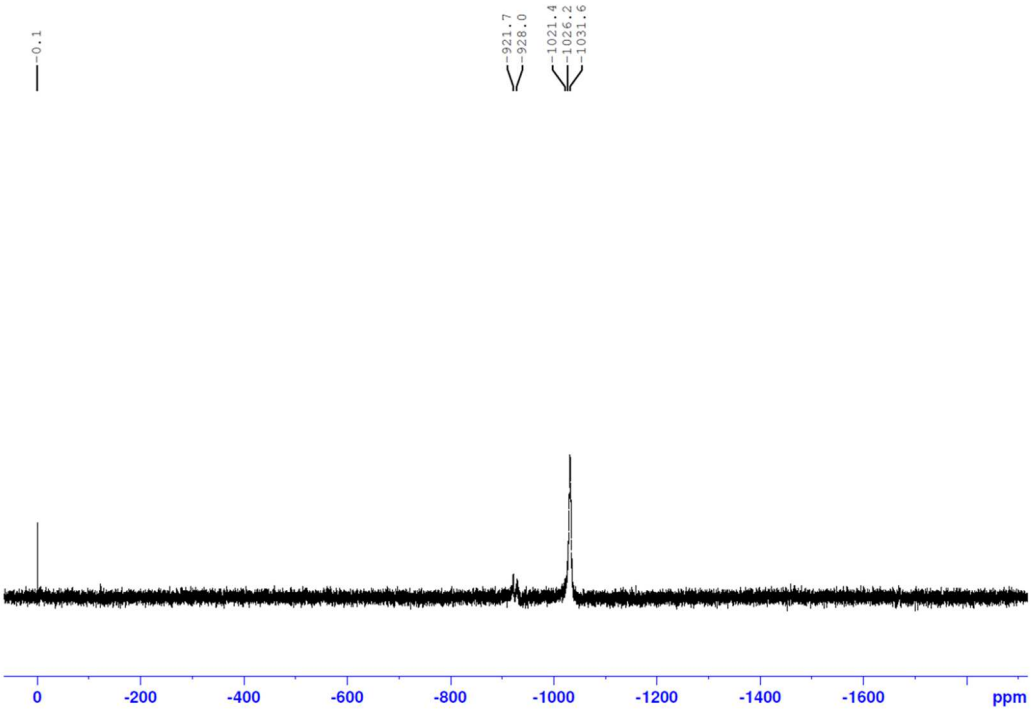

Figure 115. ^{99}Tc NMR of $[^{99}TcBr_n(CO)_3(DMF)_{3-n}]$ in DMF (9.6 mM, 300 K).

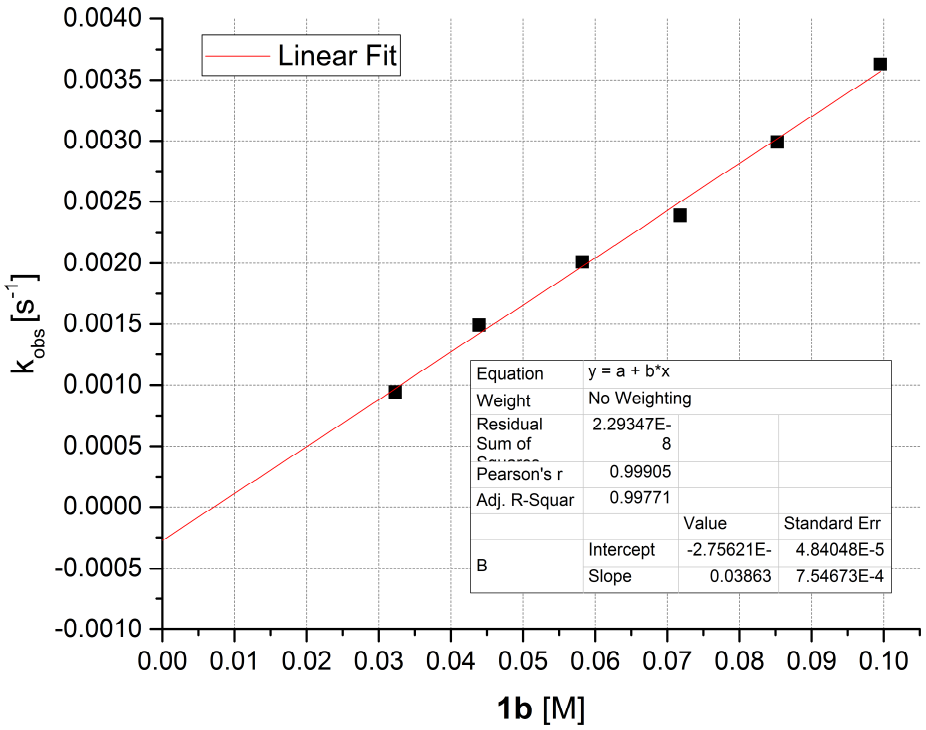

Figure 116. The observed rate constants (k_{obs}) for the formation of **2** as a function of the concentration of **1b** in d^7-DMF at 274 K.

Table 7. Observed rate constants (k_{obs}) for the formation of **2** at different concentrations of **1b** in d^7-DMF at 274 K ([^{13}CO] = 5 ± 1 mM).

1b [mM]	k_{obs} [s^{-1}]
32.3	0.00094
43.9	0.00149
58.2	0.00201
71.8	0.00239
85.2	0.00299
99.6	0.00363

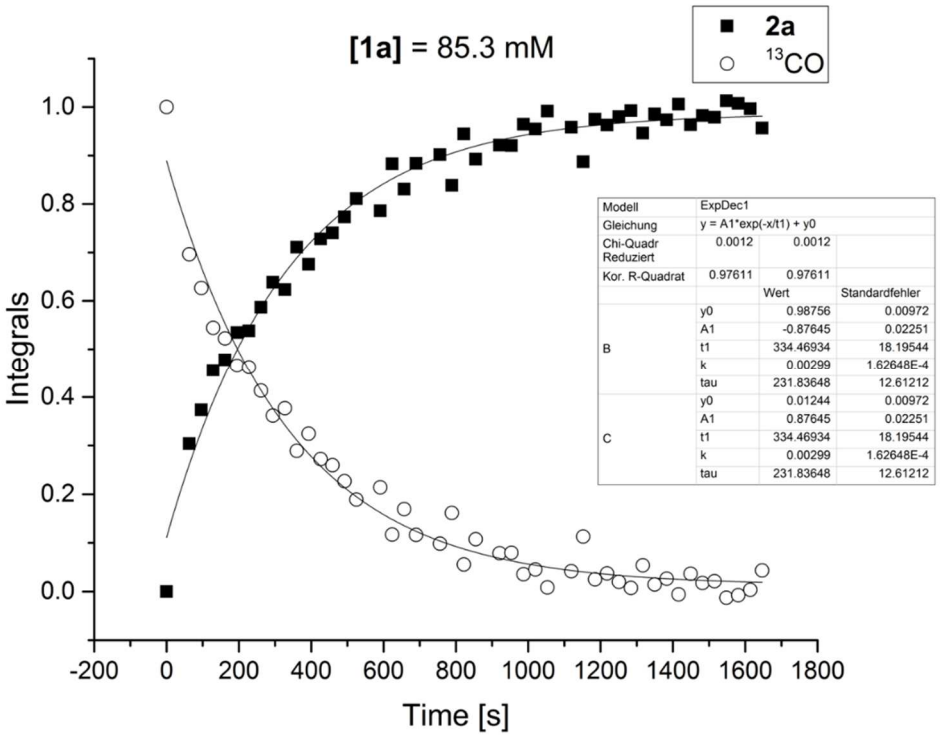

Figure 117. Example of a typical kinetic trace for **1a** (85.3 mM, 187.9 ppm) + ^{13}CO (5 mM, 185.4 ppm) in d^7-DMF at 274 K.

Table 8. Observed rate constants (k_{obs}) for the formation of **2** at different temperatures ([**1b**] = 48 mM, [^{13}CO] = 5 ± 1 mM).

T [K]	k_{obs} [s^{-1}]
253	0.000020
258	0.000071
263	0.000147
268	0.000325
274	0.001430

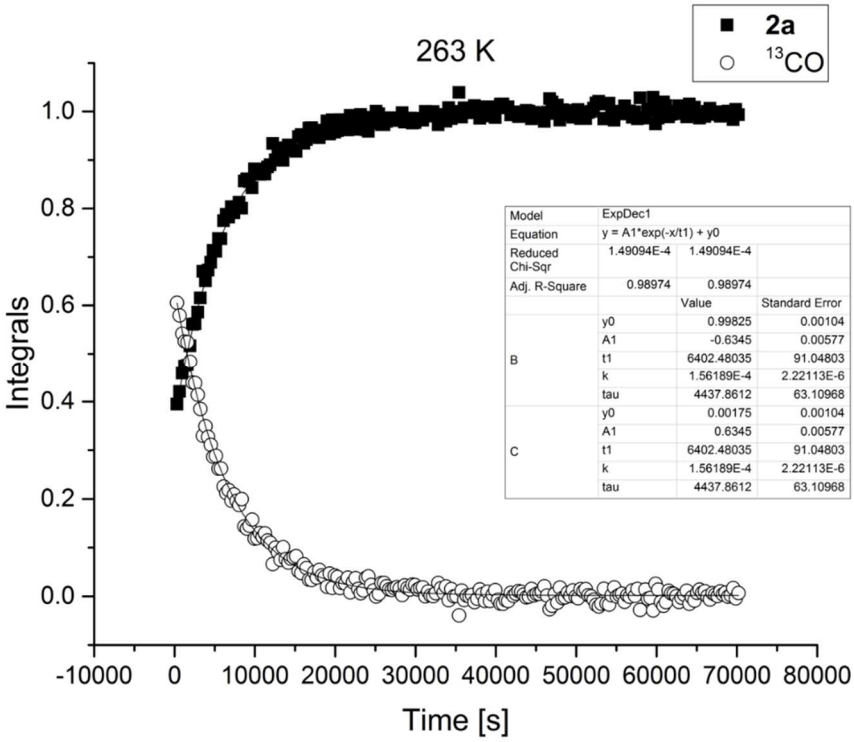

Model	ExpDec1		
Equation	y = A1*exp(-x/t1) + y0		
Reduced Chi-Sqr	1.49094E-4	1.49094E-4	
Adj. R-Square	0.98974	0.98974	
		Value	Standard Error
B	y0	0.99825	0.00104
	A1	-0.6345	0.00577
	t1	6402.48035	91.04803
	k	1.56189E-4	2.22113E-6
	tau	4437.8612	63.10968
C	y0	0.00175	0.00104
	A1	0.6345	0.00577
	t1	6402.48035	91.04803
	k	1.56189E-4	2.22113E-6
	tau	4437.8612	63.10968

Figure 118. Example of a typical kinetic trace for **1a** (48.0 mM) + ^{13}CO (6 mM) in DMF-d7 at 263 K.

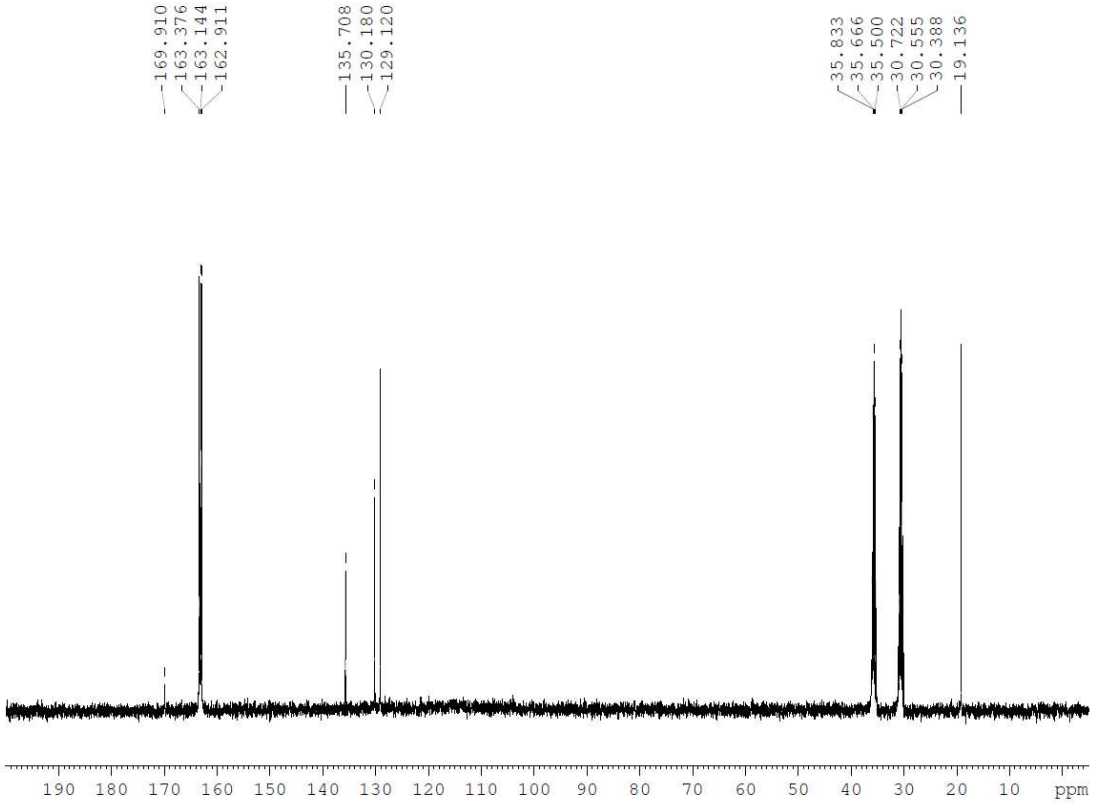

Figure 119. ^{13}C NMR of 2,6-dimethylphenyl isocyanide in d^{7}-DMF (300 K).

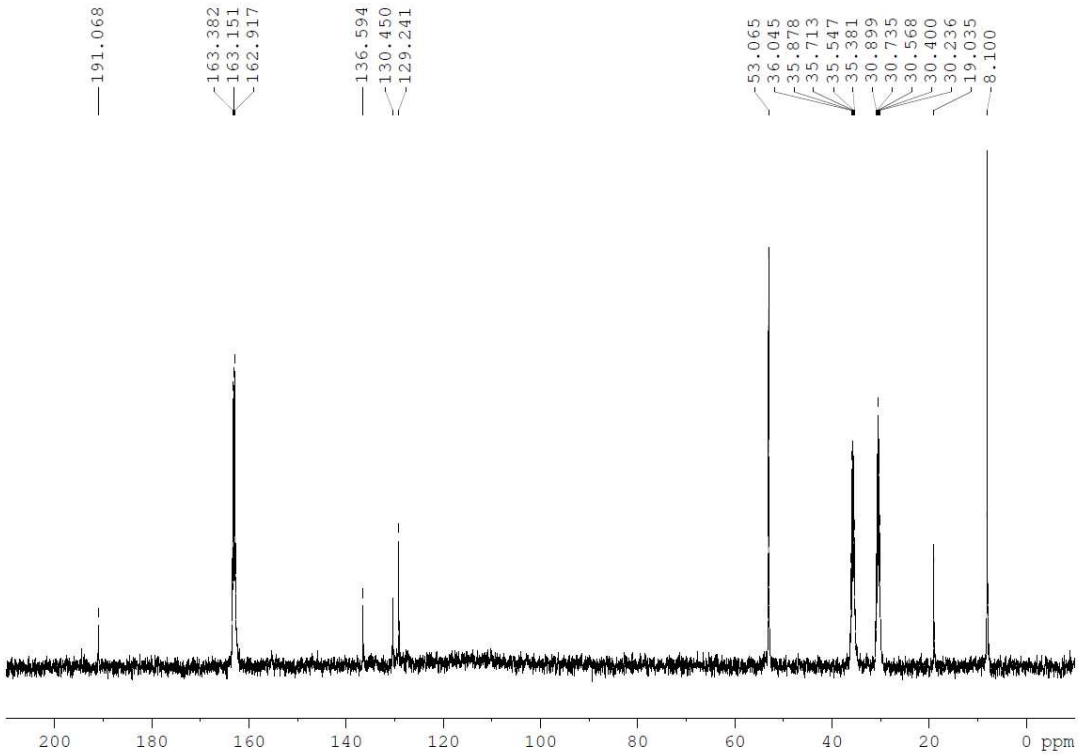

Figure 120. ^{13}C NMR of **4** in d^7-DMF (300 K).

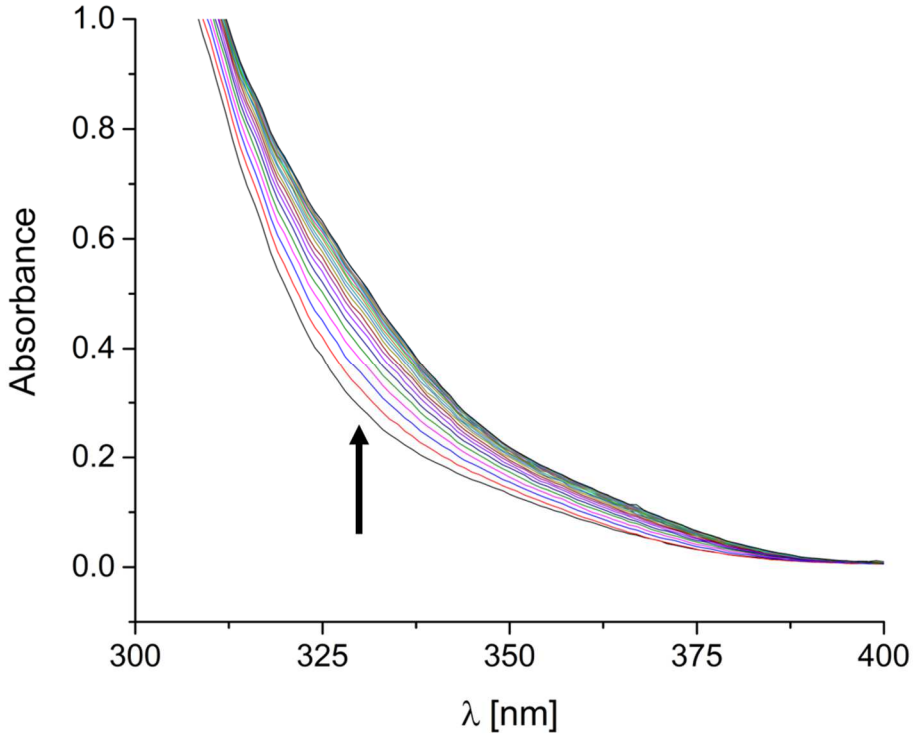

Figure 121. Selected UV/vis spectra recorded during a typical measurement of the reaction of **1b** (0.4 mM) with 2,6-dimethylphenyl isocyanide (0.04 mM) at 304 K.

Table 9. Observed rate constants (k_{obs}) for the formation of **4** at different concentrations of **1b** in d^7-DMF at 298 K ([Xyl-NC] = 0.04 mM).

1b [mM]	k_{obs} [s^{-1}]
0.2	0.000155
0.4	0.000333
0.8	0.000580
1.2	0.000899

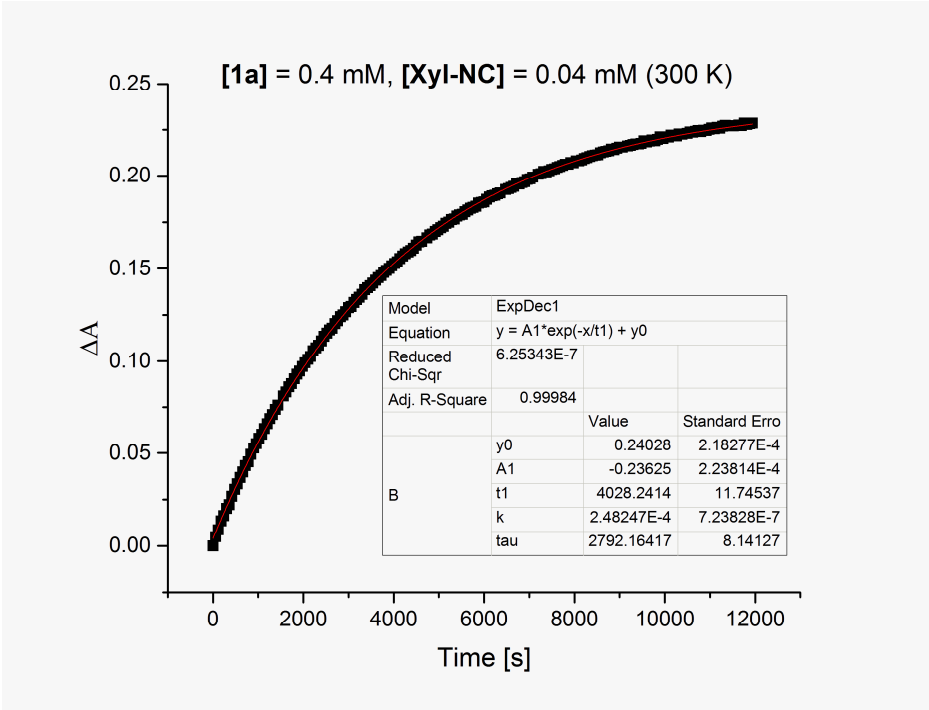

Figure 122. Example for the change in UV/Vis absorption at 326 nm for **1a** (0.4 mM) + 2,6-dimethylphenyl isocyanide (Xyl-NC, 0.04 mM) in 2.5 ml DMF at 300 K.

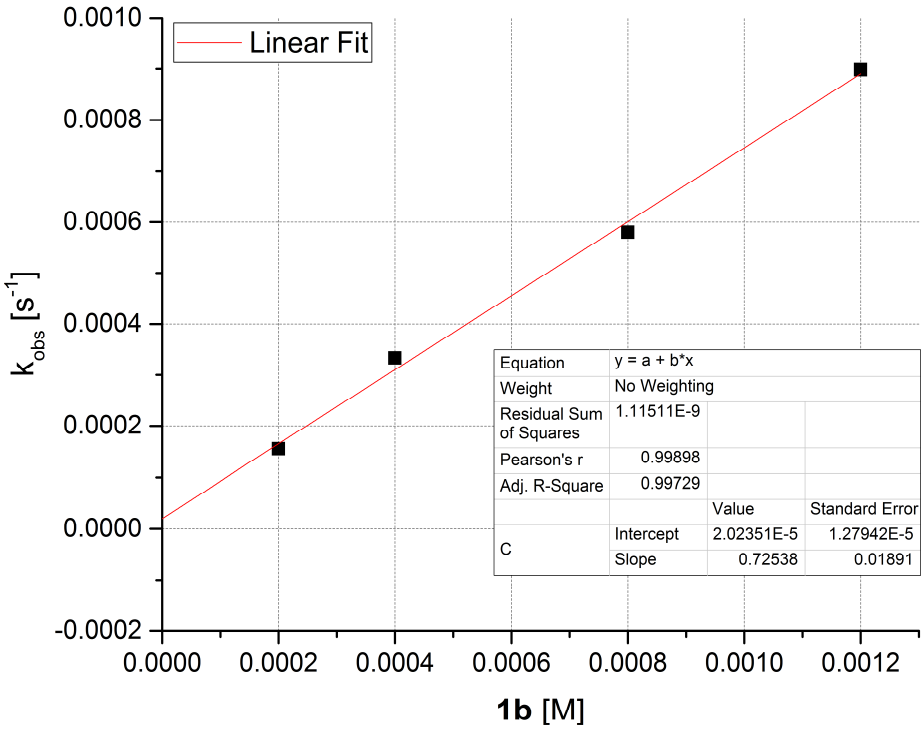

Figure 123. The observed rate constants (k_{obs}) for the formation of **4** as a function of the concentration of **1b** in d^7-DMF at 298 K.

Table 10. Observed rate constants (k_{obs}) for the formation of **4** at different temperatures ([**1b**] = 0.4 mM, [Xyl-NC] = 0.04 mM).

T [K]	k_{obs} [s^{-1}]
300	0.00025
304	0.00052
308	0.00091
315	0.00237
319	0.00336

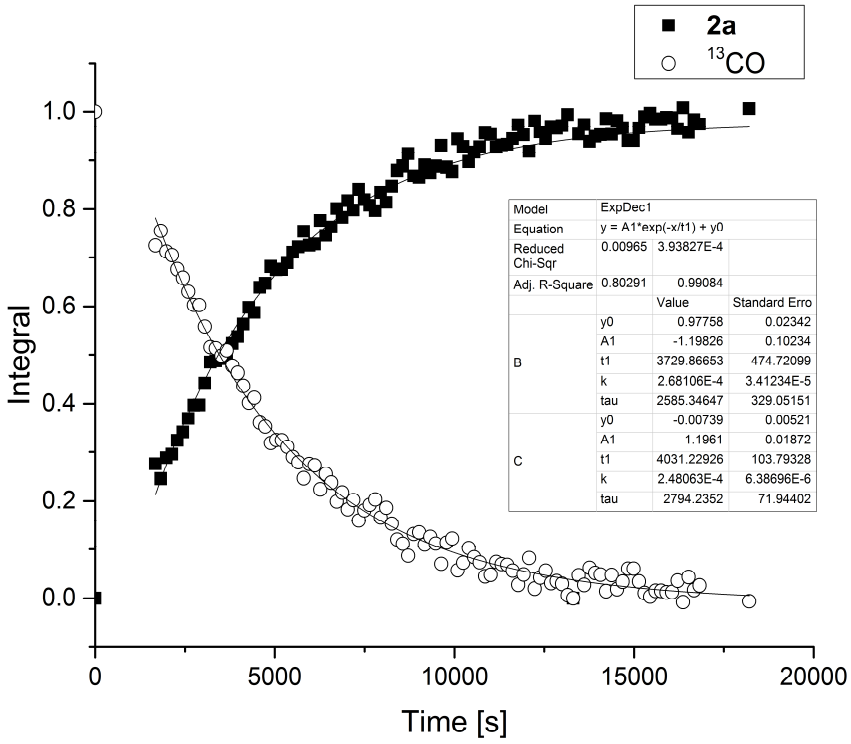

Model	ExpDec1		
Equation	y = A1*exp(-x/t1) + y0		
Reduced Chi-Sqr	0.00965	3.93827E-4	
Adj. R-Square	0.80291	0.99084	
		Value	Standard Erro
B	y0	0.97758	0.02342
	A1	-1.19826	0.10234
	t1	3729.86653	474.72099
	k	2.68106E-4	3.41234E-5
	tau	2585.34647	329.05151
C	y0	-0.00739	0.00521
	A1	1.1961	0.01872
	t1	4031.22926	103.79328
	k	2.48063E-4	6.38696E-6
	tau	2794.2352	71.94402

Figure 124. Kinetic trace for **1a** (48.0 mM, 187.6 ppm) + ^{13}CO (4 mM, 185.1 ppm) in d^3-ACCN at 274 K.

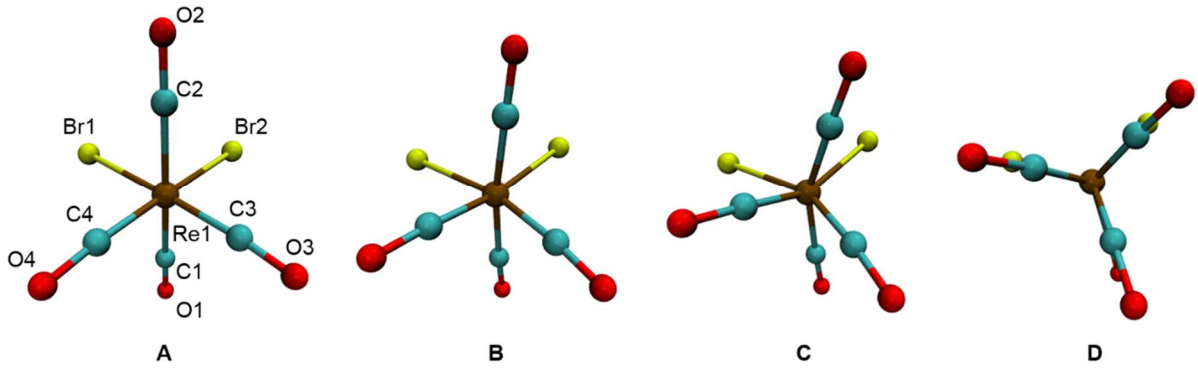

Figure 125. The first four out of eight optimized structures from the NEB calculations performed to obtain the minimum energy path for the rotation in **2**.

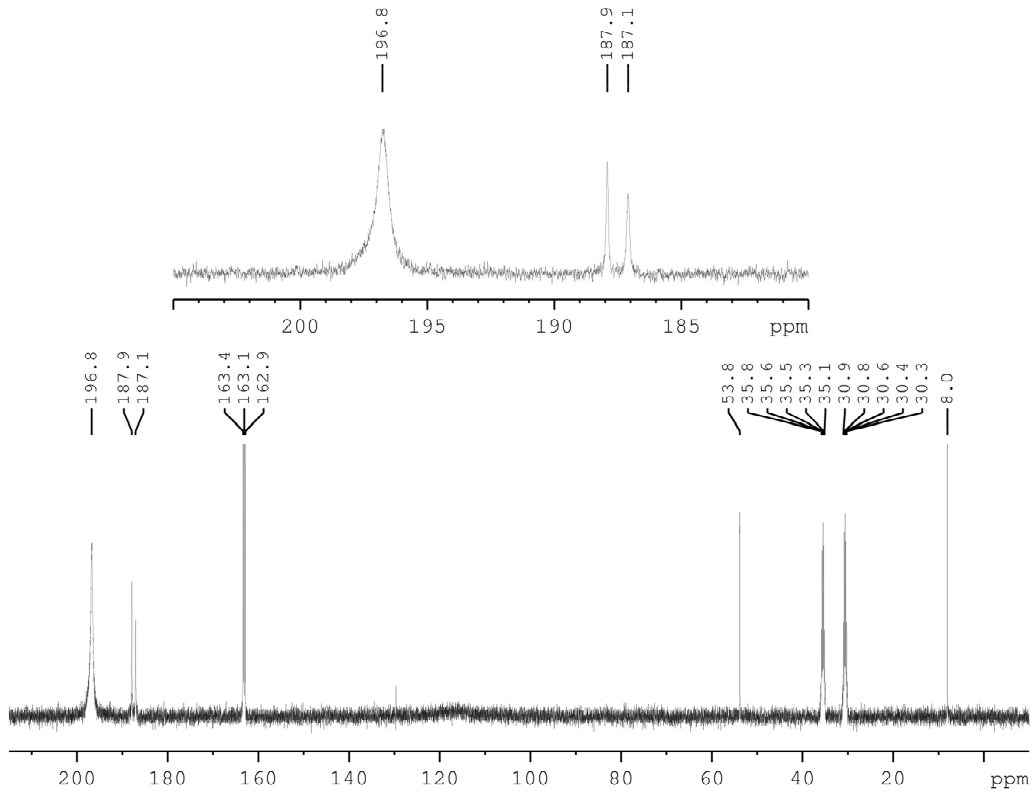

Figure 126. ^{13}C NMR spectrum of ^{13}CO enriched **1b** and **2** at 383 K (DMF-d^7, 100 mM).

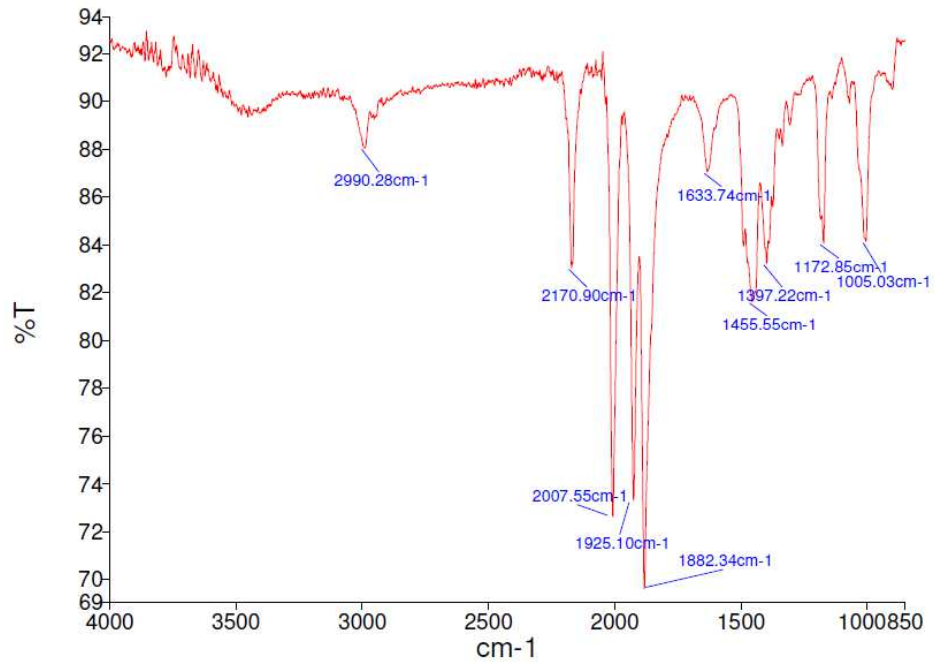

Figure 127. IR spectrum of **4** (neat).

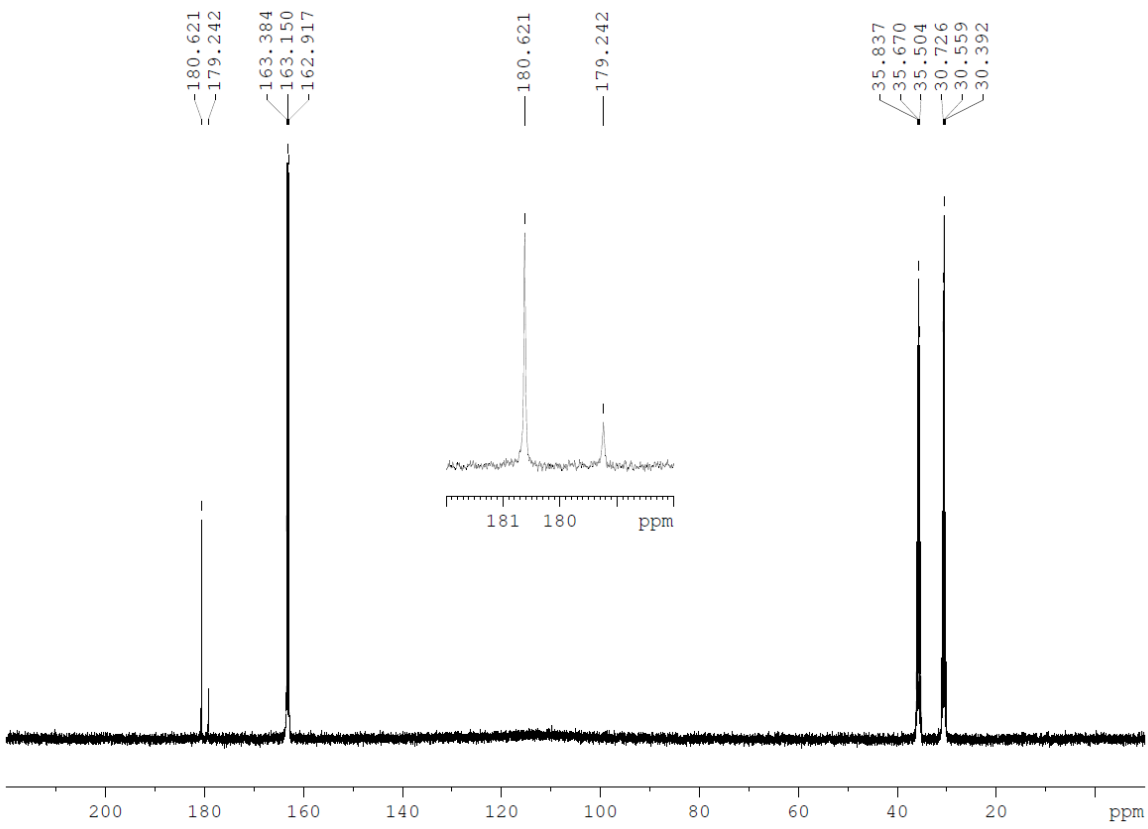

Figure 128. ^{13}C NMR of $ReBr(CO)_5$ in d^{7}-DMF (75 mM, 300 K).

Table 11. Crystal data and structure refinement for **2**.

Empirical formula	C_{12} H_{20} Br_2 N O_4 Re
Diffractometer	Xcalibur Ruby
Wavelength [Å]	0.71073
Formula weight	588.31
Crystal system	Monoclinic
Space group	$P2_1/c$
a [Å]	7.3143(3)
b [Å]	20.0387(6)
c [Å]	12.5146(4)
α [°]	90
β [°]	103.754(4)
γ [°]	90
Volume [Å^3]	1781.65(11)
Z	4
Density (calculated) [Mg/m^3]	2.193
Absorption coefficient [mm^{-1}]	11.315
F(000)	1104
Crystal size [mm^3]	0.460 x 0.140 x 0.090
Crystal description	colourless plate
Theta range for data collection [°]	2.634 to 32.810
Index ranges	-11<=h<=10, -30<=k<=30, -18<=l<=17
Reflections collected	18938
Independent reflections	6074 [R(int) = 0.0482]
Reflections observed	5270
Criterion for observation	I > 2(I)
Completeness to theta	99.9 % to 25.242°
Absorption correction	Analytical
Max. and min. transmission	0.481 and 0.049
Data / restraints / parameters	6074 / 0 / 185
Goodness-of-fit on F^2	1.048
Final R indices [I>2sigma(I)]	R1 = 0.0286, wR2 = 0.0626
R indices (all data)	R1 = 0.0353, wR2 = 0.0656
Extinction coefficient	n/a
Largest diff. peak and hole [e.Å^{-3}]	1.244 and -1.627

Table 12. Selected bond lenths (Å) and bond angles (°) for **2**.

Re(1)-C(4)	1.900(3)	C(4)-Re(1)-C(3)	90.89(13)
Re(1)-C(3)	1.914(4)	C(4)-Re(1)-C(2)	90.33(13)
Re(1)-C(2)	1.983(3)	C(3)-Re(1)-C(2)	94.53(14)
Re(1)-C(1)	2.011(3)	C(4)-Re(1)-C(1)	92.47(13)
Re(1)-Br(1)	2.6200(4)	C(3)-Re(1)-C(1)	93.90(14)
Re(1)-Br(2)	2.6395(3)	C(2)-Re(1)-C(1)	171.08(13)
C(1)-O(1)	1.125(4)	C(4)-Re(1)-Br(1)	92.89(10)
C(2)-O(2)	1.131(4)	C(3)-Re(1)-Br(1)	175.96(9)
C(3)-O(3)	1.148(4)	C(2)-Re(1)-Br(1)	86.89(9)
C(4)-O(4)	1.150(3)	C(1)-Re(1)-Br(1)	84.52(9)
C(5)-C(6)	1.508(5)	C(4)-Re(1)-Br(2)	178.12(10)
		C(3)-Re(1)-Br(2)	87.33(9)
		C(2)-Re(1)-Br(2)	89.20(8)
		C(1)-Re(1)-Br(2)	88.27(9)
		Br(1)-Re(1)-Br(2)	88.906(10)

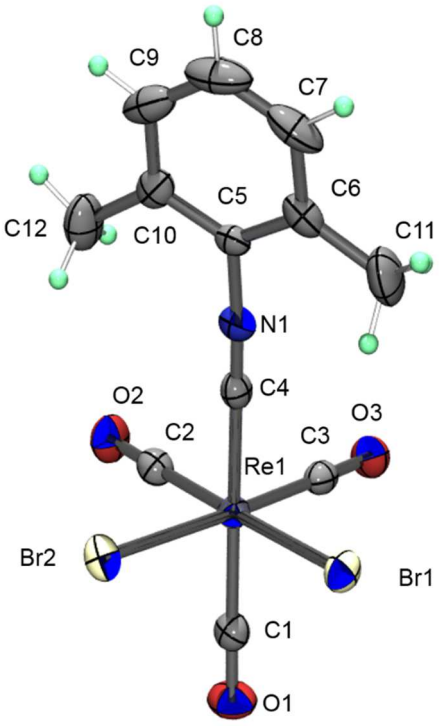

Figure 129. Crystal structure of $[NEt_4][ReBr_2(CO)_3(Xyl\text{-}NC)]$ **4** ($[NEt_4]^+$ cation omitted for clarity). Ellipsoides are drawn on the 50 % probability level.

Table 13. Crystal data and structure refinement for **4**.

Empirical formula	$C_{20}H_{29}Br_2N_2O_3Re$
Diffractometer	Xcalibur Ruby
Wavelength [Å]	0.71073
Formula weight	691.47
Crystal system	Monoclinic
Space group	$P2_1/c$
a [Å]	18.0878(8)
b [Å]	8.7429(3)
c [Å]	16.4010(7)
α [°]	90
β [°]	110.971(5)
γ [°]	90
Volume [$Å^3$]	2421.84(18)
Z	4
Density (calculated) [Mg/m^3]	1.896
Absorption coefficient [mm^{-1}]	8.338
F(000)	1328
Crystal size [mm^3]	0.400 x 0.180 x 0.170
Crystal description	colourless prism
Theta range for data collection [°]	2.497 to 32.891
Index ranges	-26<=h<=27, -13<=k<=13, -22<=l<=24
Reflections collected	24578
Independent reflections	8212 [R(int) = 0.0401]
Reflections observed	6495
Criterion for observation	I > 2(I)
Completeness to theta	99.9 % to 25.242°
Absorption correction	Analytical
Max. and min. transmission	0.372 and 0.119
Data / restraints / parameters	8212 / 16 / 292
Goodness-of-fit on F^2	1.041
Final R indices [I>2sigma(I)]	R1 = 0.0334, wR2 = 0.0616
R indices (all data)	R1 = 0.0498, wR2 = 0.0676
Extinction coefficient	n/a
Largest diff. peak and hole [$e.Å^{-3}$]	1.167 and -2.173

Table 14. Selected bond lenths (Å) and bond angles (°) for **4**.

Re(1)-C(2)	1.899(4)
Re(1)-C(3)	1.903(3)
Re(1)-C(1)	1.962(3)
Re(1)-C(4)	2.071(3)
Re(1)-Br(2)	2.6451(3)
Re(1)-Br(1)	2.6466(4)
C(4)-N(1)	1.145(4)
C(2)-Re(1)-C(3)	89.48(14)
C(2)-Re(1)-C(1)	92.97(14)
C(3)-Re(1)-C(1)	90.51(13)
C(2)-Re(1)-C(4)	92.00(13)
C(3)-Re(1)-C(4)	93.42(12)
C(1)-Re(1)-C(4)	173.69(13)
C(2)-Re(1)-Br(2)	88.42(9)
C(3)-Re(1)-Br(2)	177.77(10)
C(1)-Re(1)-Br(2)	90.37(9)
C(4)-Re(1)-Br(2)	85.89(8)
C(2)-Re(1)-Br(1)	175.63(9)
C(3)-Re(1)-Br(1)	93.29(10)
C(1)-Re(1)-Br(1)	90.38(10)
C(4)-Re(1)-Br(1)	84.47(8)
Br(2)-Re(1)-Br(1)	88.758(11)

DFT Calculations

Calculation of $\Delta G^{\ddagger}$ from Normal modes.

The energy correction H_{vib} and the entropy correction S_{vib} to the DFT energy are arising from the normal modes. They are calculated by

$$H_{vib} = \sum_{i=1}^{3N-6} \frac{1}{2} N_A h\nu_i + \frac{N_A h\nu_i e^{\frac{h\nu_i}{kT}}}{1 - e^{\frac{h\nu_i}{kT}}}$$

$$S_{vib} = -\sum_{i=1}^{3N-6} R \ln\left(1 - e^{\frac{h\nu_i}{kT}}\right) + \frac{N_A h\nu_i}{T} \frac{e^{\frac{h\nu_i}{kT}}}{1 - e^{\frac{h\nu_i}{kT}}}$$

where N is the number of atoms in the molecule, R is the gas constant, $N_A$is Avogadros number, h is plancks constant, k is Boltzmann constant, T is temperature, and ν_i is the frequency of the i'th normal mode.[61] Gibbs free energy for one state is then obtained by

$$G = U^{DFT} + H_{vib} - T\,S_{vib}.$$

[ReBr$_2$(DMF)(CO)$_3$]$^-$

In the ground state structure, the ligands adopt an octahedral geometry to Re(I). The calculated binding distance from Re to DMF is 2.22 Å, which is in good agreement with the experimental binding distance found for [Re(DMF)$_3$(CO)$_3$]$^-$ (2.2 Å).[233]

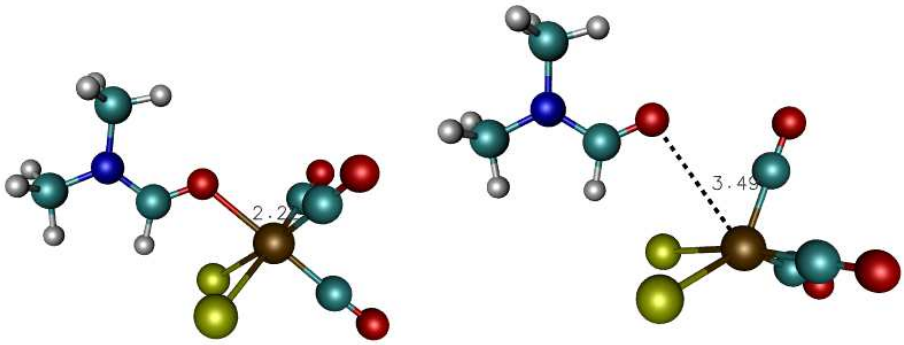

Figure 130. Left: Optimized structure of the octahedral complex **1b**. The Re-O binding distance is 2.22 Å. Right: Transition state structure of complex **1b**. The DMF is formally dissociated from the complex and the remaining $[Re(CO)_3(Br)_2]^-$ unit is between a trigonal bipyramidal and square pyramidal configuration, leaving space for another DMF (or CO) molecule to coordinate from below.

The energy of the transition state converges only very slowly, which is due to the concurrent dissociation of DMF during the rotation of the (CO)$_3$ unit. Vibrational analysis of the transition state (TS) structures gives only one negative frequency, which confirms that it is indeed a TS of this rotation. However, vibrational analysis needs the structures to be tightly converged. Otherwise, low frequency modes are not calculated

correctly. Therefore, $\Delta H^{\ddagger}$ and $\Delta S^{\ddagger}$ calculated from these frequencies are limited in their accuracy.

$[ReBr_2(CO)_4]^-$

The calculated Re-Ligand binding distances match well with the X-ray crystal structure (Table 12, vide supra)

	Crystal structure	PBE
C1	1.98	1.98
C2	2.01	1.98
C3	1.90	1.90
C4	1.91	1.90
Br1	2.64	2.67
Br2	2.62	2.67

Table 15. Binding distances of the ligands to the Re atom in $[ReBr_2(CO)_4]^-$, obtained from the DFT calculations, and X-ray crystal structure.

In this case, the transition state converges more easily and the values for $\Delta H^{\ddagger}$ and $\Delta S^{\ddagger}$ are of higher accuracy.

5.4 Experimental Section Part D

Instrumentation information and crystallographic details are given in the ESI. The Schiff bases[216, 234, 235] as well as the precursor complexes $[NEt_4]_2[ReBr_3(CO)_3]$, $[NEt_4]_2[^{99}TcCl_3(CO)_3]$, $[^{99m}Tc(OH_2)_3(CO)_3]^+$ and the trinuclear cluster **3** were prepared as described elsewhere.[166] ***Caution***! ^{99}Tc is a weak β^- emitter with a half-life of 200 ky and should be handled in specially equipped laboratories only.

Preparation of tetranuclear $^{99m}TcRe_3$ cluster 4 from 3 (path A): The pH of an aqueous $[^{99m}Tc(CO)_3(H_2O)_3]^+$-solution (0.9 ml) was adjusted to 5 with HCl and an acetate buffer (0.2M, 0.2ml). This-solution (0.5ml) was transferred to a N_2-purged microwave vial containing **3** (3.0 mg, 2.97 □mol) and heated in a microwave for 10 min at 100°C. HPLC analysis evidences 94% yield of **4**. HPLC: R_t=21.2 min.

Preparation of tetranuclear $^{99m}TcRe_3$ cluster 4 from 1 (path B): The pH of an aqueous solution of $[^{99m}Tc(CO)_3(H_2O)_3]^+$-solution (0.5ml) was adjusted to 5 as described before and transferred to a N_2-purged microwave vial containing $[NEt_4]_2[ReBr_3(CO)_3]$ (3.1mg, 4.02 □mol). Stirring at 20°C for 10 min and subsequent heating at 100°C in a microwave oven for 10 min afforded **4** in 90 % yield according to HPLC analysis.

Syntheses of 6-8 (indicated for Hsal-m-tol): $[NEt_4]_2[^{99}TcCl_3(CO)_3]$ (25mg, 0.05mmol) was dissolved in acetonitrile (3ml). Hsal-m-tol (16mg, 0.07mmol) in acetonitrile (2 ml) was added to the solution. An excess of NEt_3 (0.1 ml) was added. After stirring at 80 °C for 3 h, HPLC analysis (UV/vis and radiodetector) evidenced the quantitative formation of **6.** The solution was filtered and the solvent removed under vacuum. The $[Et_4N]Cl$ was removed by extraction of the product with THF. The yellow product **6** was crystallised from a CH_2Cl_2 solution. The product was further purified by preparative column chromatography on C18 (final yield after all purification steps: 4 %).^{1}H NMR (500 MHz, $CDCl_3$): δ (ppm) 2.54 (s, 3H), 6.79 (m, 1H), 6.94 (m, 1H),7.25 – 7.27 (m, 2H) 7.35 – 7.38 (m, 2H), 7.44 (m, 1H), 7.50 (t, 1H), 8.48 (s, 1H). ^{13}C NMR (126 MHz, $CDCl_3$): δ (ppm) 21.60, 119.34, 120.54, 121.16, 122.51, 123.84, 128.03, 129.25,

134.94, 135.42, 139.52. 154.96, 167.96, 169.23. ^{99}Tc NMR (90 MHz, $CDCl_3$): δ (ppm) -691.5 (s, $\Delta\nu_{1/2}$ = 1763 Hz).

Preparation of dinuclear ^{99m}Tc^{99}Tc complex 6*: A solution of $[^{99m}Tc(OH_2)_3(CO)_3]^+$ (0.5ml) was dried under nitrogen flow, taken up in acetonitrile (1 ml) and added to a solution of $[NEt_4]_2[^{99}TcCl_3(CO)_3]$ (40.1mg, 0.073mmol) in acetonitrile (3ml). Hsal-m-tol (17mg, 0.080mmol) in acetonitrile (2ml) and an excess of NEt_3 (0.1ml) were added and the solution was stirred at 80°C for 3 h. HPLC analysis (UV/vis) evidenced the quantitative formation of **6** together with the ^{99m}Tc^{99}Tc homologue **6*** (□-trace) as shown in Figure 4.

Preparation of dinuclear ^{99m}TcRe complex 10: A solution of $[^{99m}Tc(OH_2)_3(CO)_3]^+$ (0.5ml) was dried under nitrogen flow, taken up in acetonitrile (1ml) and added to a solution of $[NEt_4]_2[ReBr_3(CO)_3]$ (20mg, 0.026mmol) in acetonitrile (1ml). Hsal-m-tol (6mg, 0.028mmol) in acetonitrile (1ml) and an excess of NEt_3 (8 drops) were added and the solution was stirred at 80 °C for 3 h. HPLC analysis (UV/vis) showed the formation of the mononuclear rhenium complex **9** together with the mixed-element complex **10** (□-trace) as shown in Figure 4.

Characterization

^{1}H, ^{13}C, and ^{99}Tc NMR spectra were recorded on a BrukerDRX 400 MHz or BrukerDRX 500 MHz spectrometer. ^{1}H and ^{13}C chemical shifts were referenced with the residual solvent resonances relative to TMS, while ^{99}Tc was referenced relative to the signal of $[^{99}TcO_4]^-$ (δ = 0).

HPLC analyses of the ^{99m}Tc and ^{99}Tc complex was performed on a Merck Hitachi LaChrom L 7100 pump coupled to a Merck Hitachi LaChrom L7200 tunable UV detector and a radiodetector. UV/Vis detection was performed at 250 nm. The detection of radioactive ^{99m}Tc/^{99}Tc complexes was performed with a Berthold LB508 radiodetector equipped with BGO/YG cell. Separations were achieved on a Macherey-Nagel C18 reversed-phase column (Nucleosil 10 lm, 250 4 mm) using a gradient of MeOH/ 0.1% CF_3COOH as eluent, and a flow rate of 0.5 mL/min. Gradient: t = 0 – 3 min: 0% MeOH; 3 – 3.1 min: 0 – 25% MeOH; 3.1 – 9 min: 25% MeOH; 9 – 9.1 min: 25

– 34% MeOH; 9.1 – 18 min: 34 - 100% MeOH; 18 – 25 min: 100% MeOH, 25 – 25.1 min: 100 - 0% MeOH; 25.1 – 30 min: 0% MeOH. Comparison of the HPLC retention times for the ^{99m}Tc compounds with the corresponding ^{99}Tc and Re compound confirms identity.

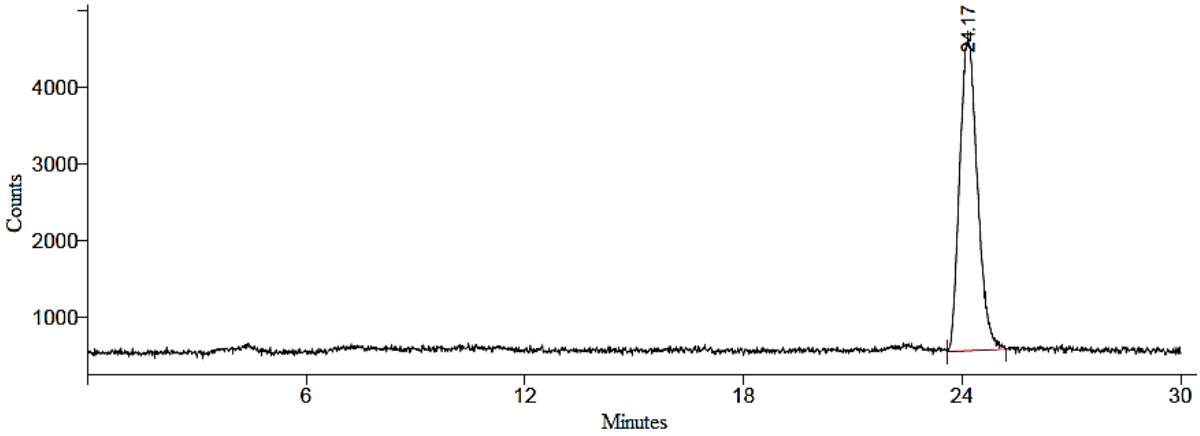

Figure 131. HPLC chromatogram obtained for [99Tc(Sal-CyHex)(CO)3]2 (β-trace).

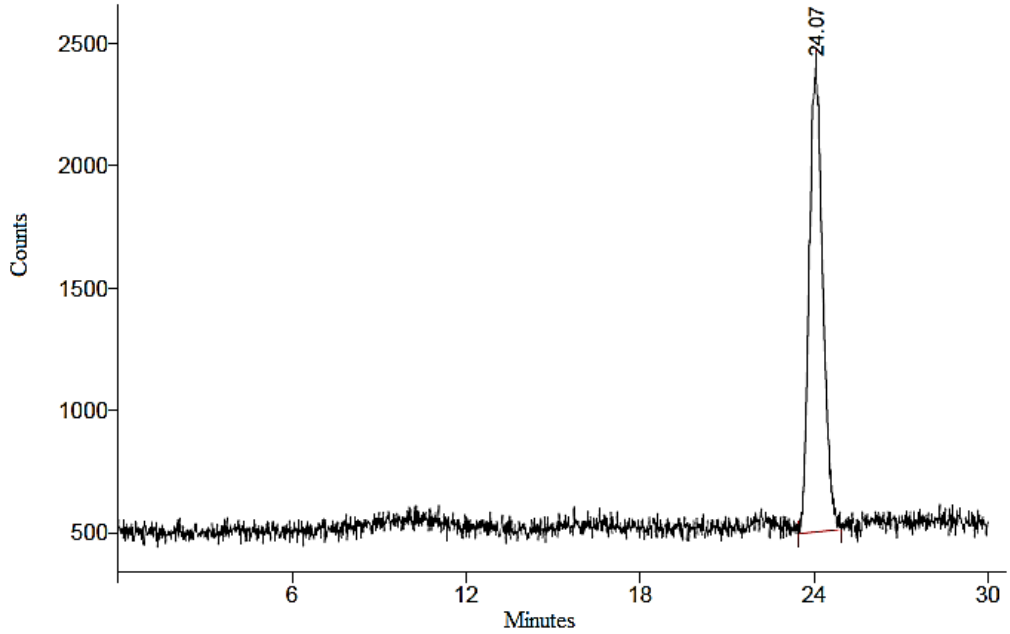

Figure 132. HPLC chromatogram obtained for [^{99}Tc(Sal-*C*yp)$(CO)_3]_2$ (β-trace).

Crystal Data

X-ray Crystallographic data were collected at 183(2) K with Mo Kα radiation (λ = 0.7107 Å). Compound **6**, **7** and **8** were measured on an Oxford Diffraction CCD Xcalibur system with a Ruby detector. Suitable crystals were covered with oil (Infineum V8512, formerly known as Paratone N), placed on a nylon loop that is mounted in a CrystalCap Magnetic™ (Hampton Research) and immediately transferred to the diffractometer. Data were corrected for Lorentz and polarisation effects as well as for absorption (numerical). The program suite CrysAlisPro was used for data collection, multi-scan absorption correction and data reduction.[62] Structures were solved with direct methods using SIR97[236] and were refined by full-matrix least-squares methods on F^2 with SHELXL-2014.[237] The structures were checked for higher symmetry with help of the program Platon.[238238] Supplementary crystallographic data can be obtained free of charge from the Cambridge Crystallographic Data Centre via www.ccdc.cam.ac.uk/structures.

Table 16: X-Ray crystallographic data and refinement parameters for *fac*-[$^{99}Tc_2(\mu_2$-O^N-m-tol$)_2(CO)_6$] (**6**), *fac*-[$^{99}Tc_2(\mu_2$-O^N- cpent$)_2(CO)_6$] **(7)** and *fac*-[$^{99}Tc_2(\mu_2$-O^N- EtPh$)_2(CO)_6$] **(8)**

	fac-[$^{99}Tc_2(\mu_2$-O^N-m-tol$)_2(CO)_6$] **(6)**	*fac*-[$^{99}Tc_2(\mu_2$-O^N-cpent$)_2(CO)_6$] (**7**)	*fac*-[$^{99}Tc_2(\mu_2$-O^N-EtPh$)_2(CO)_6$] **(8)**
Empirical formula	C_{34} H_{24} N_2 O_8 Tc_2	C_{32} H_{30} N_2 O_8 Tc_2	C_{38} H_{32} N_2 O_8 Tc_2
Formula weight	784.55	766.58	840.65
Temperature/(K)	183(2)	183(2)	183(2) K
Wavelength Å	0.71073	0.71073	0.71073
Crystal system	Triclinic	Triclinic	Monoclinic
Space group	P $\bar{1}$	P $\bar{1}$	P $2_1/n$
a/Å	7.7230(3)	8.5234(6)	7.5595(5)
b/Å	9.6213(5)	9.4839(4)	19.5030(9)
c/Å	11.4744(6)	10.3293(7)	12.0691(8)
α/°	103.910(4)	96.671(5)	90
β/°	102.384(4)	113.343(7)	97.395(7)
γ/°	99.338(4)	95.370(5)	90
Volume/Å^3	787.52(7)	752.46(9)	1764.58(19)
Z	1	1	2
Density (g.cm^{-3})	1.654	1.692	1.582
μ(mm^{-1})	0.933	0.974	0.838
F(000)	392	386	848
Crystal Colour	Yellow	Yellow	Yellow
Crystal Morphology	Plate	Plate	Plate
Theta range (°)	2.772 to 26.370	2.634 to 26.371	2.694 to 27.997
Completeness (%)	99.9	99.9	99.9
Index ranges	h = -8 to 9 k = -10 to 12 l= -13 to 14	h = -10 to 10 k = -11 to 7 l = -12 to 12	h = -9 to 9 k = -25 to 25 l = -15 to 15
Reflections collected	6179	6758	20701
Independent reflections	3217	3074	4245
R_{Int}	0.0451	0.0391	0.0638
Data/restraints/ parameters	3217 / 0 / 209	3074 / 18 / 231	4245 / 0 / 226
Goodness-of-fit on F^2	1.042	0.935	1.064
Final R indexes [I>=2σ (I)]	R1 = 0.0401 wR2 = 0.0727	R1 = 0.0342 wR2 = 0.0827	R1 = 0.0421 wR2 = 0.0712
Final R indexes [all data]	R1 = 0.0508 wR2 = 0.0779	R1 = 0.0392 wR2 = 0.0856	R1 = 0.0713 wR2 = 0.0833
ρ max, ρ min (e.Å^{-3})	0.777, -0.853	0.942, -0.714	0.720, -0.528
CCDC number	1581119	1581120	1581121

6. Curriculum Vitae

Personal Information

Name	Angelo
Surname	Frei
Date of Birth	15.09.1990
Nationality	Swiss
Place of Origin	Diepoldsau-Schmitter (SG)

EDUCATION

University of Zurich, Switzerland

03/2014 – 03/2018 **- PhD in Chemistry -**
"Multi-functional Cyclopentadienyl Complexes for Theranostic Applications".
Supervisor: Prof. Dr. Roger Alberto

09/2012 – 12/2013 **- Master of Science in Chemistry -**
Master Thesis: *"Towards Red-Light Activated Ruthenium Photosensitizers for Photodynamic Therapy".*
Supervisor: Prof. Dr. Gilles Gasser

09/2009 – 08/2012 **- Bachelor of Science in Chemistry -**
Minor: Biochemistry

Kantonsschule Romanshorn, Switzerland

08/2005 – 07/2008 **- Matura –**
Specialization 1: Chemistry and Biology
Specialization 2: Physics

PUBLICATIONS & PATENTS

- D. V. Kama, **A. Frei**, P. Mokolokolo, M. Schutte-Smith, A. Brink, H. G. Visser, C. Swart, R. Alberto and A. Roodt, *"Structure relationships and preliminary mitochondrial activity of fac-{$M^{I}(CO)_3$}$^{+}$ bis(diarylphosphino)alkyl-/arylamine complexes (M=^{99}Tc, Re)",* in preparation.

- **A. Frei**, E. Fischer, B. Childs, J. Holland and R. Alberto, *"Two is Better than One. Dimeric High-affinity PSMA Probes Based on a [CpM(CO)$_3$] Scaffold",* in preparation.
- ***A. Frei***, *B. Spingler and R. Alberto, "Multi-functional Cyclopentadiene as a Scaffold for Combinatorial Bioorganometallics in [(η^5-$C_5H_2R^1R^2R^3$)M(CO)$_3$] (M = Re, ^{99m}Tc) Piano-stool Type Complexes",* submitted.
- ***A. Frei****, P. P. Mokolokolo, R. Bolliger, H. Braband, M. S. Tsosane, A. Brink, A. Roodt, and R. Alberto,* "Self-assembled multi-nuclear complexes incorporating ^{99m}Tc"*, submitted.*
- A. Roodt, R. Alberto, **A. Frei**, P. Mokolokolo, R. Bolliger, A. Brink, *"Multinuclear Complexes and their Preparation" SA Pat. Appl. (2017), P3490ZA00.*
- P. P. Mokolokolo, **A. Frei**, M. S. Tsosane, D. V. Kama, M. Schuette-Smith, A. Brink, H. G. Visser, G. Meola, R. Alberto, and A. Roodt, *"Schiff base ligand manipulation of the nuclearity in fac-tricarbonyl complexes of Mn(I) and Re(I)". Inorg. Chim. Acta.* **2017**, *471*, 249 – 256.
- J. P. Kraack, **A. Frei**, R. Alberto, and P. Hamm, *„Ultrafast Vibrational Energy Transfer in Catalytic Monolayers at Solid-Liquid Interfaces" J. Phys. Chem. Lett.,* **2017***, 8,* 2489-2495. **DOI:** 10.1021/acs.jpclett.7b01034

  http://pubs.acs.org/doi/abs/10.1021/acs.jpclett.7b01034
- **A. Frei***, D. Sidler, P. Mokolokolo, H. Braband, T. Fo*x, B. Spingler, A. Roodt, and R. Alberto, *"Kinetics and Mechanism of CO Exchange in fac-[MBr2(solvent)(CO)3]- (M = Re, 99Tc)" Inorg. Chem.* **2016**, *55*, 9352-9360. **DOI:** 10.1021/acs.inorgchem.6b01503

  http://pubs.acs.org/doi/abs/10.1021/acs.inorgchem.6b01503
- **A. Frei**, R. Rubbiani, S. Tubafard, O. Blacque, P. Anstaett, A. Felgenträger, T. Maisch, L. Spiccia, and G. Gasser, *"Synthesis, Characterization, and Biological Evaluation of New Ru(II) Polypyridyl Photosensitizers for Photodynamic Therapy" J. Med. Chem.* **2014**, *57*, 7280-7292. **DOI:** 10.1021/jm500566f

  http://pubs.acs.org/doi/abs/10.1021/jm500566f
- Leonidova, T. Joshi, D. Nipkow, **A. Frei**, J.-E. Penner, S. Konatschnig, M. Patra, and G. Gasser, *"An Environmentally Benign and Cost-Effective Synthesis of Aminoferrocene and Aminoruthenocene" Organometallics* **2013**, *32*, 2037-2040. **DOI:** 10.1021/om400009g

  http://pubs.acs.org/doi/abs/10.1021/om400009g
- G. Gasser, A. Leonidova, T. Joshi, D. Nipkow, **A. Frei**, J.-E. Penner, S. Konatschnig and M. Patra, *"Synthesis of Amino-substituted Metallocene Compounds"* Eur. Pat. Appl. (2013), EP13157319.8

AWARDS

- Swiss National Science Foundation Early PostDoc.Mobility Fellowship (**2017**)
- Nomination and Honorable Mention for the Hofmann PhD Award (**2017**)
- CMSZH/PerkinElmer Travel Award (**2017**)
- New Zealand Institute of Chemistry Early Career Researcher Lecture Award (**2016**)
- AsBIC8 Travel Award (**2016**)
- Swiss Academy of Sciences/Swiss Chemical Society Chemistry Travel Award (**2016**)
- *J. Med. Chem. Award* for the Highly Cited Article of 2014 (**2016**)
- Alfred Werner Legat for a remarkable GPA during the Master studies (**2014**)
- Alfred Werner Legat for a remarkable GPA during the Bachelor studies (**2013**)

SCIENTIFIC CONTRIBUTIONS

Poster Communications

- *Multifunctional Cp-Ligands, a New Versatile Toolbox for the Development of Theranostic Agents.* 8th Asian Biological Inorganic Chemistry Conference, **2016**, Auckland, New Zealand.
- *Multifunctional Cyclopentadiene Ligands for Theranostic Re/99mTc Complexes.* 4th Whole Action Meeting of the COST Action CM1105, **2016**, Palma de Mallorca, Spain.
- *Multi-functional Cyclopentadienyl Complexes for Theranostic Applications*. SSAJRP Midterm Workshop, **2015**, Basel, Switzerland.
- S*ynthesis, Characterization and Biological Evaluation of New Ru(II) Polypyridyl Photosensitizers for Photodynamic Therapy.* Swiss Summer School in Chemical Biology, **2014**, Villars-sur-Ollon, Switzerland.

Oral Communications

- *A Customizable Synthetic Approach to Tune Targeting, Bioactivity and Solubility of Theranostic Cp-Re/99mTc Complexes,* ISABC14, **2017**, Toulouse, France.
- *New and Multifunctional Tailor-Made Cp-Ligands and their Re/99mTc Complexes for Theranostics.* Oral Presentation, CanBIC6, **2017**, Parry Sound, Canada.
- *Multifunctional Cp-Ligands, a New Versatile Toolbox for the Development of Theranostic Agents.* RSC Early Career Forum, **2016**, Auckland, New Zealand.
- *Not so similar after all***.** *Fundamental differences in reactivity of fac-[M(solvent)3(CO)3]+ (M = Re, 99Tc) with CO.* Oral Presentation, SCS Fall Meeting, **2016**, Zurich, Switzerland.
- *Multi-functional Re/99mTc-Cyclopentadienyl and Carbonyl Complexes for Theranostic Applications*. Flash Poster Presentation, INDABA8, **2015**, Skukuza – Kruger National Park, South Africa.

7. Appendix

7.1 Index of Compounds

7.1.1. Compounds Synthesized in Part A

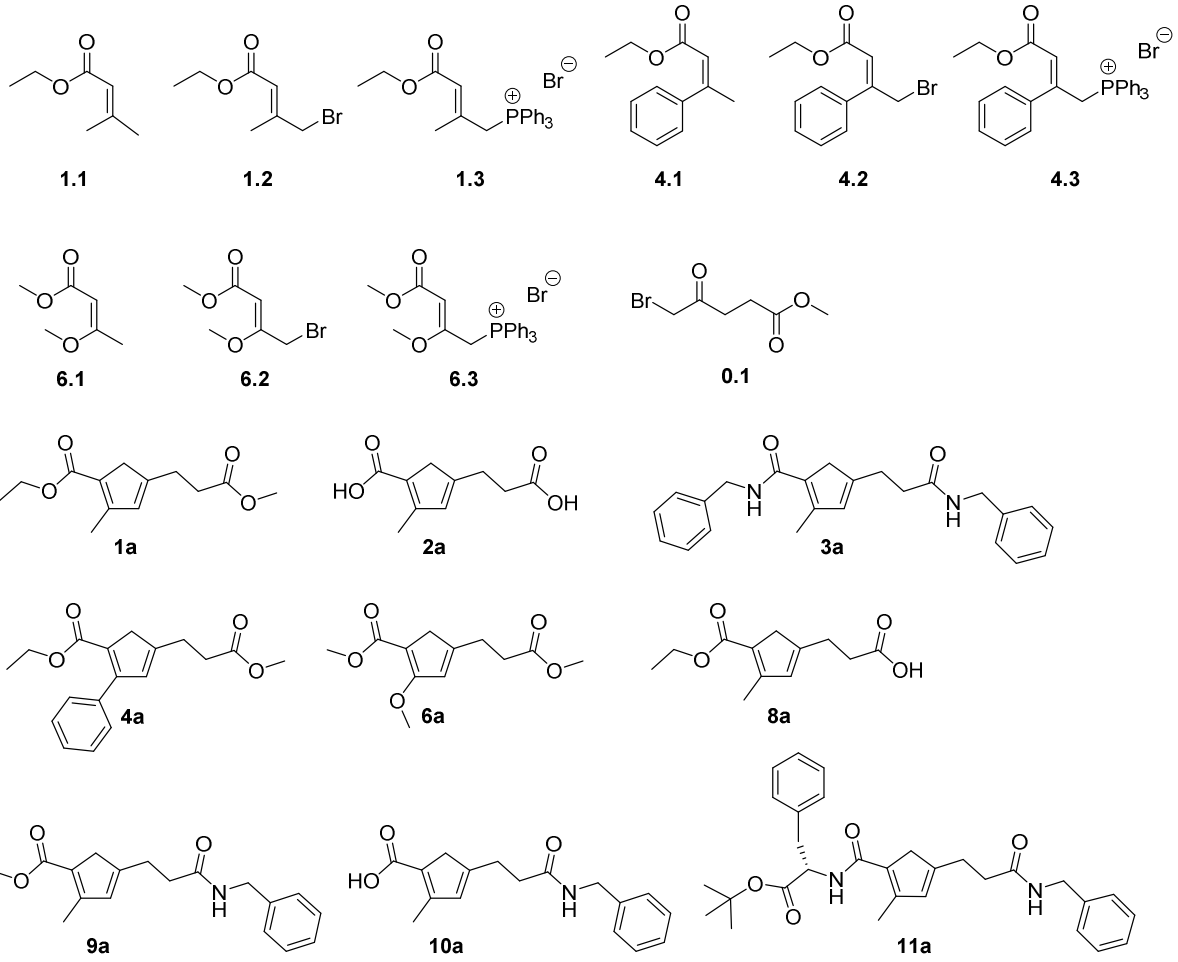

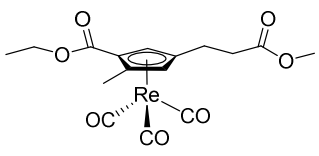

1b

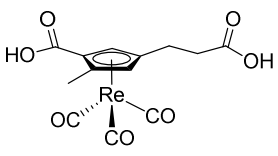

2b

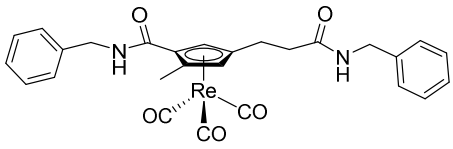

3b

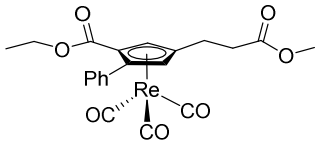

4b

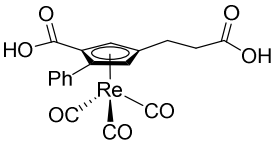

5b

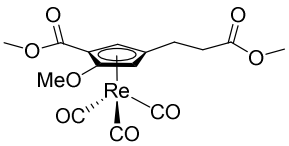

6b

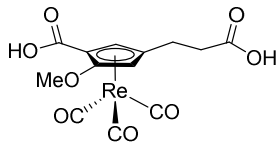

7b

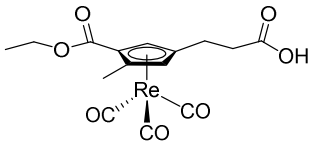

8b

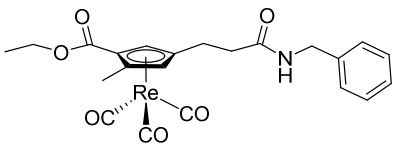

9b

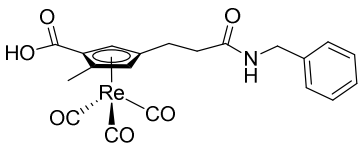

10b

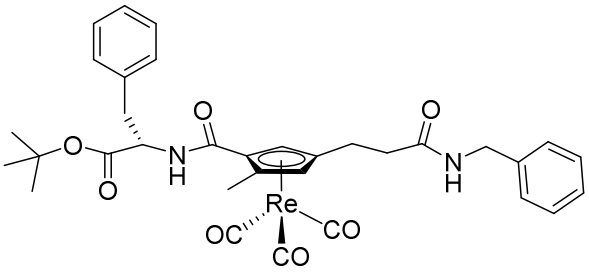

11b

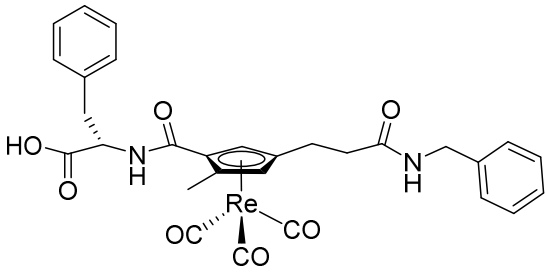

12b

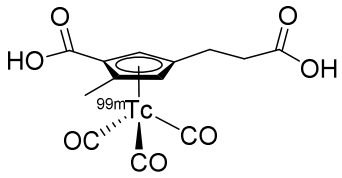

2c

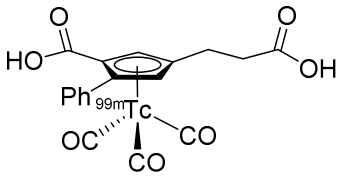

5c

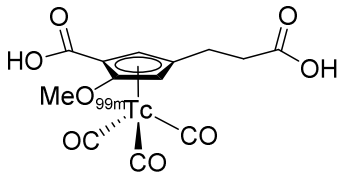

7c

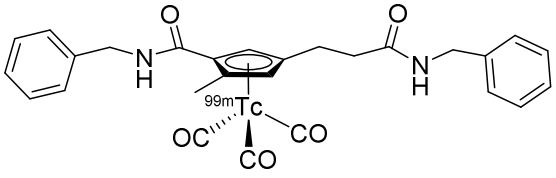

3c

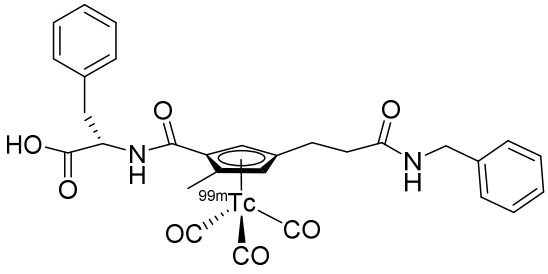

12c

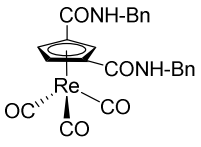

13

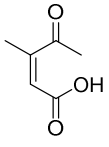

14

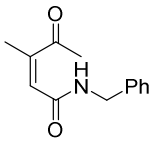

15

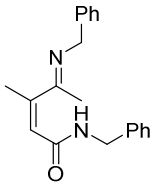

16

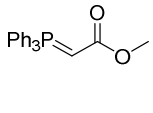

17

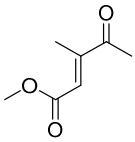

18

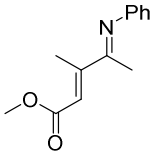

19

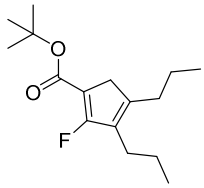

20

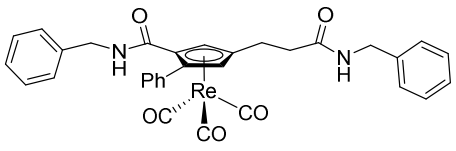

21

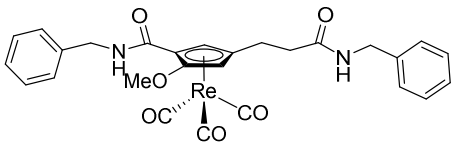

22

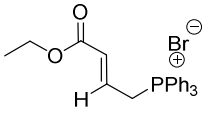

23

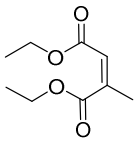

24

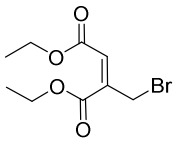

25

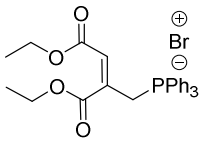

26

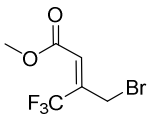

27

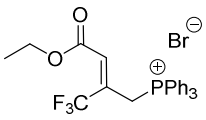

28

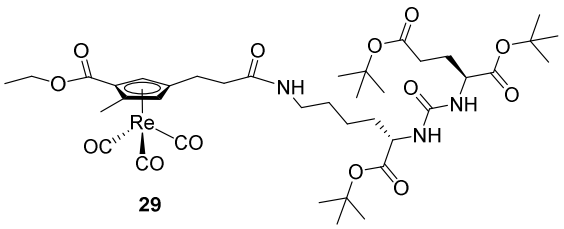

29

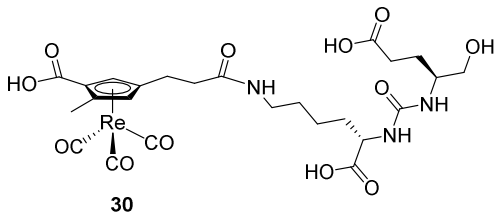

30

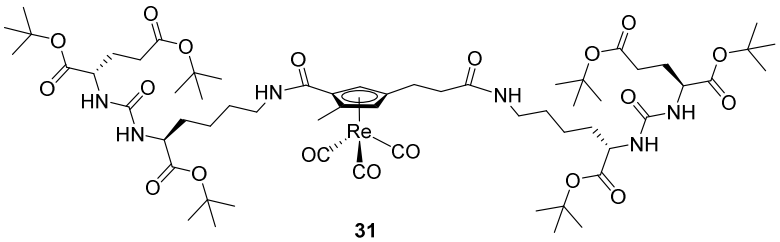

31

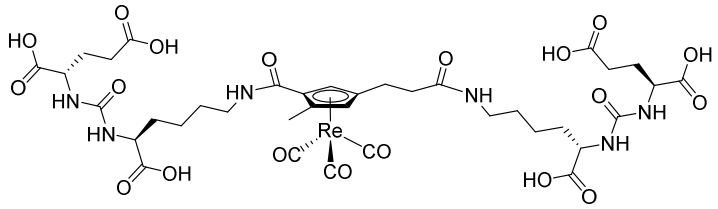

32

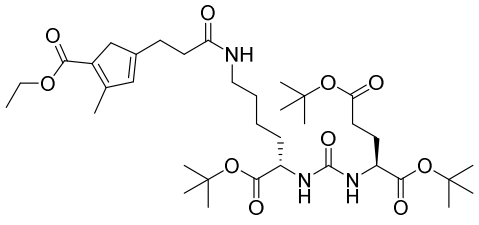

33

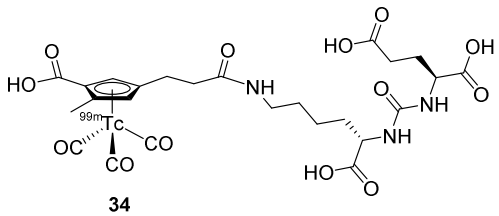

34

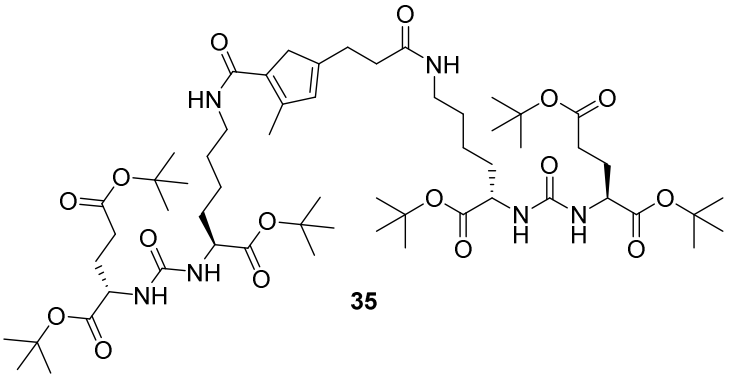

35

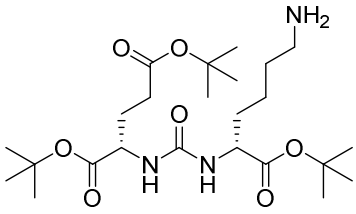

LuG

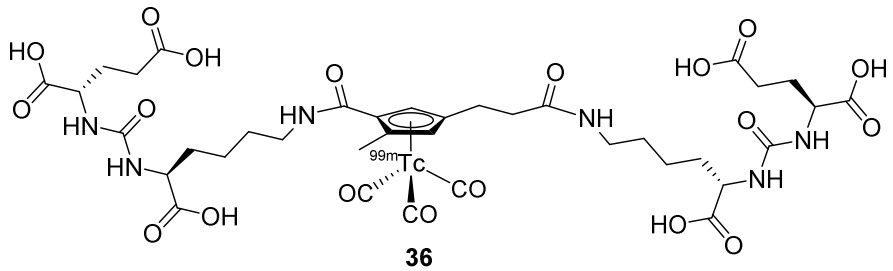

36

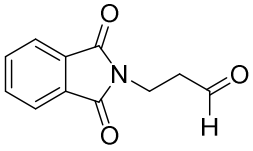

37

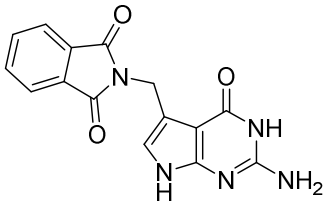

38

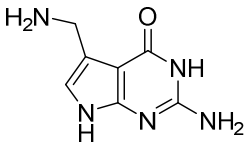

39

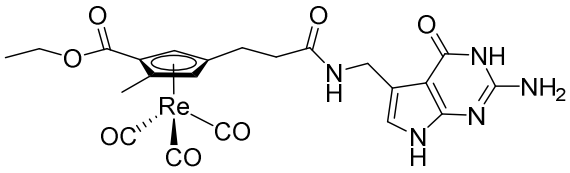

40

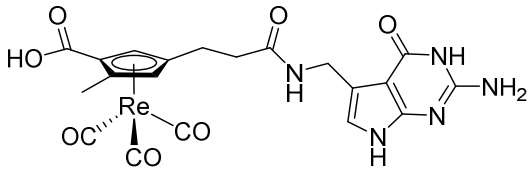

41

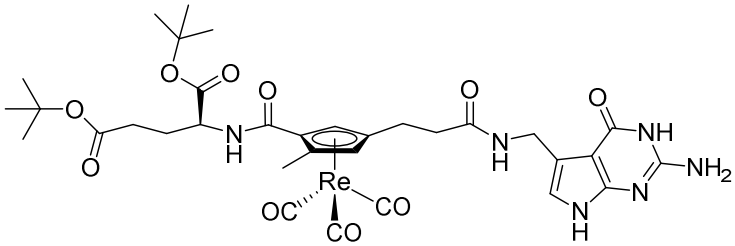

42

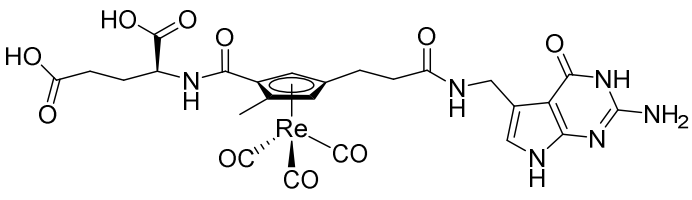

43

7.1.2. Compounds Synthesized in Part B

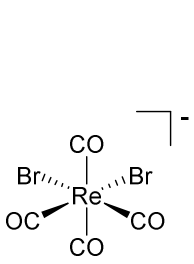

2

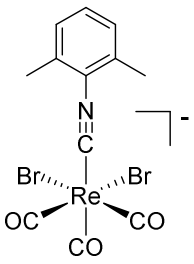

4

7.1.3. Compounds Synthesized in Part C

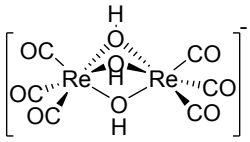

2

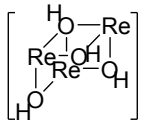

3

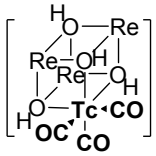

4

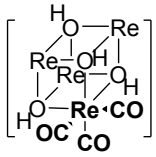

5

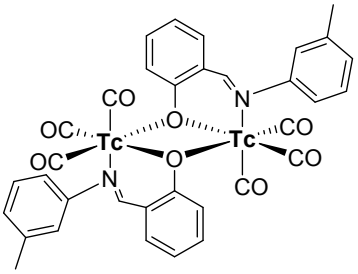

6

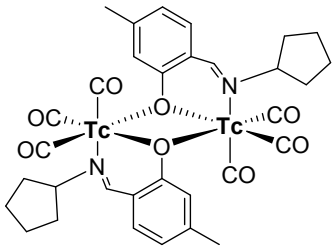

7

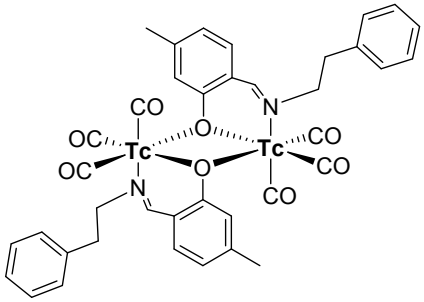

8

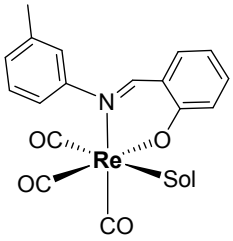

9

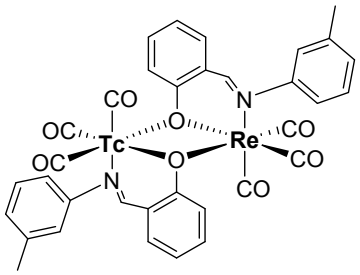

10

7.1.4. Compounds Synthesized in Part D

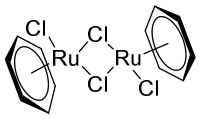

44

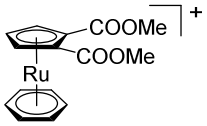

45

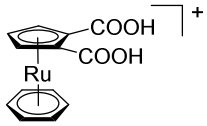

46

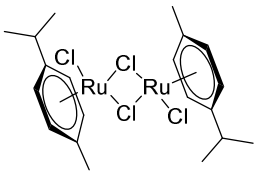

47

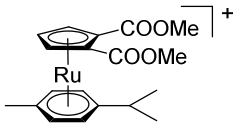

48

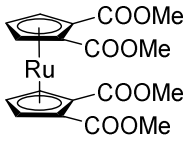

49

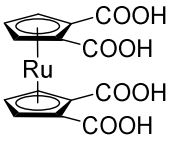

50

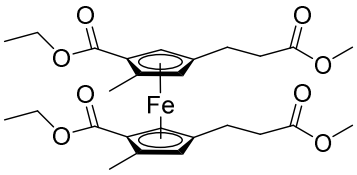

51

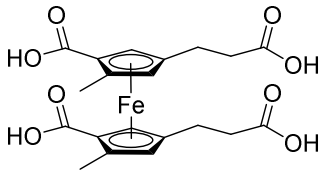

52

7.2 Abbreviations

ACN	acetonitrile
AcOH	acetic acid
AIBN	azobisisobutyronitrile
BBB	blood brain barrier
CA	carbonic anhydrase
CO	carbon monoxide
Cp	cyclopentadiene
DFT	density functional theory
DG	deoxyglucose
DIPEA	N,N-diisopropylethylamine
DLT	double ligand transfer
DMF	N,N-dimethylformamide
E.U.	European Union
EC	ethylenedicysteine
EDC	1-ethyl-3-(3-dimethyl-aminopropyl)carbodiimide
EDDA	ethylenediaminediacetic acid
EtOAc	ethyl acetate
EtOH	ethanol
Fc	ferrocene
FDA	food and drug administration
FGD	fluorodeoxyglucose
FR	folate receptor
HOBt	hydroxybenzotriazole
HPLC	high pressure liquid chromatography
HR	high resolution
HYNIC	hydrazinonicotinyl
ICP-MS	inductively coupled plasma mass spectrometry
IR	infrared
mAChR	muscarinic acetylcholine receptor
MeCN	acetonitrile
MeOH	methanol
MS	mass spectrometry
MW	microwave
NBS	N-bromosuccinimide

NEt3	triethylamine
NMR	nuclear magnetic resonance
NOE	Nuclear Overhauser Effect
NSCLC	non-small cell lung cancer
ORTEP	Oak Ridge Thermal Ellipsoid Plot
POM	polyoxometalate
PSMA	prostate specific membrane antigen
Rf	retention factor
RGD	arginine-glycine-aspartic acid
ROS	reactive oxygen species
Rt	retention time
SPECT	single photon emission computed tomography
TFA	trifluoroacetic acid
TLC	thin layer chromatography
U.S.	United States
UPLC	ultra high pressure liquid chromatography
UV	ultraviolett
VIS	visible
Xyl-NC	2,6-dimethylphenyl-isocyanide

8. References

(1) G. Gasser and N. Metzler-Nolte, *Curr. Opin. Chem. Biol.*, 2012, **16**, 84-91.

(2) G. Gasser, I. Ott and N. Metzler-Nolte, *J. Med. Chem.*, 2011, **54**, 3-25.

(3) B. Rosenberg, L. Vancamp, J. E. Trosko and V. H. Mansour, *Nature*, 1969, **222**, 385.

(4) M. Galanski, M. A. Jakupec and B. K. Keppler, *Curr. Med. Chem.*, 2005, **12**, 2075-2094.

(5) N. N. Howlader, A. M.; Krapcho, M.; Neyman, N.; Aminou, R.; Waldron, W.; Altekruse, S. F.; Kosary, C. L.; Ruhl, J.; Tatalovich, Z.; Cho, H.; Mariotto, A.; Eisner, M. P.; Lewis, D. R.; Chen, H. S.; Feuer, E. J.; Cronin, *K. A. SEER Cancer Statistics Review, 1975–2009;* , National Cancer Institute: Bethesda, MD, 2012.

(6) T. C. Johnstone, K. Suntharalingam and S. J. Lippard, *Chem. Rev.*, 2016, **116**, 3436-3486.

(7) C. Mari, V. Pierroz, R. Rubbiani, M. Patra, J. Hess, B. Spingler, L. Oehninger, J. Schur, I. Ott, L. Salassa, S. Ferrari and G. Gasser, *Chem. - Eur. J.*, 2014, **20**, 14421-14436.

(8) G. Sava, S. Pacor, G. Mestroni and E. Alessio, *Clin. Exp. Metastasis*, 1992, **10**, 273-280.

(9) E. Alessio, *Eur. J. Inorg. Chem.*, 2017, **2017**, 1549-1560.

(10) S. Leijen, S. A. Burgers, P. Baas, D. Pluim, M. Tibben, E. van Werkhoven, E. Alessio, G. Sava, J. H. Beijnen and J. H. M. Schellens, *Invest. New Drugs*, 2015, **33**, 201-214.

(11) B. K. Keppler and W. Rupp, *J. Cancer Res. Clin. Oncol.*, 1986, **111**, 166-168.

(12) M. M. Henke, H. Richly, A. Drescher, M. Grubert, D. Alex, D. Thyssen, U. Jaehde, M. E. Scheulen and R. A. Hilger, *Int. J. Clin. Pharmacol. Ther.*, 2009, **47**, 58-60.

(13) H. Holtkamp, G. Grabmann and C. G. Hartinger, *Electrophoresis*, 2016, **37**, 959-972.

(14) R. D. Hofheinz, C. Dittrich, M. A. Jakupec, A. Drescher, U. Jaehde, M. Gneist, N. Graf von Keyserlingk, B. K. Keppler and A. Hochhaus, *Int. J. Clin. Pharmacol. Ther.*, 2005, **43**, 590-591.

(15) M. A. Jakupec, M. Galanski, V. B. Arion, C. G. Hartinger and B. K. Keppler, *Dalton Trans.*, 2008, DOI: 10.1039/B712656P, 183-194.

(16) C. Biot, F. Nosten, L. Fraisse, D. Ter-Minassian, J. Khalife and D. Dive, *Parasite*, 2011, **18**, 207-214.

(17) C. Supan, G. Mombo-Ngoma, M. Kombila, C. L. Ospina Salazar, J. Held, B. Lell, C. Cantalloube, E. Djeriou, B. Ogutu, J. Waitumbi, N. Otsula, D. Apollo, M. E. Polhemus, P. G. Kremsner and D. S. Walsh, *The American journal of tropical medicine and hygiene*, 2017, **97**, 514-525.

(18) R. Alberto, R. Schibli, R. Waibel, U. Abram and A. P. Schubiger, *Coord. Chem. Rev.*, 1999, **190–192**, 901-919.

(19) O. Chiewitz and G. Hevesy, *Nature*, 1935, **136**, 754.

(20) J. G. Hamilton and M. H. Soley, *Am. J. Physiol.*, 1939, **127**, 557-572.

(21) S. Carlson, *Acta Oncol.*, 1995, **34**, 1095-1102.

(22) M. D. Bartholomä, A. S. Louie, J. F. Valliant and J. Zubieta, *Chem. Rev.*, 2010, **110**, 2903-2920.

(23) H. Luna Pais, I. Alho, I. Vendrell, A. Mansinho and L. Costa, *Dalton Trans.*, 2017, **46**, 14475-14487.

(24) W. A. Volkert and T. J. Hoffman, *Chem. Rev.*, 1999, **99**, 2269-2292.

(25) I. Amato, *Chemical & Engineering News Archive*, 2009, **87**, 58-64.

(26) A. C. Kluba and L. T. Mindt, *Molecules*, 2013, **18**.

(27) S. Banerjee, M. R. Ambikalmajan Pillai and N. Ramamoorthy, *Semin. Nucl. Med.*, 2001, **31**, 260-277.

(28) G. T. Seaborg and E. Segrè, *Phys. Rev.*, 1939, **55**, 808-814.

(29) J. R. Dilworth and S. J. Parrott, *Chem. Soc. Rev.*, 1998, **27**, 43-55.

(30) V. J. Molinski, *Int. J. Appl. Radiat. Isot.*, 1982, **33**, 811-819.

(31) B. Wolterbeek, J. L. Kloosterman, D. Lathouwers, M. Rohde, A. Winkelman, L. Frima and F. Wols, *J. Radioanal. Nucl. Chem.*, 2014, **302**, 773-779.

(32) M. R. A. Pillai and F. F. Knapp, *J. Nucl. Med.*, 2011, **52**, 15N-28N.

(33) M. R. A. Pillai, A. Dash and F. F. Knapp, *J. Nucl. Med.*, 2015, **56**, 159-161.

(34) K. D. Mjos and C. Orvig, *Chem. Rev.*, 2014, **114**, 4540-4563.

(35) M. S. Kinch and P. K. Woodard, *Drug Discovery Today*, 2017, **22**, 1077-1083.

(36) R. Alberto, K. Ortner, N. Wheatley, R. Schibli and A. P. Schubiger, *J. Am. Chem. Soc.*, 2001, **123**, 3135-3136.

(37) R. Alberto, R. Schibli, A. Egli, A. P. Schubiger, U. Abram and T. A. Kaden, *J. Am. Chem. Soc.*, 1998, **120**, 7987-7988.

(38) R. Schibli and P. A. Schubiger, *Eur. J. Nucl. Med. Mol. Imaging*, 2002, **29**, 1529-1542.

(39) S. M. Hillier, K. P. Maresca, G. Lu, R. D. Merkin, J. C. Marquis, C. N. Zimmerman, W. C. Eckelman, J. L. Joyal and J. W. Babich, *J. Nucl. Med.*, 2013, **54**, 1369-1376.

(40) C. Schmidkonz, C. Hollweg, M. Beck, J. Reinfelder, T. I. Goetz, J. C. Sanders, D. Schmidt, O. Prante, T. Bäuerle, A. Cavallaro, M. Uder, B. Wullich, P. Goebell, T. Kuwert and P. Ritt, *The Prostate*, 2018, **78**, 54-63.

(41) L. K. Meszaros, A. Dose, S. C. G. Biagini and P. J. Blower, *Inorg. Chim. Acta*, 2010, **363**, 1059-1069.

(42) S. Liu and S. Chakraborty, *Dalton Trans.*, 2011, **40**, 6077-6086.

(43) T. Kniess, M. Laube, F. Wust and J. Pietzsch, *Dalton Trans.*, 2017, **46**, 14435-14451.

(44) E. M. Hahn, A. Casini and F. E. Kühn, *Coord. Chem. Rev.*, 2014, **276**, 97-111.

(45) M. P. Coogan, R. P. Doyle, J. F. Valliant, J. W. Babich and J. Zubieta, *J. Labelled Compd. Radiopharm.*, 2014, **57**, 255-261.

(46) D. Psimadas, P. Bouziotis, P. Georgoulias, V. Valotassiou, T. Tsotakos and G. Loudos, *Contrast Media Mol. Imaging*, 2013, **8**, 333-339.

(47) M. Morais, A. Paulo, L. Gano, I. Santos and J. D. G. Correia, *J. Organomet. Chem.*, 2013, **744**, 125-139.

(48) B. Cristina, C. Davide, S. Nicola and R. Fiorenzo, *Anti-Cancer Agents Med. Chem.*, 2012, **12**, 428-461.

(49) A. Y. Maruk, A. B. Bruskin and G. E. Kodina, *Radiochemistry*, 2011, **53**, 341.

(50) C. Bolzati, F. Refosco, A. Marchiani and P. Ruzza, *Curr. Med. Chem.*, 2010, **17**, 2656-2683.

(51) F. Y. Lambrecht, *Ann. Nucl. Med.*, 2011, **25**, 1-6.

(52) V. Gutmann and E. Wychera, *Inorg. Nucl. Chem. Lett.*, 1966, **2**, 257-260.

(53) J. M. Buchanan and S. C. Hartman, in *Adv. Enzymol. Relat. Areas Mol. Biol.*, John Wiley & Sons, Inc., 2006, DOI: 10.1002/9780470122662.ch5, pp. 199-261.

(54) C. P. Leamon, M. A. Parker, I. R. Vlahov, L.-C. Xu, J. A. Reddy, M. Vetzel and N. Douglas, *Bioconjug. Chem.*, 2002, **13**, 1200-1210.

(55) A. A. Bengali, B. K. Mezick, M. N. Hart and S. Fereshteh, *Organometallics*, 2003, **22**, 5436-5440.

(56) K.-E. Gottschalk and H. Kessler, *Angew. Chem. Int. Edit.*, 2002, **41**, 3767-3774.

(57) P. C. Brooks, A. M. P. Montgomery, M. Rosenfeld, R. A. Reisfeld, T. Hu, G. Klier and D. A. Cheresh, *Cell*, 1994, **79**, 1157-1164.

(58) S. Liu, *Mol. Pharmaceut.*, 2006, **3**, 472-487.

(59) L. Wang, J. Shi, Y.-S. Kim, S. Zhai, B. Jia, H. Zhao, Z. Liu, F. Wang, X. Chen and S. Liu, *Mol. Pharmaceutics*, 2009, **6**, 231-245.

(60) Z. Zhu, W. Miao, Q. Li, H. Dai, Q. Ma, F. Wang, A. Yang, B. Jia, X. Jing, S. Liu, J. Shi, Z. Liu, Z. Zhao, F. Wang and F. Li, *J. Nucl. Med.*, 2012, **53**, 716-722.

(61) D. A. McQuarrie, *Statistical thermodynamics*, Harper & Row, New York, 1973.

(62) C. Decristoforo, S. J. Mather, W. Cholewinski, E. Donnemiller, G. Riccabona and R. Moncayo, *Eur. J. Nucl. Med.*, 2000, **27**, 1318-1325.

(63) A. Płachcińska, R. Mikołajczak, H. R. Maecke, E. Młodkowska, J. Kunert-Radek, A. Michalski, K. Rzeszutek, J. Kozak and J. Kuśmierek, *Eur. J. Nucl. Med. Mol. Imaging*, 2003, **30**, 1402-1406.

(64) ClinicalTrials.gov, https://clinicaltrials.gov/ct2/show/NCT02691078?term=HYNIC&rank=1 Accessed, 24.01.2018).

(65) D. J. Yang, C.-G. Kim, N. R. Schechter, A. Azhdarinia, D.-F. Yu, C.-S. Oh, J. L. Bryant, J.-J. Won, E. E. Kim and D. A. Podoloff, *Radiology*, 2003, **226**, 465-473.

(66) R. Alberto, R. Schibli, A. Egli, A. P. Schubiger, U. Abram and T. A. Kaden, *J. Am. Chem. Soc.*, 1998, **120**, 7987-7988.

(67) C. Schmidkonz, C. Hollweg, M. Beck, J. Reinfelder, T. I. Goetz, J. C. Sanders, D. Schmidt, O. Prante, T. Bauerle, A. Cavallaro, M. Uder, B. Wullich, P. Goebell, T. Kuwert and P. Ritt, *Prostate*, 2018, **78**, 54-63.

(68) S. S. Gambhir, *Nat. Rev. Cancer*, 2002, **2**, 683.

(69) P. Som, H. L. Atkins, D. Bandoypadhyay, J. S. Fowler, R. R. MacGregor, K. Matsui, Z. H. Oster, D. F. Sacker, C. Y. Shiue, H. Turner, C.-N. Wan, A. P. Wolf and S. V. Zabinski, *J. Nucl. Med.*, 1980, **21**, 670-675.

(70) S. Top, A. Vessières, G. Leclercq, J. Quivy, J. Tang, J. Vaissermann, M. Huché and G. Jaouen, *Chem. - Eur. J.*, 2003, **9**, 5223-5236.

(71) Y. C. J. Chen and K. D. Janda, *J. Am. Chem. Soc.*, 1992, **114**, 1488-1489.

(72) P. Wentworth, T. Wiemann and K. D. Janda, *J. Am. Chem. Soc.*, 1996, **118**, 12521-12527.

(73) S. Z. Lever, K. E. Baidoo, A. Mahmood, K. Matsumura, U. Scheffel and H. N. Wagner, *Nucl. Med. Biol.*, 1994, **21**, 157-164.

(74) S. Samnick, W. Brandau, J. Sciuk, A. Steinsträβer and O. Schober, *Nucl. Med. Biol.*, 1995, **22**, 573-583.

(75) D. Y. Chi and J. A. Katzenellenbogen, *J. Am. Chem. Soc.*, 1993, **115**, 7045-7046.

(76) R. K. Hom and J. A. Katzenellenbogen, *The Journal of Organic Chemistry*, 1997, **62**, 6290-6297.

(77) M. B. Skaddan and J. A. Katzenellenbogen, *Bioconjug. Chem.*, 1999, **10**, 119-129.

(78) C. Fan, H. Jia, W. Deuther-Conrad, P. Brust, J. Steinbach and B. Liu, *Sci. China, Ser. B: Chem.*, 2006, **49**, 169-176.

(79) D. Can, B. Spingler, P. Schmutz, F. Mendes, P. Raposinho, C. Fernandes, F. Carta, A. Innocenti, I. Santos, C. T. Supuran and R. Alberto, *Angew. Chem. Int. Edit.*, 2012, **51**, 3354-3357.

(80) J.-Y. Winum, M. Rami, A. Scozzafava, J.-L. Montero and C. Supuran, *Med. Res. Rev.*, 2008, **28**, 445-463.

(81) T. J. Kealy and P. L. Pauson, *Nature*, 1951, **168**, 1039.

(82) J. D. Dunitz, L. E. Orgel and A. Rich, *Acta Crystallogr.*, 1956, **9**, 373-375.

(83) F. Baumgaertner, E. O. Fischer and U. Zahn, *Naturwissenschaften*, 1962, **49**, 156.

(84) M. Wenzel, *J. Labelled Compd. Radiopharm.*, 1992, **31**, 641-650.

(85) T. W. Spradau and J. A. Katzenellenbogen, *Bioconjug. Chem.*, 1998, **9**, 765-772.

(86) T. W. Spradau, W. B. Edwards, C. J. Anderson, M. J. Welch and J. A. Katzenellenbogen, *Nucl. Med. Biol.*, 1999, **26**, 1-7.

(87) Y. Liu, B. Spingler, P. Schmutz and R. Alberto, *J. Am. Chem. Soc.*, 2008, **130**, 1554-1555.

(88) H. W. Peindy N'Dongo, Y. Liu, D. Can, P. Schmutz, B. Spingler and R. Alberto, *J. Organomet. Chem.*, 2009, **694**, 981-987.

(89) S. Ursillo, D. Can, H. W. P. N'Dongo, P. Schmutz, B. Spingler and R. Alberto, *Organometallics*, 2014, **33**, 6945-6952.

(90) Y. Kuninobu, Y. Nishina, T. Matsuki and K. Takai, *J. Am. Chem. Soc.*, 2008, **130**, 14062-14063.

(91) G. Iskander, R. Zhang, D. S.-H. Chan, D. S. Black, M. Alamgir and N. Kumar, *Tetrahedron Lett.*, 2009, **50**, 4613-4615.

(92) M.-J. Villa and S. Warren, *J. Chem. Soc., Perkin Trans. 1*, 1994, DOI: 10.1039/P19940001569, 1569-1572.

(93) M. E. Abbasov, B. M. Hudson, D. J. Tantillo and D. Romo, *J. Am. Chem. Soc.*, 2014, **136**, 4492-4495.

(94) T. Ichitsuka, T. Fujita, T. Arita and J. Ichikawa, *Angew. Chem. Int. Edit.*, 2014, **53**, 7564-7568.

(95) M. Hatanaka, Y. Himeda and I. Ueda, *J. Chem. Soc., Perkin Trans. 1*, 1993, DOI: 10.1039/P19930002269, 2269-2274.

(96) Y. K. Yan, M. Melchart, A. Habtemariam and P. J. Sadler, *Chem. Commun.*, 2005, DOI: 10.1039/B508531B, 4764-4776.

(97) E. Meggers, *Angew. Chem. Int. Edit.*, 2011, **50**, 2442-2448.

(98) S. Imstepf, V. Pierroz, R. Rubbiani, M. Felber, T. Fox, G. Gasser and R. Alberto, *Angew. Chem. Int. Edit.*, 2016, **55**, 2792-2795.

(99) F. Roesch and F. F. Knapp, *Handbook of Nuclear Chemistry*, Kluwer Academic Publishers,, 2003.

(100) I. Amato, *Chemical & Engineering News*, 2009, **87**, 58 - 64.

(101) C. A. Kluba and T. L. Mindt, *Molecules*, 2013, **18**, 3206-3226.

(102) W. Eckelman, *Nucl. Med. Biol.*, 2011, **38**, 613-616.

(103) M. U. Akbar, M. R. Ahmad, A. Shaheen and S. Mushtaq, *J. Radioanal. Nucl. Chem.*, 2016, **310**, 477-493.

(104) S. Achilefu, *Chem. Rev.*, 2010, **110**, 2575-2578.

(105) M. Morais, A. Paulo, L. Gano, I. Santos and J. D. G. Correia, *J Organomet Chem*, 2013, **744**, 125-139.

(106) G. R. Morais, A. Paulo and I. Santos, *Organometallics*, 2012, **31**, 5693-5714.

(107) Y. Liu, J.-K. Pak, P. Schmutz, M. Bauwens, J. Mertens, H. Knight and R. Alberto, *J. Am. Chem. Soc.*, 2006, **128**, 15996-15997.

(108) G. L. Lu, S. M. Hillier, K. P. Maresca, C. N. Zimmerman, W. C. Eckelman, J. L. Joyal and J. W. Babich, *J. Med. Chem.*, 2013, **56**, 510-520.

(109) K. P. Maresca, S. M. Hillier, G. L. Lu, J. C. Marquis, C. N. Zimmerman, W. C. Eckelman, J. L. Joyal and J. W. Babich, *Inorg. Chim. Acta*, 2012, **389**, 168-175.

(110) G. L. Lu, K. P. Maresca, S. M. Hillier, C. N. Zimmerman, W. C. Eckelman, J. L. Joyal and J. W. Babich, *Bioorg. Med. Chem. Lett.*, 2013, **23**, 1557-1563.

(111) S. M. Hillier, K. P. Maresca, G. L. Lu, R. D. Merkin, J. C. Marquis, C. N. Zimmerman, W. C. Eckelman, J. L. Joyal and J. W. Babich, *J. Nucl. Med.*, 2013, **54**, 1369-1376.

(112) S. Vallabhajosula, A. Nikolopoulou, J. W. Babich, J. R. Osborne, S. T. Tagawa, I. Lipai, L. Solnes, K. P. Maresca, T. Armor, J. L. Joyal, R. Crummet, J. B. Stubbs and S. J. Goldsmith, *J. Nucl. Med.*, 2014, **55**, 1791-1798.

(113) A. Afshar-Oromieh, J. W. Babich, C. Kratochwil, F. L. Giesel, M. Eisenhut, K. Kopka and U. Haberkorn, *J. Nucl. Med.*, 2016, **57**, 79s-89s.

(114) J. Wald, R. Alberto, K. Ortner and L. Candreia, *Angew. Chem. Int. Edit.*, 2001, **40**, 3062-3066.

(115) J. Bernard, K. Ortner, B. Spingler, H. J. Pietzsch and R. Alberto, *Inorg. Chem.*, 2003, **42**, 1014-1022.

(116) H. W. Peindy N'Dongo, Y. Liu, D. Can, P. Schmutz, B. Spingler and R. Alberto, *J. Organomet. Chem.*, 2009, **694**, 981-987.

(117) S. Liu, *Mol. Pharmaceut.*, 2006, **3**, 472-487.

(118) S. D. Ji, A. Czerwinski, Y. Zhou, G. Q. Shao, F. Valenzuela, P. Sowinski, S. Chauhan, M. Pennington and S. Liu, *Mol. Pharmaceut.*, 2013, **10**, 3304-3314.

(119) E. Brenna, F. G. Gatti, A. Manfredi, D. Monti and F. Parmeggiani, *Adv. Synth. Catal.*, 2012, **354**, 2859-2864.

(120) N. Junzo, T. Takashi, O. Hideki and W. Shoji, *Chem. Lett.*, 1986, **15**, 541-544.

(121) B. A. Pawson, K.-K. Chan, J. DeNoble, R. J. L. Han, V. Piermattie, A. C. Specian, S. Srisethnil, P. W. Trown and O. Bohoslawec, *J. Med. Chem.*, 1979, **22**, 1059-1067.

(122) R. L. Siegel, K. D. Miller and A. Jemal, *Ca-Cancer J. Clin.*, 2018, **68**, 7-30.

(123) S. Perner, M. D. Hofer, R. Kim, R. B. Shah, H. Li, P. Möller, R. E. Hautmann, J. E. Gschwend, R. Kuefer and M. A. Rubin, *Hum. Pathol.*, 2007, **38**, 696-701.

(124) E. Gourni and G. Henriksen, *Molecules*, 2017, **22**, 523.

(125) ClinicalTrials.gov, https://clinicaltrials.gov/ct2/results?cond=&term=Ga-PSMA&cntry=&state=&city=&dist= (Accessed 11.02.2018)).

(126) A. Meyer, J. Auernheimer, A. Modlinger and H. Kessler, *Curr. Pharm. Des.*, 2006, **12**, 2723-2747.

(127) S. Liu, *Bioconjug. Chem.*, 2015, **26**, 1413-1438.

(128) M. Schäfer, U. Bauder-Wüst, K. Leotta, F. Zoller, W. Mier, U. Haberkorn, M. Eisenhut and M. Eder, *EJNMMI Research*, 2012, **2**, 23.

(129) P. Misra, V. Humblet, N. Pannier, W. Maison and J. V. Frangioni, *J. Nucl. Med.*, 2007, **48**, 1379-1389.

(130) B. S. Angelo Frei, Roger Alberto, *submitted*, 2018.

(131) M. Felber, M. Bauwens, J. M. Mateos, S. Imstepf, F. M. Mottaghy and R. Alberto, *Chem. - Eur. J.*, 2015, **21**, 6090-6099.

(132) M. Benešová, U. Bauder-Wüst, M. Schäfer, K. D. Klika, W. Mier, U. Haberkorn, K. Kopka and M. Eder, *J. Med. Chem.*, 2016, **59**, 1761-1775.

(133) F. Zelder, M. Sonnay and L. Prieto, *ChemBioChem*, 2015, **16**, 1264-1278.

(134) F. Klepper, K. Polborn and T. Carell, *Helv. Chim. Acta*, 2005, **88**, 2610-2616.

(135) E. C. Taylor, D. Kuhnt, C. Shih, S. M. Rinzel, G. B. Grindey, J. Barredo, M. Jannatipour and R. G. Moran, *J. Med. Chem.*, 1992, **35**, 4450-4454.

(136) H. L. Pearce and M. Alice Miller, *Adv. Enzyme Regul.*, 2005, **45**, 229-255.

(137) J. Tönnemann, J. Risse, Z. Grote, R. Scopelliti and K. Severin, *Eur. J. Inorg. Chem.*, 2013, **2013**, 4558-4562.

(138) W. L. Jolly, *Inorg. Synth.*, New York, 1968.

(139) K. Ogawa, T. Mukai, Y. Arano, A. Otaka, M. Ueda, T. Uehara, Y. Magata, K. Hashimoto and H. Saji, *Nucl. Med. Biol.*, 2006, **33**, 513-520.

(140) G. Ferro-Flores and C. Arteaga de Murphy, *Adv. Drug Delivery Rev.*, 2008, **60**, 1389-1401.

(141) P. J. Blower, A. G. Kettle, M. J. O'Doherty, A. J. Coakley and F. F. Knapp, Jr., *Eur. J. Nucl. Med.*, 2000, **27**, 1405-1409.

(142) P. Bernal, J. L. Raoul, J. Stare, E. Sereegotov, F. X. Sundram, A. Kumar, J. M. Jeong, P. Pusuwan, C. Divgi, P. Zanzonico, G. Vidmar, J. Buscombe, T. T. Chau, M. M. Saw, S. Chen, R. Ogbac, M. Dondi and A. K. Padhy, *Semin. Nucl. Med.*, 2008, **38**, S40-45.

(143) L. Helm, *Coord. Chem. Rev.*, 2008, **252**, 2346-2361.

(144) M. P. Coogan, R. P. Doyle, J. F. Valliant, J. W. Babich and J. Zubieta, *J. Labelled Compd. Radiopharm.*, 2014, **57**, 255-261.

(145) G. Jaouen, S. Top and A. Vessières, in *Bioorganometallics*, Wiley-VCH Verlag GmbH & Co. KGaA, 2006, DOI: 10.1002/3527607692.ch3, pp. 65-95.

(146) R. G. Balasingham, M. P. Coogan and F. L. Thorp-Greenwood, *Dalton Trans.*, 2011, **40**, 11663-11674.

(147) M. Morais, A. Paulo, L. Gano, I. Santos and J. D. G. Correia, *J. Organomet. Chem.*, 2013, **744**, 125-139.

(148) J. D. Correia, A. Paulo and I. Santos, *Curr. Radiopharm.*, 2009, **2**, 277-294.

(149) R. Alberto, in *Medicinal Organometallic Chemistry*, eds. G. Jaouen and N. Metzler-Nolte, Springer Berlin Heidelberg, Berlin, Heidelberg, 2010, DOI: 10.1007/978-3-642-13185-1_9, pp. 219-246.

(150) M. Bartholoma, J. Valliant, K. P. Maresca, J. Babich and J. Zubieta, *Chem. Commun.*, 2009, DOI: 10.1039/B814903H, 493-512.

(151) M. L. Bowen and C. Orvig, *Chem. Commun.*, 2008, DOI: 10.1039/B809365B, 5077-5091.

(152) S. Liu, *Adv. Drug Delivery Rev.*, 2008, **60**, 1347-1370.

(153) G. Bandoli, F. Tisato, A. Dolmella and S. Agostini, *Coord. Chem. Rev.*, 2006, **250**, 561-573.

(154) R. Alberto, *J. Nucl. Radiochem. Sci.*, 2005, **6**, 173-176.

(155) A. T. Taylor, M. Lipowska and H. Cai, *J. Nucl. Med.*, 2013, **54**, 578-584.

(156) M. Lipowska, H. He, E. Malveaux, X. Xu, L. G. Marzilli and A. Taylor, *J. Nucl. Med.*, 2006, **47**, 1032-1040.

(157) P. V. Grundler, B. Salignac, S. Cayemittes, R. Alberto and A. E. Merbach, *Inorg. Chem.*, 2004, **43**, 865-873.

(158) K. Koike, N. Okoshi, H. Hori, K. Takeuchi, O. Ishitani, H. Tsubaki, I. P. Clark, M. W. George, F. P. A. Johnson and J. J. Turner, *J. Am. Chem. Soc.*, 2002, **124**, 11448-11455.

(159) K. Koike, J. Tanabe, S. Toyama, H. Tsubaki, K. Sakamoto, J. R. Westwell, F. P. A. Johnson, H. Hori, H. Saitoh and O. Ishitani, *Inorg. Chem.*, 2000, **39**, 2777-2783.

(160) O. Ishitani, M. W. George, T. Ibusuki, F. P. A. Johnson, K. Koike, K. Nozaki, C. Pac, J. J. Turner and J. R. Westwell, *Inorg. Chem.*, 1994, **33**, 4712-4717.

(161) J. V. Caspar, B. P. Sullivan and T. J. Meyer, *Inorg. Chem.*, 1984, **23**, 2104-2109.

(162) P. Grundler, Ph.D. Thesis, Ph.D. Thesis, 2005.

(163) P. V. Grundler, L. Helm, R. Alberto and A. E. Merbach, *Inorg. Chem.*, 2006, **45**, 10378-10390.

(164) S. F. Lincoln and A. E. Merbach, in *Adv. Inorg. Chem.*, ed. A. G. Sykes, Academic Press, 1995, vol. Volume 42, pp. 1-88.

(165) B. Salignac, P. V. Grundler, S. Cayemittes, U. Frey, R. Scopelliti, A. E. Merbach, R. Hedinger, K. Hegetschweiler, R. Alberto, U. Prinz, G. Raabe, U. Kölle and S. Hall, *Inorg. Chem.*, 2003, **42**, 3516-3526.

(166) A. Egli, K. Hegetschweiler, R. Alberto, U. Abram, R. Schibli, R. Hedinger, V. Gramlich, R. Kissner and P. A. Schubiger, *Organometallics*, 1997, **16**, 1833-1840.

(167) U. Prinz, U. Koelle, S. Ulrich, A. E. Merbach, O. Maas and K. Hegetschweiler, *Inorg. Chem.*, 2004, **43**, 2387-2391.

(168) F. A. Dunand, L. Helm and A. E. Merbach, in *Adv. Inorg. Chem.*, Academic Press, 2003, vol. Volume 54, pp. 1-69.

(169) N. Aebischer, R. Schibli, R. Alberto and A. E. Merbach, *Angew. Chem. Int. Edit.*, 2000, **39**, 254-256.

(170) J. D. Atwood and T. L. Brown, *J. Am. Chem. Soc.*, 1976, **98**, 3160-3166.

(171) R. Alberto, A. Egli, U. Abram, K. Hegetschweiler, V. Gramlich and P. A. Schubiger, *J. Chem. Soc., Dalton Trans.*, 1994, DOI: 10.1039/DT9940002815, 2815-2820.

(172) F. Cotton, *Chemical applications of group theory*, Wiley, New York, 1990.

(173) R. Carter, *Molecular symmetry and group theory*, Wiley, New York, 1998.

(174) G. F. P. Warnock, L. C. Moodie and J. E. Ellis, *J. Am. Chem. Soc.*, 1989, **111**, 2131-2141.

(175) R. Krämer, E. Lippmann, K. Noisternig, M. Steimann, U. Nagel and W. Beck, *Chem. Ber.*, 1993, **126**, 927-932.

(176) J. VandeVondele, M. Krack, F. Mohamed, M. Parrinello, T. Chassaing and J. Hutter, *Comput. Phys. Commun.*, 2005, **167**, 103-128.

(177) M. Sandström, I. Persson and P. Persson, *Acta Chem. Scand.*, 1990, **44**, 653-675.

(178) K. A. Johnson, Z. B. Simpson and T. Blom, *Anal. Biochem.*, 2009, **387**, 20-29.

(179) J. P. Kraack, A. Frei, R. Alberto and P. Hamm, *J. Phys. Chem. Lett.*, 2017, **8**, 2489-2495.

(180) P. P. Mokolokolo, A. Frei, M. S. Tsosane, D. V. Kama, M. Schutte-Smith, A. Brink, H. G. Visser, G. Meola, R. Alberto and A. Roodt, *Inorg. Chim. Acta*, 2018, **471**, 249-256.

(181) K. D. Mjos and C. Orvig, *Chem. Rev.*, 2014, **114**, 4540-4563.

(182) C. S. Allardyce and P. J. Dyson, *Dalton Trans.*, 2016, **45**, 3201-3209.

(183) E. A. Hillard and G. Jaouen, *Organometallics*, 2011, **30**, 20-27.

(184) G. Gasser and N. Metzler-Nolte, *Curr. Opin. Chem. Biol.*, 2012, **16**, 84-91.

(185) G. Jaouen, A. Vessieres and S. Top, *Chem. Soc. Rev.*, 2015, **44**, 8802-8817.

(186) E. Hillard, A. Vessieres, L. Thouin, G. Jaouen and C. Amatore, *Angew. Chem. Int. Edit*, 2006, **45**, 285-290.

(187) S. Top, A. Vessieres, P. Pigeon, M. N. Rager, M. Huche, E. Salomon, C. Cabestaing, J. Vaissermann and G. Jaouen, *ChemBioChem*, 2004, **5**, 1104-1113.

(188) D. Dive and C. Biot, *ChemMedChem*, 2008, **3**, 383-391.

(189) M. Navarro, W. Castro and C. Biot, *Organometallics*, 2012, **31**, 5715-5727.

(190) F. Dubar, C. Slomianny, J. Khalife, D. Dive, H. Kalamou, Y. Guerardel, P. Grellier and C. Biot, *Angew. Chem. Int. Ed.*, 2013, **52**, 7690-7693.

(191) S. Blanck, J. Maksimoska, J. Baumeister, K. Harms, R. Marmorstein and E. Meggers, *Angew. Chem. Int. Edit.*, 2012, **51**, 5244-5246.

(192) E. Meggers, *Angew. Chem. Int. Edit.*, 2011, **50**, 2442-2448.

(193) A. C. Komor and J. K. Barton, *J. Am. Chem. Soc.*, 2014, **136**, 14160-14172.

(194) A. Leonidova and G. Gasser, *ACS Chem. Biol.*, 2014, **9**, 2180-2193.

(195) D. Can, B. Spingler, P. Schmutz, F. Mendes, P. Raposinho, C. Fernandes, F. Carta, A. Innocenti, I. Santos, C. T. Supuran and R. Alberto, *Angew. Chem. Int. Edit.*, 2012, **51**, 3354-3357.

(196) S. Imstepf, V. Pierroz, R. Rubbiani, M. Felber, T. Fox, G. Gasser and R. Alberto, *Angew. Chem. Int. Edit.*, 2016, **55**, 2792-2795.

(197) C. Yvon, A. J. Surman, M. Hutin, J. Alex, B. O. Smith, D. L. Long and L. Cronin, *Angew. Chem. Int. Ed.*, 2014, **53**, 3336-3341.

(198) L. E. Joyce, J. D. Aguirre, A. M. Angeles-Boza, A. Chouai, P. K. L. Fu, K. R. Dunbar and C. Turro, *Inorg. Chem.*, 2010, **49**, 5371-5376.

(199) N. I. Shtemenko, H. T. Chifotides, K. V. Domasevitch, A. A. Golichenko, S. A. Babiy, Z. Y. Li, K. V. Paramonova, A. V. Shtemenko and K. R. Dunbar, *J. Inorg. Biochem.*, 2013, **129**, 127-134.

(200) H. T. Chifotides and K. R. Dunbar, *Acc. Chem. Res.*, 2005, **38**, 146-156.

(201) E. Orhan, A. Garci and B. Therrien, *Inorg. Chim. Acta*, 2017, **461**, 78-83.

(202) E. Orhan, A. Garci, T. Riedel, M. Soudani, P. J. Dyson and B. Therrien, *J. Organomet. Chem.*, 2016, **803**, 39-44.

(203) E. Orhan, A. Garci, T. Riedel, P. J. Dyson and B. Therrien, *J. Organomet. Chem.*, 2016, **815-816**, 53-58.

(204) F. F. Li, J. G. Collins and F. R. Keene, *Chem. Soc. Rev.*, 2015, **44**, 2529-2542.

(205) H. Liu, C. H. Jiang, J. S. L. Yeo, K. F. Mok, L. K. Liu, T. S. A. Hor and Y. K. Yan, *J. Organomet. Chem.*, 2000, **595**, 276-284.

(206) C. H. Jiang, T. S. A. Hor, Y. K. Yan, W. Henderson and L. J. McCaffrey, *Dalton Trans.*, 2000, 3204-3211.

(207) R. Alberto, A. Egli, U. Abram, K. Hegetschweiler, V. Gramlich and P. A. Schubiger, *J. Chem. Soc., Dalton Trans.*, 1994, 2815-2820.

(208) R. Alberto, R. Schibli, R. Waibel, U. Abram and A. P. Schubiger, *Coord. Chem. Rev.*, 1999, **192**, 901-919.

(209) M. Karthikeyan and B. Manimaran, *J. Organomet. Chem.*, 2014, **769**, 130-135.

(210) B. Manimaran, A. Vanitha, M. Karthikeyan, B. Ramakrishna and S. M. Mobin, *Organometallics*, 2014, **33**, 465-472.

(211) R. Alberto, R. Schibli and P. A. Schubiger, *Polyhedron*, 1996, **15**, 1079-1089.

(212) W. A. Herrmann, A. Egli, E. Herdtweck, R. Alberto and F. Baumgärtner, *Angew. Chem.*, 1996, **108**, 486.

(213) S. B. Copp, S. Subramanian and M. J. Zaworotko, *J. Chem. Soc., Chem. Comm.*, 1993, 1078-1079.

(214) W. A. Herrmann, R. Alberto, P. Kiprof and F. Baumgärtner, *Angew. Chem. Int. Ed. Engl.*, 1990, **29**, 189-191.

(215) P. P. Mokolokolo, A. Frei, M. S. Tsosane, D. V. Kama, M. Schutte-Smith, A. Brink, H. G. Visser, G. Meola, R. Alberto and A. Roodt, *Inorg. Chim. Acta*, 2018, **471**, 249-256.

(216) A. Brink, H. G. Visser and A. Roodt, *Inorg. Chem.*, 2014, **53**, 12480-12488.

(217) C. Aggelidou, T. A. Theodossiou, A. R. Gonçalves, M. Lampropoulou and K. Yannakopoulou, *Beilstein J. Org. Chem.*, 2014, **10**, 2414-2420.

(218) V. Sharma, G. T. Kelly and C. M. H. Watanabe, *Org. Lett.*, 2008, **10**, 4815-4818.

(219) R. Riclea and J. S. Dickschat, *Chem. - Eur. J.*, 2011, **17**, 11930-11934.

(220) S. Bittner, M. Gorodetsky, I. Har-Paz, Y. Mizrahi and A. E. Richmond, *Phytochemistry*, 1977, **16**, 1143-1151.

(221) L.-w. Liu, Z.-z. Wang, H.-h. Zhang, W.-s. Wang, J.-z. Zhang and Y. Tang, *Chem. Commun.*, 2015, **51**, 9531-9534.

(222) S. Essig, S. Bretzke, R. Müller and D. Menche, *J. Am. Chem. Soc.*, 2012, **134**, 19362-19365.

(223) M. V. Mavrov and V. F. Kucherov, *Bull. Acad. Sci. USSR, Div. Chem. Sci. (Engl. Transl.)*, 1972, **21**, 1395-1397.

(224) S. Da Ros, A. Linden, K. K. Baldridge and J. S. Siegel, *Org. Chem. Front.*, 2015, **2**, 626-633.

(225) A. Altomare, M. C. Burla, M. Camalli, G. L. Cascarano, C. Giacovazzo, A. Guagliardi, A. G. G. Moliterni, G. Polidori and R. Spagna, *J. Appl. Cryst.*, 1999, **32**, 115-119.

(226) G. M. Sheldrick, *Acta Cryst.*, 2008, **A64**, 112-122.

(227) J. P. Perdew, K. Burke and M. Ernzerhof, *Phys. Rev. Lett.*, 1996, **77**, 3865-3868.

(228) S. Goedecker, M. Teter and J. Hutter, *Phys. Rev. B*, 1996, **54**, 1703-1710.

(229) C. Hartwigsen, S. Goedecker and J. Hutter, *Phys. Rev. B*, 1998, **58**, 3641-3662.

(230) M. Krack, *Theor. Chem. Acc.*, 2005, **114**, 145-152.

(231) J. VandeVondele and J. Hutter, *J. Chem. Phys.*, 2007, **127**, 114105.

(232) G. Henkelman, B. P. Uberuaga and H. Jónsson, *J. Chem. Phys.*, 2000, **113**, 9901-9904.

(233) H. C. Horng, C. P. Cheng, C. S. Yang and G.-H. Lee, *Organometallics*, 1996, **15**, 2543-2547.

(234) A. Brink, H. G. Visser and A. Roodt, *Inorg. Chem.*, 2013, **52**, 8950-8961.

(235) A. Brink, H. G. Visser and A. Roodt, *Polyhedron*, 2013, **52**, 416-423.

(236) A. Altomare, M. C. Burla, M. Camalli, G. L. Cascarano, C. Giacovazzo, A. Guagliardi, A. G. G. Moliterni, G. Polidori and R. Spagna, *J. Appl. Cryst.*, 1999, **32**, 115-119.

(237) G. Sheldrick, *Acta Cryst.*, 2008, **A64**, 112-122.

(238) A. Spek, *J. Appl. Crystallogr.*, 2003, **36**, 7-13.


CMSZH
CHEMICAL MOLECULAR SCIENCES ZURICH
GRADUATE SCHOOL